Federal University of Rio Grande do Sul

School of Engineering

Graduate Program in Civil Engineering

Comprehensive Analysis of Cemented Mine Tailings Granular Materials Anisotropy Under Multiaxial Loading

Gustavo Dias Miguel

Porto Alegre

2024

GUSTAVO DIAS MIGUEL

Comprehensive Analysis of Cemented Mine Tailings Granular Materials Anisotropy Under Multiaxial Loading

A thesis presented to the Graduate Program in Civil Engineering of the Federal University of Rio Grande do Sul as part of the requirements of the Degree of Doctor in Engineering – Geotechnical subject.

Porto Alegre

2024

CIP - Catalogação na Publicação

Dias Miguel, Gustavo
Comprehensive Analysis of Cemented Mine Tailings Granular Materials Anisotropy Under Multiaxial Loading / Gustavo Dias Miguel. -- 2024.
231 f.
Orientador: Lucas Festugato.

Tese (Doutorado) -- Universidade Federal do Rio Grande do Sul, Escola de Engenharia, Programa de Pós-Graduação em Engenharia Civil, Porto Alegre, BR-RS, 2024.

1. cement stabilization. 2. multiaxial loading. 3. mining. 4. tailings. 5. soil anisotropy. I. Festugato, Lucas, orient. II. Título.

Elaborada pelo Sistema de Geração Automática de Ficha Catalográfica da UFRGS com os dados fornecidos pelo(a) autor(a).

GUSTAVO DIAS MIGUEL

Comprehensive Analysis of Cemented Mine Tailings Granular Materials Anisotropy Under Multiaxial Loading

This Doctoral Thesis was assessed by the Board of Examiners and was considered suitable to obtain the title of DOCTOR IN ENGINEERING in Geotechnical Engineering. The supervising professor and the Graduate Program in Civil Engineering of the Federal University of Rio Grande do Sul approved its final version.

Porto Alegre, April 2024.

Prof. Lucas Festugato
Ph.D., University of Bristol, United Kingdom
Supervisor

Prof. Nilo C. Consoli
PPGEC/UFRGS Head of Department

BOARD OF EXAMINERS

Prof. Erdin Ibraim (University of Bristol)
PhD., École Nationale des Travaux Publics (ENTPE) of Lyon, France

Prof. Nilo Cesar Consoli (UFRGS)
Ph.D., Concordia University, Canada

Prof. Pedro D. M. Prietto (Universidade de Passo Fundo)
PhD., Federal University of Rio Grande do Sul, Brazil

To my family, Zélio, Loreni, and Leonardo. You are the base of everything! Thank you for supporting me every single day. Love u!

ACKNOWLEDGMENT

The present thesis was written in English to become easily widespread, however, in the Acknowledgement section let me shift to Portuguese:

Uma infinidade de pessoas acaba circulado por nossas vidas neste período de quatro anos, no entanto, pode se dizer que são poucas aquelas que realmente influenciam e impactam no trabalho final. Dentre as “poucas” gostaria de agradecer algumas delas que sem dúvida me fizeram chegar até aqui.

Primeiramente à minha família, Zélio, Loreni e Leonardo, pessoas as quais eu gostaria que fossem eternas. Pessoas que sempre me apoiaram, incentivaram e foram formadoras do meu caráter, fica aqui o meu muito obrigado de coração, amo muito vocês! No quesito família, posso incluir meu melhor amigo Luciano Adriani Ferrari, que nos seus quase 15 anos de amizade conseguimos construir histórias que sempre serão lembradas. Obrigado pela força e apoio de sempre, mesmo nos momentos mais difíceis!

Gostaria de agradecer também meu orientador e amigo Lucas, torcedor do mesmo time (Vamooo Colorado!), que nos gerou mais tristezas do que alegrias nesses anos que se passaram. Agradecer pelo incentivo pela busca do desconhecido, sair da zona de conforto e pelas longas discussões geotécnicas.

Não poderia deixar de agradecer aqui aqueles que me ajudaram, literalmente, no trabalho braçal desta tese, Andressa, João Vitor (01), Pablo e Renato (Renight). Muito obrigado pela parceria, pelos longos dias de LEGG, sem dúvida vocês contribuíram para que este trabalho ocorresse.

Aos meus inúmeros amigos de LEGG, em especial, Dudi, Gonça, Mozara, Dionatas, Eclesielter, Estéfano, São Hugo, João Vitor (01), Mariana, Paulo, Renight, Sérgio, Vini e Helena. Obrigado pela vivência, auxílio, amizade e companheirismo. Vocês além de contribuírem para este trabalho, fizeram com ele se tornasse mais leve.

A Fulbright Brasil pela possibilidade de realizar parte desta tese no exterior, mais especificamente na universidade Colorado School of Mines. Na figura da Fulbright destaco a Carolina Martins, pessoa cativante e de uma energia surreal. Carol obrigado por ter sido essa mãezona de sempre. Aos 40 bolsistas Fulbs tóxicos, os quais tive a possibilidade de conhecer graças a Fulbright, nossas trocas de experiência só enriqueceram minha estadia nos Estados Unidos além de não me deixarem surtar ao longo do caminho. Obrigado por tudo!

Aos amigos que o doutorado sanduíche me deu Arthur, Cesar, Gustavo (mexicano), Conrado e Débora. A pacata Golden-CO e os -30ºC tornaram-se muito melhor com vocês, com nossos incessantes dias jogando sinuca, os dias de karaokê, além do sagrado Chunch de todas às terças-feiras. Levo vocês no coração!

To the Colorado School of Mines in the name of Professors Marte Gutierrez and Jennifer L. Miskimins, thank you for assisting me and for giving me the possibility to use your laboratories.

Por fim, um agradecimento às agências de fomento que contribuíram para a execução da parte experimental desta tese, dentre elas o CNPq e a Capes.

Obrigado!

"Just keep swimming."

Finding Nemo movie, 2003.

ABSTRACT

MIGUEL, G. D. (2024). **Comprehensive Analysis of Cemented Mine Tailings Granular Materials Anisotropy Under Multiaxial Loading**. 2024. Doctoral Thesis (Doctor of Engineering) – Graduate Program in Civil Engineering, Federal University of Rio Grande do Sul, UFRGS, Porto Alegre.

The mining sector is one of the most important economic sources in spite of the country. This economic sector is also in charge of producing tons of waste like tailings, which come from ore extraction and beneficiation. Soil dams, levees, and stack piles are the most common ways to dispose of this kind of residue, and in general encompasses considerable material volumes. Regardless of the methodology adopted, mine tailings disposal remains the major concern in the mining sector. Apart from the visual aspect that sometimes may affect natural landscapes, there is also a concern about water pollution and the soil structures' safety. This latter aspect attracted worldwide experts' attention after considerable geotechnical catastrophes increased in the last decade. Topics like tailings mechanical comprehension, soil liquefaction susceptibility, and tailings mechanical improvements have been spotted in the geotechnical area of study. Several possibilities have emerged aiming to enhance tailings' mechanical behavior and thus avoid new structure failures. Within the possibilities, conventional and alternative binders, and synthetic fibers inclusion in the soil matrix demonstrated to be promising. Inserted into the mine tailings perspective, the scope of the present thesis concerns studying the geomechanical behavior of two cemented granular materials: (i) iron ore tailing, and (ii) ordinary sand, when subjected to multiaxial loading conditions. Unconfined compressive, splitting tensile, ultrasonic pulse velocity, triaxial, and true triaxial tests were carried out to a wide range of dry unit weights (16.0, 16.5, 17.5, 19.0, 20.5, and 22.0 kN/m³) and ordinary Portland cement contents (3, 2.66, 4.38, 5, 7, and 14.65%) when subjected to distinct loading stress paths. Some of the conclusions are: (i) The porosity/volumetric cement content index (η/C_{iv}) proved to be useful and a reliable dosage tool for cement-treated soils even for a multiaxial loading condition. Despite of the cement content and porosity combinations, a single η/C_{iv} index outcame the same engineering properties. (ii) The dry unit weight (porosity) impact on specimens' engineering properties is described by a power function, whereas the cement content linearly impacted the same properties. (iii) The cement content dictated the specimens' final stiffness. (iv) Mean effective stresses (p') higher than the yielding threshold point may lessen the cement benefits on the ultimate failure strength. (v) On the other hand, a mean effective stress higher than the yielding threshold point did not influence the specimens' stiffness. (vi) The induced Z-axis molding compaction anisotropy is erased with cement inclusion. However, this phenomenon is only evidenced for samples tested under the yielding threshold point.

Key-words: cement stabilization, multiaxial loading, mining, tailings, soil anisotropy, high pressure;

RESUMO

MIGUEL, G. D. (2024). **Análise Extensiva da Anisotropia de Materiais Granulares e Rejeitos de Mineração Cimentados Sob Carregamento Multiaxial**. 2024. Tese (Doutorado em Engenharia) – Programa de Pós-Graduação em Engenharia Civil, Universidade Federal do Rio Grande do Sul, UFRGS, Porto Alegre.

Independentemente do país, o setor de mineração é uma das mais importantes fontes econômicas. Este setor econômico é responsável por produzir um grande volume de resíduos também conhecidos por rejeitos, que são oriundos da lavra e beneficiamento de minérios. Barragens de terra, diques, e pilhas são as formas mais comuns de dispor estes rejeitos, formas estas que demandam grandes volumes de solo. A despeito da metodologia adotada para dispor estes resíduos, sua correta disposição ainda é uma grande fonte de preocupação no setor minerário. Além do impacto visual em áreas naturais, há também apreensão quanto à possibilidade da poluição de corpos hídricos e a segurança destas estruturas executadas em solo. Este último aspecto veio à tona nos últimos anos, e atraiu a atenção de profissionais do mundo todo. Tópicos de estudo como a compreensão geomecânica dos rejeitos, sua susceptibilidade a liquefação, e metodologias para melhora de suas características se tornaram comuns na área geotécnica. Diversas alternativas surgiram na busca da melhora geomecânica destes materiais como o uso de agentes cimentantes clássicos e alternativos, e a utilização de fibras sintéticas se mostraram promissores. Este trabalho encontra-se inserido nesta perspectiva do tratamento de materiais granulares sob a ótica de rejeitos de mineração. O escopo deste trabalho é estudar o comportamento geomecânico de dois solos granulares (rejeito de minério de ferro e areia comum de rio) estabilizados pela inclusão de cimento Portland quando submetidos a um estado multiaxial de tensões. Ensaios como o de resistência à compressão, resistência à tração, pulso ultrassônico, triaxial e true triaxial foram realizados para uma ampla faixa de pesos específicos (16.0, 16.5, 17.5, 19.0, 20.5, e 22.0 kN/m³) e teores de cimento Portland (3, 2.66, 4.38, 5, 7, e 14.65%). São conclusões deste estudo: (i) o índice porosidade/teor volumétrico de cimento (η/C_{iv}) provou ser útil, demonstrando ser uma robusta ferramenta de dosagem para materiais cementados mesmo quando submetidos a um estado multiaxial de tensões. A despeito da porosidade ou teor de cimento utilizado, um mesmo η/C_{iv} resultará nas mesmas propriedades de engenharia. (ii) O impacto do peso específico (porosidade) na dosagem de solos cimentados pode ser descrito através de uma função do tipo potência, já o teor de cimento impacta de forma linear estes mesmos materiais. (iii) A quantidade de cimento inserido irá ditar a rigidez de amostras estabilizadas. (iv) Tensões efetivas médias (p') acima da tensão de plastificação do material estabilizado resultam em perda parcial do benefício da inserção do cimento. Isto pode ser explicado pela quebra da cimentação quando da utilização de tensões elevadas. (vi) A anisotropia induzida pela compactação das amostras é eliminada com a inserção de cimento Portland. Entretanto,

este fenômeno só é evidenciado em amostras submetidas a tensões efetivas médias inferiores a tensão de plastificação do material.

Palavras-chave: estabilização com cimento, carregamento multiaxial, mineração, rejeitos de mineração, anisotropia do solo, altas pressões;

LIST OF FIGURES

LIST OF TABLES

SUMMARY

1 INTRODUCTION

1.1 RESEARCH RELEVANCE

Mining has emerged as one of the most important economic sources despite the country. In Brazil, for instance, according to the Brazilian Mining Institute (IBRAM, 2020) mining production in February/2020 was estimated in US$ 40 billion, being responsible for around of 3% of the Brazilian Gross Domestic Product (GDP). Concerning the Brazilian worldwide ore resources representativeness, Brazil emerges as one of the greatest iron ore deposits with an unextracted amount estimated at 33,731,000 (10^3 tons) that might be subject to mining. Such amount represents around 20% of the global iron ore resources. The second and third most important Brazilian ore resources are, in this sequence, mineral coal and bauxite with a global representativeness of 0.4 and 9.6%, respectively (ANM, 2020). This highlights the present thesis relevance, where ore and consequently mine tailings deserve attention from both internal market and academics to improve their production efficiency and safety.

The mining sector drawbacks regard to waste materials production, also known as tailings, which are produced from ore extraction and beneficiation (Zhang et al. 2020). Such residues are generally disposed in artificial pounds, which result in tailing dams over time; other disposal methods have also been reported and have been implemented nowadays (Figure 1) (Nguyen and Boger, 1998; Chen et al., 2019). Regardless of the methodology adopted, mine tailings disposal remains the major concern in mining. Apart from the visual aspect that sometimes affects natural landscapes, there is also a concern due to water pollution, which may be attributed to the discharge of water contaminated with solids, heavy metals, and mill reagents, that are responsible for polluting both surface water and groundwater (Chalkley et al. 1989; Wills & Finch, 2015).

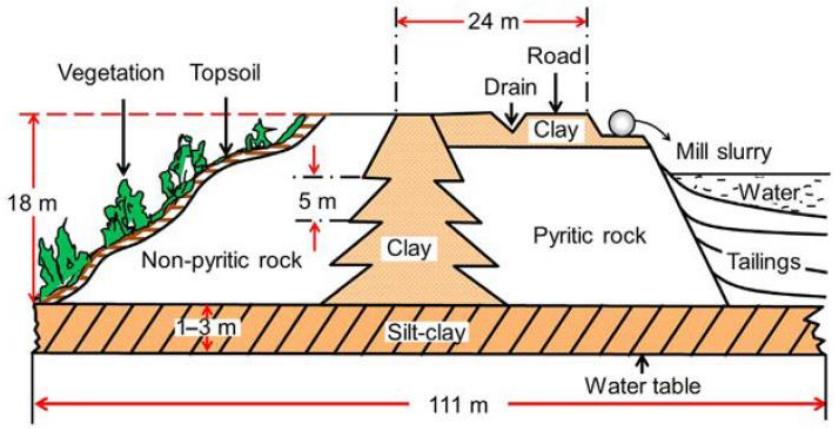

(a)

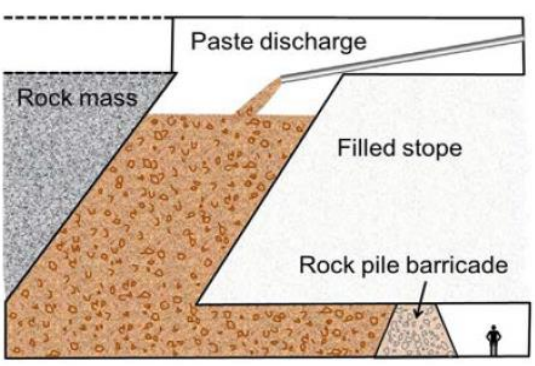

(b)

(c)

Figure 1: Alternative mining tailings disposal techniques: a) Flambeau impoundment (WILLS & FINCH, 2015); b) Backfill disposal design (WILLS & FINCH, 2015); and c) Ring dikes design (RIO TINTO, 2022).

In addition, the safety of tailing dams has attracted experts' attention, which joins environmental, social, and health concerns. Because of the mining sector increase, tailing dams have been forced to expand their storage capacity, which is directly reflected in tailing dams' height once the ground area is sometimes limited. Therefore, it is common to find dams surpassing heights of a hundred meters. That is the case of eleven tailing dams located in Brazil, where the height varies between 100 to 375 m (ANM, 2021). Similarly, it occurs in other countries such as Chile where a tailing dam was reported at 108 m (James et al. 2011), in Mexico with a dam of 100 m (Hu et al. 2017), and in China with tailing dams reaching around 200 m height (Wu et al. 2017). These continuous height increment demands caution, once at the same pace of dams' height, the failure of these structures has also increased (Figure 2).

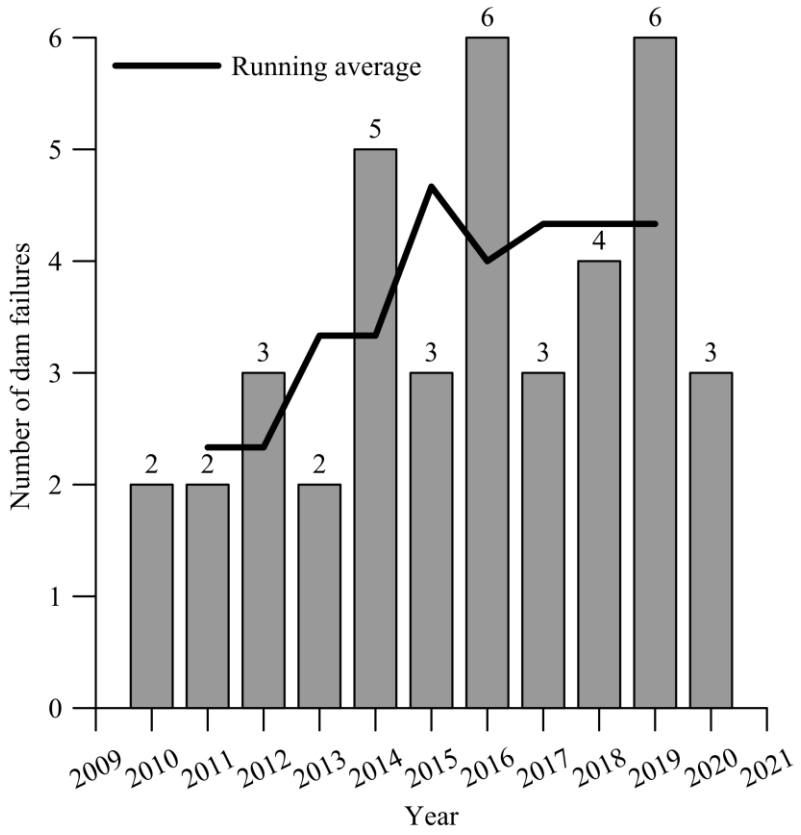

Figure 2: Worldwide dam failures throughout the years (after WISE, 2021).

In Brazil, the most recent accident happened in the year 2019 when a dam break occurred in the state of Minas Gerais, precisely in the city of Brumadinho. Several people died, which was considered one of the most important mining disasters in Brazil. Additionally, before Brumadinho's dam break, a few years back another dam accident happened. This accident was known as Mariana's dam break. Despite the small number of deaths, this second accident was responsible for the greatest environmental damage due to mining in the history of Brazil. Other authors have reported similar accidents around the world that were the case of Van Niekerk & Viljoen (2005), which mentioned a gold tailings dam failure in the Free State Province of South Africa where 17 deaths were reported as well as several houses damaged. Yin et al. (2011) referred to a dam failure that occurred in China, Shanxi province, which resulted in 277 deaths and large natural areas covered by iron ore tailings. Similarly, Li & Coop (2018a) quoted a tin ore tailings impoundment failure in Guangxi province, China, which also caused 277 deaths and a surprising economic loss of 3.4 million yuan.

Such catastrophes led the Brazilian Government to update the tailings disposal policy seeking to increase dams' safety. Therefore, in September 2020 the National Dams' Safety Policy (Brazilian law number 12.334) was updated prohibiting, for example, the upstream tailings disposal methodology. In the same way, this policy encourages companies to look for alternative disposing techniques in order to avoid waterway disposal methods. Thereby, nowadays in Brazil, mining tailings must be gradually filtered; in addition, the existing dams that do not follow such requirements must be closed and the natural site rehabilitation provided.

As a consequence, the Brazilian scenery is predominantly depicted by tailings disposed of in artificial pounds; according to the Tailing Dams Brazilian National Register, a number of 878 tailing dams were accounted for in the last census (ANM, 2021). A small number compared to China for instance, where more than 12,000 tailing dams were accounted for (Yin et al. 2008). Among these hundreds of Brazilian tailing dams, the construction methodology varies in a wide range, few of them were constructed by downstream and centerline techniques, whereas some were first settled upstream, or the construction methodology remains uncatalogued; and now these latter are unable to receive further tailings discharges.

Alternatively, some companies converted their production plant to dewatered processes, which result in filtered tailings. These filtered tailings can no longer be transported through pipelines, representing an important disadvantage compared to waterways methods. Otherwise, trucks and conveyors are implemented to transport these materials from the deposit to the site compaction which turns it into an unsaturated stable "dry" stack (Davies & Rice, 2001; Dixon-Hardy & Engels, 2007). "Dry" stack methods do not require retention embankments and are less susceptible to the liquefaction phenomenon (Dixon-Hardy & Engels, 2007). Despite the smallest concern due to liquefaction, such technique also demands caution. Firstly, because of the "dry" stack slope stability once several meters of height can be achieved. On the other hand, soil foundation carrying capacity must also be verified to avoid a generalized failure.

Several possibilities have emerged aiming to enhance tailings' mechanical behavior and thus avoiding new structure failures. In this scenario, the Graduate Program of Civil

Engineering at the Federal University of Rio Grande do Sul has succeeded among the proposals. Within the possibilities, conventional and alternative binders and fibers inclusion demonstrated to be promising. For instance, Consoli (1997) and Consoli & Sills (2000) studied the soil formation process from tailings disposal, where the transport, sedimentation, and consolidation of sediments were modeled to accurately estimate waste reservoir capacities. Festugato et al. (2013, 2015) in turn, performed monotonic and cyclic direct simple shear tests on fiber-reinforced (cemented or uncemented) gold mining tailings. Regardless of the presence of Portland cement, fiber inclusions conferred to the material a very pronounced hardening behavior. Nevertheless, in the case of monotonic loadings, it was noticed a decrease in materials' rigidity due to fiber inclusion, fact that was not observed in strain-controlled cyclic loading conditions, where fiber inclusion improved the cyclic shear response of mine waste tailings. Recently, Consoli et al. (2017, 2018a) focused on studying the durability, strength, and stiffness of cemented gold mining tailings, where fibers were included as soil reinforcement. Similarly, Bruschi et al. (2021) proposed an innovative green soil stabilization, which was based on the alkali activation technique aiming to stabilize bauxite mining tailings.

Inserted in the previous perspective, the scope of the present thesis concerns studying the multiaxial response of cemented granular materials in the context of mine waste tailings. The main goal of the present work can be driven by the following questions: Is it reasonable to use small percentages of ordinary cement Portland to improve todays' mine waste tailings structures safety? How does the loading condition may affect materials strength?

The thesis's main scope, literature background, methodologies and test results are thereafter presented.

1.2 SCOPE

Design, construction, and operation of tailings structures represent the major concern to new geotechnical mining projects, which may include both environmental and mechanical aspects. Therefore, it became mandatory to fully understand the behavior of materials that might compose such structures to avoid further disasters.

The main objective of the present thesis is to provide a better understanding of cemented and uncemented granular materials when subjected to a multiaxial loading condition. Nevertheless, the main objective can be split into the following minor objectives:

a) to understand the mechanical behavior of cemented and uncemented granular materials in the domain of mine waste tailings;

b) to evaluate/study the effects of multiaxial loading on cemented-granular materials;

c) to evaluate/study the effects of cementing on soil induced anisotropy;

d) to compare experimental test results with predicting models;

1.3 THESIS HYPOTHESIS

Mine waste tailings are majoritarily composed by silt and sand grain sizes, and thus considered a challenging construction material in the mining sector. Challenges that surround these materials regard to their peculiarities, once they are strongly dependent of the ore processing plant. Crushing and grinding methods as well as froth flotation, gravity, and magnetic separation may lead to distinct final products and residues. These materials disposal methods will also impact their behavior. Foundation carrying capacity, slope stability, and liquefaction susceptibility are the main concerns when working with mining tailings. Thence, it is mandatory to look for new strategies to enhance both foundation-bearing capacity and slope stability, likewise, decrease the liquefaction potential. Based on this, it is presumed that ordinary Portland cement addition may be able to improve granular materials mechanical

characteristics by hydrated compounds precipitation. Ordinary Portland cement (OPC) is a worldwide known binder, where several dosage methodologies were already developed. This fact may simplify the OPC usage after this thesis outcomes.

1.4 ASSUMPTIONS

It is well known that ordinary Portland cement has applicability to soil stabilization, where the main variables were already satisfactorily documented. Similarly, the OPC application was extended to mining tailings in the last years and it demonstrated to be promising. Nonetheless, the economic drawbacks have sometimes avoided the OPC applications. Therefore, looking to overcome the economic drawbacks, the present thesis studies a wide range of cement contents, which includes reduced binder amounts. At the same time, despite the lack of novelty concerning ordinary Portland cement usage, it is undocumented until the moment studies on cemented-granular materials (like tailings) that comprises the intermediate principal stress effect on the soil matrix mechanical behavior.

1.5 DELIMITATIONS

The present thesis is delimited to use a restricted number of materials, namely, an iron ore tailing from the ‘Quadrilátero Ferrífero’, located in the south of Minas Gerais – Brazil, ordinary sand from Denver, western of United States, and ordinary Portland cement. Experimental programs were set to evaluate ordinary Portland cement contents and dry unit weights in order to capture controllable variables' impact on response variables.

1.6 LIMITATIONS

Laboratory and test restrictions must be herein apprised to provide the reader with important explanations. Laboratory and equipment limitations are described below:

- Iron ore tailing and ordinary sand amount restrictions. The present thesis is composed by three materials as aforementioned. The ordinary Portland cement is industrialized and does not represent a concern in terms of quantities. Nonetheless, both the iron ore

tailing and ordinary sand had amount restrictions, which dictated the number samples and tests carried out;

- Molding framework loading capacity. Both cylindrical and cubical samples fabricated in the present thesis followed the moist tamping methodology by means of the undercompaction technique. Therefore, dry unit weights chosen were limited to the hydraulic jack loading capacity. On the other hand, cubical samples were manually molded, thus the dry unit weights, in this case, were limited to the maneuverer ability;
- The Federal University of Rio Grande do Sul true triaxial limitations. True triaxial tests are conventionally characterized to maintain the mean effective stress constant under the shear procedure. Thus, despite the several stress paths that the equipment may follow on the octahedral stress plane, at least one of the principal stresses must be gradually decreased to assure the mean effective stress constant. For instance, the standard triaxial compression test simulated in the true triaxial apparatus, which is represented by the angle $\theta = 0°$ (zero). This test type is characterized by a principal stress increment in Z-axis whereas both X and Y-axis are proportionally decreased to maintain the mean effective stress. Nonetheless, both X and Y-axis are restricted by the pressure valve capacity, which means that if X and Y-axis attain a null pressure magnitude; the experimental test must be finished. This fact occurs owing to the pressure valve's inability to promote suction (*i.e.*, the pressure valve is unable to apply a negative stress pressure suctioning the rubber cushion). Therefore, vigorous soil specimens may not attain the peak strength condition before the pressure valve limitation. To avoid the previous described condition the true triaxial soil samples developed at the Federal University of Rio Grande do Sul were molded aiming to attain unconfined compression strengths of 180 kPa;
- The Colorado School of Mines true triaxial limitation relies on the lack of backpressure. Such true triaxial was developed for rock samples, where the backpressure (porepressure) is not a reliable concern. The backpressure drawback was overcame by means measuring soil suction after the shearing procedure.
- In addition, the Colorado School of Mines equipment differs from the Federal University of Rio Grande do Sul true triaxial due to its loading frame structure.

Whereas the Federal University of Rio Grande do Sul true triaxial has flexible loading interfaces (cushions), the Colorado School of Mines true triaxial holds rigid platen interfaces. The rigid boundaries were composed by steel heavy platens which turned the in loco molding inconceivable; the untreated soil strength was lower than the platens weight, and it resulted in specimens' strain before the test start;

- In the case of ordinary sand-ordinary Portland cement blends the cement content upward threshold of 15% (q_u = 3.5 MPa) was chosen, otherwise we might be subject to be migrating from soil theory into the concrete theory which is not the intention here. Also, the ordinary sand-ordinary Portland cement blends experimental program considers conventional triaxial tests. Therefore, the cement content upward threshold of 15% takes into account the triaxial loading frame maximum capacity in advance;
- The Federal University of Rio Grande do Sul true triaxial has a stress range from 0 to 1000kPa, whereas the Colorado School of Mines true triaxial has a stress range from 0 to 70000kPa.
- The ordinary Portland cement soil stabilization inefficiency for cement dosages up to 2% by the soil dry mass in the case of cemented iron ore tailings specimens. Several preliminary tests were conducted to determine the cement content range that would be studied for cemented iron ore tailings samples (Section 3.2 describes the controlled variables). According to the preliminary test results, cement contents lower than 2% by the soil dry mass were unable to develop cemented compounds. Thereby, the present work is limited to the use of cement contents greater than 2%.

1.7 CONTRIBUTION TO THE STATE OF THE ART

Soil stabilization science has been gradually incremented where the ordinary Portland cement remains in the center of the stage despite the large number of innovative binders created throughout the years. Ordinary Portland cement accounts for the advantage of being worldwide commercialized, which might be an economic advantage. Therefore, the present thesis intends to contribute to the soil stabilization state of the art by providing an alternative to tailings disposals in a matter of granular materials treatment. In addition, true triaxial tests on artificially cemented materials are rather scarce (e.g., Reddy *et al*. 1992; Reddy and

Saxena 1993; Festugato et al. 2019, 2023; Silvani et al. 2022), thence, this thesis also seeks to overcome this database shortage.

1.8 THESIS STRUCTURE

Looking to organize the present work, the thesis was divided into several minor parts. Therefore, the present thesis was sorted according to the following sections: 1) research relevance and scope; 2) literature background; 3) experimental program conception and execution; 4) Analysis and modeling of experimental test results; and 6) discussion of the main conclusions.

The first section, named research relevance and scope, was previously discussed and was responsible to present to the reader basic concepts about the mining sector and problems that surround granular materials (e.g., liquefaction susceptibility). Accordingly, this section was also responsible to introduce to the reader thesis's main scope, its minor objectives, and materials employed.

Afterward, the second section is in charge to provide a literature background about the main subjects that comprise this manuscript. Thereby, to perform a high-recognized literature review, both international and national journal papers including renowned books were consulted. The literature background plays an important role to determine the variables that are going to be studied in the experimental program. Therefore, the main variables apprised herein were well-defined based on the theoretical background exhibited in section two.

The experimental program, the third section, determines the variables studied and the laboratory experiments carried out. Each controlled variable, for instance, ordinary Portland cement content and blends dry unit weight, were varied alongside each experiment where their impacts were measured by each response variable (e.g., unconfined compressive strength, tensile strength, initial shear modulus, etc.). The third section in turn is divided into two phases, Phase I – introductory tests and Phase II – advanced tests. Phase I comprises regular geotechnical tests like unconfined compressive and tensile strength tests, whereas phase II regards to more advanced tests like triaxial and true triaxial tests.

Concluding, the remaining four and five sections are responsible to compare experimental and modeled data and discuss the main conclusions obtained. For a detailed thesis structure, where sections one to five are distinguished, please refer to Figure 17.

2 LITERATURE BACKGROUND

Chapter 2 is responsible to discuss the main topics apprised in the present thesis through an extensive literature background review. The literature background begins discussing the soil matrix in a perspective of mine waste tailings. In the sequence, insights of soil stabilization by ordinary Portland cement addition and true triaxial tests are apprised.

2.1 MINE WASTE TAILINGS

Mining waste tailings or just mining tailings are described as a residual material derived from ore processing (*i.e.,* mineral extraction and beneficiation) (DIXON-HARDY & ENGELS 2007; LI et al. 2018; KOSSOFF et al. 2014; ZHANG et al. 2020; CONSOLI et al. 2022).

On the other hand, a mineral is designated as an inorganic chemical compound naturally found in the Earth's crust, which was created by geological processes (LAMBE & WHITMAN, 1979; WILLS & FINCH, 2015). Minerals are formed by basic structural units, which are barely idealized for better understanding. Among these basic structural units, some of them are largely known such as the silicon-oxygen tetrahedron and the aluminum-oxygen octahedron. Connecting basic structural units result in stable or unstable atomic structures. Stable structures naturally exist in the nature, for instance, minerals Gibbisite and Brucite. Whereas unstable atomic structures must be combined with analogous structures to build up other components (*e.g.,* the Silica, which is composed by a connection of silicon-oxygen tetrahedron structures) (LAMBE & WHITMAN, 1979).

Distinct stable units can also be connected between each other by hydrogen bonding or secondary valence forces, and result in further minerals. For instance, the brucite units stacked on silicate units resulted in a serpentine mineral; The gibbsite units piled on silica units giving the kaolinite mineral, etc. (LAMBE & WHITMAN, 1979). According to Lambe & Whitman (1979), such minerals are also known as two-layer sheet minerals, once one basic unit comes on the top of another. Other minerals are also created through *isomorphous substitutions*, where atoms are replaced inside the existing structures. That is the case of silicon replacement by aluminum atoms in the silicon-oxygen tetrahedron, which is readily

seen in halloysite minerals where the aluminum atom takes place of a silicon atom in the reason of 1/400 (*i.e.*, one substitution occurs for every four hundredth silicon atoms).

Every atom substitution is in charge to create a kind of new mineral; nonetheless, a new mineral formation might be also conditioned to the net unit charge resulting from the isomorphous substitution. A net unit charge deficiency [*e.g.*, the aluminum atom (+3) replacing a silicon atom (+4)] can attract randomly basic structural units and result in additional mineral structures, for example, the muscovite mineral (LAMBE & WHITMAN, 1979).

Therefore, based on the atoms substitution and the possibility to have unbalanced compounds, highly reactive metals become prone to make part of unstable structures neutralizing these ones. Wills & Finch (2015) suggest as example the olivine mineral, where Mg and Fe atoms might replace Si and O atoms using an isomorphous substitution without affecting the crystallography structure at all. These previous high-reactive metals are industrially attractive to be mined likewise aluminum, iron, and magnesium. Thus, once mineral deposits are found and become profitable to be extracted, these are converted to ore deposits (WILLS & FINCH, 2015).

Nonetheless, a mineral deposit cannot be described as a homogeneous body. A mixture of profitable minerals and extraneous nonvaluable materials, also known as *gangue*, are subjected to be mined simultaneously (WILLS & FINCH, 2015; SANTOS, 2009; CARVALHO, 2012). For instance, the minerals galena and sphalerite are generally associated with copper production; however, such minerals are commonly found with the pyrite mineral, a nonvaluable mineral when compared to copper for instance (WILLS & FINCH, 2015).

Galena and sphalerite depict a single example, where the pyrite mineral might be present. However, diverse other nonvaluable minerals are also found associated with profitable components as well. Despite the gangue presence or not, during the ore beneficiation both valuable and nonvaluable materials must be mined, once there is the necessity to separate the *paymineral* from the gangue (WILLS & FINCH, 2015; LUZ & LINS, 2010). Thus, the mineral dressing consists of the mining process, particle breakage, and particle physical or

chemical separation. This latter is responsible to access the most valuable components, which will be addressed for alloys production for instance. Whereas the discarded phase, namely, the components considered unprofitable (the gangue), are referred to as *tailings*.

Thence, tailings are described as a mining residue resulting from ore processing. Such residues are disposed according to a varied techniques like in sludge form, backfilling deactivated mines, by subaqueous disposals, among others (a detailed review of tailings disposal methods is appraised in section 2.1.2). According to Hu et al. (2017), tailings volume has significantly increased over the last few decades, which might be explained owing to the ore demand for metal production and because of the low-grade ores' beneficiation. Low-grade ores tend to produce meaningfully higher tailings volume than concentrated deposits. Major advances in productivity and technologies have also boosted mineral processing, where the production costs were reduced, whereas the volume of residues increased (WILLS & FINCH, 2015).

Mining waste tailings concern the main core of the present thesis and will be designated hereafter as soil matrix. Both the iron ore tailing from the 'Quadrilátero Ferrífero', a lean clay with sand, and the ordinary sand from Denver area seek mimic two distinct tailings gradation.

2.1.1 Ore processing and end products

As already mentioned, ore processing or ore beneficiation consists of several treatments responsible to improve natural Earth compounds turning it profitable products. These final products will be in charge to be further producing alloys and metals for instance. According to Wills & Finch (2015), two major processing steps must be highlighted: the size reduction and the concentration processes.

The size reduction process contributes to particle size reduction aiming to liberate the paymineral from the gangue. Whereas, the concentration process, a subsequent step, seeks to concentrate the previously treated material using physical and/or chemical separation (GRAY, 1984; BARBERY, 1991). The concentration process is then accounted to produce both the enriched part and the residue part (tailings).

Paymineral liberation consists in material particle breakage that is carried out by crushing and grinding processes, and results in a mixture of valuable materials and residues. In agreement with Radziszewski (2013), crushing and grinding processes are in charge of the greatest energy consumption during the ore beneficiation, attaining around 50% of the entire energy spent in the whole process. Thus, it is important to be aware of the mining site characteristics and ore availability, once lower-grade ores might demand more pre-treatments. Looking to achieve a great paymineral liberation, Wills & Finch (2015) stated that particle size dimensions must attain dimensions lesser than 100 μm in order to avoid gangue contamination. Nonetheless, this is not a pattern and depends on the site and ore characteristics, ore destination, etc.

Heavily ground minerals tend to produce both very fine ores and tailings as well, which may raise some concerns. Firstly, highly thin ores might be lost during tailings disposals once it turns difficult to separate fine ore particles from gangue. Thus, important ore amounts are susceptible to be lost during tailings discharge. Secondly, very thin tailing particles tend to deserve caution on tailings disposals, fine tailings are easily prone to liquefaction and need caution according to the disposal methodology (WILLS & FINCH, 2015; CONSOLI et al. 2022). Therefore, there is not a well-defined amount of grinding content, and such a process must be balanced according to the energy costs, ore quality recovery, and process outcomes. Wills & Finch (2015) suggest that small-scale or laboratory pilot tests must be previously carried out to achieve the optimum grinding ratio.

A complete ore liberation is something almost impossible, once some gangue portions tend to remain coupled with valuable minerals (DIXON-HARDY & ENGELS 2007; WILLS & FINCH, 2015). Wills & Atkinson (1993) suggested that it is possible to separate the gangue-mineral compound nearly to its interface, thus, avoiding valuable mineral losses. This methodology comprises the mineral extraction by microwaves and/or scanning techniques. Microwaves heat each portion in different a way, which produce dilation and cracks around the gangue-ore interface (KINGMAN et al., 2004). On the other hand, scanning microscopy techniques can assess the ore mineralogy, ore availability, and recovery potential, helping to formulate distinct strategies to achieve the greatest ore beneficiation (Guerney et al., 2003; Baum et al., 2004; Hoal et al., 2009; Evans et al., 2011; Lotter, 2011; Smythe et al., 2013).

This blend of profitable material with gangue is also known by *middlings* and is readily susceptible to be reprocessed on a grinding plant or subjected to the next step, the concentration process.

The next stage, the concentration process, is widely applied to separate the ore from the gangue, enriching the former. Several concentration techniques exist and all of them seek to exploit ore's physical properties such as mineral density, magnetic susceptibility, and electrical conductivity, etc. (RITCEY 1989; VICK 1990; EC 2004; WILLS & FINCH, 2015). The most ancient technique regards optical ore concentration, which was formerly man-made by hands and in the sequence shifted to machines. The handmade concentration remains in use and is commonly seen, for instance, in illegal sites in the meddle-west and north of Brazil. On the other hand, other up-to-date processes were also implemented, which tend to work in a mass-produced chain. Some of these processes are gravity concentration, froth flotation, and magnetic/electrostatic separation.

The gravity concentration methodology exploits the density of each compound in the ore-gangue blend. Dense particles tend to sink whereas light particles are prone to float in a dense liquid, which can be either water or artificial suspensions. In alternative, the froth flotation methodology concentrates the paymineral attaching these on-air bubbles. The air bubbles are produced by synthetic mixtures and a shaking pulp. The pulp density and chemistry are adjusted according to ores' nature, producing hydrophobic or hydrophilic materials. The hydrophobic portion, the valuable mineral in this case, seeks to be enclosed by the pulp bubbles and tends to float; whereas the hydrophilic part, the gangue, sinks in the tank.

Other methodologies also take the advantage of ores' physical properties, that is the case of iron ore processing. High magnetic ores, generally depicted by iron ores (e.g., magnetite - Fe_3O_4), are readily attracted by magnetic forces and can easily be separated from the gangue when subjected to magnetic fields. Even low magnetic ores can also experience such treatment, however, demanding great magnetic sources. Finally, electrostatic separation consists of separating conductive minerals from non-conductive minerals based on minerals' electrical differences in conductivity.

2.1.2 Tailings disposal methods

Tailings disposal methods are surrounded by a huge concern and are undoubtedly recognized as the most harmful source to the environment independent of technique (VICK 1990; WILLS & FINCH, 2015). According to the EPA (1995), tailings structures must be able to satisfactorily remain stable throughout their entire life, avoiding site contamination and being capable to provide site rehabilitation as well.

The way of disposing such residues will mandatorily follow tailings' characteristics, site restrictions, ore sort, etc. (VICK 1984; DIXON-HARDY & ENGELS 2007). Arid locations are prone to receive dry stack operations, enabling them to easily achieve the target moisture content during compaction. On the contrary, dry stacks located in arid zones are also responsible to dust production and fences must be projected. Other example regards to gold extraction which in general must be mined by cyanide employment. In this case, the tailings storage facilities (TSF) accounted to stock residues from gold extraction must have a bottom liner to avoid site contamination. Therefore, as can be seen tailings source dictates the final deposition method choice.

Nonetheless, the ancient and most common disposal method regards hydraulic deposition, which was made in the past by direct discharges in watercourses, neglecting eventual environmental damages (VICK 1990). Nowadays hydraulic-based methods regard to pump residues to artificial ponds by pipelines. On the artificial ponds, residues are spigotted off and allowed to sediment/consolidate under their own weight. Residues consolidation may take several years owing to its characteristics like the low hydraulic conductivity (JAMES et al. 2011; CONSOLI & SILLS 2000, HU et al. 2017; CONSOLI et al. 2022).

In general, valleys, depressions, in-pit, and ring dikes (also known as paddock or cell) are alternatives to stock slurry mining residues. However, dams, embankments, and other types of surface impoundments are by far the most common storage techniques (VICK 1990). In the case of surface impoundments, likewise, dams and ring-dikes, the formers are built aiming to block natural river streams in valleys – the preexisting natural flow is reallocated – and then enabling tailings residues storage (e.g., Figure 3a). Whereas ring-dikes are characterized to have dikes surrounding the tailings and are positioned on flat sites (e.g.,

Figure 3b). These are some characteristics that differentiate dams, ring-dikes, and dry stacks facilities. Dams and ring-dikes have the conception to support tailings and water backward load, whereas dry stacks are thought to be self-supporting.

(a) (b)

Figure 3: Tailings storage facilities: a) Cross-valley impoundment (Berger, 2018); and b) ring-dike design (Davidson, H - The Guardian, 2019).

Several materials, which include mine waste tailings and borrowed materials, are susceptible to be used as construction materials for tailings storage facilities. Despite the impoundment type, dams or ring-dikes, the structured zone will follow at least one of these concepts: 1) upstream; 2) downstream; and/or 3) centerline construction design.

Embankments' design will be adopted accordingly to site characteristics and project requirements like site seismic activity, foundation carrying capacity, hydrological conditions, etc. (AZIZLI et al. 1995). Furthermore, the design adopted must look for to be reducing the Operational (OPEX) and Capital (CAPEX) expenditures. The disposal methodology is critical in determining the final ore production costs.

The upstream embankments' design is supposed to be the most affordable design. This kind of impoundment rising is so named because of the upward movement of the main embankment into the pond. Figure 4 depicts the upstream design. According to Wills & Finch (2015), the upstream design advantages rely on the low-cost construction and speed of the dam rising. Dam embankments' rising at a high pace are favorable in terms of cost reduction, but the least favorable in terms of safety. Figure 4 exemplifies the main reason, where every subsequent new dike settles on coarse, loose, and saturated material.

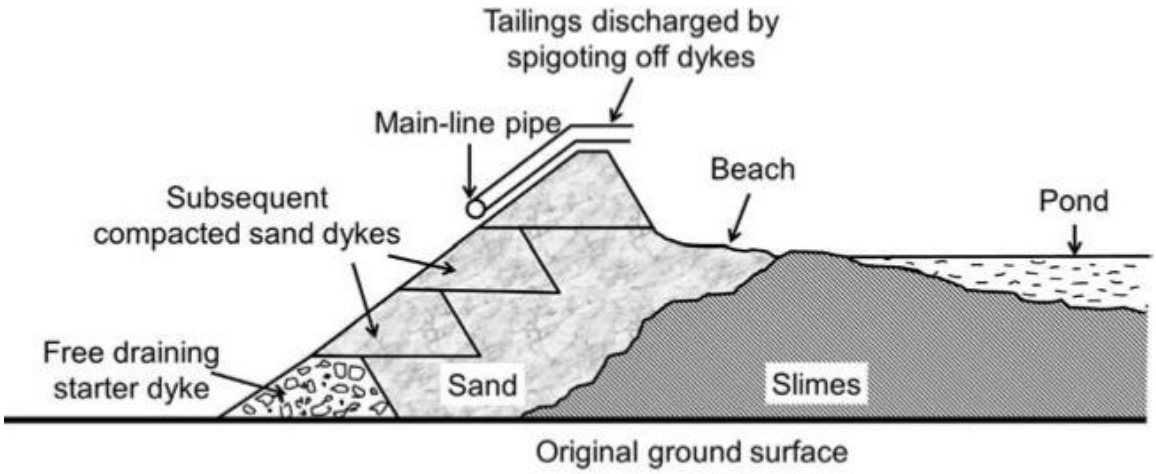

Figure 4: The upstream design (after WILLS & FINCH, 2015).

Coarse, loose, and saturated materials are prone to contract upon shear and promote positive pore water pressure increase, thence, a decrease in the mean effective stress (CASTRO 1969; CASTRO & POULOS 1977; CASTRO et al. 1982; TERZAGHI et al. 1996; CONSOLI et al. 2022; FESTUGATO et al. 2022). In line with Andersen (2009), positive pore water pressure build-up is susceptible to occur by both monotonic (e.g., dikes increment) or cyclic loads (e.g., compaction, seismic loads, etc.), which might be characterized by a sharp and sudden increase resulting in soil liquefaction. This latter corresponds to a state where temporary null mean effective stress is reached and the soils start flowing indeterminately (JEFFERIES & BEEN, 2015; SANTAMARINA et al. 2019; FESTUGATO et al. 2022).

Among those dam failures shown in Figure 2, several of them were associated with liquefaction phenomenon. For this reason, the upstream design was restricted in many countries including in Brazil. The most recent National Dams' Safety Policy (Brazilian law number 12.334) prohibited such methodology, where downstream and centerline designs come out as safer options.

Conversely to the upstream design, in the downstream methodology the dam centerline moves downward, opposite to the pond. Thus the dam settles on compacted pre-treated materials instead of saturated, fine, loose materials (Figure 5a). Another advantage of the downstream design regards to the ongoing drainage layer at the dam foot, whereas its disadvantages lay in the amount of material required for starting (WILLS & FINCH, 2015).

The centerline design option is assumed to be a variation of downstream design, where the dam crest remains in the same vertical position throughout the dam raising (Figure 5b). In spite of the downstream or centerline designs, both of them are sometimes criticized to cause landscape detriments, once embankments revegetation is not possible until its closing. Also, this fact may lead to erosion concerns along the dam construction.

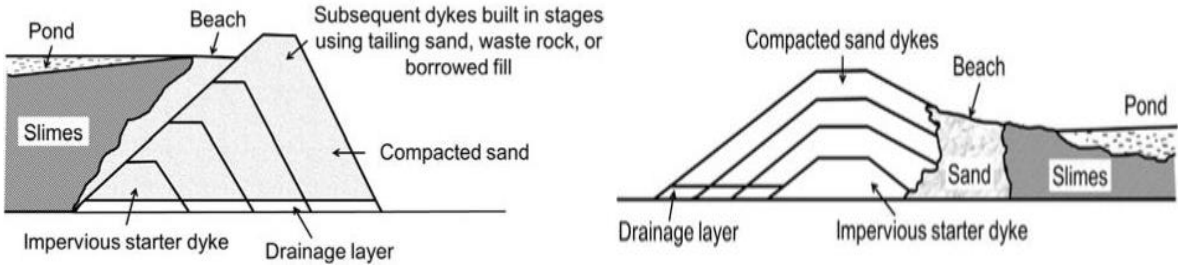

Figure 5: Dam embankments design: a) the downstream design; and b) the centerline design (after WILLS & FINCH, 2015).

In the previous designs tailings are disposed of by waterways methodologies. Otherwise, other alternatives exist in terms of densified tailings deposition. Wills & Finch (2015) suggest three main alternatives, namely, dry stacking (or filtered tailings), thickened tailings, and paste tailings – the semi-dried disposal techniques.

Of course, the main advantage of such designs regard to materials' liquefaction potential decrease. In addition, the water-reagent recovery and tailings footprint decrease are benefits as well (AMSDEN 1974; COOLING AND GLENISTER, 1992). However, the densifying process might induce to cost increase, which comprises the insertion of filter-based steps and truck transportation until deposition site. Thickened tailings are no longer possible to be transported by pipelines accordingly to fines concentration. Nguyen & Boger (1998) highlight the fact that thickened tailings also demand more complex understanding (e.g., rheology parameters) when compared to waterway disposal techniques.

Among the previous three possibilities, thickened and paste tailings remain prone to be pumped even though water is partially extracted. The former technique is characterized to have solid contents around 50% to 70%, enabling a homogeneous, self-supporting material (CHANDLER, 1987; POHLAND & TIELENS, 1987; ROBINSKY, 1987; ROBINSKY,

1999). Otherwise, paste tailings are characterized to have solids content around 70% to 85%, which may improve materials geomechanical performance (BUSSIÈRE, 2007). Inter-layer water reduction allows inserting hydraulic binders in tailings throughout the production chain, which helps tailings bearing capacity, durability, stiffness, contaminants stabilization, etc. (BENZAAZOUA et al. 2004; CONSOLI et al. 2022). Nonetheless, water reduction also contributes to increase pumping energy and wear in pipelines and pumps (COLOMBERA & WANT, 1982; NGUYEN & BOGER, 1987, 1998).

The “dry” stacking methodology (Figure 6) is characterized to have solids over 85% (WILLS & FINCH, 2015). For Crystal et al. (2018) almost all tailings might be filtered and the adoption or not depends on the cost. Filters and thickeners insertion into the process allude to costs increase, thence, the challenging process regards handling with the desired (target) final moisture content and the achievable moisture content – tailings re-processing may severely increase production costs.

Figure 6: Tamanduá “dry” stacking facility, probably the largest dry stacking in Brazil (VALE S.A., 2019).

Dry stacking benefits are set, for instance, in affordable capital expenditures (CAPEX), and the rate of embankments increases. Otherwise, in terms of drawbacks, dry stacking may have higher costs to operation and maintenance (OPEX) when compared to conventional disposal

methods (CRYSTAL et al. 2018). Of course, these costs are highly dependent on the average haul distance, stacking methodology, re-handling of off-spec materials, etc. In addition, the fact that the dried cake is no longer able to be pumped, then demanding to be transported by trucks and conveyor belts.

Figure 7 depicts a traditional “dry” stacking cross-section where two main zones are distinguished. Firstly, and most important, the structured zone which is responsible to support the whole tailings mass. Structured zones are in general submitted to 95% or 98% standard Proctor effort compaction degrees, namely, at or slightly below optimum moisture content (CRYSTAL et al. 2018). This stacking pattern decreases materials’ liquefaction potential, because of their dilative behavior, unsaturated condition and the quality assurance and quality control (QA/QC) of tailings' physical properties. Also, well-compacted unsaturated tailings help to ensure embankments increase rate and avoid excessive deformations.

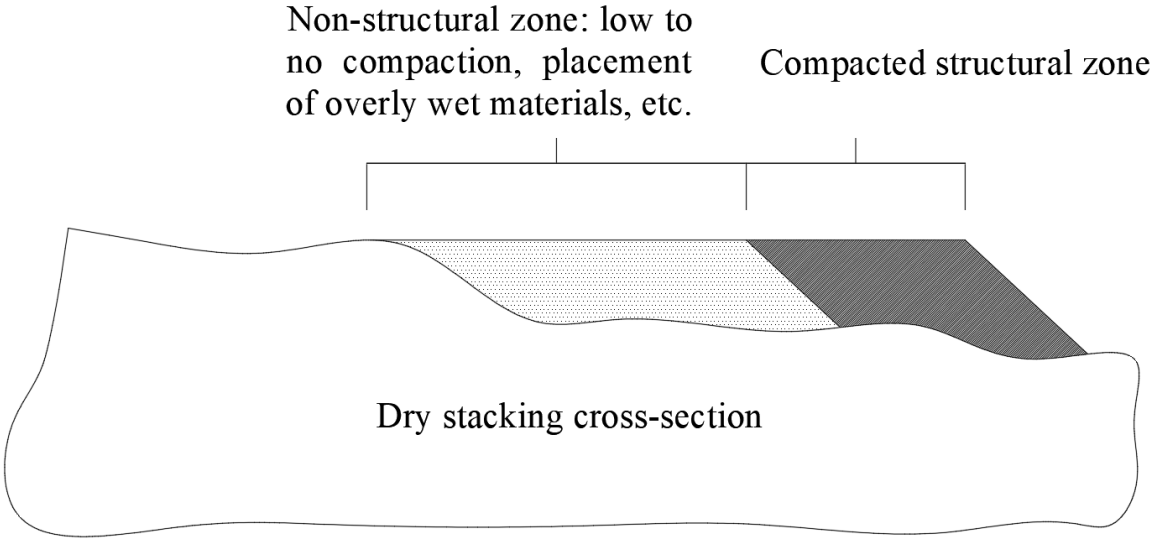

Figure 7: Conventional dry stacking cross-section (after DAVIES et al. 2011).

According to Davies & Rice (2001), the “dry” stack design is in general indicated for arid sites, which is confirmed by Table 1 and Figure 8 when comparing the annual average precipitation and evaporation of each deposition site. Figure 8 y-axis compares the difference between precipitation and evaporation in which most of the dry stack facilities lay on the orange trapezoidal form, that is, the average evaporation is higher than precipitation.

Table 1: Dry stacking facilities examples (after SLR CONSULTING, 2016).

LOCAL	RAGLAN	GREEN SCREEK	POGO	MANTOS BLANCOS	LA COPIA	EL SAUZAL	EL PEÑON	CERRO LINDO	ALAMO DORADO	TAMANDUÁ	ROSEMONT (project)	MAGINO (project)
Production rate (tpd)	2,400	800	1,250	12,000	18,000	5,300	2,600	5,000	4,000	65,000	68,000	35,000
Deposition method	Dry stack	Dry stack	Dry stack	Dry stack	Dry stack	Dry stack	Dry stack	Dry stack	Dry stack	Dry stack	Dry stack	Conventional/Densified
Reason	Hydrological management. Reactive tailings.	Seismic stability.	Location	Hydrological management. Seismic stability.	Hydrological management. Seismic stability.	Location	Hydrological management. Seismic stability.	Hydrological management. Seismic stability.	Location	-	Hydrological management.	Production rate
Distribution Method	Trucks	Trucks	Trucks	Conveyors	Conveyors	Conveyors	Trucks	Trucks	Conveyors	-	Conveyors	By pipe
Location	Canada	EUA	EUA	Chile	Chile	Mexico	Chile	Peru	Mexico	Brazil	EUA	EUA
Annual Ave. Temperature	-8°C	5°C	-3°C	16°C	Iced all year	18°C	-	-	26°C	22°C	22°C	3°C
Annual Ave. Precipitation	500	1,530	280	<50	<50	800	<50	200	800	1205	440	820
Annual Ave. Evaporation	-	510	-	>2,000	>2,000	2,400	>2,000	1,500	-	1,295	1,820	455

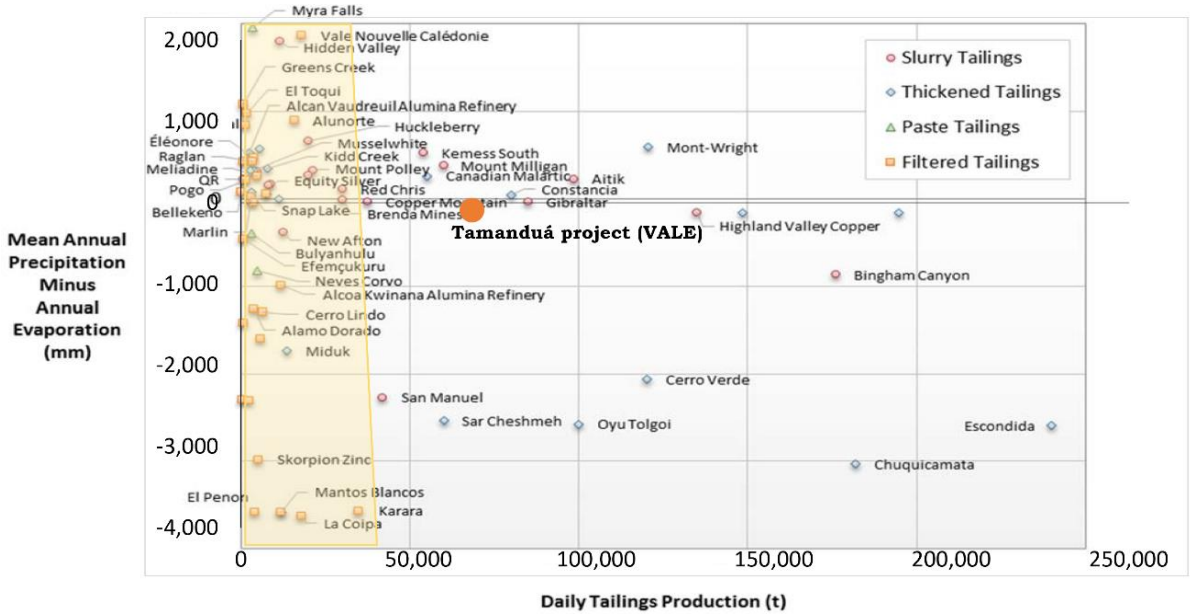

Figure 8: Dry stacking facilities around world (MEND 2017).

Arid sites are good for water management and tailings moisture control for further compaction. In addition, small water percentages assist the mixture between dried cakes and hydraulic binders (e.g., CONSOLI et al. 2022), if necessary. On the other hand, dried sites may also be responsible for other concerns like tailings' dust, which demand the use of surrounding fences, polymers, etc. Filtered dry stacks are growing throughout the world and are well established in some countries whereas remain as new alternative in others like Brazil.

Other disposal techniques (e.g., Figure 1) are underground deposition and comprise backfilling, in-pit and submarine disposals. Both backfill and in-pit designs regards to backfilling mined-out areas or pits, with the former being characterized to be mixed with hydraulic binders whereas the second is stored in its natural form. The submarine deposition regards to a de-aeration/mixing process with seawater and discharge in the seabed using gravity deposition. Sometimes submarine deposition may be an alternative to avoid Acid Rock Drainage (ARD), a natural oxidation of sulfidic minerals by air and water (WILLS & FINCH, 2015) – oxygen solubility and diffusion in water are several times lower compared to air (Davé et al. 1994).

2.1.3 Granular materials (tailings) characteristics

Tailings', hereafter also referred as granular materials, characteristics are highly variable and depend on the ore type, clay mineralogy, extraction, and beneficiation methods, etc. (VICK 1990; HU et al. 2017; CONSOLI et al. 2022). For instance, copper ore is recognized to have great extents of tough silicate particles which result in a coarse particle size. Conversely, Florida phosphate tailings are in general clay-based materials (VICK 1990). Other example is the laterite-based tailings cyclic resistance, which seems to be sensitive to the initial mean effective stress whereas cooper-gold-zinc and gold tailings do not (WIJEWICKREME et al. 2005; JAMES et al. 2011).

For instance, in the case of iron ore tailings, one of the most impacting factors on tailings physical properties and mechanical characteristics regards to iron concentration. This characteristic impacts in tailings' specific gravity, grain size distribution, plasticity, etc. According to Quaresma (2009), the Brazilian iron ore is divided into two main sources: highly concentrated and slightly lower concentration iron ores; with the latter more usual than the former. Among the existing ferrous minerals hematite, magnetite, goethite, and siderite are the most widespread (QUARESMA 2009; ESPÓSITO 2000). Hematite mineral is present in high concentrated Brazilian iron ores, with concentrations varying between 50 and 70%. Otherwise, low concentrated iron ores are locally known as itabirite and are characterized to have concentrations ranging between 40 and 50% (or lower) (QUARESMA 2009). Other authors reported similar concentrations around the world such as Hu et al. (2017), where iron ores concentration varied around of 70% in the Yuhezhay mine.

Iron mineral source and concentration will dictate, for instance, the paymineral extraction methodology. High concentrated iron ores are prone to be subjected to gravity and magnetic separation, the former due to the elevated particles specific gravity and the latter because of iron magnetic properties (VICK 1990). Otherwise, nonmagnetic lower-grade iron ores are regularly composed by unprofitable minerals such as quartz and kaolinite. These lower-grade ores may demand extra treatments to attain the desired iron concentration (e.g., froth flotation) (VICK 1990; SANTOS 2009; CARVALHO 2012).

Therefore, in case of tailings outcome from iron ores, its particles specific gravity and gradation may vary according to, firstly, the iron amount remaining in tailings paste and, secondly, the production plant extraction effectiveness.

Hematite specific gravity may reach values around of 5.25, several times higher than quartz (2.65) for instance (ESPÓSITO 2000; LOPES 2000; DUTRA 2021). Therefore, it is expected that high concentrated iron ores result in great tailings specific gravity. Vick (1990) shows some worldwide materials' specific gravities, which are presented in Table 2.

Table 2: Worldwide tailings specific gravity (After Vick 1990).

Location	Material	Tailings type	Specific gravity	Source
Quebec	Iron ore tailing	Fine	3.0-3.4	Guerra (1979)
Quebec		Coarse	3.0	Guerra (1973)
Minnesota		Fine	3.1	Klohn (1979)
Brazil		-	2.839	Brazilian mining company (private)
Brazil (present study)		Fine	3.18	-
USA (present study)	Ordinary sand	-	2.67	-

The 2.839 value depicts an iron ore tailings specific gravity exception, which might be due to ore extraction effectiveness; as less as iron minerals, more tailings specific gravity approaches to quartz specific gravity. Figure 9 summarizes the iron ore concentration influence in tailings specific gravity, where a directly proportional relation can be observed.

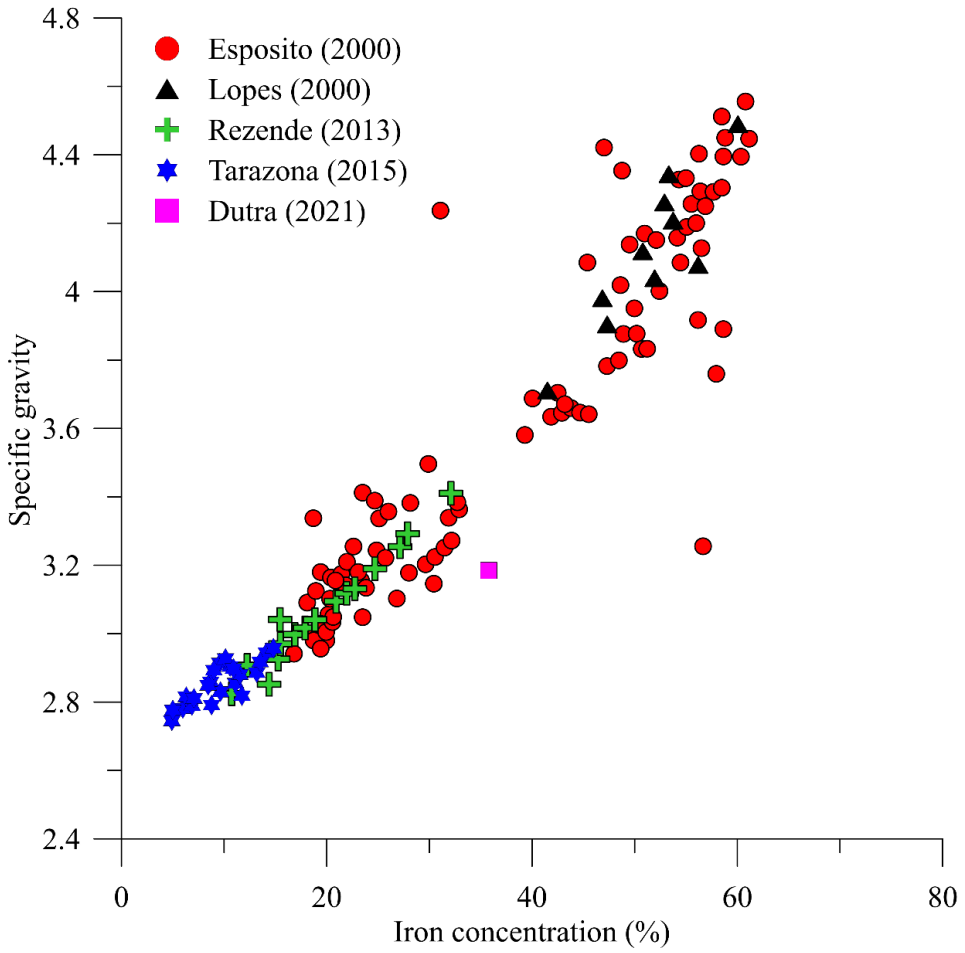

Figure 9: Iron ore concentration influence in tailings specific gravity (After DUTRA 2021).

Once iron concentration dictates the beneficiation process adoption, this indirectly affects tailings final gradation. Vick (1990) stated that the United States iron ore is massively composed by the taconite mineral, where gravity and magnetic separation are usually employed resulting in coarse, predominantly composed by sand, tailings. On the other hand, low-grade minerals demand further concentration methods likewise froth flotation. The flotation method demands very fine ore particles to achieve its greatest effectiveness.

Thence, in a single ore beneficiation plant both coarse and fine tailings gradation can exist simultaneously according to ore characteristics (VICK 1990). In general, iron ore tailings can vary in size from colloidal (below of 0.005 mm) to sand dimensions (grater then 0.075 mm) (VICK 1983; SARSBY 2013). Figure 10 compares distinct iron ore tailings gradation curves, and also includes the USA ordinary sand gradation applied in this work.

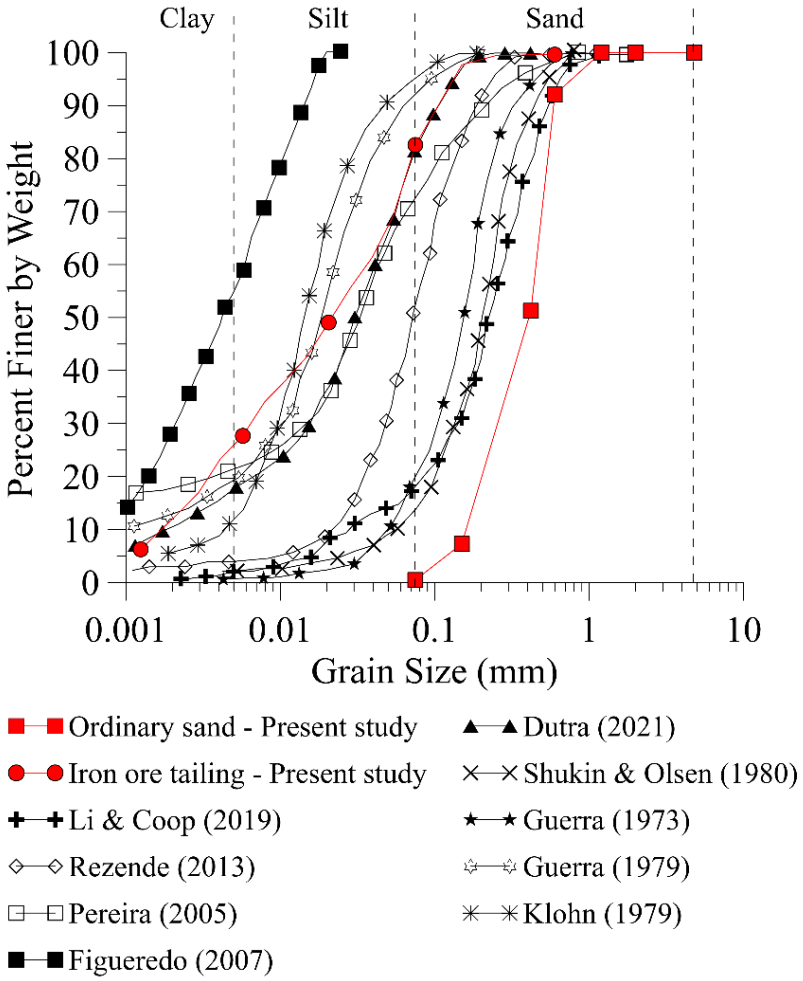

Figure 10: Gradation range of iron ore tailings.

Tailings' properties are interconnected and depend on the treatment employed for ore extraction. For example, tailings' specific gravity and gradation might be a result of iron concentration, which will dictate the beneficiation process needed for ore extraction. Once the beneficiation process affects tailings' parameters, it will also impact on tailings' deposition inside the TSF. Tailings' coarse particles are expected to deposit around the discharge point (RIBEIRO & ASSIS 1999). In agreement, ore concentration will also impact on tailings' consistency like the plasticity parameter.

Tailings' consistency is very important and may help to avoid the liquefaction phenomenon on tailings. Plastic fine matter (e.g., clay minerals fraction) is able to bring soil particles together, thus, avoiding liquefaction (DUTRA 2021). For instance, iron ore tailings are expected to be composed predominantly by iron minerals and quartz, thence, behaving like

non-plastic materials (GUERRA 1973). Fines content and particles surface activity can also affect tailings' plasticity (VICK 1990; DUTRA 2021).

Dutra (2021) states that sand and silt-size materials are prone to be liquefiable for fine contents (clay fraction) less than 5%, but that plastic fines inclusion tend to increase the liquefaction resistance. A similar conclusion is also reported by Chang et al. (1982) and Amini & Qi (2000). Nonetheless, tailings clay-size particles are in general inert, without plasticity itself (ISHIHARA et al. 1980).

On the other hand, studies also reported liquefaction even in sands with plastic or non-plastic fines (e.g., Ishihara et al. 1980; Perlea et al. 1999; Bayat & Bayat 2012). Benghalia et al. (2015) and Marto et al. (2016) studied the effect of fines inclusion on a sandy soil, where fines with plastic indexes ranging from 12 to 20% were included. Both authors reported a liquefaction resistance decrease for fines inclusion thresholds of 5% (Benghalia et al. 2015) and 22.5% (Marto et al. 2016), further inclusions resulted in liquefaction resistance increase. In summary, tailings liquefaction resistance varies according to particles' mineralogy, beneficiation process, etc., and plastic fines presence might not be able to avoid the liquefaction phenomenon.

It was naturally seen that tailings' mechanical properties are straightforward connected to the beneficiation process, which will also impact tailings' strength parameters. Ore grinding tends to result in sharp sub-angular particles (LINDOLFO 2010; ROBERTSON et al. 2019), which may affect ore internal friction angle (LAMBE & WHITMAN 1979). Particles' angularity and gradation affect the internal friction angle by two mechanisms, in terms of material void ratio and particles interlocking. Well-graded soils predominantly composed by angular particles tend to have more particles interaction, thence, better stress distribution and higher internal friction angles. On the other hand, particles' mineral type does not severely impact on internal friction angle (LAMBE & WHITMAN 1979). Based on this, Figure 11 shows some of iron ore critical state friction angles.

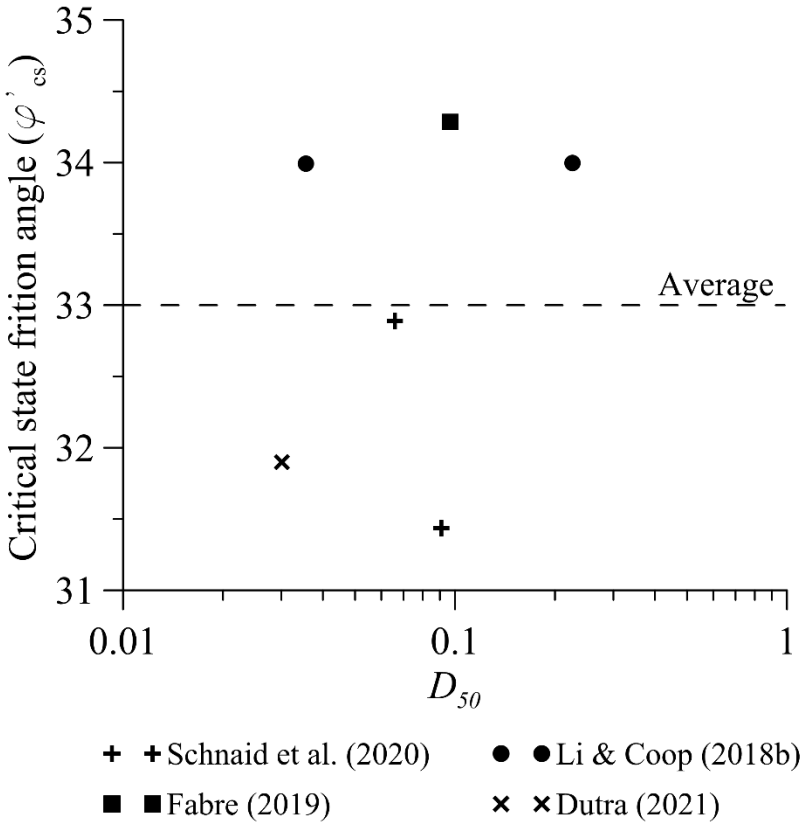

Figure 11: Usual iron ore critical state friction angles (after DUTRA 2021).

2.2 SOIL STABILIZATION

Soil, the most versatile construction material. Accordingly, soil might be thought as an alternative to build houses, embankments, roads, and several other men demands (INGLES & METCALF 1972; MITCHELL 1981). Such flexibility is leading to natural soil deposits depletion to fulfill market demand. At the same pace, despite the world population rate decrease (ONU 2019), urban centers are continuously expanding their boards. This results in new land occupation and qualified soil site extinction. Suitable soil extinction alludes to land occupation in poor soil sites, which is associated with landslides and natural catastrophes or extra expenses for soil treatment (MITCHELL 1981; BEHNOOD 2018; SILVANI et al. 2022).

On the other hand, in spite of poor soil presence or not, it is readily seen that engineering structures are continuously incrementing their loads owing to tall buildings construction (MIGUEL 2020). In addition, today's building projects demand minimal displacements in order to avoid, for example, differential settlements and ensure structure functionality.

Undesired soil properties improvement is known as Soil Stabilization and look primarily for volume stability, permeability decrease, strength, and durability increment of soil (INGLES & METCALF 1972; MITCHELL 1981; U.S Army Corps of Engineers 1984). In a general view, soil stabilization can be divided in two major methods, namely, physical and chemical soil treatments. Examples of physical treatments are soil compaction, thermal, vibrating, freezing treatments, etc. Whereas chemical stabilization is funded in soil particles chemical modification by means chemical stabilizers addition like ordinary Portland cement, lime, bitumen, polymers, lignins, etc. (INGLES & METCALF 1972). Other soil treatment alternatives have emerged throughout the last decade, which are primarily based on residues and by products (e.g., fly ash, rice husk ash, ground granulated blast-furnace slag, glass, etc.). Either the traditional ones or the alternative binders both can also be used together (e.g., ordinary Portland cement plus fly ash) as a composite or even alone (e.g., fly ash type C) (TUNCER & BASMA 1991; AÏTCIN 2000; CONSOLI et al. (2002, 2003, 2005, 2007a, 2007b, 2007c, 2009d, 2009e, 2010a, 2011b, 2012b, 2012c, 2013, 2017, 2019c, 2019d, 2020a , 2020b, 2021a, 2021b, 2022; NALBANTOGLU 2006; KANAZAWA 2015; QUIÑÓNEZ

SAMANIEGO 2015; BITTAR MARÍN 2017, SCHUERMANN FILHO 2019, 2022; SCHUERMANN FILHO et al. 2021a, 2021b, 2022; MIGUEL 2020; MIGUEL et al. 2021a, 2021b, 2021c, 2022a, 2022b; DARONCO et al. 2022; DA SILVA et al. 2022; SILVANI et al. 2022).

The ancient and widespread physical soil improvement method relays on soil compaction, which is done by either dynamic or monotonic compaction loads. Compaction aims to decrease soil voids and promote soil particles interaction (MITCHELL 1981). Nonetheless, soil compaction is sometimes insufficient in terms of soil bearing capacity and stiffness, which may demand other soil treatments like chemical stabilization. Chemical stabilization by soil admixtures is the second most widespread soil improvement technique according to Mitchell (1981). The early chief reagents are cement and lime with cement being the most common by far. Both cement and lime are applied to soil mechanical properties enhancement (INGLES & METCALF 1972).

The term ‘cement’ refers in general to any cementitious material able to produce hydraulic compounds. Nonetheless, hereafter the term cement will designate the ordinary Portland cement. Cement was firstly employed for road construction like in base and sub-base treatments and afterwards expanded to other engineering purposes. In agreement with Ingles e Metcalf (1972), cement stabilization can be extended to every soil type, with some restrictions to heavily organic soils.

2.2.1 Ordinary Portland cement soil stabilization

The ordinary Portland cement (OPC) soil stabilization consists of break up soil lumps and afterwards mix it with cement, usually by spreading on the surface, and water. At the end of blending, the soil-cement-water mixture is compacted in the usual manner (INGLES & METCALF 1972). “When the cement hydrates the soil is stabilized and will be stronger, more resistant to water, etc.” (INGLES & METCALF 1972). Namely, the cement agent creates bonds between soil particles, removes moisture excess and fills empty voids in soil skeleton (SAS & GLUCHOWSKI 2013).

As previous discussed, hydraulic cement compounds come to be developed by several insertions either in natural or artificial forms (SAXENA & LASTRICO, 1978; CLOUGH et al., 1981; CORTE, 2020; ANDREGHETTO, 2022). The ordinary Portland cement was herein chosen because of its widely application in the current engineering practice and commercial popularity around the world. Of course, it is recognized the OPC environmental drawbacks assigned to its production process. However, this study seeks to immediate engineering field solutions. Also, the fact of Brazil be an emergent country it is reasonable to use a well-settled solution, avoiding thus the new technologies acquirement. Furthermore, the existing OPC cemented materials literature background promotes a better understanding of the treatment apprised here. Other cementitious treatments can also be tested later.

2.2.2 Ordinary Portland cement main reaction

Ordinary Portland cement main reactions differ according to soil type and characteristics. For example, cementitious reactions may differ according to clay minerals type and amount. Silt-sand size particles are in general recognized to be inert, whereas clay minerals are prone to react with the stabilizing agent (VAN OLPHEN, 1963; HEINZEN & ARULANANDAN, 1977; HOLMGREN & FLANAGAN, 1977; McELROY, 1987; MIGUEL 2020). Therefore, on the contrary of silt-sand size soils, secondary reactions also take place in clay-cement mixtures (HERZOG & MITCHELL, 1963).

Clayey soils and cement reactions were assessed by Herzog & Mitchell (1963). According to the authors, clay-cement mixtures hydration results in (i) hydrolysis and (ii) cement hydration. Hydrolysis is the chemical phenomenon of molecules brakeage in the presence of water, thence, the primary main reaction regards to compounds dissolution. Once the primary reactions are set, cement hydrated products begin to develop concomitantly with environment pH increase and lime release [$Ca(OH)_2$]. The alkali environment produced is responsible to degrade clay particles. This process is in charge to release amorphous silica and alumina. Free silica and alumina will afterwards combine with calcium, provided from lime, and result in secondary cementitious compounds (LAMBE, MICHAELS & MOH, 1960); HERZOG & MITCHELL, 1963). In this sense, it is expected that amorphous materials are far more inclined to be degraded when compared to crystalline ones (ANDREGHETTO, 2022). On

the other hand, inert silt-sandy soils hardening occurs in general solely due to the hydration of cement phase (HERZOG & MITCHELL, 1963).

Either in clayey or sand-silt soils the free lime is not completely consumed throughout the entire process and enables further reactions. These further reactions are the basis for high strength cements production, likewise the Brazilian ordinary Portland cement Type V (equivalent to Type III – ASTM C150/C150M-21), where extra silica sources (e.g., fly-ash, rice husk ash, etc.) are inserted to react with the free lime.

In accordance with Harrisson (2019), the OPC-water basic reactions are (i) the dissolution of cement clinker and other non-inert components, and (ii) precipitation and reprecipitation of cementitious compounds. These reaction are responsible to be producing Calcium Silicate Hydrate (C-S-H), Calcium Hydroxide [$Ca(OH)_2$] and AFm(AFt).

The C-S-H product is a result of C_3S (Alite) or C_2S (Belite) reaction with water, which is known to be a gel, without a well-defined structure and difficult to be detected in X-ray diffraction tests (HARRISSON, 2019). Accordingly, compounds notation is designated as C = CaO, A = Al_2O_3, S= SiO_2, H = H_2O, $\overline{S}$ = SO_3, where Alite and Belite are represented as Ca_3SiO_5 and Ca_2SiO_4, respectively. The C-S-H gel does not have a well-defined arrangement, with calcium oxides being in general twice as much as the silicon dioxide which justifies the acronym C-S-H (HARRISSON, 2019). Nonetheless, the final products main composition is affected by the setting precursors, which is described in (Eq. 1 and (Eq. 3 for instance.

$$Ca_2SiO_4 + H_2O > CaO - SiO_2 - H_2O \quad \text{(Eq. 1)}$$

$$Ca_2SiO_4 + H_2O > C - S - H \quad \text{(Eq. 2)}$$

Belite hydration (expressed in (Eq. 1 and (Eq. 2) results predominately in calcium silicate hydrate compounds. Otherwise, Alite hydration results in extra calcium oxide and C-S-H (expressed in (Eq. 3 and (Eq. 4). The extra calcium oxide is susceptible to react with water and produce extra calcium hydroxides (HARRISSON, 2019).

$$Ca_3SiO_5 + H_2O > CaO - SiO_2 - H_2O + Ca(OH)_2 \quad \text{(Eq. 3)}$$

$$Ca_2SiO_4 + H_2O > C - S - H + CH \quad \text{(Eq. 4)}$$

Free lime can also be provided from both Alite hydration and in some extent from cement clinker (HARRISSON 2019), which represents another source of calcium hydroxides when in contact with water (Eqs. 5 and 6). These extra calcium hydroxides are prone to react with free silica and alumina, otherwise, it will turn to discrete crystals throughout the time (HARRISSON, 2019).

$$CaO + H_2O > Ca(OH)_2 \quad \text{(Eq. 5)}$$

$$C + H > CH \quad \text{(Eq. 6)}$$

The C_3S reaction, apprised in (Eq. 3 and (Eq. 4, is characterized to be set quickly hindering the paste workability. In addition, this process is unreversed, and it is sometimes responsible to cause problems at the construction site. Sulfate inclusion into the system helps to delay cement setting time. In the cement industry the sulfate source comes from calcium sulfate addition into OPC powder (HARRISSON 2019). Gypsum and anhydrite are the most common sulfate sources, which shifts the clinker hydration reaction for following:

$$Ca_3A + 3C\bar{S} + H_2 + 26H > C_6A\bar{S}3H_{32} \quad \text{(Eq. 7)}$$

The rightward compound is known by ettringite, and it is characterized to be needlelike crystals and responsible to coat the Alite surface delaying the concrete setting time (HARRISSON, 2019). The AFm(AFt) product previous stated regards to ettringite crystals, where A = Al_2O_3, F = Fe_2O_3 and t = three moles of calcium sulfate (HARRISSON, 2019). Ettringite formation happens until C_3A, water and sulfates availability occur. Once sulfates run out, ettringite formation may cease and starts to be dissolved. Ettringite dissolution shifts this mineral to one mole calcium sulfate compounds like AFm (m = single mole). Either AFt or AFm compounds can cause adverse reaction to cement paste, once both of them are volume expansive minerals. Miguel (2020) and Consoli et al. (2021a, b) assessed the damage caused by the sulfate presence in sulfated soils treated with calcium-based stabilizers. Sulfate adverse reactions can be minimized by calcium carbonate inclusion into cement powder, where the remaining C_3A seeks to interact with $CaCO_3$ and thus producing monocarbonate instead of ettringite (HARRISSON, 2019).

2.2.3 Parameters controlling soil-cement mixtures

2.2.3.1 Cement content effect

Cement can broadly affect soil properties even in small percentages (e.g., cement contents below 2% by soil dry mass) or when soil treatment occur with high inclusions (e.g., greater than 5% by soil dry mass) (PCA 1995). The U.S. Army Corps of Engineers (1984) termed soil-cement low percentages as ‘modified soil’, whereas soil-cement high percentages as ‘stabilized soil’. In fact, these terms are not a consensus and vary according to authors, even though the term stabilized soil is broadly used in engineering.

Despite of the term, small cement contents are responsible to modify soil properties like plastic index, permeability and granulometry. In case of clayey soils, cement inclusion results in ion exchange and thereafter the Diffuse Double Layer (DDL) reduction (flocculation). Once particles are flocculated, it is expected a soil plastic index decrease and permeability increase; Soil particle dimensions are expected to increase as well (INGLES & METCALF 1972).

Soil-high cement contents, also termed as “lean” or “rolled” concrete (U.S. ARMY CORPS OF ENGINEERS 1984), tend to behave a concrete-like material and aim to attain substantial strengths and stiffness gain. Of course, high strengths and stiff materials are not synonyms of great performance. Consoli et al. (2021b) demonstrated that stiff soil samples exhibited poor behavior when subjected to fatigue life tests.

Despite of cement content itself, soil-cement dosages were scarce in the earlies of 2000s and became widespread with works like Foppa (2005) and Consoli et al. (2007c). Most of the existing dosages were based on laboratory tests trial and error, with cement content adoption accordingly with the desired soil property (U.S. ARMY CORPS OF ENGINEERS 1984). For instance, the EM 1110-3-137 Engineer Manual of U.S. Army Corp of Engineers (1984) suggests for soil swelling treatment, mold several soil samples with different cement contents; the dosage will be that yields the desired swelling magnitude.

Among the traditional tests carried out to assess soil-cement stabilizations, the unconfined compressive strength (UCS) became widely employed due to its convenience. Strength, durability, and permeability are some samples' characteristics that can be directly or indirectly assessed by the UCS tests, turning it the first test to be carried out for stabilized samples' evaluation. For instance, Consoli et al. (2007c) carried out several UCS tests to assess cement content effect on a sandy soil, the UCS test results are depicted in Figure 12.

Figure 12 apprises UCS test results of four soil-cement dosages, where both cement content and dry unit weights are varied throughout the experimental program. From Figure 12, it is readily seen the linear trend exhibited by cement addition, which means that soil-cement unconfined strength is directly proportional to cement inclusion. Another relevant aspect from Figure 12 is the cement higher effectiveness for heavily compacted soil blends, namely, increasing blends dry unit weight seem to result in great strength gain rates.

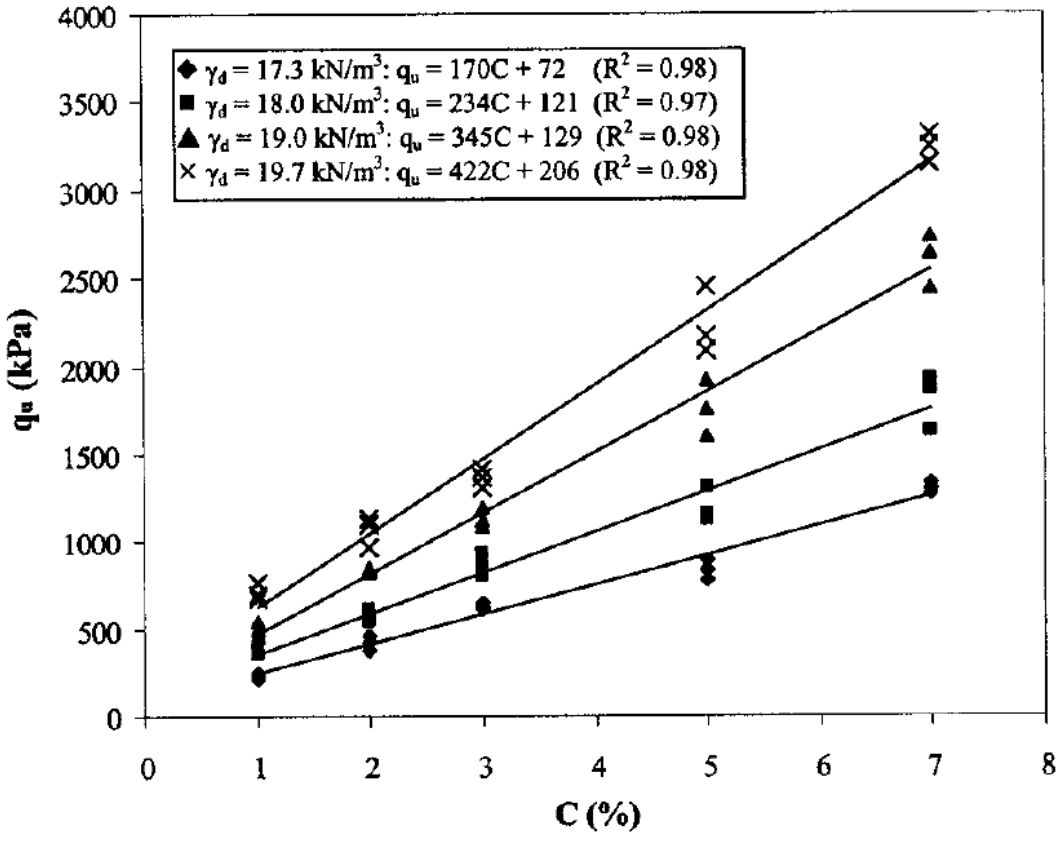

Figure 12: Cement content effect on soil-cement stabilization (CONSOLI et al. 2007c).

2.2.3.2 Effect of blends' porosity

The previous topic introduced blends' compaction impact on cement effectiveness, the present matter will further discuss it. Soil properties likewise unconfined compressive strength, hydraulic conductivity and volumetric strain are closely related to soils' compaction degree. Focusing first on untreated soil samples, soil porosity or in other words soil void ratio plays an important role in terms of soil behavior, which was well discussed in terms of soil over-consolidation ratio (OCR) to clayey soils and the state parameter to sandy soils (BEEN & JEFFERIES 1985).

Basically, void ratio decrease promotes soil grains interaction, thence, it leads to frictional resistance development. In addition to soil grains interaction increase, the inexistence (or partial) of voids turns soil prone to dilation. Soil dilation means to attain higher peak strengths in terms of drained conditions, or negative pore water pressure generation in terms of undrained conditions. This is evidenced in Figure 13, which highlights the porosity (voids) impact on soil samples unconfined compressive strength. Figure 13 shows UCS increase accordingly to porosity (voids) decrease; this trend extends to untreated soils, lime treated soils and cement treated soils (e.g., Consoli et al. 2006, 2007c, 2009b).

In terms of treated soils, Hausmann (1990), Baghdadi et al. (1995) and Nalbantoglu (2006) mention the influence of binder inclusion on soil compaction characteristics. Fine grained particles, like cement particles, are avid for water and tend to increase mixture optimum moisture content. At the same time, binder inclusion is inclined to turn Proctor test compaction curves flat, it depicts soil-binder blends less susceptibility to moisture change. Less susceptibility to moisture change turns the soil mixture less susceptible to volume change as well. Finally, binder inclusion promotes particles flocculation thus soil gradation increase which may difficult site soil compaction.

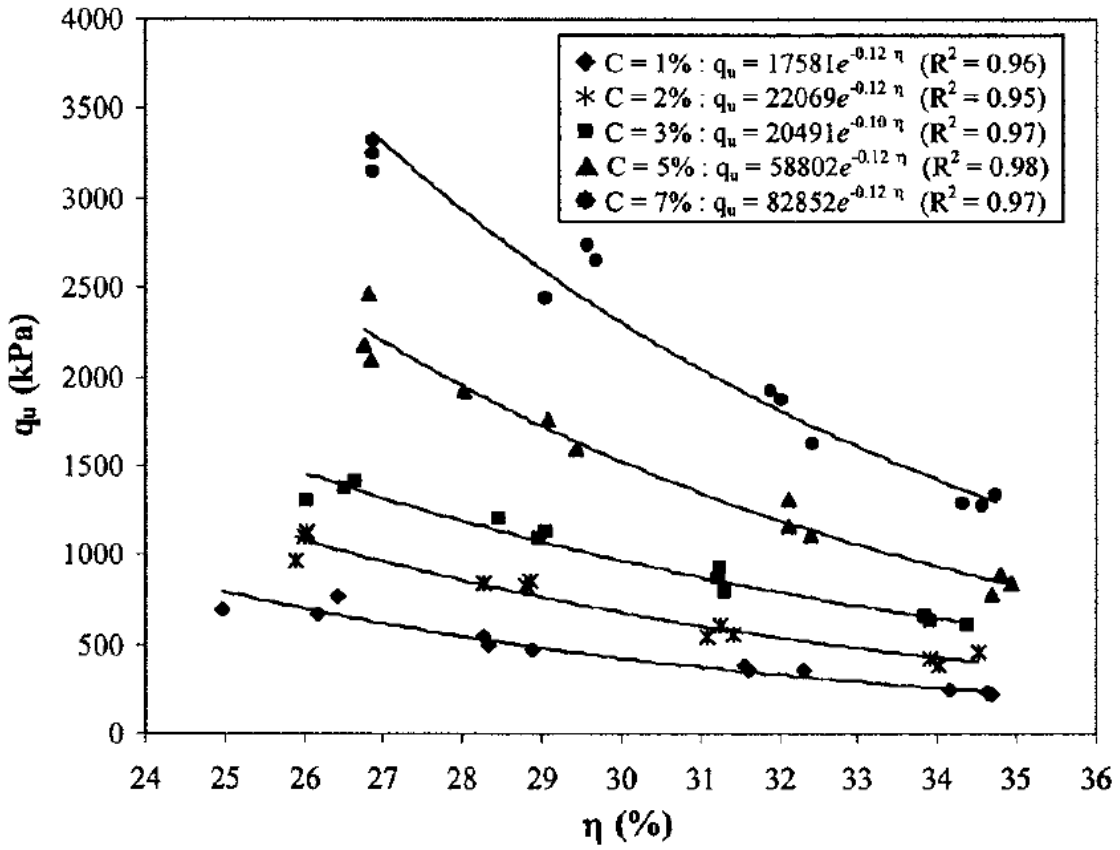

Figure 13: Effect of blends' porosity in unconfined compressive strength (after CONSOLI et al. 2007c).

2.2.3.3 Moisture content effect

Water in soil-cement mixtures perform two actions: (i) water lubricate soil particles helping them to get closer one another, it helps to achieve higher soil densities; and (ii) water promotes environment hydration, which is responsible to produce cementitious compounds and increase soil mechanical properties (PCA 1995). Ingles & Metcalf (1972) and Austroads (2019) do not mention water quality requirements, and solely suggest the use of potable water. Nonetheless, water containing salts like sulphates or chlorides must be avoided. Such compounds might be responsible to be producing ettringite and efflorescence problems (MITCHELL & DERMATAS 1992; DERMATAS 1995; MIGUEL 2020; CONSOLI et al. 2020a, 2020b, 2021a, 2021b).

Consoli et al. (2007c) assessed the moisture effect in terms of molding moisture content by means several UCS tests. UCS test results increased up to a threshold molding moisture

content, after that the UCS decreased. The molding moisture content threshold for the highest UCS test result was almost identical to the optimum moisture content determined by the Proctor test. Therefore, molding moisture influence might be restricted to particles interlocking increase and not necessarily responsible to promote higher cementation degree. Nonetheless, it is important to highlight that Consoli et al. (2007c) soil samples had only 5% of clay fraction, which may impact in such conclusions.

Mateos (1961) found that fine soils may demand higher molding moisture contents than coarse soils, with the former achieving higher UCS test results with moisture content increase. Similarly, Sas & Gluchowski (2013) reported cement inclusion impact on the soils' optimum moisture content. According to the authors cement fines inclusion have a directly proportional relation with the soils' optimum moisture content.

In consonancy with Consoli et al. (2007c), Austroads (2019) states the following "the quantity of water added to a cement-stabilized mixture is determined by the requirements of maximum density. Curing water may be needed to keep […] moist while hydration takes place".

2.2.3.4 Curing time effect

Rong-Rong & Dong-dong (2020) studied the curing time effect on mechanic properties of cement-stabilized silty clay by means UCS tests. The peak strength increased with time, whereas the strain to the peak decreased. This trend influenced on specimens' failure mode, which changed from plastic to brittle failures. In addition, it was noticed that the strength gain occurred mostly in the first curing day, which represented around of 45% of the entire strength achieved (at the 28^{th} day); other 27% of strength gain occurred in the next two days (at the 29^{th} and 30^{th} days), further strength gains were marginal.

Xiao & Lee (2008) studied the curing time effect (7 to 180 days) on cement treated marine clay behavior through UCS and triaxial tests. Xiao & Lee (2008) UCS test results are in line with Rong-Rong & Dong-dong (2020). Regarding to triaxial tests results, cured under stress samples' stress-strain behaviors were dependent of consolidation stress magnitude and cement content. Specimens consolidated to stresses lower than the curing stress exhibited

peak strength increase with curing time. On the other hand, specimens consolidated to stresses higher than the curing stress demonstrated to be affected by the consolidation stress magnitude and cement content. This trend is draw due to treated soils bonds breakage when the curing stress was overcome. After that, the mean effective stress is more relevant than the cement content itself (DARONCO 2022). Also, high cement contents are inclined to modify soil gradation, fine grained soils tend to shift to lower extent coarse grained soils which will impact on soil mechanical behavior as well.

Summing up, the curing time effect may vary according to the loading condition (e.g., soil samples cured under stress, consolidation pressure, stress path, etc.), however, in a general view, it is expected that the peak strength increases with time being more prominent at the beginning of cement hydration.

2.3 THE TRUE TRIAXIAL

Conventional or standard triaxial apparatus is probably the most employed equipment for soil mechanics understanding in terms of laboratory testing. Nonetheless, the term triaxial might sometimes lead to ambiguous understanding, once the conventional triaxial apparatus has only two degrees of freedom and thus an axisymmetric stress state condition (SADEK, 2006; CORTE, 2020); this is due because of the intermediate principal stress (σ_2) equivalence to either the major (σ_1) or minor (σ_3) principal stresses. Lambe & Whitman (1979) in the earlies of 60s highlighted the necessities of three-dimensional failure laws, and at the same time the demand of versatile devices to assist different loading conditions.

Robust testing devices were then projected to soil behavior better understanding. Test devices like the Direct Simple Shear (DSS), True Triaxial (TT) and Hollow Cylinder (HC) apparatus were developed (ANDREGHETTO 2022). Such devices are able to reproduce distinct field loading conditions, which comprises the intermediate principal stress variation/control. In the DSS device, for instance, the intermediate principal stress can rotate throughout the test. Whereas the TT device allows the intermediate principal stress control; the latter varying according to the intermediate principal stress *b* parameter. Finally, the HC apparatus,

probably the most robust geotechnical equipment, allows the principal stresses magnitude and directions (rotation) control.

Thence, a real three independent axis device with six degrees of freedom is known by True Triaxial (KO & SCOTT 1967; AIREY & WOOD 1988; LADE & DUNCAN 1973; LADE 2016; CORTE 2020; ANDREGHETTO 2022).

The true triaxial apparatus has in general a cubical design, where cubical soil specimens are set and tested through a wide range of stress or strain possibilities; *viz*. this equipment can be either a principal stress or strain-controlled equipment (WILLIAMS, 2004). The principal stresses are conventionally known as σ_1, σ_2 and σ_3. Where σ_1 refers to the major principal stress, σ_3 is the minor principal stress, and σ_2 is the intermediate principal stress. Likewise, this extends to the principal strains known as ε_1, ε_2 and ε_3.

Thereby, the true triaxial device allows to study soil by means a three-dimensional approach, where the intermediate principal stress can assume values equal to the major and minor principal stresses or even values between them. For this reason, the true triaxial equipment is broadly applied to study the intermediate principal stress influence on soil behavior and soil anisotropy comprehension. Therefore, the true triaxial test stills nowadays as one of the most reliable tool for soil behavior understanding.

Figure 14 depicts the 'principal stress space' through a Cartesian coordinate system, where the vertical z-axis agrees with the axis of material symmetry. In accordance, the σ_x, σ_y, σ_z, stresses can also be expressed in terms of σ_1, σ_2, σ_3, the principal stresses. Table 3 summarizes the loading condition for both notations. Thence, in Figure 14 and in true triaxial tests, the principal stresses are able to be represented by x, y and z axis.

Figure 14 states several concepts like the hydrostatic axis which is the line where all the principal stresses are identical ($\sigma_1 = \sigma_2 = \sigma_3$). The deviatoric plane or octahedral plane[1], the π plane, where the distortional stress magnitude is given by the distance between the

[1] See Andreghetto (2022) for 'octahedral plane' detailed definition.

hydrostatic axis and the current principal stresses states. The distortional stress is responsible to materials' change of shape, thence, plastic strains (WOOD, 1991).

Also, Figure 14 depicts the intermediate stress parameter *b* firstly introduced by Habib (1953), which is determined according to (Eq. 8.

$$b = \frac{\sigma_2 - \sigma_3}{\sigma_1 - \sigma_3} \qquad \text{(Eq. 8)}$$

The *b* parameter assumes, in general, the following values: (i) zero when ($\sigma_2 = \sigma_3$), which alludes to a conventional triaxial compression stress path; (ii) one when ($\sigma_2 = \sigma_1$), stress path which is equivalent to a laterally loaded sample in the conventional triaxial test. For these reasons true triaxial *b* values equal to zero and one are known by compression and extension tests respectively. When σ_2 differs from σ_1 and σ_3, namely, values between them, the *b* parameter assumes values among zero and the unity (Lade & Duncan, 1975). The *b* value of 0.5 sounds like a simple shear test state condition, where the intermediate principal stress (σ_2) remain immutable throughout the test whereas σ_1 and σ_3 vary in order to attain, in this case, a plane stress condition. Table 3 describe the stress paths according to the parameter *b* adopted.

And finally, Figure 14 also introduces the loading θ angle concept. The loading θ angle hereafter used to describe the true triaxial loading condition, derives from the Lode angle (θ_L) firstly introduced by the scientist Walter Lode (ANDREGHETTO, 2022). By definition, the θ_L angle interval is $0 \leq \theta_L \leq \pi/3$, *i.e.* it ranges from 0° to 60°, where θ_L is assumed to be referenced by the minor principal stress (σ_3) (ANDREGHETTO, 2022; DANAS & CASTAÑEDA, 2012). Nonetheless, once the θ_L interval is from 0° to 60°, it would be necessary to divide the octahedral stress plane into three stress sectors to differentiate sample stress states; each sector with the range of 0° to 60°.

In order to avoid the octahedral stress plane division, the true triaxial stress path loading condition can be expressed in terms of the loading θ angle instead of the Lode angle (θ_L). The loading θ angle is alternatively referenced by the z-axis of specimen and ranges between 0° and 180°. Figure 14 and Table 3 apprise the loading θ angle values. The loading θ angle

can be coupled to the intermediate stress parameter *b*, where the *b* parameter assumes a value of 0 for θ = 0° and 120° and equal to 1 when θ = 60° and 180°.

Alternatively, Figure 15 expresses the octahedral plane in terms of vectors of stresses. Figure 15 restates which was apprised in Figure 14, however, in terms of stress vectors to assist the reader comprehension. In this case, the vector $\overrightarrow{OP}$ describes an arbitrary stress state represented by the stress point P. The same stress state can also be described by the sum of $\overrightarrow{OO'}$ and $\overrightarrow{O'P}$ vectors projected on both the hydrostatic axis and deviatoric stress plane, respectively (SILVANI et al. 2022). The distortional stress magnitude describes in the previous paragraph, here depicted by the $\overrightarrow{O'P}$ vector, is also known as the octahedral or deviatoric shear stress (τ_{oct}).

True triaxial further details such as equipment aspects, main variables, test procedures and response variables can also be accessed through section 3.3.5.

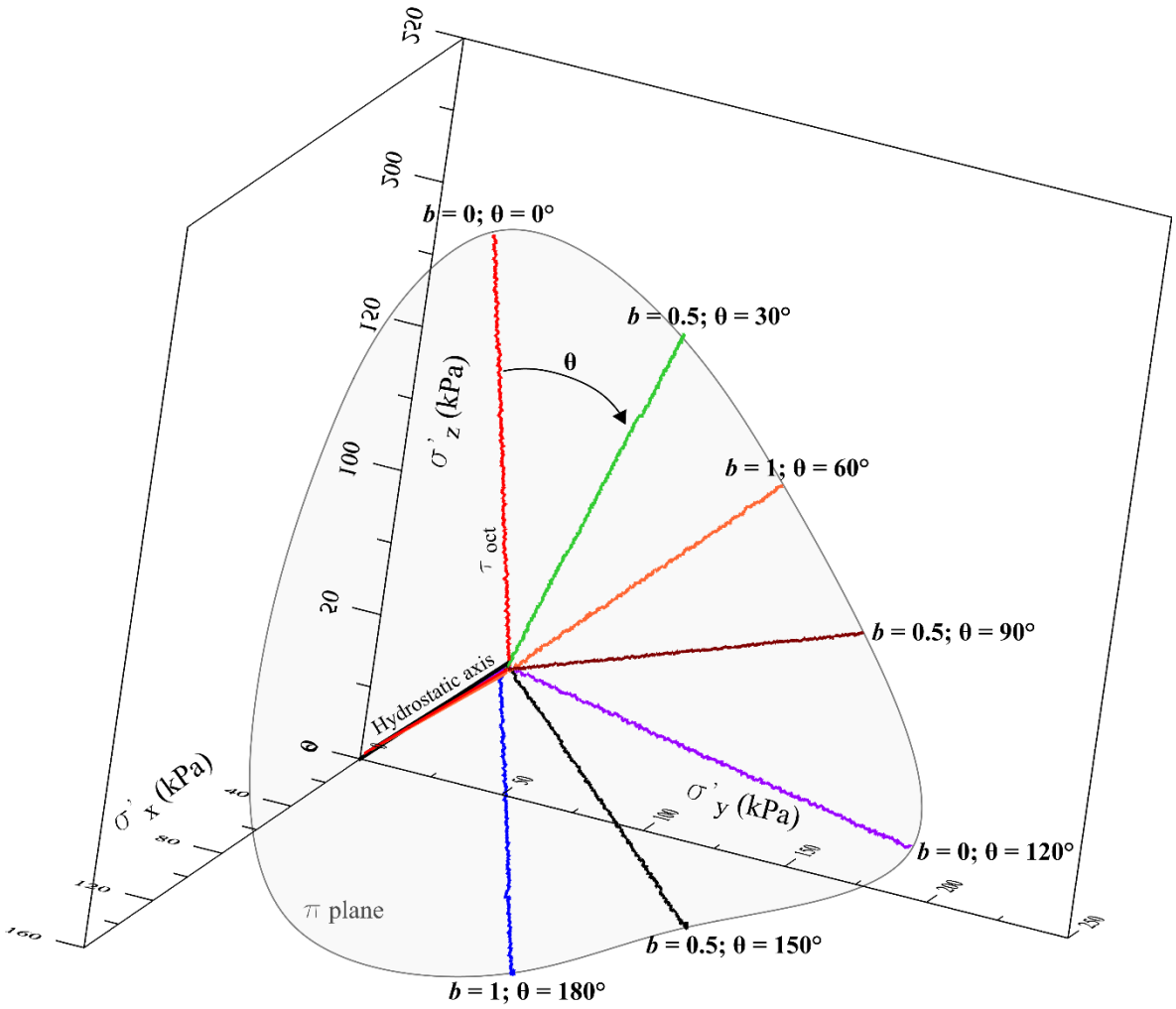

Figure 14: Representation of the stress states in a three-dimensional principal stress space, including the hydrostatic axis, the intermediate principal stress *b* parameter, the deviatoric plane or π plane and, the loading θ angle.

Table 3: The true triaxial main loading conditions.

θ (°)	*b*	X pressure	Y pressure	Z pressure	Principal stresses equivalence
0	0	Decreases	Decreases	Increases	$\sigma_1 = \sigma_Z$; $\sigma_2 = \sigma_3 = \sigma_X = \sigma_Y$
30	0.5	Decreases	Stands	Increases	$\sigma_1 = \sigma_Z$; $\sigma_2 = \sigma_Y$; $\sigma_3 = \sigma_X$
60	1	Decreases	Increases	Increases	$\sigma_1 = \sigma_2 = \sigma_Y = \sigma_Z$; $\sigma_3 = \sigma_X$
90	0.5	Decreases	Increases	Stands	$\sigma_1 = \sigma_Y$; $\sigma_2 = \sigma_Z$; $\sigma_3 = \sigma_X$
120	0	Decreases	Increases	Decreases	$\sigma_1 = \sigma_Y$; $\sigma_2 = \sigma_3 = \sigma_X = \sigma_Z$
150	0.5	Stands	Increases	Decreases	$\sigma_1 = \sigma_Y$; $\sigma_2 = \sigma_X$; $\sigma_3 = \sigma_Z$
180	1	Increases	Increases	Decreases	$\sigma_1 = \sigma_2 = \sigma_X = \sigma_Y$; $\sigma_3 = \sigma_Z$

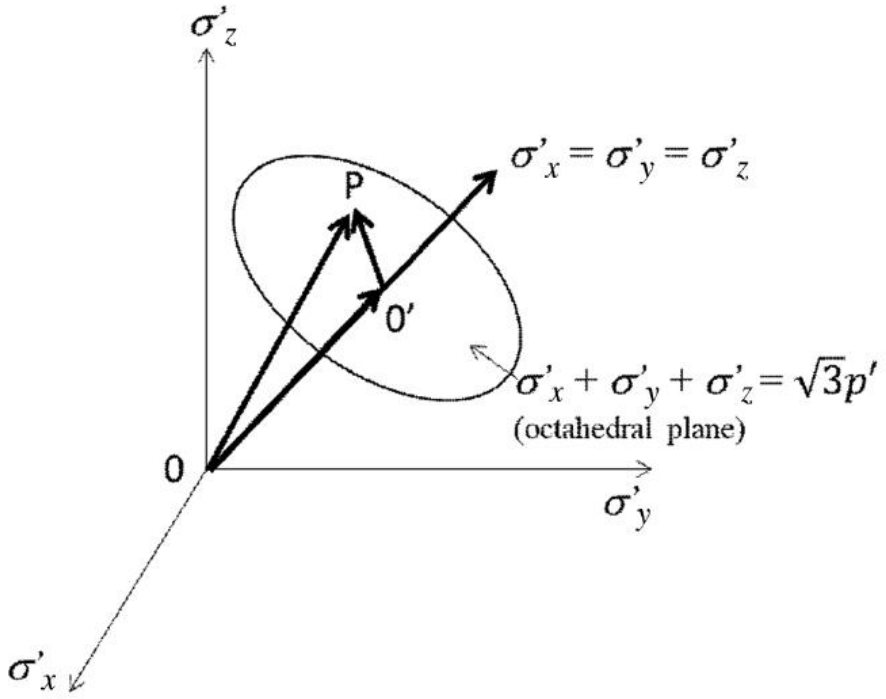

Figure 15: Representation of the stress states in a three-dimensional principal stress space, a vectorial approach (after SILVANI et al. 2022).

2.3.1 The existing True Triaxial apparatus

According to Sadek (2006) the first true triaxial apparatus was developed by Kjellman (1936), which was further split into three different categories: (i) rigid boundary equipment (Hambly, 1969; Wood, 1974; Airey & Wood, 1988); (ii) flexible boundary equipment (Ko & Scott, 1967; Sture & Desai, 1979); and (iii) a mix of rigid and flexible boundaries (Green, 1971; Lade & Duncan, 1973).

Pearce (1970, 1971) describes a rigid boundary true triaxial where the soil specimen is enclosed by a thin membrane and thereafter surrounded by six rigid platens, one for each cubical specimen's face (LADE & DUNCAN, 1973). The six rigid platens superimpose one another in a manner to avoid edges conflict, Sadek (2006) depicts the rigid platens arrangement. Rigid boundaries true triaxial equipment are in general strain-controlled equipment, in this case the induced loads are response variables. The rigid boundary strain-

controlled benefit relays on capturing the post-peak failure condition by the data logger systems. Scenery unlikely to occur in stress-controlled flexible boundary equipment.

Lade & Duncan (1973) states that some of this rigid boundary equipment are able to attain strains up to 30%, which enables to approach soil critical state condition. Rigid boundary equipment cons settle on equipment complex structure, higher expenses when compared to other models, and the excessive shear stress prone to be developed between the specimen's faces and the rigid platens (LADE & DUNCAN 1973; MOGI 1981); lubricants are sometimes applied to reduce the specimen/platen friction, however, setting up the possibility to radial stresses development (e.g., Sakurai & Serata, 1967; Niwa et al. 1967; Bieniawski, 1971).

The flexible boundary equipment emerges as option to the rigid ones. A flexible boundary equipment with six degrees of freedom, where cubical are able to be loaded by six flexible membranes, was developed by Ko & Scott (1967). Each of the six membranes are able to be individually controlled/pressurized or, alternatively, x-x, y-y and z-z faces might be connected one another. The Ko e Scott (1967) equipment has the advantage of does not develop shear stress at the specimen's edge. Nevertheless, Green (1971), Arthur & Menzies (1968) and Bell (1968) raise up two aspects that may lead to data misunderstanding: (i) the friction developed between flexible membrane and equipment frame; and (ii) flexible membrane edges interferences. Both drawbacks may cause strength overestimated.

A flexible boundary equipment is also found at the University of Bristol, where six flexible boundaries are composed by top-hat-shaped rubber membranes (cushions); Sadek (2006), Corte (2020) and Silvani et al. (2022) carried tests on it. Despite of the six degrees of freedom possibility, Silvani et al. (2022) noticed samples' rotation when the six rubber membranes were attached. Samples' rotation throughout the tests may lead to results misunderstanding. Samples' rotations are minimized by replacing some of the flexible boundaries by rigid platens, which results in a mixed boundary condition.

The true triaxial third design regards to a mix between flexible and rigid boundaries, namely, pairs of axis composed by both rigid and flexible conditions. Following the previous patterns, the mixed apparatus comprises flexible boundaries in three of the six faces, whereas in its

opposite side/face a rigid platen is clamped. Despite of this design avoid undesired specimens' motion; such design may cause asymmetry loading condition, which may limit the stress space exploration (SADEK 2006). Furthermore, mixed designs may induce specimens' failure in certain preferential failure planes that is the case where the flexible faces were installed (SADEK 2006).

All of the previous designs have pros and cons. In this study two designs were employed, namely, a stress-controlled mixed boundary true triaxial and a stress-controlled rigid boundary true triaxial. The former is held at the Federal University of Rio Grande do Sul (Brazil) whereas the latter at the Colorado School of Mines (USA). The Federal University of Rio Grande do Sul true triaxial equipment is based on the University of Bristol true triaxial, and it is a mix of Ko & Scott (1967) and Lade & Duncan (1973) concepts. The Colorado School of Mines true triaxial equipment has six rigid faces and resembles the Pearce (1970, 1971) design. Both equipment are detailed in section 3.3.5.

2.3.2 The intermediate principal stress influence

Soil, brittle rocks, among other materials are markedly influenced by the current stress state. Conventional triaxial compression tests, for instance, assume the equivalence between minor and intermediate principal stresses. Based on this assumption and the fact that failure planes may lay on the intermediate principal stress direction, it is reasonable to adopt the Mohr-Coulomb failure criteria for soil modelling. According to this failure criterion, the intermediate principal stress does not influence on materials' strength nor in the normal or shear stresses acting on the failure plane (MOGI, 1981; AL-AJMI & ZIMMERMAN, 2005).

However, several authors have demonstrated the intermediate principal stress influence on soil and rock geomechanical properties. Murrell (1965), Handin et al. (1967) and Mogi (1967) assessed the intermediate principal stress influence of some rocks, where test results outcome substantial differences between compression ($\sigma_1 > \sigma_2 = \sigma_3$) and extension ($\sigma_1 = \sigma_2 > \sigma_3$) test conditions. Precisely, it was reported a major principal stress increase when the intermediate principal stress was increased as well (Figure 16); Figure 16 depicts the relation between minor (x-axis) and major (y-axis) principal stresses, where solid-square/rounded

symbols regard to the extension condition (*i.e.*, $b = 1$) whereas open-rounded symbols to the compression condition (*i.e.*, $b = 0$) (MOGI, 1981).

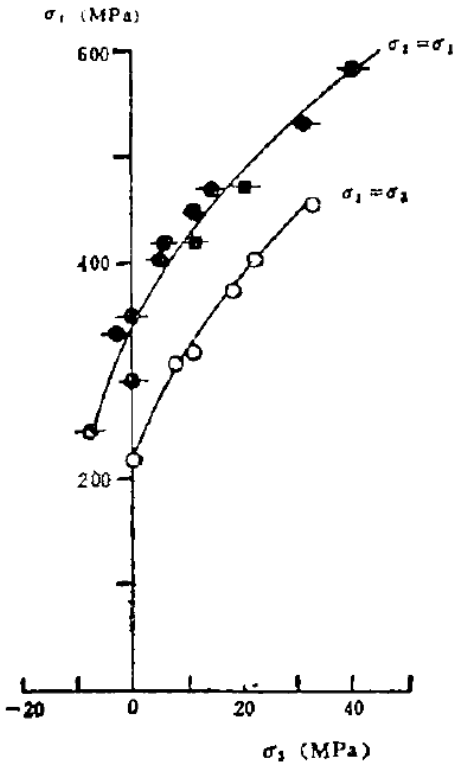

Figure 16: The intermediate principal stress influence on rock strengths according to Mogi (1967) (after MOGI, 1967).

From Figure 16, it is feasible to observe the intermediate principal stress influence for Dunham dolomite samples. Nevertheless, the intermediate principal stress impact is much lower than the minor principal stress. Further intermediate principal stress influences were reported by Mogi (1981). Intermediate principal stress seems to impact on the angle of failure plane occurrence, where fault plane angle decreased with σ_2 increase. Also, specimens' ductility appeared to be a function of both σ_2 and σ_3, where this mechanical parameter increased with σ_3 increase but decreased with σ_2 increase. Specimens under high intermediate principal stress values experienced anisotropic dilatancy.

The intermediate principal stress influence was also studied by means the stress parameter *b*. In this scenario, Ko & Scott (1967) carried out true triaxial tests on a medium dense and medium loose state Ottawa sand. The internal friction angle increased from a *b* value equal

to zero (*i.e.*, $\sigma_2 = \sigma_3$) up to a maximum, and then slightly decreased when the *b* parameter reaches a value of one (*i.e.*, $\sigma_2 = \sigma_1$) (KO & SCOTT, 1968).

Lade & Duncan (1973) stated that the strength of Monterrey No. 0 sand increased by increasing the stress parameter *b* up to a value around of 0.75 to 0.90, and then slight decreased when *b* approached a value of one. In addition, the authors also reported that the strain-to-failure was great to $b = 0$ tests, and that brittle failures were observed for large *b* values (which is in line with Mogi, 1981). Concerning to the specimens' volumetric change, the dilation rate increased with increasing the stress parameter *b* value. Furthermore, the authors believed that the studied sand was not influenced by the deposition method, with specimens approaching almost to an isotropic body. This was inferred owing to the major and intermediate principal strains equivalence during extension tests ($b = 1$), even though the major principal stress (σ_1) being applied on the specimen's deposition direction. Lastly, Lade & Duncan (1973) declare the following, "as the magnitude of *b* increases, the friction angle increases to a maximum before decreasing slightly close to the extension condition". Similar conclusions were addressed by Rodriguez & Lade (2013).

The previous conclusions must be carefully evaluated. It is worth mentioning that the Mogi (1967, 1981), Ko & Scott (1967) and Lade & Duncan (1973) experimental true triaxial tests were conducted on a σ_3 = constant stress condition. A minor principal stress constant condition produces distinct mean effective stresses (p') at failure, to the whole of the intermediate stress parameter *b*. For instance, for $b = 0$ tests where $\sigma_2 = \sigma_3$ the mean effective stress at failure will certainly be lower compared to $b = 1$ tests where $\sigma_2 = \sigma_1$. Once granular materials are dependent of the mean effective stress, it is reasonable to assume that $b = 1$ tests can outcome great strengths in this case. This scenario is not replicated here, where the mean effective stress is maintained constant instead like Corte (2020) and Andreghetto (2022) studies.

Lade & Duncan (1975) performed true triaxial tests on a sandy soil in order to explore the intermediate principal stress influence. According to the authors, when the intermediate principal stress shifts from its minimum value (*i.e.* $\sigma 2 = \sigma 3$) to its highest value (*i.e.* $\sigma 2 = \sigma 1$), some test characteristics were observed as follows: (i) the major principal strain (ε_1) remained in compression, however, succeeding in a lower rate; (ii) the minor principal strain

(ε_3) was kept in extension, with an increase in the dilation rate; and (iii) soil samples were subjected to great volumetric strains, where both contraction and dilation rates were severely increased.

Reddy and Saxena (1993) investigated the constitutive behavior of cemented Monterey No. 0/30 sand under distinct stress paths. The outcomes described in the sequence were observed to the entire cemented Monterey No. 0/30 samples. Monterey No. 0/30 specimens exhibit contraction in the major principal stress direction, expansion throughout the minor principal stress direction. Otherwise, Monterey No. 0/30 specimens shifted their behavior from expansive to compressive according to the intermediate principal stress direction change, it was observed when the stress parameter *b* was changed from 0 to 1. Also, a dilation rate increase was observed when the stress parameter *b* was changed from 0 to 1.

Distinctly from the previous authors, Abelev & Lade (2003) true triaxial test results on a sandy soil exhibited an increase in the internal friction angle up to a stress parameter *b* value of 0.5, and after that the internal friction angle remained almost constant. Corte (2020) and Andreghetto (2022) observed, in this sequence, great deviatoric stress/mean effective stress ratios ($q/p' = M$) for samples subjected to stress parameter *b* values of 0 (zero), 0.5 and 1. It suggests that compression stress paths led to great strength parameters when compared to extension stress paths; this assumption is here stated and was not assumed by the authors, of course, such assumption ignores the possibility to have an effective cohesion intercept due to the cementitious phase, as well as, the lack of tests on different octahedral stress planes.

2.4 LITERATURE BACKGROUND SUMMARY

The previous works highlighted the intermediate stress and soil anisotropy influence on soil mechanical behavior, which can be fully apprised by true triaxial tests. Nonetheless, true triaxial tests on artificially cemented materials are scarce, even more in material like mining waste tailings. Few works already studied the cementing, intermediate stress and soil anisotropy effects, and all of them focused most on natural soil matrices (*e.g.*, Reddy & Saxena, 1993; Festugato et al. 2019; Corte 2020; Silvani et al. 2022 and Andreghetto 2022). This study focuses on comprehend cemented mine waste tailings mechanical behavior when

exposed to a multiaxial loading condition, and then increment the multiaxial loading existing database. In this point of view, the test results outcome of this present study will undoubtedly enhance materials geomechanical comprehension.

3 EXPERIMENTAL PROGRAM

The experimental program conceived here has two main reasons, (i) it seeks to comprehend the mechanical response of two granular materials in a perspective of mining waste tailings-ordinary Portland cement blends; and (ii) it also looks for examining blends experimental response when subjected to a multiaxial loading condition. Several laboratory tests were carried out to determine and comprehend the controlling variables influence on test results.

As previous discussed in section 1.8, the experimental program was divided into two minor subsections, which were named as follow: Phase I – Preliminary tests and Phase II – Advanced tests. The first subsection, hereafter alluded to Phase I, was designed to comprehend materials (soil matrix and cementing agent) interaction. Specimens with a wide range of dry unit weights and cement contents were tested by means of unconfined compressive strength (UCS), unconfined tensile strength (UTS) and ultrasonic pulse velocity (UPV) tests. Therewith, Phase I is responsible to determine blends dosage which will thereafter be tested in Phase II – Advanced tests.

Phase II – Advanced tests concerns to the phase where multiaxial response of the previous dosages are tested by means of conventional triaxial and true triaxial tests. Therefore, Phase II main objective regards to study ordinary Portland cement stabilization effectiveness when subjected to distinct loading stress paths. This phase also seeks to investigate the intermediate stress influence on samples geomechanical response.

The following chapter, Chapter 3, is going to be responsible to describe both Phase I and Phase II experimental program. This chapter details the controlled variables, response variables acquired, test conditions and materials' characterization. Thesis structure along with Phases I and II is depicted in Figure 17, whereas Chart 1 summarizes materials and experimental tests carried out throughout this thesis.

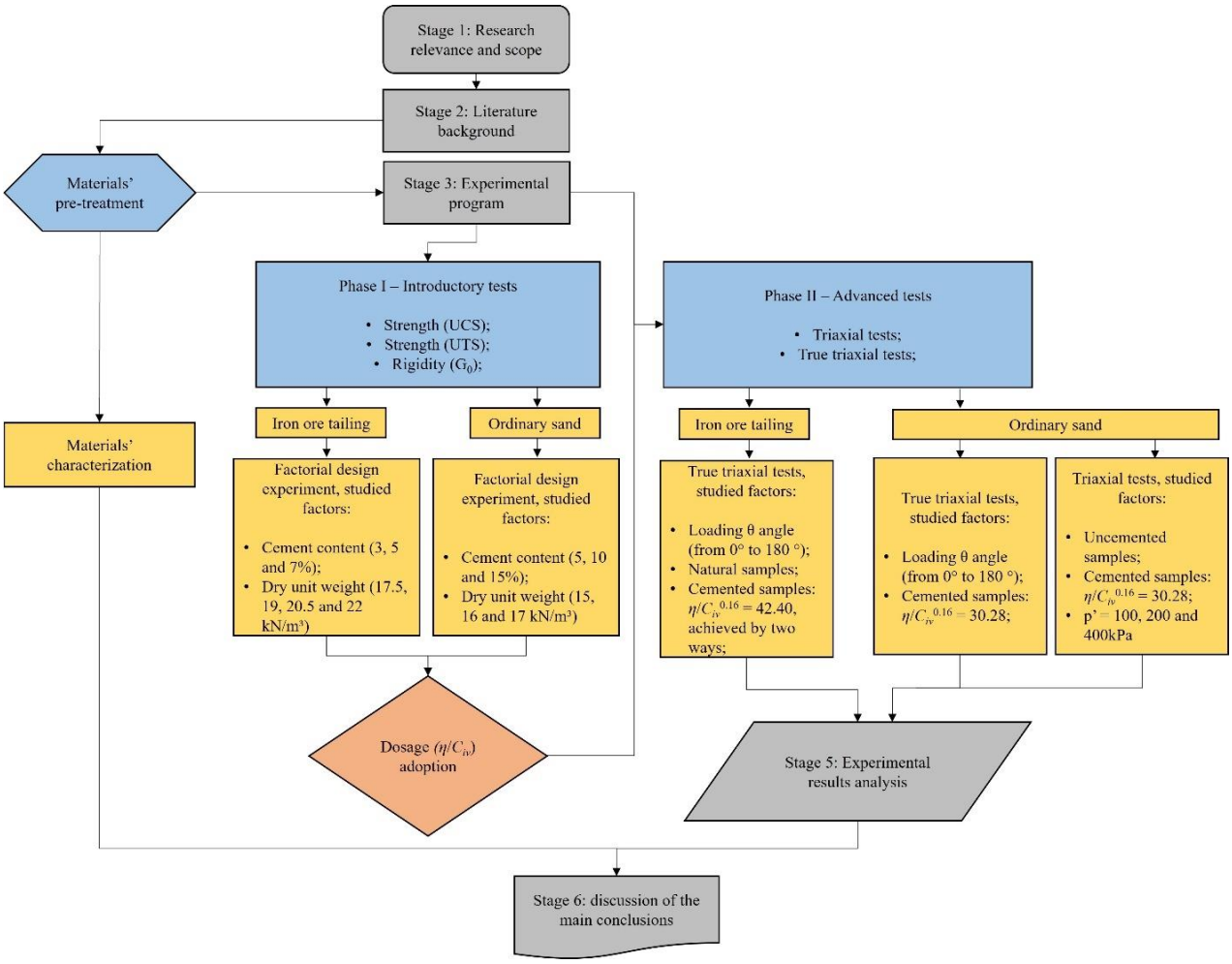

Figure 17: Thesis and experimental program structure.

Chart 1: Materials and experimental tests summary.

Experimental Plan	Materials	Treatments and test types
Materials Treatment and Characterization	• Iron ore tailing; • Ordinary sand; • Ordinary Portland cement;	→ Treatment: • Gridding; • Sieving; → Tests: • Specific gravity; • Grain size distribution; • Liquid limit; • Plastic limit; • Compaction (Proctor test);
Phase I	• Iron ore tailings-Ordinary Portland cement blends; • Ordinary sand-Ordinary Portland cement blends;	• Unconfined compressive strength tests (UCS); • Unconfined tensile strength tests (UTS);[2] • Ultrasonic pulse velocity tests (UPV);[2]
Phase II		• Triaxial tests;[3] • True triaxial tests;

3.1 MATERIALS

3.1.1 Soil matrices: the iron ore tailing and ordinary sand

Two soil matrices were employed in the present study and comprehend both the iron ore tailings and ordinary sand.

The iron ore tailing was sampled from a mining production plant located near of Belo Horizonte, southeast of Brazil, which settles around of 600 km from the Brazilian district capital, Brasília (Figure 18a). The iron ore tailing employed in the present thesis experimental program came from a “dry” stack disposal methodology, where both fine and coarse tailings aggregates are mixed to be afterwards dewatered by a combination of compression thickeners and filter presses. The result is “dry” cake with a moisture content around of 20%, which is

[2] These tests were conducted only for the iron ore tailing matrix.
[3] These tests were conducted only for the ordinary sand matrix.

transported by trucks and conveyors to the stacks. At the mining site, earthwork equipment are responsible for tailings disposal and the dry stack construction. According to the Unified Soil Classification System (ASTM D2487-17), the iron ore tailing studied here is classified as Lean Clay with Sand (CL), and it is predominantly composed by quartz, kaolinite, gibbsite and hematite. Figure 19a shows the iron ore tailing visual aspect.

The ordinary sand was sampled from a construction site located near of Golden, western of United States, which settles around of 20 km from the Colorado state capital, Denver (Figure 18b). According to the Unified Soil Classification System (ASTM D2487-17), the ordinary sand applied here is classified as Poorly Graded Sand (SP), and it is predominantly composed by quartz. Figure 19b shows the ordinary sand visual aspect.

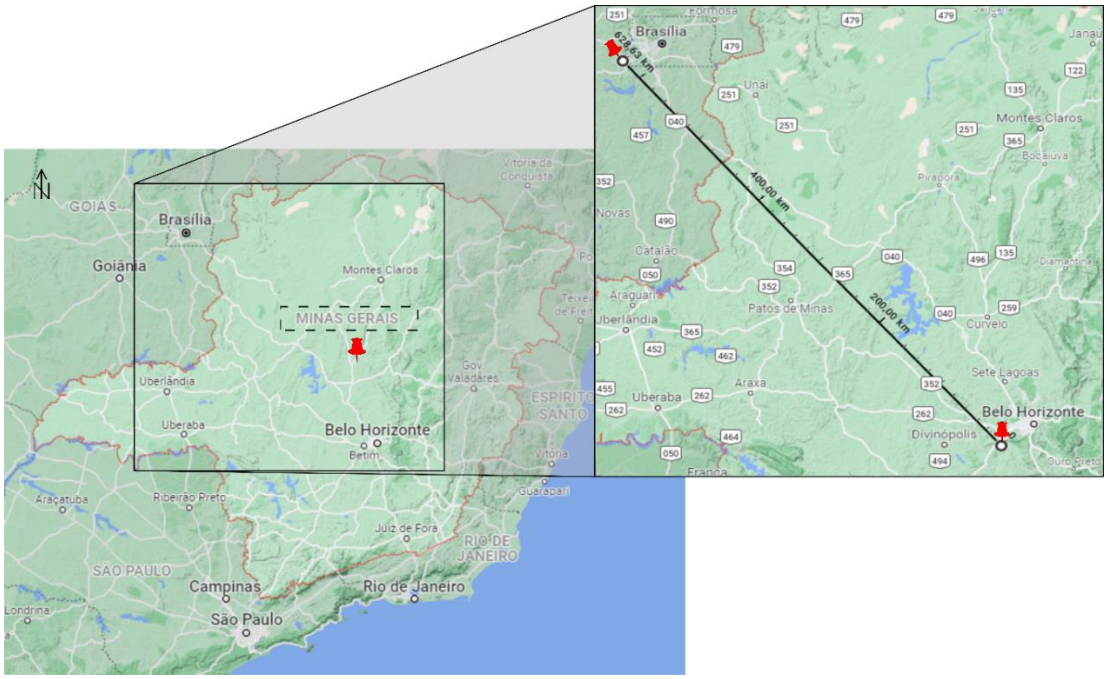

(a)

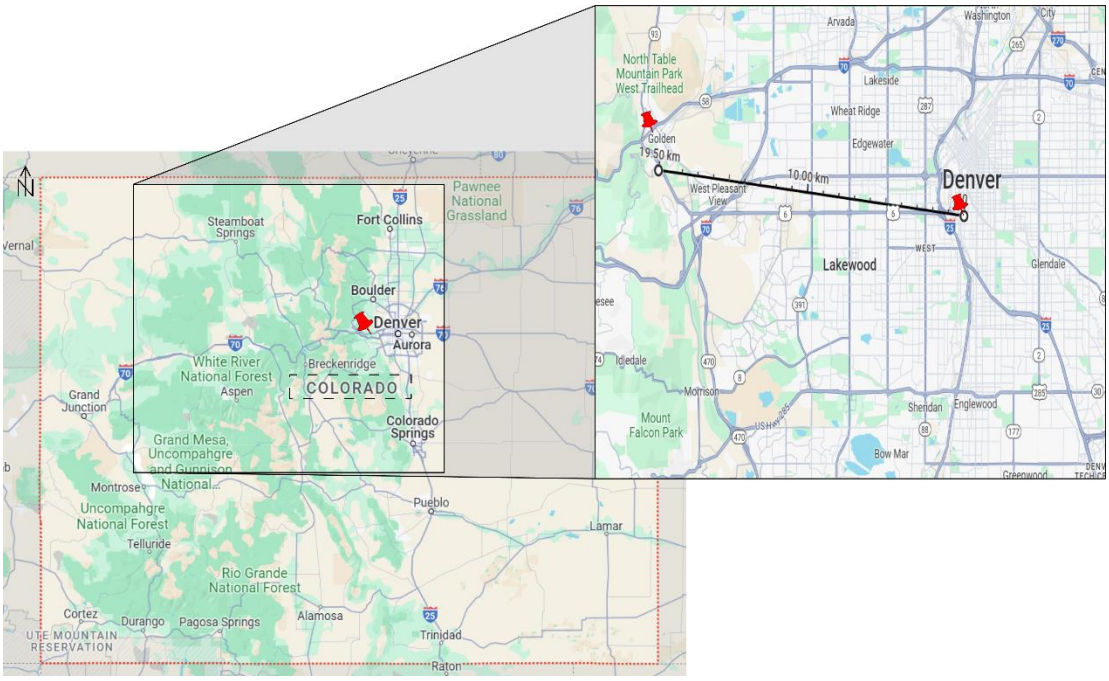

(b)

Figure 18: Deposit location: (a) Iron ore tailing, and (b) Ordinary sand (modified from Google, 2023).

(a) (b)

Figure 19: Materials visual aspect: (a) Iron ore tailing, and (b) Ordinary sand.

The iron ore tailing gradation and physical properties were determined at the Federal University of Rio Grande do Sul facilities at the Geotechnical Engineering and Environmental Geotechnology laboratory. Whereas the ordinary sand main properties were determined at the Colorado School of Mines at the Geotechnical and Rock Mechanics Engineering laboratory. Both iron ore tailing and ordinary sand gradation were carried out in accordance with ASTM D6913M-17. Materials' particle size distributions are displayed in Figure 20, whereas Table 4 comprises materials' physical properties.

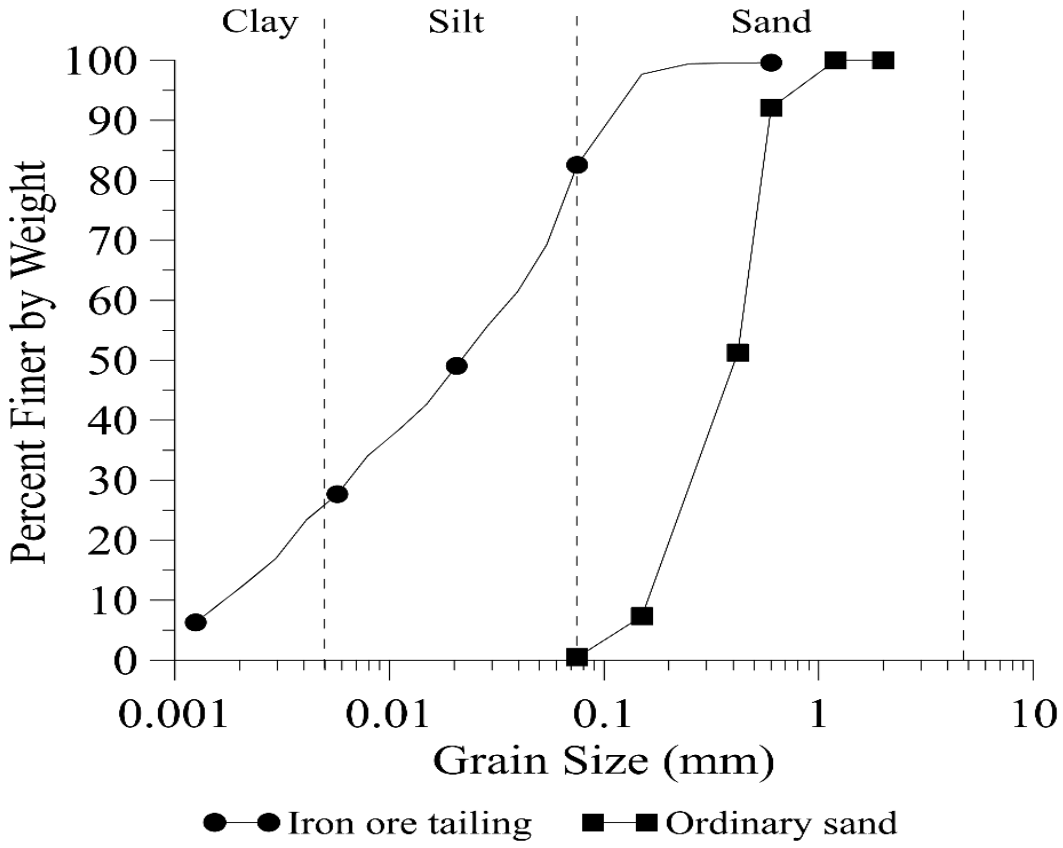

Figure 20: Iron ore tailing particle size distribution.

Table 4: Iron ore tailings physical indexes.

Index	Iron or tailing	Ordinary sand	Standard / Method
Liquid limit - LL (%)	27	NL	ASTM D4318-17
Plastic limit - PL (%)	18	NP	ASTM D4318-17
Plastic index - PI (%)	9	NP	ASTM D4318-17
Specific Gravity of Soil Solids (Gs)	3.18	2.67	ASTM D854-14
Hygroscopic moisture (%)	2.92	0.17	
Gravel (%)	0.00	0.00	
Coarse sand (%)	0.00	0.00	
Medium sand (%)	1.00	47.50	ASTM D6913M-17
Fine sand (%)	16.45	52.50	
Silt (%)	54.87	0.00	
Clay (%)	27.68	0.00	
D_{50} (mm)	0.021	0.40	ASTM D2487-17
Maximum void ratio (e_{max})	1.450	0.750	ASTM D4254-16
Minimum void ratio (e_{min})[4]	0.440	0.552	-
pH	8.6	-	ASTM D4972-19
USCS classification	CL	SP	ASTM D2487-17

3.1.2 Cementing phase: Ordinary Portland cement

Brazilian ordinary Portland cement Type V (equivalent to the ASTM C150/C150M-21 Type III) was adopted to the present thesis. The cementing agent is characterized by the earlier setting time (~1 hour) and fast gain of strength (80% of the total strength is achieved in seven days), which allows short curing times. According to the cement manufacturer, the cement specific gravity is 3.15. The ordinary Portland cement was here chosen because of its characteristic to be worldwide known and commercialized, which might be an economic advantage. Figure 21 depicts the ordinary Portland cement visual aspect.

[4] Estimated according to the Proctor test.

Figure 21: The ordinary Portland cement visual aspect.

3.1.3 Distilled water

Distilled water was used to the whole tests performed throughout this thesis, which comprises the Phase I – Preliminary tests and Phase II – Advanced tests.

3.2 VARIABLES INVESTIGATED

3.2.1 Phase I – Preliminary tests experimental program

Phase I comprehends basic experiments, preliminary tests, which were destinated for comprehend materials interaction and determine your dosages. In this sense, the design and analysis of experiments theory was employed to boost the current experimental program. The design and analysis of experiments theory, which is stablished in statistical concepts, is a reliable tool to structure and optimize experimental campaigns providing to it a clear and concise experimental path through researcher objectives (RIBEIRO & CATEN, 2014).

Thereby, for Phase I general factorial designs were proposed to investigate two main independent variables like dry unit weight and cement content for both soil matrices. The

factorial design is the most efficient instrument and exhibits several research advantages like: (i) it allows to assess the effect of a factor in a wide range of possibilities; and also (ii) this kind of design is indicated to investigate variables interaction (MONTGOMERY 2001). Nonetheless, there are several factorial designs that may fit to each experimental condition. Among the design possibilities, the most useful design regards to the general factorial design or complete factorial design, also known by crossed factorial design.

The general factorial design considers the whole combinations between a series of distinct factors with their i^{th} levels. Thus, a general factorial design might have an *A* factor with *a* levels (*e.g.*, *A* = temperature and *a* = 10°C, 15°C and 20°C) and a *B* factor with *b* levels (*e.g.*, *B* = moisture content and *b* = 10% and 15%), which may result in a number of *ab* combinations or experimental runs to each replication. Montgomery (2001) adverts that, if all interactions are included in the experimental model, at least one replication is recommended to estimate the pure error. Therefore, the previous experimental runs amount turns to be (at least) duplicated 2*x*(*ab*).

The effect of a factor is assessed by shifting its i^{th} level, where its impact is evaluated on the response variables. The impact of each factor on the response variable (*e.g.*, *A* = temperature and *B* = moisture content) is called main effects, whereas the interaction between factors is known as secondary effects. Secondary effects can be thought as the effect that one factor can cause to another (MONTGOMERY, 2001).

Therewith two complete factorial designs were proposed in order to study both soil matrices ordinary Portland cement blends:

I) Iron ore tailing-ordinary Portland cement blends:

This complete factorial design is composed by two main factors, which consists in blends' dry unit weight and cement content. Blends' dry unit weight factor is made of 4 distinct levels, whereas blends' cement content is made of 3 levels. As a consequence, this experimental design test base is composed by 4*x*3 = 12 experimental runs. Three specimens' replication were considered, which results in 36 experimental runs (tests) that were carried out to iron ore tailing-ordinary Portland cement blends. Thereby, thirty-six (36) experiments

were carried out for ultrasonic pulse velocity, unconfined compressive and unconfined tensile strength tests. Specimens' replications were separated in three randomized blocks, which allowed tests to be carried out in different times without some statistical detriment.

II) Ordinary sand-ordinary Portland cement blends:

This complete factorial design is composed by two main factors, which consists in blends' dry unit weight and cement content. Both blends dry unit weight and blends cement content factors are made of 3 distinct levels. As a consequence, this experimental design test base is composed by 3*x*3 = 9 experimental runs. Three specimens' replication were considered, which results in 27 experimental runs (tests) that were carried out to ordinary sand-ordinary Portland cement blends. Thereby, twenty-seven (27) experiments were carried out for unconfined compressive strength tests. Specimens' replications were separated in three randomized blocks, which allowed tests to be carried out in different times without some statistical detriment.

The following section describes the independent and dependent variables apprised in Phase I, and in what manner each factor level was determined as well.

3.2.1.1 Unconfined compressive, unconfined tensile strength and ultrasonic pulse velocity tests

I) Independent variables

Independent variables can be constant, controlled, and uncontrollable factors (nuisance factors).

a) Constant factors

Constant factors are fixed factors, which remain unchanged throughout the experiment campaign. Curing temperature (23 ± 2ºC), specimens' curing period (7 days), molding moisture content for both proposed blends (w_{opt} = 11.3%, see Figure 22), materials batch and molding operator are the constant factors for Phase I.

Curing time (7 days) and molding temperature constant factors were stablished according to laboratory physical restrictions. Both ordinary Portland cements adopted in this thesis are characterized by earlier setting times which justifies the short curing time adopted. Laboratory curing temperature was defined in agreement with the laboratory mixing rooms, moist cabinets and water storage tanks physical constraints.

b) Controlled factors

Controlled factors are those changed throughout the experiment campaign and aim to detect factors' effects on response variables. Phase I controlled factors are blends dry unit weight (γ_d) and ordinary Portland cement content (C).

Blends' dry unit weights were determined based on standard (600 kN-m/m³) and modified effort (2,700 kN-m/m³) Proctor tests. These tests are standardized by the ASTM D698-12$^{\varepsilon 2}$ and ASTM D1557-12, respectively. Figure 22 depicts standard and modified effort compaction curves for both studied soil-cement blends. Iron ore tailing (Gs = 3.18) and ordinary sand (Gs = 2.67) saturation curves are also illustrated in Figure 22.

The iron ore tailing maximum dry unit weight achieved by modified effort Proctor test was 22 kN/m³. The ordinary sand maximum dry unit weight achieved by standard effort Proctor test was 17.2 kN/m³. Other dry unit weights, lower than the maximum achieved by the Proctor tests, were chosen in order to have more porous specimens. Therefore, iron ore tailing dry unit weights are composed by four levels, namely, 17.5, 19, 20.5 and 22.0 kN/m³. On the other hand, ordinary sand dry unit weights are composed by three levels, namely, 15, 16 and 17 kN/m³. Figure 22 highlights both soil matrices specimens' molding points.

The ordinary Portland cement content factor was set by both experimental assessments and the international literature. The international literature reports experiments with cement contents ranging from 1% to 20% (e.g., MITCHELL 1981; SCHNAID et al. 2001; CONSOLI et al. 2009a, 2009b, 2009c, 2011a, 2012a, 2013, 2016a, 2016b, 2016c, 2019a, 2019b; RIOS et al. 2012, 2013; WILLS & FINCH, 2015; FESTUGATO et al. 2017; MOLA-ABASI et al. 2017; CONSOLI & TOMASI, 2018b; DE PAULA et al. 2019; HENZINGER & SCHÖMIG 2020; BALDOVINO et al. 2021; SCHEUERMANN FILHO et al. 2022).

An introductory assessment for both soil matrices with cement contents ranging from 1 to 15% was carried out. The introductory experimental assessment outcomes unsuccessful soil treatment for cement contents lower than 2%. As a consequence, the ordinary Portland cement contents for the iron ore tailing-cement blends are 3, 5 and 7%, whereas the ordinary Portland cement contents for the ordinary sand-cement blends are 5, 10 and 15%. The upward threshold of 15% was chosen, otherwise, we might be subject to be migrating from soil theory into the concrete theory which is not the intention of this research.

Table 5 summarizes the Iron ore tailing-ordinary Portland cement experimental campaign, whereas Table 6 summarizes the Ordinary sand-ordinary Portland cement experimental campaign. Appendix A presents both blends experimental runs.

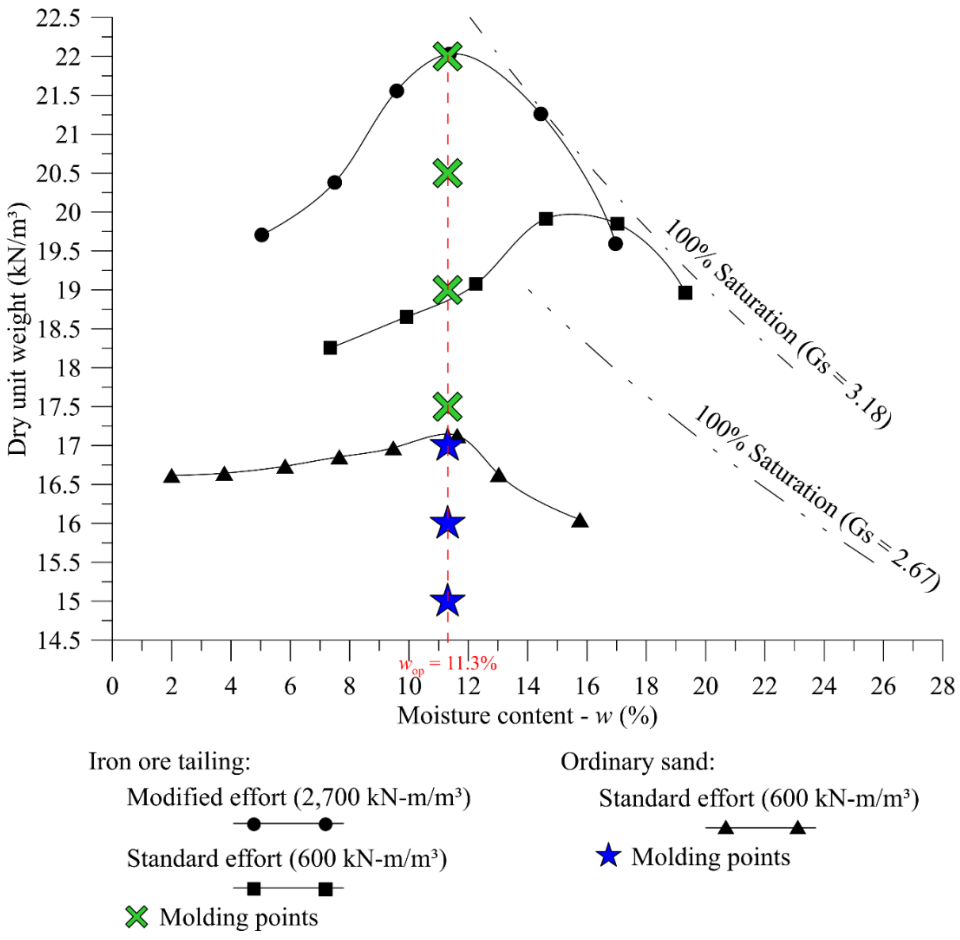

Figure 22: Compaction curves and Phase I molding points.

c) Nuisance factors

Nuisance factors are those responsible to produce undesired variability on test results. Environment moisture and temperature variations are considered nuisance factors. In the present thesis the nuisance factors were suppressed by environment temperature and moisture control.

II) Dependent variables (Response variables)

Response variables are those extracted from the experimental runs and are for Phase I the following variables: unconfined compressive strength – q_u (MPa), secant Young Modulus – $E_{sec\ peak}$ (MPa), unconfined tensile strength – q_t (MPa) and the initial shear modulus – G_0 (MPa).

Table 5: Phase I – Iron ore tailing-ordinary Portland cement experimental campaign.

Test type	Experimental treatment	Controlled factors	Constant factors	Response variable	Experimental runs
UCS	Complete factorial design	•γ_d = 17.5, 19.0, 20.5 and 22.0 kN/m³; •C = 3, 5 and 7%;	•Materials: soil matrix and cement type; •Curing time: 7 days; •Curing temperature: 23±2ºC; •w_{opt} = 11.3%;	q_u (MPa), $E_{sec\ peak}$ (MPa)	36
UTS				q_t (MPa)	36
UPV				G_0 (MPa)	36
				Total of experimental runs:	108

Table 6: Ordinary sand-ordinary Portland cement experimental campaign.

Test type	Experimental treatment	Controlled factors	Constant factors	Response variable	Experimental runs
UCS	Complete factorial design	•γ_d = 15, 16, and 17 kN/m³; •C = 5, 10 and 15%;	•Materials: soil matrix and cement type; •Curing time: 7 days; •Curing temperature: 23±2ºC; •w_{opt} = 11.3%;	q_u (MPa), $E_{sec\ peak}$ (MPa)	27
				Total of experimental runs:	27

3.2.2 Phase II – Advanced tests experimental program

The factorial designs are widely recognized to be introductory studies, and it seeks to detect variables importance into a study. Dry unit weight (porosity) and cement content-controlled variables significance were apprised in Phase I test design, which outcome the possibility to use the $\eta/C_{iv}^{0.16}$ index as a dosage tool. Hereafter the Phase II – Advanced Tests focus on investigate the $\eta/C_{iv}^{0.16}$ index as a state parameter to cement treated soils when subjected to a multiaxial loading condition.

This section restricts to study a single $\eta/C_{iv}^{0.16}$ index for each soil matrix and their impact on true triaxial tests results. The $\eta/C_{iv}^{0.16}$ indexes chose and how it was done is described in the sequence:

I) Iron ore tailing-ordinary Portland cement blends:

The $\eta/C_{iv}^{0.16}$ adopted for this soil-cement blends is equal to 42.40, and it is depicted in Figure 40. This $\eta/C_{iv}^{0.16}$ was chosen in order to fulfill section 1.6 restrictions, namely, it avoids vigorous soil specimens (q_u = 180kPa), and it adjusts to the true triaxial equipment lack of pressure capacity. Nonetheless, the $\eta/C_{iv}^{0.16}$ index can either be achieved by varying soil porosity or blend's cement content. Therefore, in the case of iron ore tailing-ordinary Portland cement blends the $\eta/C_{iv}^{0.16}$ = 42.40 is achieved by means of two ways:

a) by heavily compacted specimens and small cement contents; and,
b) by lightly compacted specimens and high cement contents;

II) Ordinary sand-ordinary Portland cement blends:

The $\eta/C_{iv}^{0.16}$ adopted for this soil-cement blends is equal to 30.28 (q_u = 3500kPa or 3.5MPa), and it is depicted in Figure 56. The Colorado School of Mines true triaxial holds stresses capacity up to 70 MPa, section 3.3 details it, which it allows to test a wide range of strength possibilities. Nonetheless, the $\eta/C_{iv}^{0.16}$ = 30.28 for ordinary sand-ordinary Portland cement blends considers the upward threshold of 15% previous set to avoid being migrating into the concrete theory and, the conventional triaxial loading frame maximum capacity. In the case of ordinary sand-ordinary Portland cement blends the $\eta/C_{iv}^{0.16}$ = 30.28 is achieved by a single way, whereas soil-cement specimens are experimented by means two consolidating pressures.

Both iron ore tailing-OPC blends and ordinary sand-OPC blends main variables are discussed in the following paragraphs. The next sections detail independent and dependent (response) variables and discuss the upward $\eta/C_{iv}^{0.16}$ adopted.

3.2.2.1 True triaxial tests

I) Independent variables
   a) Constant factors

Phase II constant factors vary according to blends' dosage, and they are explained below.

- Iron ore tailing-ordinary Portland cement blends

The iron ore tailing-ordinary Portland cement blends constant factors are as follows:

- soil matrix;
- cement type (when applicable);
- curing time of 7 days (when applicable);
- curing temperature of 23±2ºC (when applicable);

- the loading stress plane (π plane) of 100 kPa;
- molding moisture content (w_{opt} = 11.3%);
- materials batch;
- molding operator; and,
- $\eta/C_{iv}^{0.16}$ value of 42.40.

Table 7 summarizes the constant and further factors for the iron ore tailing-ordinary Portland cement blends.

➢ Ordinary sand-ordinary Portland cement blends

The ordinary sand-ordinary Portland cement blends constant factors are as follows:

- soil matrix;
- cement type;
- curing time of 7 days;
- curing temperature of 23±2ºC;
- dry unit weight of 16 kN/m³ (≡ η = 40.85);
- cement content of 14.65%;
- molding moisture content (w_{opt} = 11.3%);
- materials batch;
- molding operator; and,
- $\eta/C_{iv}^{0.16}$ value of 30.28.

Table 8 summarizes the constant and further factors for the ordinary sand-ordinary Portland cement blends. Constant factors reasons of adoption were previously explained.

b) Controlled factors

Phase II controlled factors vary according to blends' dosage, and they are explained below.

➢ Iron ore tailing-ordinary Portland cement blends

The iron ore tailing-ordinary Portland cement blends-controlled factors are as follows:

- dry unit weight (16.5 and 17.5 kN/m³);
- cement content (0.00 and 4.38%); and,
- Lode loading angle (θ° = 0, 30, 60, 90, 120, 150 and 180°).

The iron ore tailing-ordinary Portland cement blends dry unit weights and cement contents-controlled factors were adopted to achieve the $\eta/C_{iv}^{0.16} = 42.40$. The following combinations were chosen: (i) γ_d = 16.5 kN/m³ ($\eta \approx 48.09$) and C = 4.38%, and (ii) γ_d = 17.5 kN/m³ ($\eta \approx 44.95$) and C = 2.66%. The adoption of these previous combinations was guided by, firstly, it was tried to remain into the range of parameters studied in Phase I, thence, the dry unit weights (porosities) were initially determined and then the cement contents (the C_{iv} portion); Secondly, the 16.5 kN/m³ dry unit weight was not apprised in Phase I, however, once the true triaxial specimens were manually molded, it was thought that lower dry unit weight would help to perform it; Lastly, in the case of cement content, the 2% lower bound restriction (see section 1.6) was taken into consideration.

- Ordinary sand-ordinary Portland cement blends

The ordinary sand-ordinary Portland cement blends-controlled factors are as follows:

- loading stress plane (π plane) of 2,000 and 4,000 kPa; and,
- Lode loading angles (θ° = 0, 30, 60, 90, 120, 150 and 180°)

The ordinary sand-ordinary Portland cement blends-controlled factors were adopted according to the Colorado School of Mines true triaxial restrictions. This apparatus is a kind of rigid boundary equipment, and it did not have backpressure in and outlets. The rigid boundaries were composed by steel heavy platens which turn the in loco molding inconceivable; the untreated soil strength was lower than the platens weight, and it resulted in specimens' strain before the test start. The backpressure drawback was overcame by soaking the specimens previous each test and by measuring soil specimens' suctions after the shearing procedure. Therefore, it was decided to mold and cure specimens outside of the equipment and turn the loading stress plane and Lode loading angle into controlled variables. The loading stress planes (π planes) of 2,000 and 4,000 kPa were chosen according to specimens' maximum unconfined compressive strength. The ordinary sand-OPC specimens

for true triaxial tests were molded to attain an unconfined compressive strengths of 3,500 kPa (see Figure 56), thence, it was chosen loading stress planes below and above of the target unconfined compressive strength. This stress range adoption settles on the Silva et al. (2024) findings, where the unconfined compressive strength could be adopted as the cement treated soils yielding point.

c) Nuisance factors

Environment moisture and temperature variations are considered nuisance factors. In the present thesis the nuisance factors were suppressed by environment temperature and moisture control.

II) Dependent variables (Response variables)

The true triaxial test outcomes several response variables like samples' multiaxial strength, the intermediate principal stress influence (σ'_2), X, Y and Z stress and strain samples' geomechanical behavior, among others.

Table 7 and Table 8 detail Phase II the true triaxial main variables.

3.2.2.2 Conventional triaxial tests

Conventional triaxial test were performed only for ordinary sand-ordinary Portland cement blends.

I) Independent variables

a) Constant factors

- Ordinary sand-ordinary Portland cement blends

The ordinary sand-ordinary Portland cement blends constant factors are as follows:

- soil matrix;
- initial mean effective stresses (p'_0 = 100, 200 and 400kPa);
- dry unit weight (γ_d = 16 kN/m³);
- molding moisture content (w_{opt} = 11.3%);

- Curing time of 7 days;
- Curing temperature of 23±2ºC; and,
- $\eta/C_{iv}^{0.16}$ value of 30.28.

These constant factors go towards the constant factors already adopted for the true triaxial tests.

b) Controlled factors

The ordinary sand-ordinary Portland cement blends-controlled factors are as follows:

- triaxial loading condition [drained (CID) and undrained (CIU)]; and,
- cement content (C = 0.00 % and C = 14.65 %);

The conventional triaxial controlled factors were chosen in order to further guide the strength envelope of ordinary sand-ordinary Portland cement blends.

c) Nuisance factors

Environment moisture and temperature variations are considered nuisance factors. In the present thesis the nuisance factors were suppressed by environment temperature and moisture control.

II) Dependent variables (Response variables)

Conventional triaxial test response variables are the deviatoric stress (q), mean effective stress (p'), axial strain (ε_a), volumetric strain (ε_v), porepressure variation (ΔU), stress *vs* strain relationship, stress paths, strength parameters, among others. Table 8 details Phase II the true triaxial main variables.

Table 7: Phase II – Advanced tests summary for iron ore tailing-ordinary Portland cement blends.

Test type	Controlled factors	$\eta/C_{iv}^{0.16}$	Constant factors	Response variable	Experimental runs
True triaxial tests	•γ_d = 17.5 kN/m³; •C = 0.00 %; •θ (°) = 0, 30, 60, 90, 120, 150 and 180°	-	•Materials: soil matrix; •π plane = 100 kPa; •w_{opt} = 11.3%;	Stress vs strain relationship, peak strength, stress path, strength parameters, among others.	7
	•γ_d = 16.5 kN/m³; •C = 4.38 %; •θ (°) = 0, 30, 60, 90, 120, 150 and 180°	42.40	•Materials: soil matrix and cement type; •Curing time: 7 days; •Curing temperature: 23±2ºC; •π plane = 100 kPa; •w_{opt} = 11.3%;		7
	•γ_d = 17.5 kN/m³; •C = 2.66%; •θ (°) = 0, 30, 60, 90, 120, 150 and 180°				7
				Total of experimental runs:	21

Table 8: Phase II – Advanced tests summary for ordinary sand-ordinary Portland cement blends.

Test type	Controlled factors	$\eta/C_{iv}^{0.16}$	Constant factors	Response variable	Experimental runs
Conventional triaxial tests	•Consolidated isotropic drained (CID); •C = 0.00 %;	-	•Materials: soil matrix; •p'_0 = 100, 200 and 400kPa; •γ_d = 16 kN/m³; •w_{opt} = 11.3%;	Stress *vs* strain relationship, peak strength, stress path, strength parameters, among others.	3
	•Consolidated isotropic undrained (CIU); •C = 0.00 %;				3
	•Consolidated isotropic drained (CID); •C = 14.65 %;	30.28	•Materials: soil matrix and cement type; •Curing time: 7 days; •Curing temperature: 23±2ºC; •p'_0 = 100, 200 and 400kPa; •γ_d = 16 kN/m³; •w_{opt} = 11.3%;		3
	•Consolidated isotropic undrained (CIU); •C = 14.65 %;				3
True triaxial tests	•θ (°) = 0, 30, 60, 90, 120, 150 and 180°; •π plane = 2,000 kPa;		•Materials: soil matrix and cement type; •Curing time: 7 days; •Curing temperature: 23±2ºC; •γ_d = 16 kN/m³; •C = 14.65 %; •w_{opt} = 11.3%;		7
	•θ (°) = 0, 30, 60, 90, 120, 150 and 180°; •π plane = 4,000 kPa;				7
				Total of experimental runs:	26

3.3 EXPERIMENTAL PROCEDURES AND LABORATORY FACILITIES

3.3.1 Specimens' molding and curing

A single specimens' molding method was adopted for both Phase I and II experimental tests, whereas specimens' dimensions vary according to the test type. The following paragraphs describe the molding condition for each test type.

Cylindrical specimens of 50 mm in diameter and 100 mm in height (Figure 23a) were adopted for Phase I (UCS, UTS and UPV tests) and for Phase II (conventional triaxial tests). On the other hand, true triaxial tests were carried out with cubical samples of 100 mm (Figure 23b) and 200 mm (Figure 23c) in side, the former at the Federal University of Rio Grande do Sul and the latter at the Colorado School of Mines.

The specimens' preparation method consists of, firstly, soil matrix, ordinary Portland cement and distilled water weighing with a 0.01 g weighing-machine precision. Secondly, the soil matrix and ordinary Portland cement mixture in a dried state until it acquires a homogeneous state. And lastly, the distilled water inclusion and further blends' mixture. The next step consists of taking three mixture small portions for moisture content determination. Figure 24 exemplifies this procedure.

(a)

(b)

(c)

Figure 23: Split molds: a) cylindrical specimens; b) 100 mm cubical specimens; and c) 200 mm cubical specimens.

(a)

(b) (c)

Figure 24: Samples' confection: a) soil, ordinary Portland cement and distilled water weighed according to the blends' dosage; b) materials homogenization and c) moisture content determination and specimens' layers division.

The homogeneous paste previously described it is then divided into four small portion which it will compose the four specimens' layers of molding. Both cylindrical and cubical specimens' geometry were molded by means the undercompaction molding procedure proposed by Ladd (1978). This molding procedure consists of pouring the mixture into the molds and then statically compact it. Interlayers upward contacts were slightly scarified during the ongoing molding procedure. The molding procedure (materials' arrangement, mixing and compaction) maximum elapsed time was set to one hour in order to remain under the ordinary Portland cement setting time.

As much as the ending of the molding procedure, cylindrical specimens were then removed from the rigid split molds, and their weights, diameters, and heights measured with precisions of 0.01 g and 0.1 mm. The final height and diameter were the average of three determinations.

On the other hand, cubical specimens were maintained into the split molds for at least one day; this procedure aimed to avoid specimens' damage. Specimens' weight and dimensions were taken after specimens' unpacking.

Unpacked specimens were cured for 7 days (a constant factor for both Phase I and II) Thereby, cylindrical and cubical specimens were carefully sealed to avoid moisture content

losses during the 7 days curing period. After that, the sealed specimens were carried to a humid room at 23 ± 2°C and a relative humidity of 95% (ASTM C511-21).

Despite of specimens' dimensions, soil matrix-OPC specimens were considered suitable for testing if the following tolerances were met: a dry density within ± 1.5% of the target value; moisture content within ± 1% of the target value; diameter within ± 0.5 mm of the target value; and, height within ± 1.0 mm of the target value.

3.3.2 Unconfined compressive strength test methods

Unconfined compressive strength tests of cylindrical specimens were carried out based on the procedures described in the ASTM C39/C39M (ASTM 2021) standard. This test method consists of applying a compressive axial load on the top of a cylindrical specimen up to its failure (Figure 25). The unconfined compressive strength tests apprised here were carried out with a constant displacement rate of 1.4 mm/min. The reaction load was measured by a 10 kN loading cell with resolution of 0.005 kN.

Figure 25: Unconfined compressive strength test ongoing.

3.3.3 Unconfined tensile strength test methods

Splitting tensile strength tests were carried out in accordance with the C496/C496M (ASTM 2017) standard. This test method consists of applying a compressive load along the diametrical specimen's length up to its failure (Figure 26). The unconfined tensile strength tests apprised here were carried out with a constant displacement rate of 1.4 mm/min. The reaction load was measured by a 10 kN loading cell with resolution of 0.005 kN.

Figure 26: Unconfined splitting tensile strength test ongoing.

3.3.4 Ultrasonic pulse velocity test methods

Small strain initial shear modulus (G_0) was assessed by means ultrasonic pulse velocity tests. This test consists of measure the shear wave time travel throughout the specimen's length. The ASTM D2845 (ASTM 2008) standard was adopted as reference for these testes. The ultrasonic pulse velocity tests were carried out in the same unconfined compressive tests specimens; the UPS tests were carried out and then the UCS tests in the sequence. This test type consists of coupling two transducers on the specimens' edges, a shear coupler gel helps in transducers accommodation and surface adherence (Figure 27). Both transducers are

senders and receptors, and they are responsible for issuing the shear wave that crosses the specimen. The equipment outcome is the shear wave time travel, which it will further correlated for the G_0 determination; the UPS tests were carried out with 54 kHZ for determining the p-waves, and 250 kHZ for s-waves.

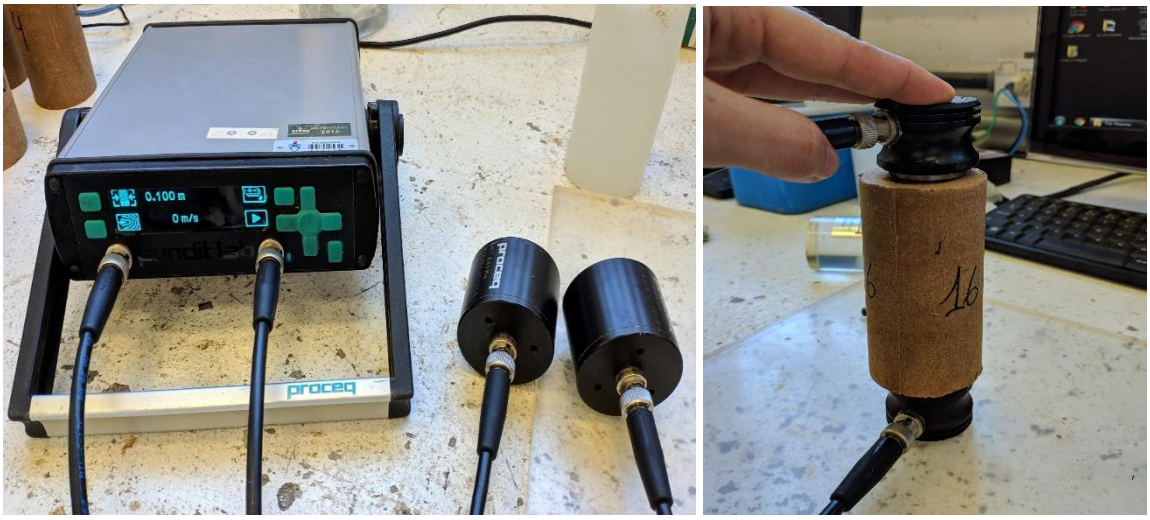

(a) (b)

Figure 27: The UPV test apparatus: a) UPV equipment and transducers; b) UPV test ongoing (MIGUEL, 2020).

3.3.5 The Federal University of Rio Grande do Sul true triaxial test method and equipment

An automated stress-controlled true triaxial apparatus was built at the Federal University of Rio Grande do Sul by Andreghetto (2022), and this equipment was employed here for studying the multiaxial response of iron ore tailing-OPC blends. Further equipment details are also found in Andreghetto et al. (2022).

The true triaxial test consists of subjecting in general cubical soil specimens (other geometries are also applicable) to a multiaxial stress or strain state condition. This kind of test is widely employed for studying soil mechanical behavior, the intermediate principal stress influence, and soil anisotropy. One of the main true triaxial advantages regards to the principal stresses or strains control (SADEK, 2006).

Figure 28 exemplifies a general stress state of an infinitesimal soil cube, where both normal and shear stresses are shown. This figure depicts the test six degrees of freedom, one for each cube face. If we hypothetically have a null friction state between the soil specimen and loading mechanism, then, the normal stresses (σ_x, σ_y, σ_z) and strains (ε_x, ε_y, ε_z) can be considered the principal stress and principal strain tensor components (CORTE, 2020).

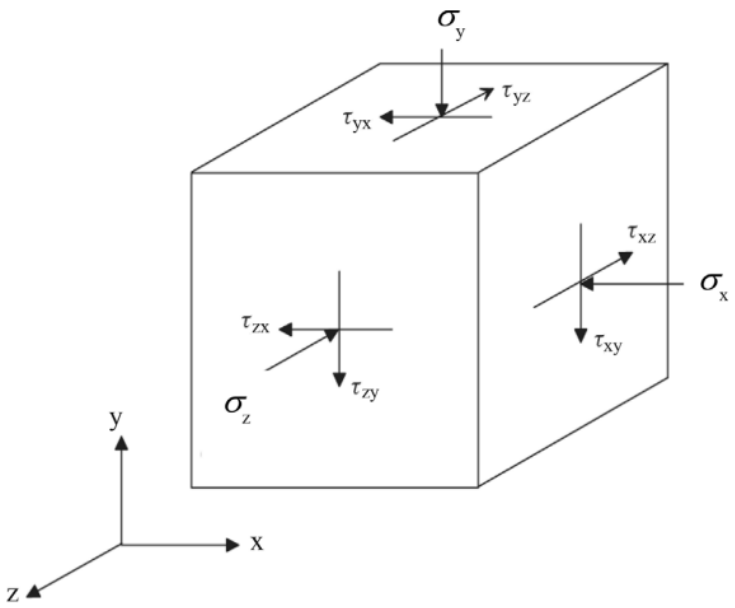

Figure 28: Stress state at a point in a one phase solid (FREDLUND, 2016).

In case of the Federal University of Rio Grande do Sul true triaxial apparatus, the test is similar to conventional triaxial phases. Such phases comprehend (i) to flush carbon dioxide (CO_2) and distilled water through soil specimen, (ii) specimen's saturation by distilled water, (iii) specimen's consolidation, and (iv) specimen's shearing last phase. The last phase, the searing phase, had to be executed on the 7th curing day. Therefore, in the 6th day specimens were accommodated into the true triaxial chamber, paper-based filters and cushion top-hat-shaped membranes installed to proceed with CO_2 and water flushing.

Despite of the true triaxial six degrees of freedom possibilities, the Federal University of Rio Grande do Sul true triaxial apparatus has only three controlled faces whereas the remaining faces are restrained. Thus, this true triaxial apparatus is a kind of mixed boundary condition. Where the loading moving faces are composed by rubber membranes, also known by

cushions, whereas in the restrained faces are made of rigid aluminum plates. Flexible-rigid boundary conditions help to avoid undesired specimen's rotation (SILVANI et al. 2022).

The true triaxial configurations are depicted in Figure 29, Figure 34 and Figure 35, where three flexible top-hat-shaped cushions (100 x 100 mm) are clamped on three true triaxial cubical faces; talcum powder was previously spread to suppress the rubber-aluminum friction contact.

The next step regards to LVDTs (Linear Variable Differential Transformers) screwing on flexible faces. Figure 29 exemplifies the three LVDTs arrangement for a single flexible face, this procedure repeats for the other two flexible faces which it results in 9 LVDTs. The rubber membrane-LVDTs contacts were ensured by magnets glued on the top-hat-shaped cushions.

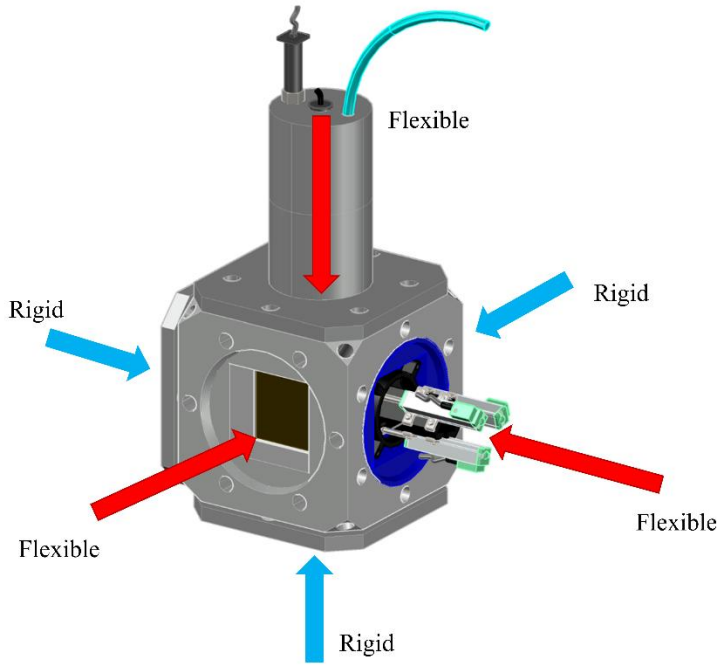

Figure 29: The true triaxial tests boundary conditions (modified from ANDREGHETTO 2022 and ANDREGHETTO et al. 2022).

As soon as the LVDTs are positioned, the top-hat-shaped cushions are air-infilled to promote specimens' loading. The next step consists of the CO_2 specimen's flushing under an effective stress of 30 kPa; a time of 15 minutes of CO_2 flushing it was assumed to be sufficient. Once the CO_2 flushing ceases, distilled water flushing starts for a period of 24 hours under the same

effective stress. The 30 kPa effective stress was achieved by air-infilling the three top-hat-shaped cushions with 48 kPa, whereas the water backpressure was set to 18 kPa (see Figure 30).

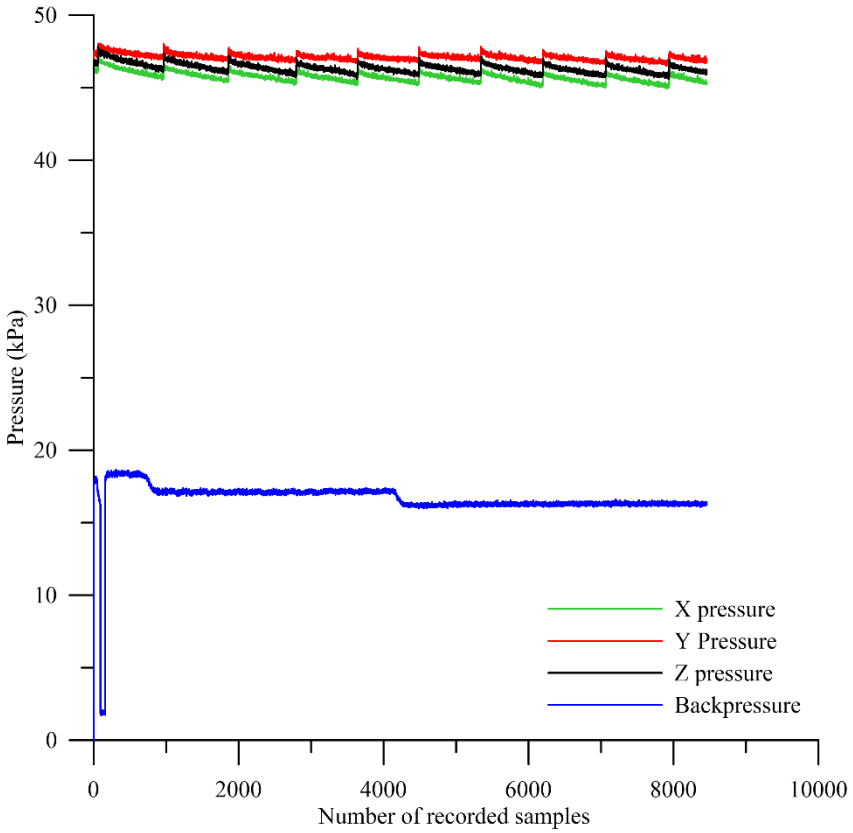

Figure 30: Example of percolation phase.

The saturation phase takes place where both confining and backpressures are incrementally raised. Both pressures were equally increase in a rate of 11.3 kPa/min. The saturation phase proceeds until reach a backpressure of 300 kPa (see Figure 31). The Federal University of Rio Grande do Sul true triaxial restrictions did not allow the B parameter (Skempton 1954) determination nor a backpressure increase over 400 kPa; a backpressure threshold of 400 kPa is widely used for air bubbles dissolution. A backpressure of 300 kPa was assumed to be sufficient to specimens' saturation. Specimens' moisture content at the end of the tests were determined, which it suggested an average saturation degree of 91.85% for all specimens.

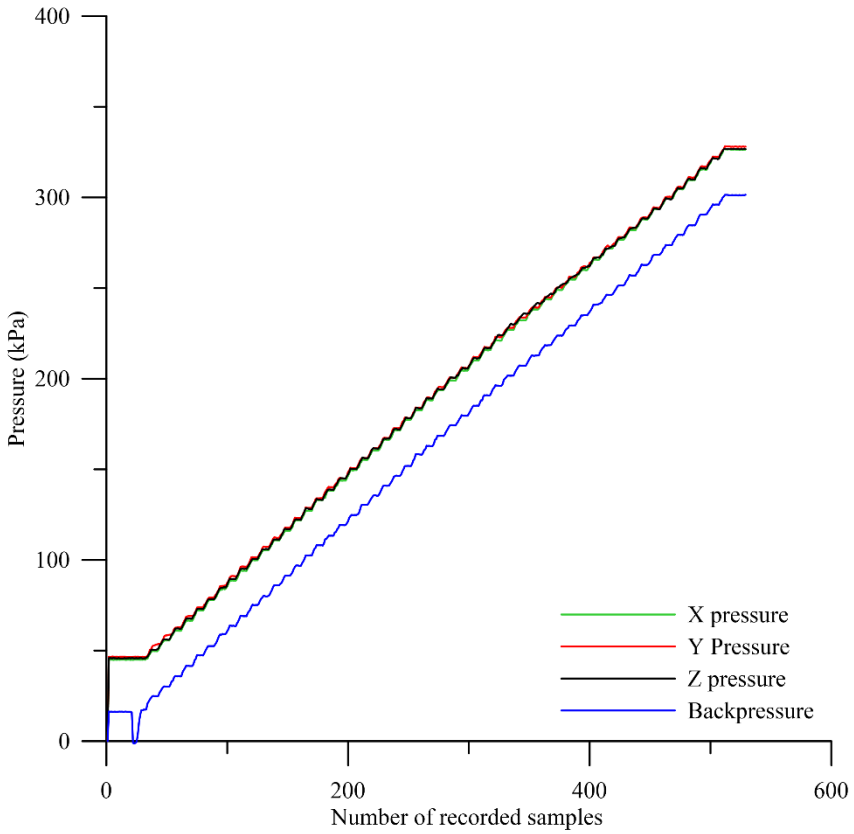

Figure 31: Example of saturation phase.

The consolidation next phase consists of increasing the confining pressure whereas the backpressure remains constant. For the true triaxial tests apprised here the confining pressure was raised to obtain an effective stress of 100 kPa (a π plane of 100 kPa); once we already had an effective stress of 30 kPa as previous described, the stress magnitude increment was of 70 kPa. The confining pressure rate of increment was of 2.8 kPa/min. Figure 32 depicts the consolidation phase.

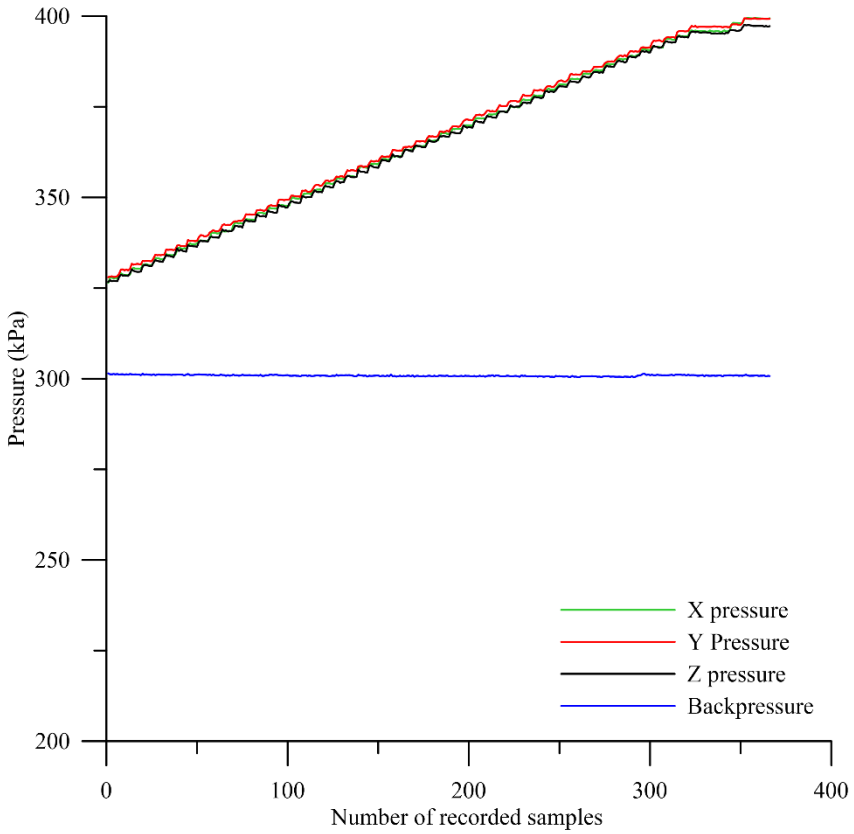

Figure 32: Example of consolidation phase.

Lastly, the Federal University of Rio Grande do Sul true triaxial last step consisted in shearing the cubical specimen by means choosing a loading θ angle. The loading θ angle dictates the test stress path and how each specimen's face is loaded; Table 3 describes ordinary loading stress paths and how each specimen's face is loaded according to the chosen path. Figure 33 exemplifies a θ = 0° loading stress path, where the intermediate stress parameter *b* is equal to zero which means an equivalence between the σ_2 and σ_3 principal stresses; this loading condition is analogous to the conventional triaxial compression stress path.

In the shearing phase the octahedral plane remains constant, and it was equal to 100 kPa in the case of the Federal University of Rio Grande do Sul true triaxial experimental campaign. Following the previous test example, namely, a loading condition of θ = 0°, the octahedral is maintained constant by increasing the major principal stress and decreasing a half of both intermediate and minor principal stresses. Figure 33 exemplifies this procedure. Either stresses increments or decrements obeyed a 2 kPa/min loading rate. The end of the test was

assumed to be when one of the following conditions were fulfilled: 1) by specimen and/or top-hat-shaped cushions failure; or, 2) when the minor principal stress approached to the backpressure stress magnitude. The second condition was set to avoid LVDTs damage, once a backpressure higher than the minor principal stress would cause LVDTs water soaking.

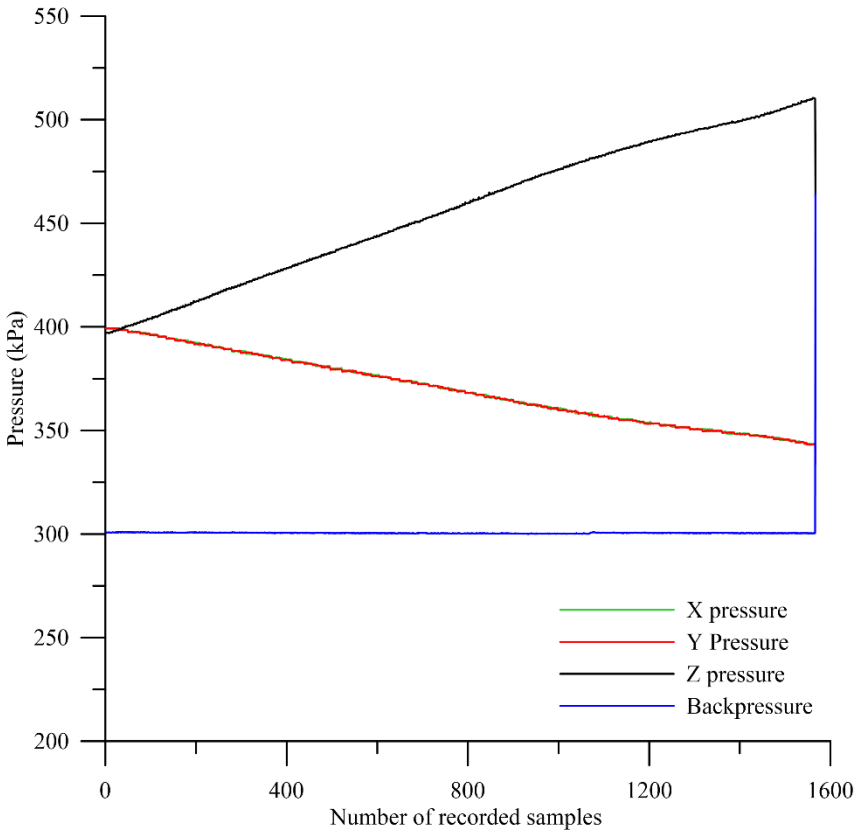

Figure 33: Example of shearing phase, angle θ = 0° equivalent to the conventional triaxial compression test where ($\sigma'_2 = \sigma'_3$).

The Federal University of Rio Grande do Sul true triaxial main components are depicted in Figure 34 whereas Figure 35 portrays the true triaxial main chamber. Nine (9) Lemaq LR 12-50 LVDTs with 50 mm in range are used for displacement measurement; three in each flexible equipment face. Other components are four (4) Ashcroft pressure transducers responsible for measuring the X, Y and Z air-pressurized lines. The fourth pressure transducer is assigned for measuring the backpressure and it was assembled in the present work in concomitance with an air-water pressure interface device; all of these transducers have working pressure ranges of zero to 1000 kPa. Four (4) steeper motors are responsible

to be controlling four (4) pressure precision valves; these set of components are designated as actuators into Figure 34. The steeper motors are controlled by two (2) Arduino Uno R3 and two (2) motor shields L293D H bridge; a pair of motors for each Arduino. Finally, the data acquisition is made by one (1) Arduino Nano where four (4) analogic-to-digital converters ADS 1115 are installed. A LabView based algorithm is responsible to control and acquire the testing data. A comprehensive true triaxial equipment description is be found in Andreghetto (2022) and Andreghetto et al. (2022).

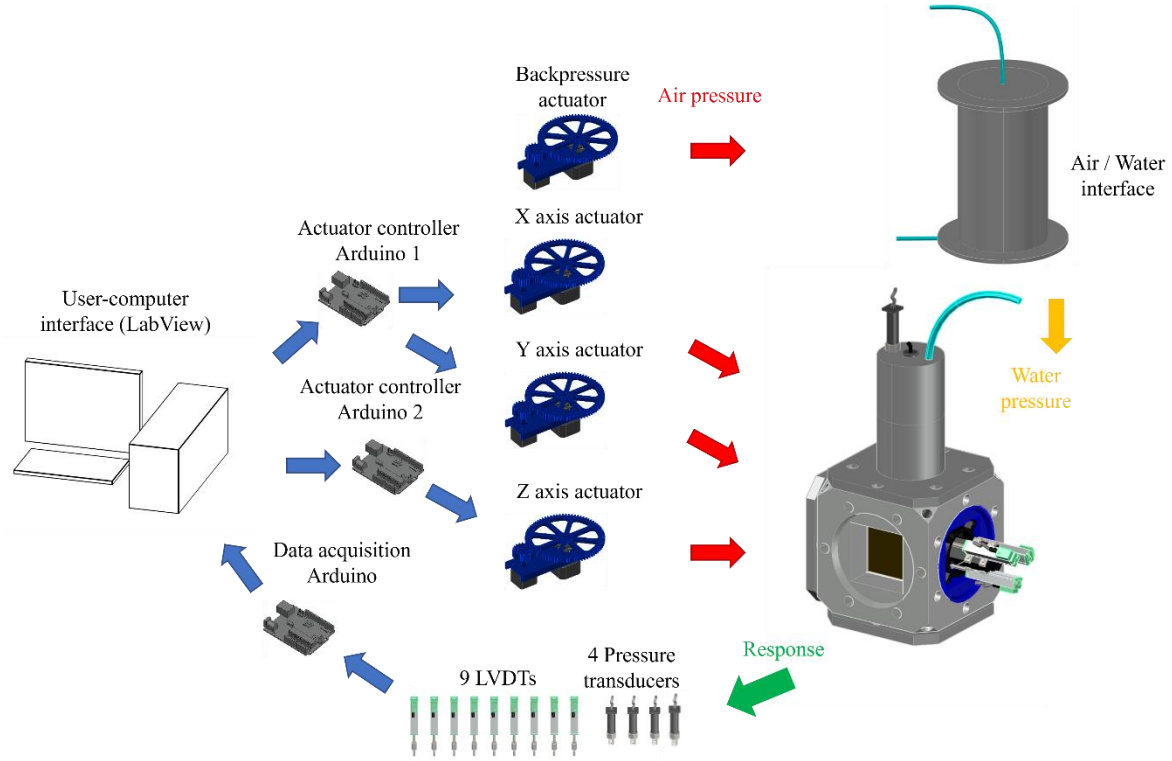

Figure 34: The true triaxial components (modified from ANDREGHETTO 2022 and ANDREGHETTO et al. 2022).

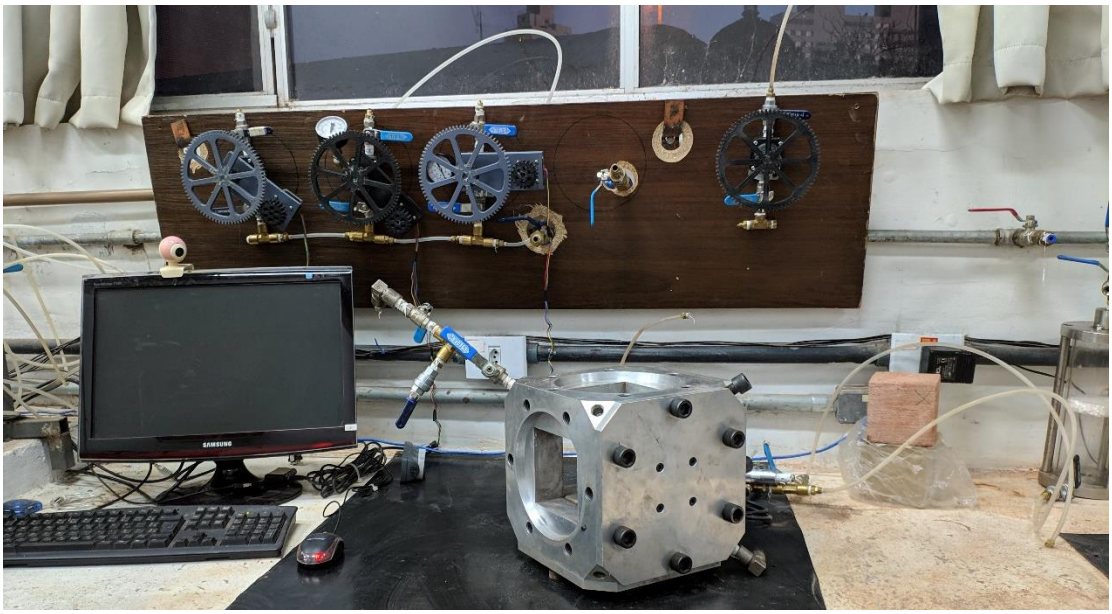

Figure 35: The Federal University of Rio Grande do Sul true triaxial apparatus.

3.3.6 The Colorado School of Mine true triaxial test method and equipment

A manual stress-controlled true triaxial apparatus was built at the Colorado School of Mines (Figure 36), and this equipment was employed here for studying the multiaxial response of ordinary sand-OPC blends.

The Colorado School of Mines true triaxial differs from the previous one, where its main difference settles in a lack on a backpressure line; this equipment is focused on rock mechanics a hydraulic fracturing, where backpressure is some kind not relevant like in soils. Therefore, phases like specimen's CO_2 and water flushing, and specimen's saturation are not feasible. The Colorado School of Mines true triaxial tests were then carried out with two main phases like (i) specimen's consolidation, and (ii) specimen's shearing. The last phase, the searing phase, had to be executed on the 7^{th} curing day. Therefore, in the 6^{th} day specimens were immersed into a water tank seeking to at least soak them; this procedure aimed to suppress the suction effect on the specimens' shear strength.

In terms of degrees of freedom possibilities, the Colorado School of Mines true triaxial is comparable to the previous true triaxial, where it has three controlled faces whereas the remaining faces are restrained (see Figure 36a). The moving faces are composed by steel

heavy plates that are impelled against the specimen by means three hydraulic jacks (see Figure 36a); this true triaxial framework has the possibility to achieve stress magnitudes of 70,000 kPa (70 MPa).

The true triaxial configurations are depicted in Figure 36. The test assembling first step consisted of arranging the specimen (200 x 200 mm) into the true triaxial chamber, which it was followed by the three steel heavy plates and hydraulic jacks positioning. A slight pressure was set in each hydraulic jack to hold the steel heavy plates in place, then the top loading framework was slid over the triaxial chamber. The assembling final step consisted of positioning three LVDTs in each X, Y and Z loading faces (Figure 36b depicts, for instance, the LVDT positioned on the X loading specimen face). Figure 36a partially depicts the test final arrangement, where the top steel plate was suppressed for the photo to be taken.

Once the test was assembled, its first phase consisted of the consolidation phase. This phase was similar to the Federal University of Rio Grande do Sul true triaxial phase, however, without the backpressure device. Therefore, in this case it was not able to hold the backpressure constant, and only the confining pressure was incrementally increased for the Colorado School of Mines true triaxial tests. Octahedral planes (π planes) of 2,000 and 4,000 kPa were chosen (section 3.2.2.1 details it) that were achieved by manual pressure increments of 250 kPa; such pressure increments were made with Enerpac manually controlled hydraulic pumps. A resting time of 10 min was adopted between each increment.

The Colorado School of Mines true triaxial last step consisted in shearing the cubical specimen. During the shearing phase both pressure increments and decrements were conducted with the same Enerpac hydraulic pumps; for pressure decrements the hydraulic pumps were slight release util attain the desired pressure. Either stresses increments or decrements obeyed stress magnitudes of 150 kPa. A resting time of 5 min was adopted between each increment/decrement of stress. The end of the test was assumed to be when one of the following conditions were fulfilled: 1) by specimen failure; or, 2) when the minor principal stress approached to zero; the test set up was unable to apply suction on specimen's surface.

The Colorado School of Mines true triaxial main components are depicted in Figure 36. Three (3) Gefran PY2 LVDTs with 50 mm in range are used for displacement measurement; one in each specimen's loading face. Other components are three (3) Ashcroft pressure transducers responsible for measuring the X, Y and Z air-pressurized lines; all of these transducers have working pressure ranges of zero to 100 MPa. Three (3) Enerpac hydraulic jacks, which are manually controlled by three (3) hydraulic pumps. Finally, the data acquisition is made by a Keithley multichannel data acquisition (DAQ) and logging, multimeter system; this DAQ system was responsible for logging only the pressure transducer readings. The LVDTs systems were built in the present thesis, where a laptop in addition of an Arduino UNO R3 were applied for data acquisition. Moreover, a LabView based algorithm was developed and it was responsible to make the software and hardware interactions.

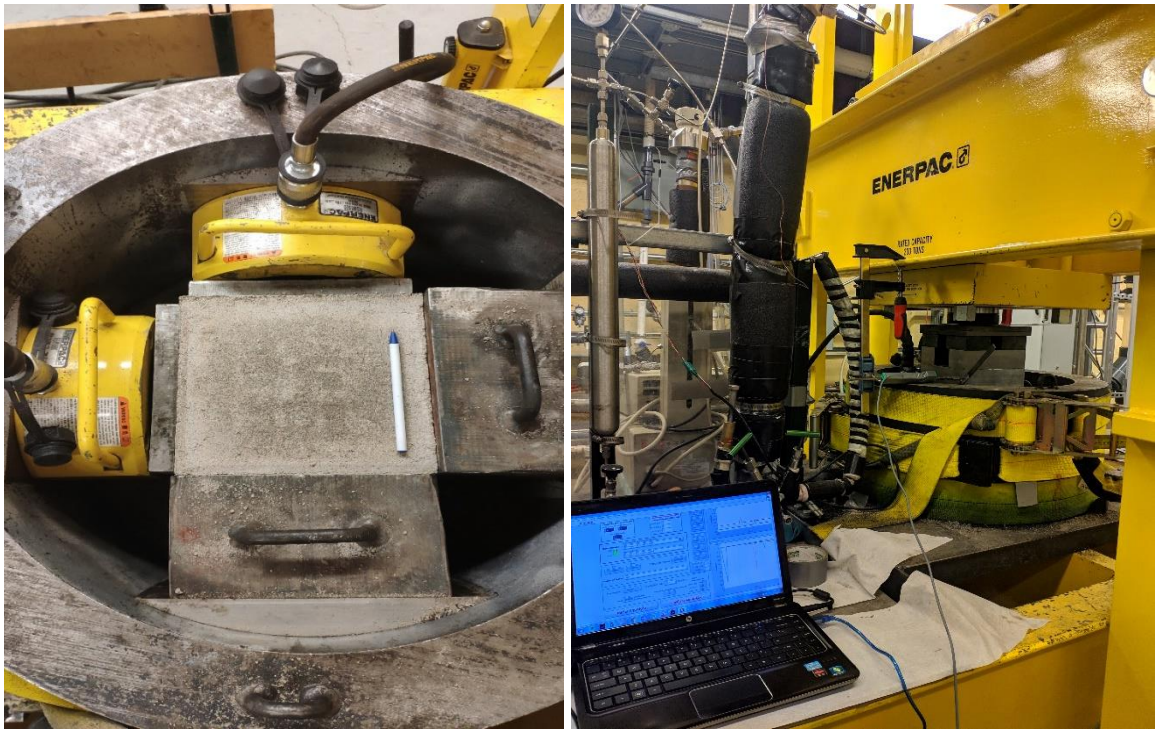

(a) (b)

(c)

Figure 36: The Colorado School of Mines true triaxial apparatus.

3.3.7 The Colorado School of Mine conventional triaxial test methods and equipment

Conventional triaxial tests were carried out on both the natural soil, ordinary sand, and in ordinary sand-OPC blends and it followed ASTM D4767 (ASTM, 2020a) and ASTM D7181 (ASTM, 2020b) test standards. In the case of ordinary sand-OPC blends, the specimens were cured for seven days, where in the 6th day the atmospheric cured samples were assembled into the triaxial chamber for CO_2 and water flushing. The 7th day was held for the saturation, consolidation, and shear phases; uncemented specimens were molded and tests carried out in the same day. Either cemented or uncemented specimens triaxial tests were conducted under effective stresses of 100, 200 and 400 kPa; the range of pressures consider the Humboldt triaxial chamber limiting conditions.

Test procedure consisted of CO_2 specimens' flushing under an effective stress of 30 kPa; a time of 15 minutes of CO_2 flushing it was assumed to be sufficient. Once the CO_2 flushing ceases, distilled water flushing started. The distilled water flux was maintained until: (i) the effluent water volume was equivalent to twice of the specimens' voids volume, or (ii) for 24 hours. The percolation phase aims to replace air bubbles that exists into the specimens' voids, and because of the cardon dioxide solubility that is great then the oxygen in water.

The saturation phase takes place by increasing simultaneously the confining and backpressure; an increasing rate of 8 kPa/min was adopted in this case. The end of the saturation phase was assumed to be when the backpressure reached a pressure magnitude of 400 kPa. The B parameter (Skempton, 1954) was determined at the end of each specimens' saturation phase; the B parameter was considered suitable for values higher than 95%.

The consolidation next phase consisted of increasing the confining pressure whereas the backpressure remained constant. For the conventional triaxial tests apprised here the confining pressure was raised to effective stresses of 100, 200 and 400 kPa depending on the test characteristics; the confining pressure was incrementally increased in steps 25 kPa, where a period of 5 min was held between each loading increment. Lastly, the shear phase comprises of specimens axial loading that occurred under a vertical displacement rate of 0.01mm/h; either drained or undrained tests followed the same displacement rate.

The Colorado School of Mines conventional triaxial main components are one (1) external LVDT with a resolution of 10 μm that was used for measuring the relative displacement between the triaxial chamber and the loading piston. Two (2) digital GDS computer-controlled pumps responsible for the tests pressure and volume control. One (1) GDS USB 8 Channel Logger (PAD) was responsible to acquire and log the tests outcomes. Figure 37a depicts the conventional triaxial framework, whereas Figure 37b shows the shear phase ending condition for a cemented specimen.

(a) (b)

Figure 37: Conventional triaxial: a) test framework; and, b) the shear phase ending condition.

4 EXPERIMENTAL TEST RESULTS

4.1 PHASE I TEST RESULTS

The Phase I of the experimental program is responsible to comprehend materials' interactions. This phase assisted the Phase II of the experimental program variables determination (see section 3.2).

Phase I test results are presented in function of porosity, cement content and the porosity/volumetric cement content index (η/C_{iv}). At the end of each presented response variable a brief statistical analysis is provided. The porosity/volumetric cement content index (η/C_{iv}) was firstly introduced by Foppa (2005) and later by Consoli et al. (2007c) and can be described as follows:

$$\frac{V_{voids}}{V_{cement}} = \frac{\frac{V_{voids}}{V_{total}}}{\frac{V_{cement}}{V_{toal}}} = \frac{\eta}{C_{iv}} \qquad \text{(Eq. 9)}$$

Where V_{voids} regards to the specimen's voids volume; V_{cement} the absolute volume cement content; and V_{total} the specimen's total volume. In (Eq. 9 (η) refers to the porosity physical index, and (C_{iv}) to the volumetric cement content. Distinct engineering properties (q_u, $E_{sec\ peak}$, q_t, G_0, among others) were empirically related to this index (*e.g.*, Consoli et al. 2007c, 2009a, 2009b, 2018a, 2018c). Furthermore, Diambra et al. (2017) theoretically explained the physical meaning backing the proposed index and concluded that the unconfined compressive strength of cement treated soils can be expressed by the following expression.

$$q_u = A \left[\frac{\eta}{C_{iv}^{\ k}}\right]^{-B} \qquad \text{(Eq. 10)}$$

Where the terms k and B are predominately related to the soils' characteristics, whereas the scalar A is associated to both soil fabric and cement matrix; the k and B terms are related by each other according to the following expression $B \approx 1/k$.

Phase I test results are presented in the sequence. Based on that and the η/C_{iv} index, hereafter considered a dosage tool, Phase II main variables will be further determined.

4.1.1 The iron ore tailing-ordinary Portland cement blends test results

I. Unconfined compressive strength (UCS) tests

The following arrangement was chosen to present test results: (i) the response variable in function of specimens' porosity; (ii) the response variable in function of ordinary Portland cement content; and (iii) the response variable in function of the porosity/volumetric cement content index (η/C_{iv}).

Figure 38 starts depicting the unconfined compressive strength (q_u) of iron ore tailing-ordinary Portland cement blends as a function of specimens' porosity. By this figure we can observe blends porosity influence on the q_u response variable, where blends' porosity decrease (*i.e.*, an increase in the dry unit weight) resulted in unconfined compressive strength gain. Consoli et al. (2007c, 2009a, 2009b, 2018a, 2018c) found identical soil behavior patterns. Such behavior occurs owing to soil voids decrease, which promotes soil grains interaction. Soil grains interaction increase results in particles interlocking and stress spreading due to external loads. Figure 38 experimental test results were mathematically fitted by a power function; the fitting equation is depicted into the figure frame.

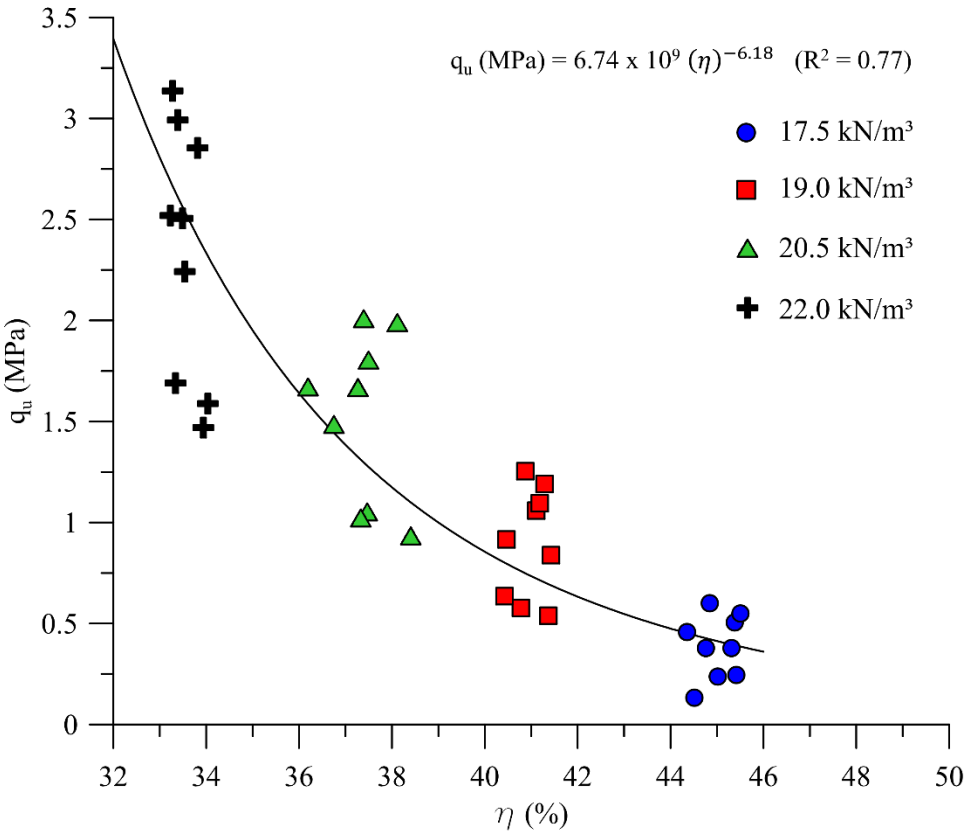

Figure 38: Iron ore tailings-ordinary Portland cement unconfined compressive strength in function of blends' porosity.

Cement content effect in q_u response variable is apprised in Figure 39. By the same figure it is also possible to indirectly detect the cement content-dry unit weight interaction. Concerning to the cement content effect, the q_u response variable increased accordingly to cement inclusion. In addition, the unconfined compressive strength linearly increased to the whole blends tested, which suggests that with further cement inclusions the q_u response variable might still increasing.

Ordinary Portland cement inclusion is responsible to (i) promote soil grains flocculation because of Ph increasing, and (ii) particles isomorphic substitutions [monovalent ions are inclined to be substituted by high valent ions like Ca^{+2} provided from cement powder (MIGUEL, 2020)]. These both reactions are responsible to decrease soil dispersion and increase soil permeability. Cement further reactions are Alite and Belite hydration, which will continuously produce C-S-H gel while the hydrated environment persists. The C-S-H gel starts to harden the soil-cement composite with strength and stiffness increase up to a

threshold; the hardening limit is when blends' Ph decreases and the hydrated environment cease.

From Figure 39 it is also possible to detect the cement content-dry unit weight interaction. The linear fit among the experimental data addresses it by the straight-lines gradient (*i.e.*, the first multiplying coefficient, see fitting equations into Figure 39). Heavily compacted specimens, namely, specimens molded with dry unit weights of 22 kN/m³, present a straight-line first multiplying coefficient of 0.353. On the other hand, lightly compacted specimens show a straight-line first multiplying coefficient of 0.086. This suggests that increasing blends' compaction degree may help to cement bonds development.

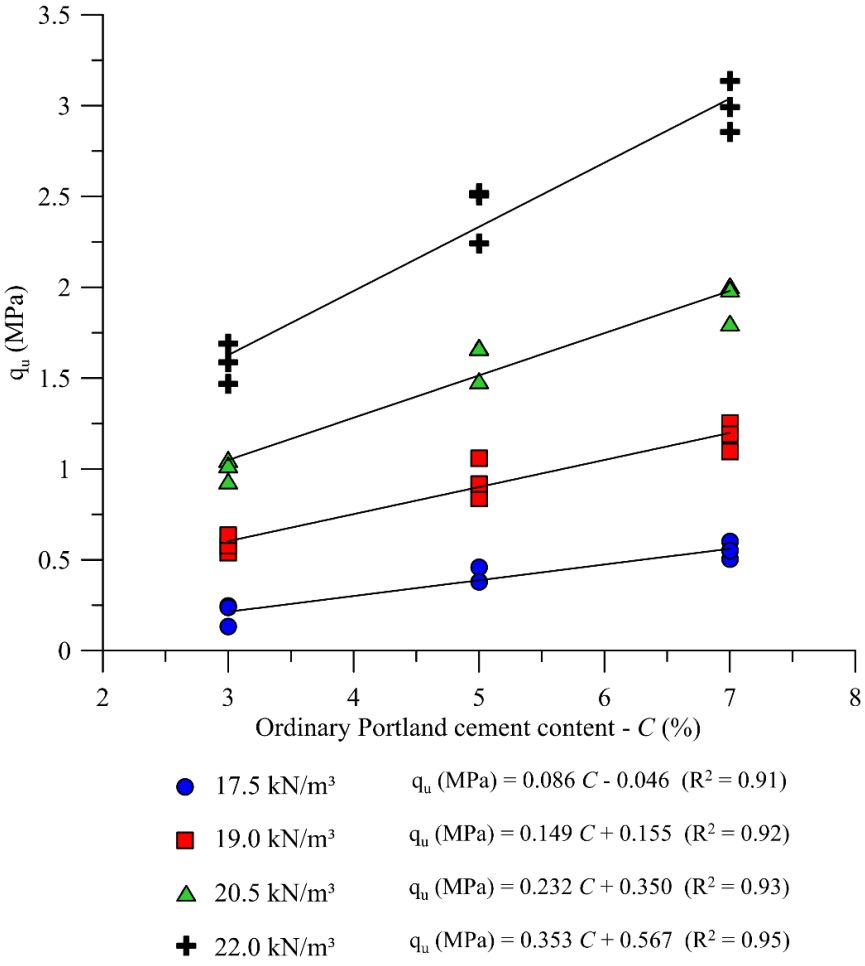

Figure 39: Iron ore tailings-ordinary Portland cement unconfined compressive strength in function of blends' cement content.

Figure 40 depicts the UCS test results in function of the porosity/volumetric cement content index (η/C_{iv}). The η/C_{iv} index joints into a single variable both blends' porosity (η - expressed by the ratio between samples' voids volume and samples' total volume) and cement content (C_{iv} - expressed by the ratio between samples' voids volume and samples' total volume) influence on the response variables. In this case, this index suggests an inversely proportional relation between both porosity and the volumetric cement content, which suggests for example that the same unconfined compressive strength can be attained by both decreasing samples' porosity (i.e., increasing the compaction degree) and cement content or, alternatively, increasing samples' porosity (i.e., decreasing the compaction degree). The η/C_{iv} versatility enables to the field engineer to choose by either increase material's compaction or increase the cement content; in general, increase material's compaction is less expensive than increase cement content.

Furthermore, it is reasonable to use porosity as a physical index to dictates the blends' behavior for granular soils, which is intimately connected with the materials' voids index. At the same pace, the volumetric cement content addresses the cement amount which was previously demonstrated to influence in the blends strength. In the present thesis a mathematical artifact was used to express the relative importance between both porosity and volumetric cement content, thence, C_{iv} portion was elevated to a power of 0.16 expressing the relative major importance of porosity compared to the volumetric cement content. Therefore, in line with Diambra et al. (2017) the external exponent was determined in accordance with the $B \approx 1/k$ relation, namely, $B \approx 1/0.16 \approx 6.25$.

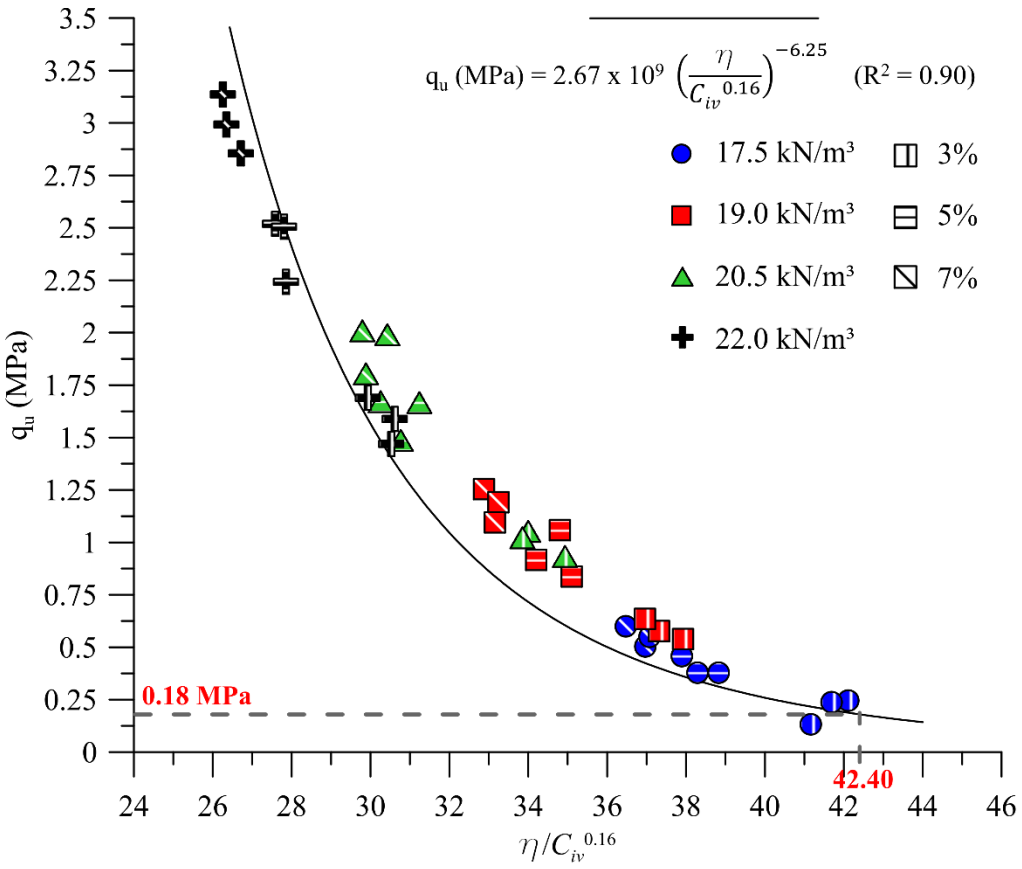

Figure 40: Iron ore tailings-ordinary Portland cement unconfined compressive strength in function of the porosity/volumetric cement content index ($\eta/C_{iv}^{0.16}$).

Even though the great number of variable levels, four dry unit weights and three cement contents, the power function fits well to the experimental data where a coefficient of determination (R^2) of 0.90 is achieved. A general equation opens the possibility to opt among cement content and dry unit weight combinations in order to achieve the desired blends strength. Therefore, the porosity/volumetric cement content settled on the power function proposed turns into a dosage tool for the materials apprised here.

The dashed line inserted into the Figure 40 regards to the Federal University of Rio Grande do Sul true triaxial limiting condition, namely, a specimens' unconfined compression strength of 0.18 MPa. Section 1.6 details such physical limiting condition; the same dashed line links the 0.18 MPa strength to its respective $\eta/C_{iv}^{0.16}$ value of 42.20. Thence, in order to fulfill the Federal University of Rio Grande do Sul equipment restrictions a $\eta/C_{iv}^{0.16}$ = 42.40 was chosen to carry out the Phase II – Advanced tests. Phase II detailed aspects are discussed in section 660.

Figure 41 presents the statistical analysis of UCS test results. The statistical analysis is presented (i) by means a line scatter plot of the first order main effects (Figure 41a), and (ii) by the standardized effects Pareto's chart (Figure 41b). The first order main effects line scatter plot is the most effective way to display independent variables impact on test results; in this plot the solid line means response variables average test results.

Pareto's chart is a useful manner to exhibit controlled factors statistical significance, where each chart bar refers to a controlled factor. If the factor standardized effect crosses the dashed line, then the parameter is considered statistically significant to the significance level (α) adopted. The dashed line is known as the quantile (1 - α/2) in the Student's t-distribution and depends of α; for this study the α value adopted is 5%. An α = 5% means that there is 5% of chance of the conclusions presented here to be wrong. In this chart the controlled factors are referred as letters like (A) cement content and (B) dry unit weight.

Figure 41a restates which was previous concluded, namely, the act of increasing either cement content or compaction degree results in unconfined compression increase. Figure 41b shows the Pareto's chart where both cement content and dry unit weight variables are statistically significant and are able to promote changes on the q_u response variable; both cement content and dry unit weight appeared to have the same standardized effect on this response variable (bar length/magnitude). Cement content and dry unit weight interaction is also statistically significant, which supports the η/C_{iv} relationship to predict/dosage blends unconfined compressive strength.

The dry unit weight and cement content impact on unconfined compressive strength regards to great particles interaction and cementitious compounds precipitation respectively. Besides Alite and Belite hydration, pozzolanic reactions also occur between free calcium hydroxides and the existing clay minerals (Thompson, 1966); this kind of reactions require long periods to be developed (Consoli et al. 2009e; 2018c; 2019d).

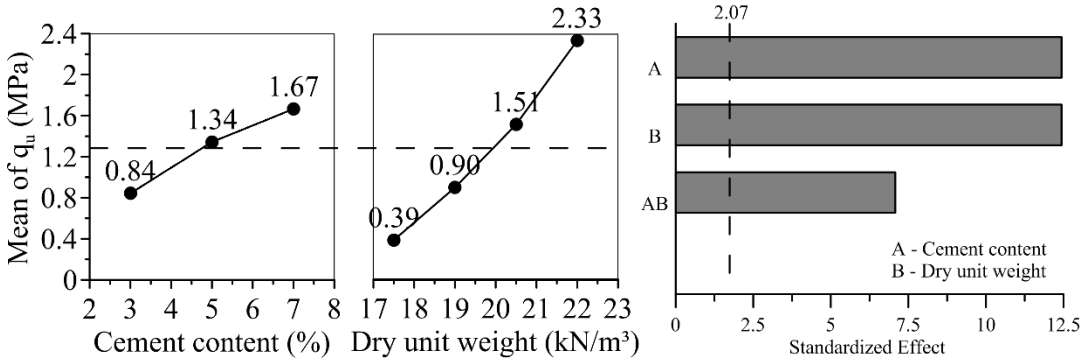

(a) (b)

Figure 41: Unconfined compressive strength statistical analysis.

II. Specimens' secant Young Modulus ($E_{sec\ peak}$)

The previous presentation pattern of the unconfined compressive strength test results was extended here for specimens' stiffness. Specimens' stiffness here apprised by the Young modulus was determined by the ratio between the peak unconfined compressive strength and its corresponding strain. It is worth mentioning that the $E_{sec\ peak}$ variable apprised in the sequence regards to a qualitative outcome once specimens' axial strains were not directly measured on the specimens' surface. The specimens' stiffness was indeed estimated according to specimens' time to failure; the UCS tests were conducted at a strain rate of 1.4 mm/min.

Comparable unconfined compressive strength conclusions can be extended to specimens' Young modulus. For instance, specimens' stiffness increased with porosity decrease and cement content increase, these both patterns are depicted in Figure 42 and Figure 43. In terms of voids decrease impact, specimens' stiffness increased due to compaction promotes particles interaction.

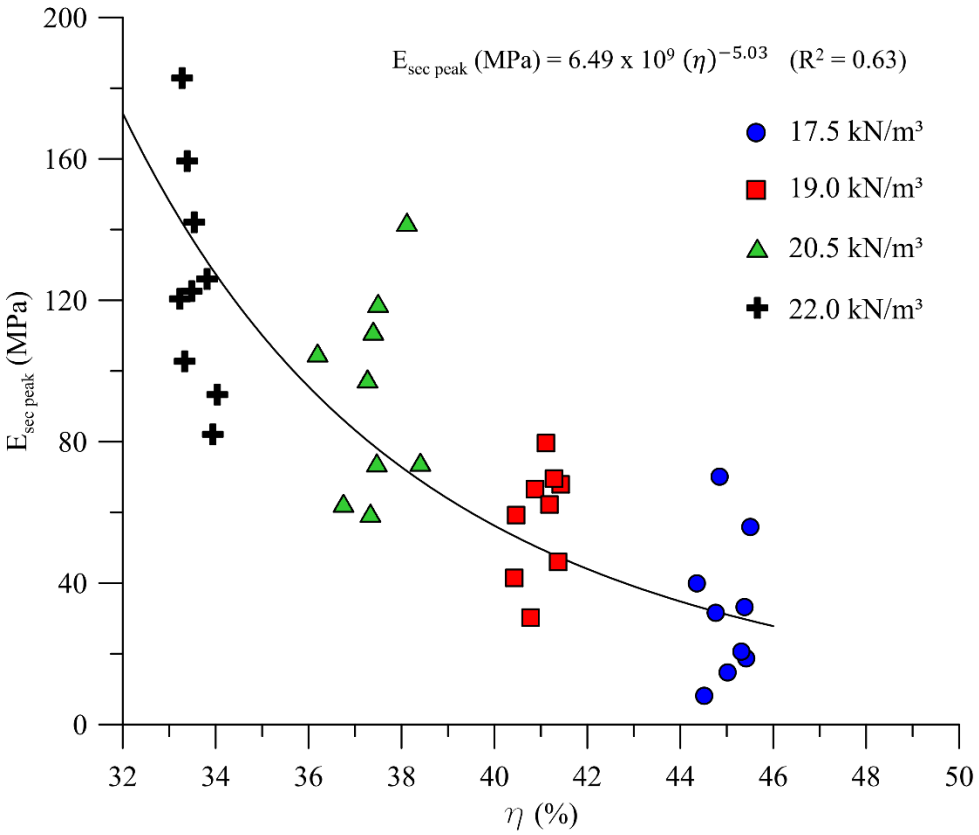

Figure 42: Iron ore tailings-ordinary Portland cement Young modulus in function of blends' porosity.

Accordingly, the ordinary Portland cement inclusion linearly contributed to specimens' stiffness growth. In spite of the scattered data observed in 19 kN/m³ samples (the red-square boxes), the Young modulus appear not to be greatly influenced by a cement-dry unit weight interaction; this is stated because of the lines parallelism. This statement is further proven by the statistical analysis presented in Figure 45b. Soil compaction clearly improved specimens' stiffness, however, it did not boost stiffness with cement inclusion (the fitted line did not turned stepper increasing soil compaction). Specimens' stiffness increased because of cement hydration (hardening) and voids filling (filler effect).

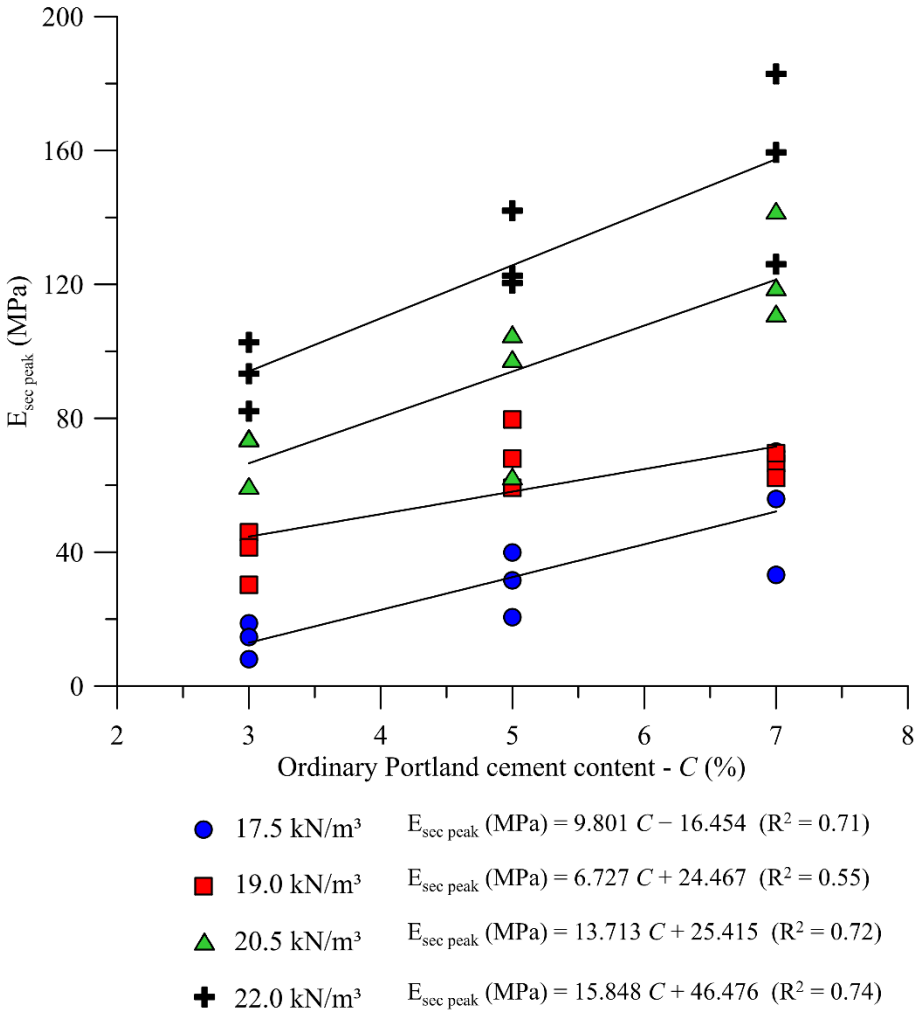

Figure 43: Iron ore tailings-ordinary Portland cement Young modulus in function of blends' cement content.

As previously demonstrated, both porosity (dry unit weight) and cement content exerted influence on specimens' stiffness. Therefore, it makes sense to adjust Young modulus experimental data to the porosity/volumetric cement content index as well. Figure 44 shows specimens' Young modulus in function of the $\eta/C_{iv}^{0.16}$ index. A power function was fitted to the experimental data outcoming a coefficient of determination of R^2 = 0.82, this mathematical adjustment allows to achieve the same specimens' stiffness by either changing specimens' porosity or cement content.

Figure 45 depicts specimens' stiffness statistical analysis and restates which was previously discussed; cement content-dry unit weight [AB] interaction is not statistically significant confirming the Figure 43 previous conclusion.

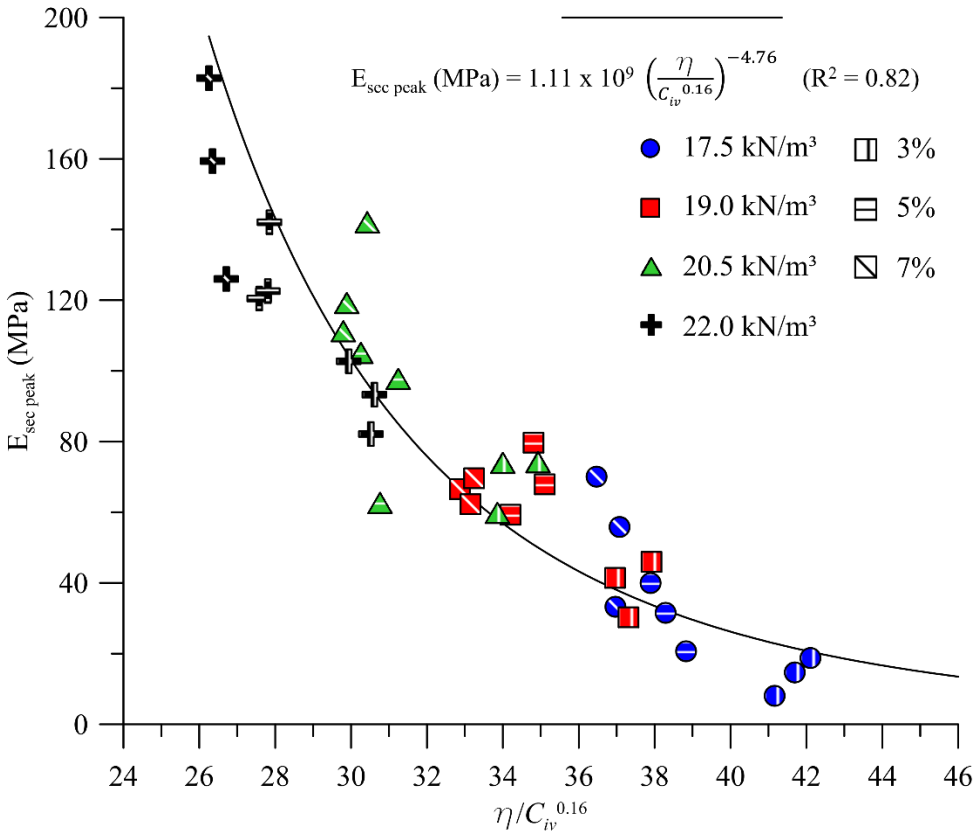

Figure 44: Iron ore tailings-ordinary Portland cement Young modulus in function of the porosity/volumetric cement content index ($\eta/C_{iv}^{0.16}$).

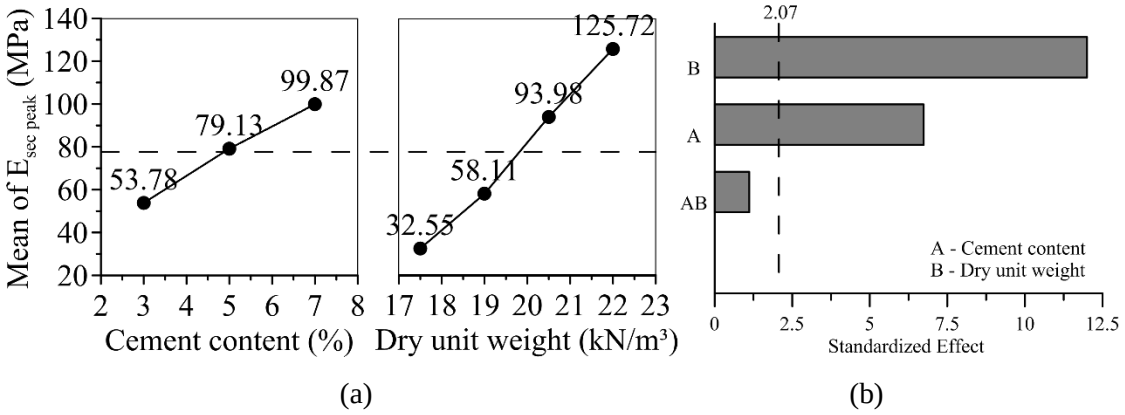

Figure 45: Young modulus statistical analysis.

III. Unconfined tensile strength (UTS) tests

This item presents the unconfined tensile strength test results (UTS or q_t). The same trends observed for q_u and $E_{sec\ peak}$ were appraised here for q_t response variable. Figure 46 portrays the porosity impact in blends tensile strengths, where blends' porosity increase led to blends' tensile strength decrease.

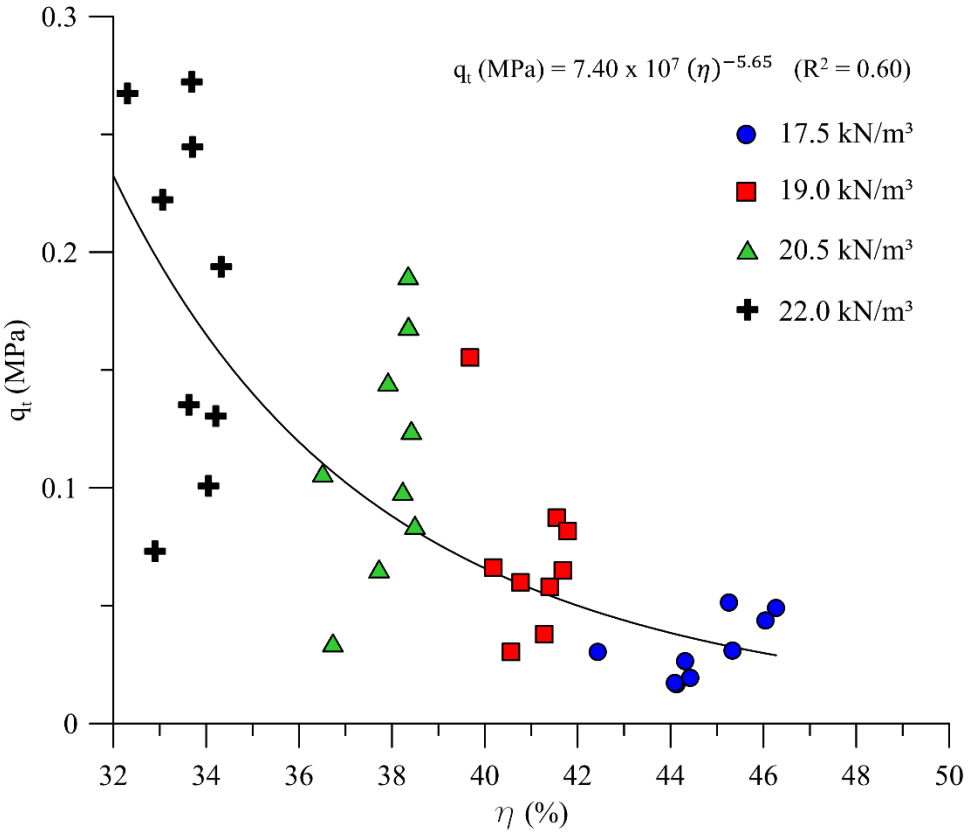

Figure 46: Iron ore tailings-ordinary Portland cement unconfined tensile strength in function of blends' porosity.

Figure 47 reports the cement content effect in blends' tensile strength, which it resembles the effect produced on q_u response variable. That is, specimens' tensile strength linearly increased with cement content growth; the q_u and q_t linear trend was already reported by other authors like Consoli et al. 2007c. Figure 47 suggests the existence of an interaction between cement content and blends' dry unit weight. Nonetheless, this assertion is not supported by the statistical analysis provided (Figure 49b).

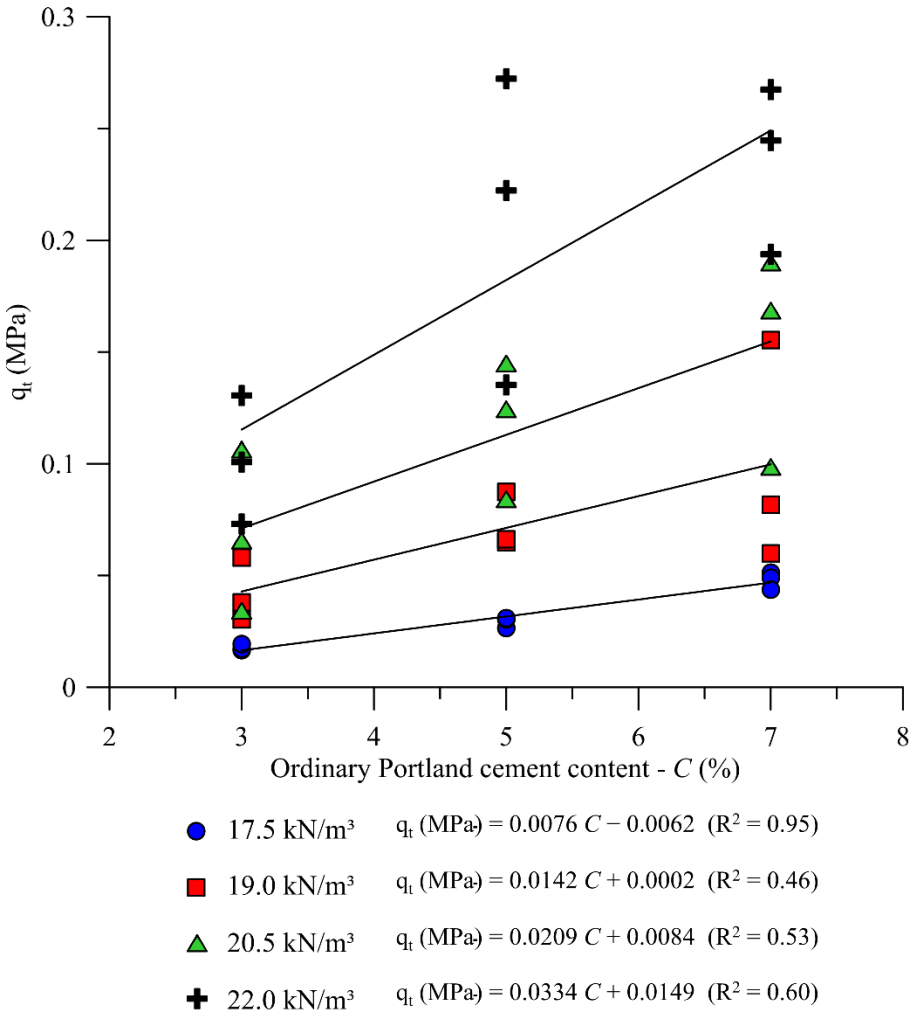

Figure 47: Iron ore tailings-ordinary Portland cement unconfined tensile strength in function of blends' cement content.

Figure 48 shows the q_t response variable in function of the the $\eta/C_{iv}^{0.16}$ index. Even though the scattered data, which might be addressed to the test methodology, a good coefficient of determination ($R^2 = 0.74$) is attained.

The $\eta/C_{iv}^{0.16}$ index assists in determining the ratio between specimens' tensile and compressive strengths even though a wide range of dry unit weights and cement contents were tested. The q_t/q_u ratio is achieved by dividing both power functions apprised in Figure 52 and Figure 29; this relation is useful in modelling and failure criterion strength estimation. The actual thesis q_t/q_u ratio for iron ore tailing-ordinary Portland cement blends is 0.08, which states a relation between blends' tensile and compressive strengths allowing their estimative thence, a straight relation can be stated between the UCS and UTV test results in other words,

tone by another. Other authors report q_t/q_u ratios ranging between 0.10 and 0.20 like Consoli et al. 2010b, 2014; Silvani 2013; Pasche 2016 and Godoy 2018. Corte (2020) reported an equal value of 0.08 to cemented treated Hostun sand specimens.

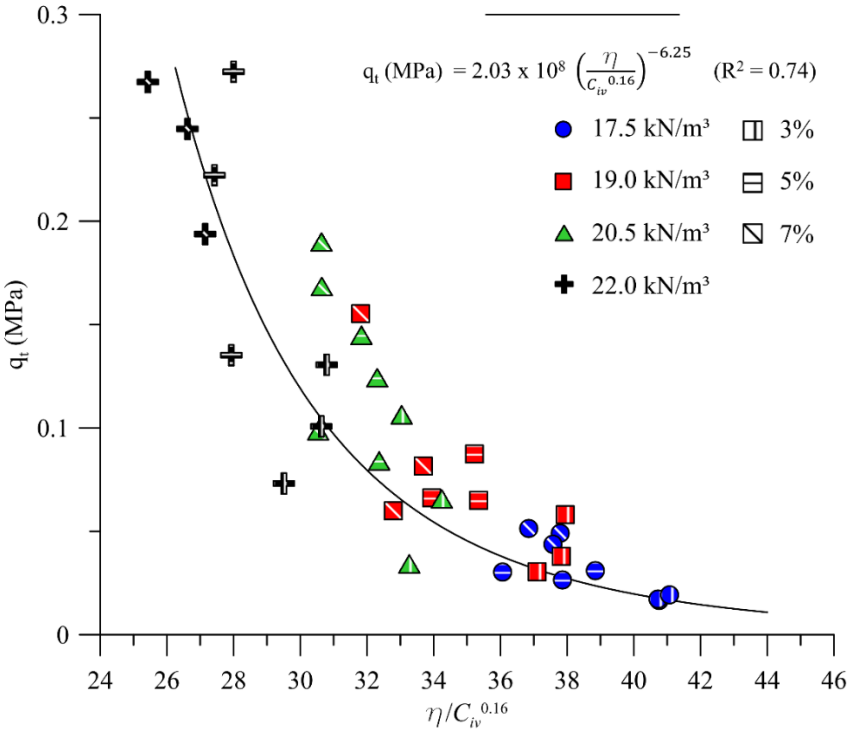

Figure 48: Iron ore tailings-ordinary Portland cement unconfined tensile strength in function of the porosity/volumetric cement content index ($\eta/C_{iv}^{0.16}$).

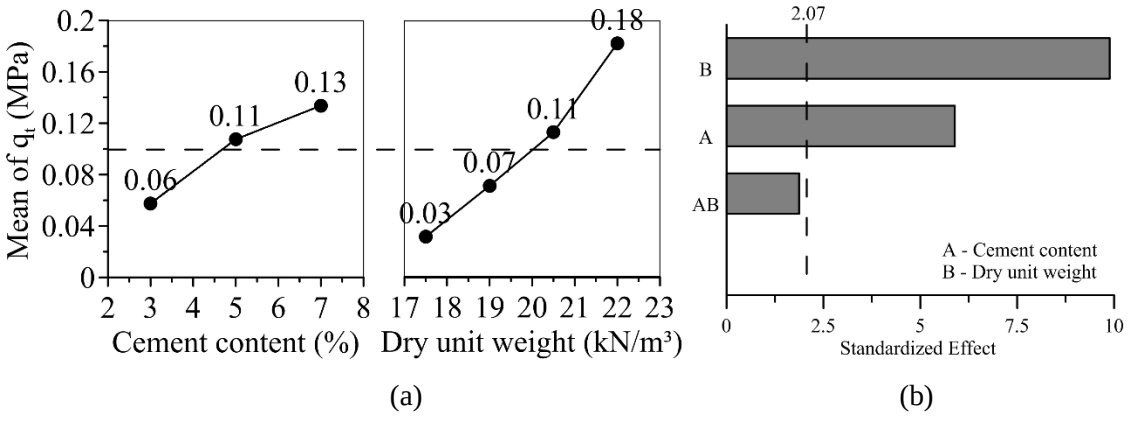

Figure 49: Unconfined tensile strength statistical analysis.

IV. Ultrasonic pulse velocity tests (UPV) tests

The initial shear modulus (G_0) was assessed by means ultrasonic pulse velocity tests; these are described in section 3.3.4. The ultrasonic pulse velocity test outcomes the shear wave time travel (t_s) throughout specimens' length, which it is measured by two transducers coupled on each opposite specimens' surface. Once specimens' lengths are known, the shear wave velocity (V_s) can be determined. Thus, the initial shear modulus is estimated by means (Eq. 11), where ρ regards to the material's density. It is worth mentioning that (Eq. 11) is only valid for an elastic, continuum, homogenous and isotropic media (SANTAMARINA *et al.* 2001; BORTOLOTTO, 2017); this last condition is partially ignored, once iron ore tailing-OPC blends cannot be considered continuum, homogeneous nor an isotropic media, thence, the G_0 presented here regards to an approximation.

$$G_0 = \rho \, .V_s^2 \qquad \text{(Eq. 11)}$$

Figure 50 presents the small strain stiffness of the iron ore tailings-OPC bends in function of blends' porosity. The pattern observed for the G_0 response variable looks like which it was previously seen for the Young modulus. That is, the G_0 decreases by increasing blends' porosity. The shear wave does not travel through water and air, thence, voids increase tends to difficult the shear wave propagation and then decrease specimens' stiffness; specimens' stiffness is also decreased because of the soil particles are moved away one another. Following the procedure already stated, a power function fits the experimental data. Consoli et al. (2020a) reports a leftward threshold behavior for power function adjustments, namely, the threshold behavior would occur for the lowest specimens' porosity as possible (*i.e.*, the specimens' minimum void ratio); it suggests that, if it would be possible to increase blends' compaction degree (which it is not expected, once specimens' are already in a compaction degree of 100%), it would not have impact on G_0. This limiting threshold is not clear in the present thesis test results, more compacted specimens should be tested in order to check this assertion.

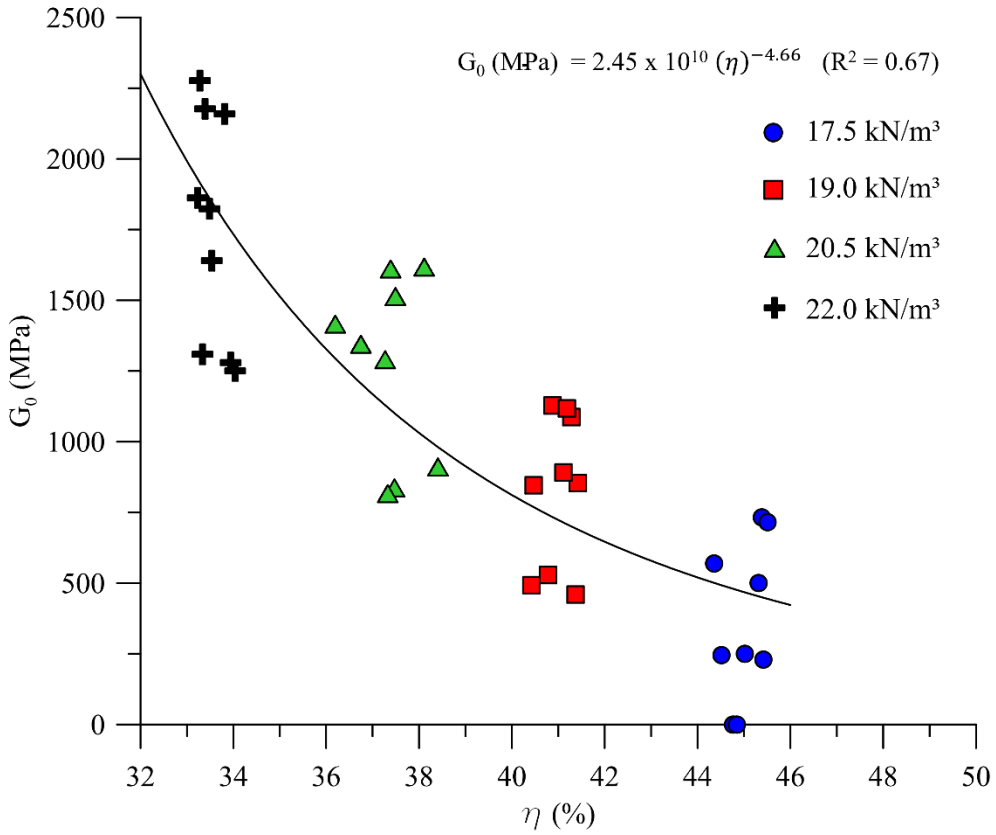

Figure 50: Iron ore tailings-ordinary Portland cement initial shear modulus in function of blends' porosity.

Figure 51 exhibits the cement content effect on G_0, where a proportional linear trend is noticed. The G_0 small strain stiffness seems to differ from the Young modulus large strain stiffness. Accordingly to Figure 51, the former seems to be affected by the interaction between specimens' cement content and porosity; this will be further validated by the statistical analysis. Cementitious compounds precipitation (*e.g.*, C-S-H gel) help in voids occupation which must enlarge particles interaction and promote the initial stiffness increase; this eventual 'continuous' media promoted by cementitious compounds precipitation is broken at large strains, which might explain the interaction between specimens' cement content and porosity not to be statistically significant in the case of the samples Young modulus. Figure 53 confirm the hypothesis previously rose by means the statistical analysis.

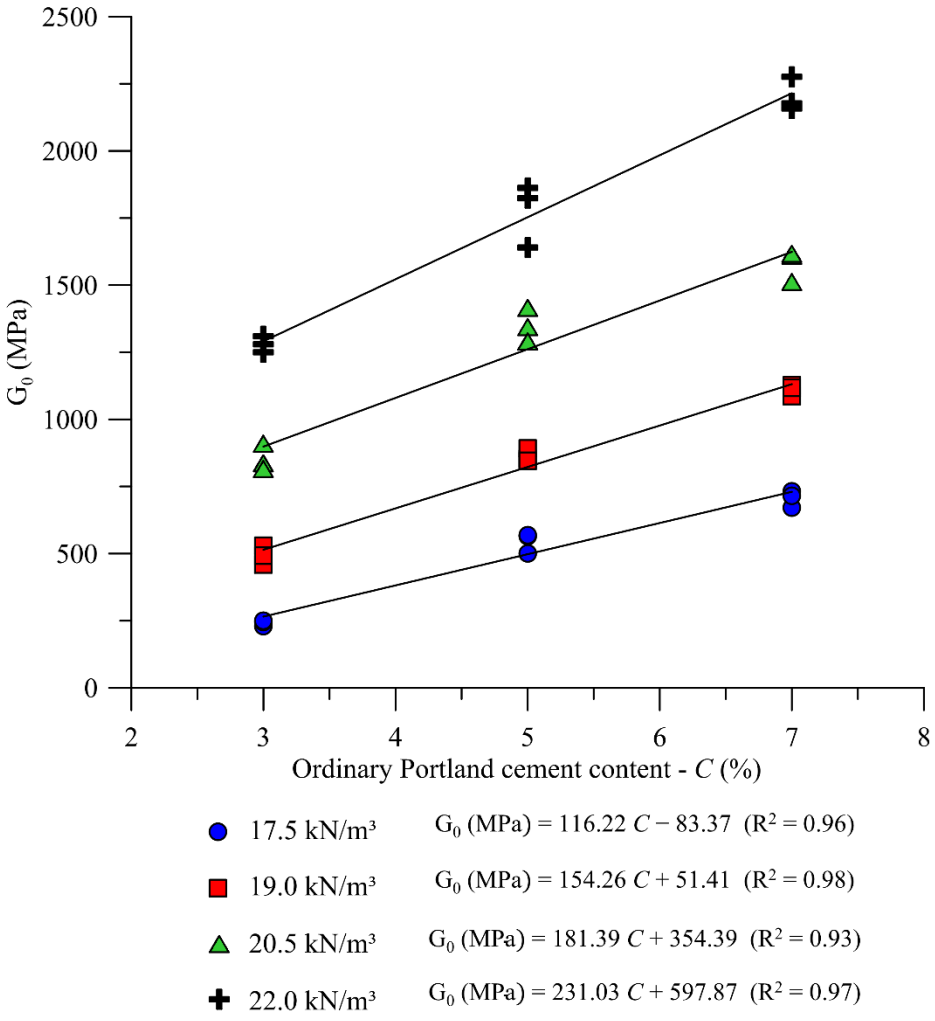

Figure 51: Iron ore tailings-ordinary Portland cement initial shear modulus in function of blends' cement content.

Figure 52 combines the cement and porosity effect on blends G_0 by means the $\eta/C_{iv}^{0.16}$ index. It is highlightable the coefficient of determination of $R^2 = 0.90$ which it is achieved after the $\eta/C_{iv}^{0.16}$ index usage; $\eta/C_{iv}^{0.16}$ index was able to suppress the experimental data scattering. Small strain stiffness can be increased by either increasing blends' compaction degree or blends' OPC content.

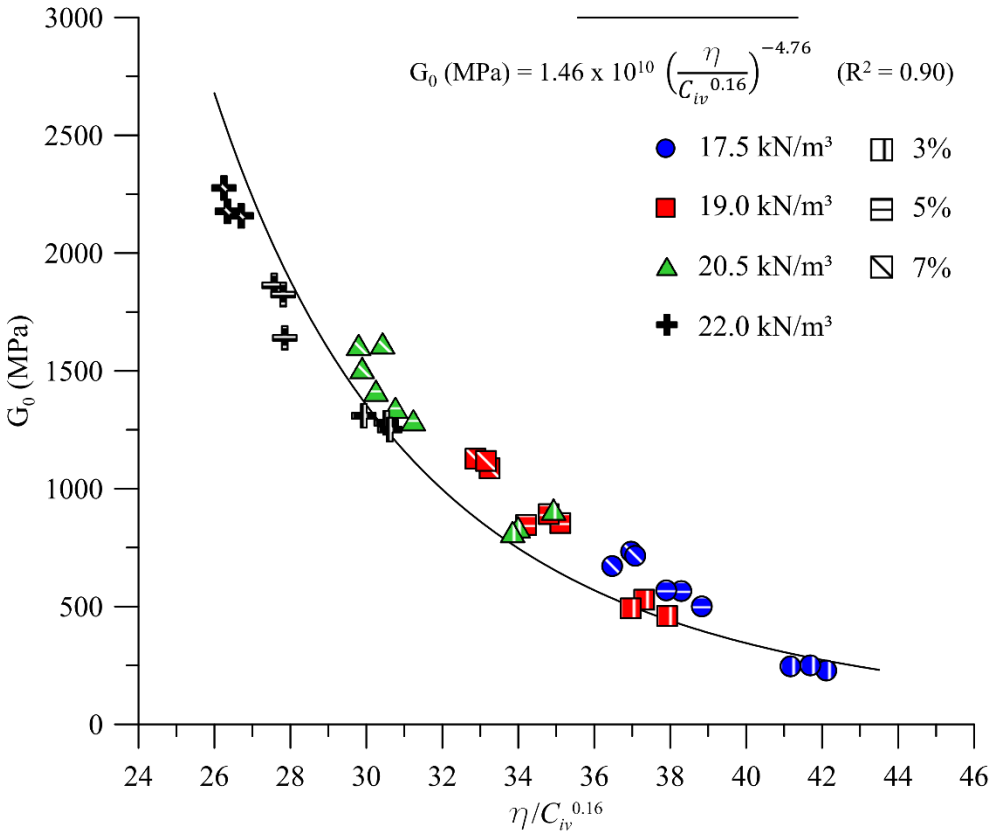

Figure 52: Iron ore tailings-ordinary Portland cement initial shear modulus in function of the porosity/volumetric cement content index ($\eta/C_{iv}^{0.16}$).

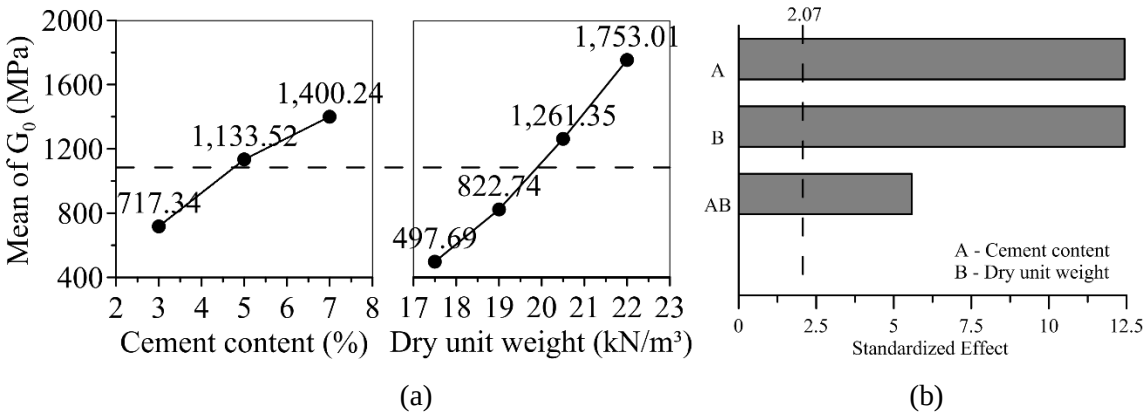

Figure 53: Initial shear modulus statistical analysis.

4.1.2 The ordinary sand-ordinary Portland cement blends test results

I. Unconfined compressive strength (UCS) tests

This section is responsible for presenting the ordinary sand-ordinary Portland cement blends test results. The same pattern previous adopted for showing the iron ore tailing-ordinary Portland cement blends test results is replicated here.

Figure 54 depicts the q_u response variable in function of porosity where the same conclusions addressed for the iron ore tailing-ordinary Portland cement blends can be restated here. Like, the unconfined compressive strength increased as much compaction was applied. Also, the porosity variable seems not to be the best variable to express q_u response variable due to the scattered data and low coefficient of determination. This problem overcome by the η/C_{iv} index adoption.

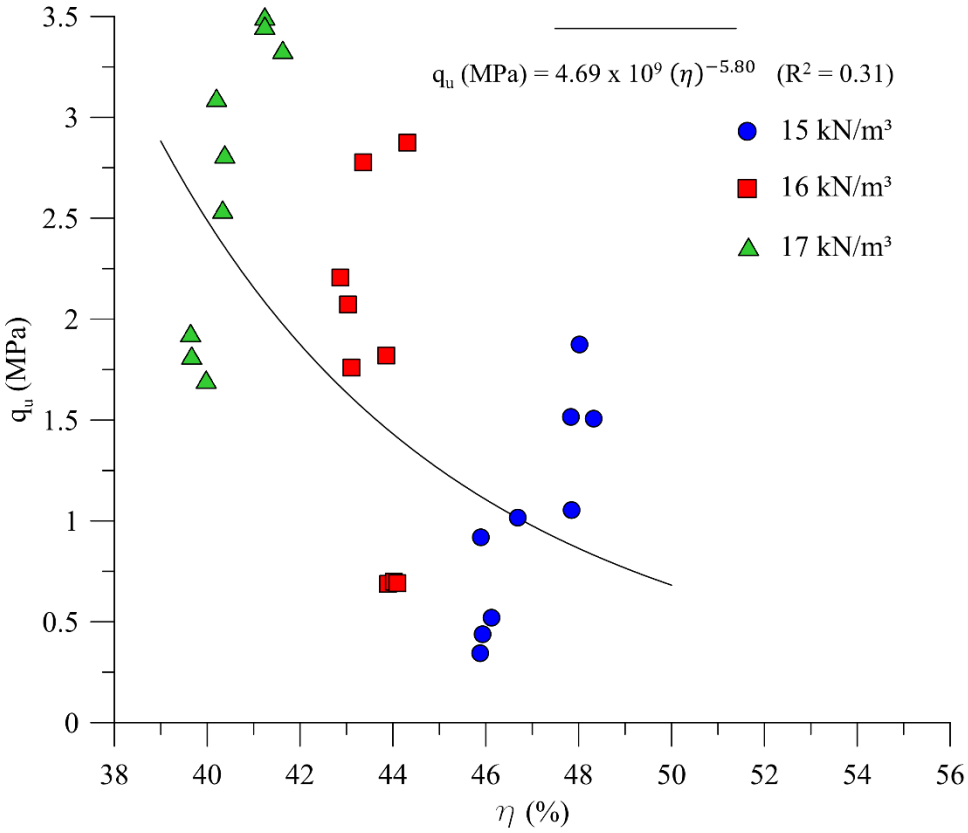

Figure 54: Ordinary sand-ordinary Portland cement unconfined compressive strength in function of blends' porosity.

Figure 55 and Figure 56 present both the cement content effect and the η/C_{iv} index normalization for the q_u response variable. The cement content effect also linearly impacts the response variable as previously seen for the other soil matrix. By the Figure 55, it is not clear whether the dry unit weight might boost the cementing phase creation; it is further clarified by the statistical analysis. Figure 56 displays all the unconfined strength test results normalized by the η/C_{iv} index, where a power function is adjusted to the test data; a very high coefficient of determination is achieved for this soil matrix.

Also, into Figure 56 a dashed line depicts the unconfined compression strength of 3.5 MPa, which was adopted as strength target for the Colorado School of Mines true triaxial specimens of Phase II; the dashed line links the 3.5 MPa strength to its respective $\eta/C_{iv}^{0.16}$ value of 30.28. Curiously, the same exponent of 0.16 applied on C_{iv} of the iron ore tailing matrix could be replicated here for the ordinary sand matrix. Diambra et al. (2017) suggests that this exponent is associated with soil characteristics, even though the difference between the matrices used here, the 0.16 exponent value fits well for both of them.

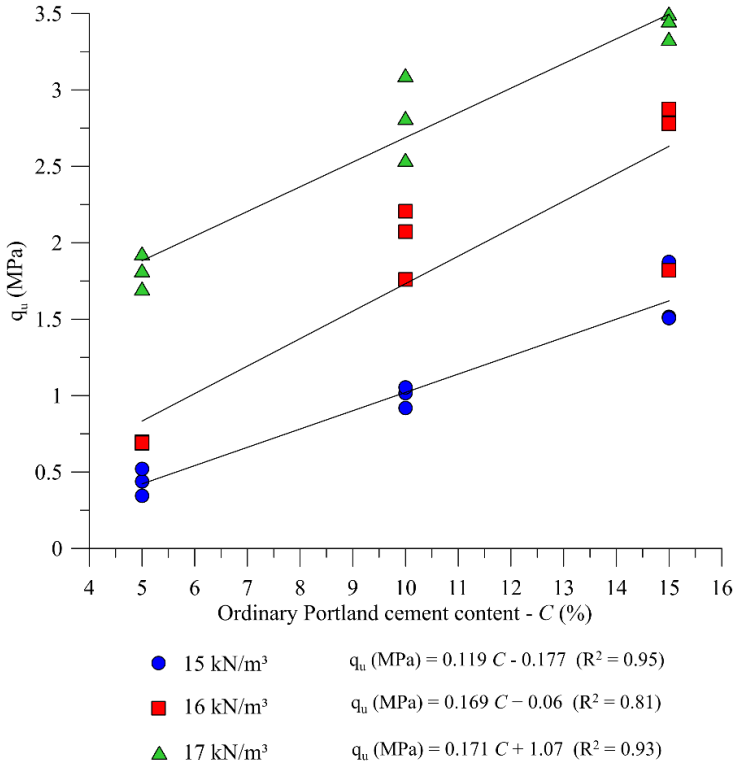

Figure 55: Ordinary sand-ordinary Portland cement unconfined compressive strength in function of blends' cement content.

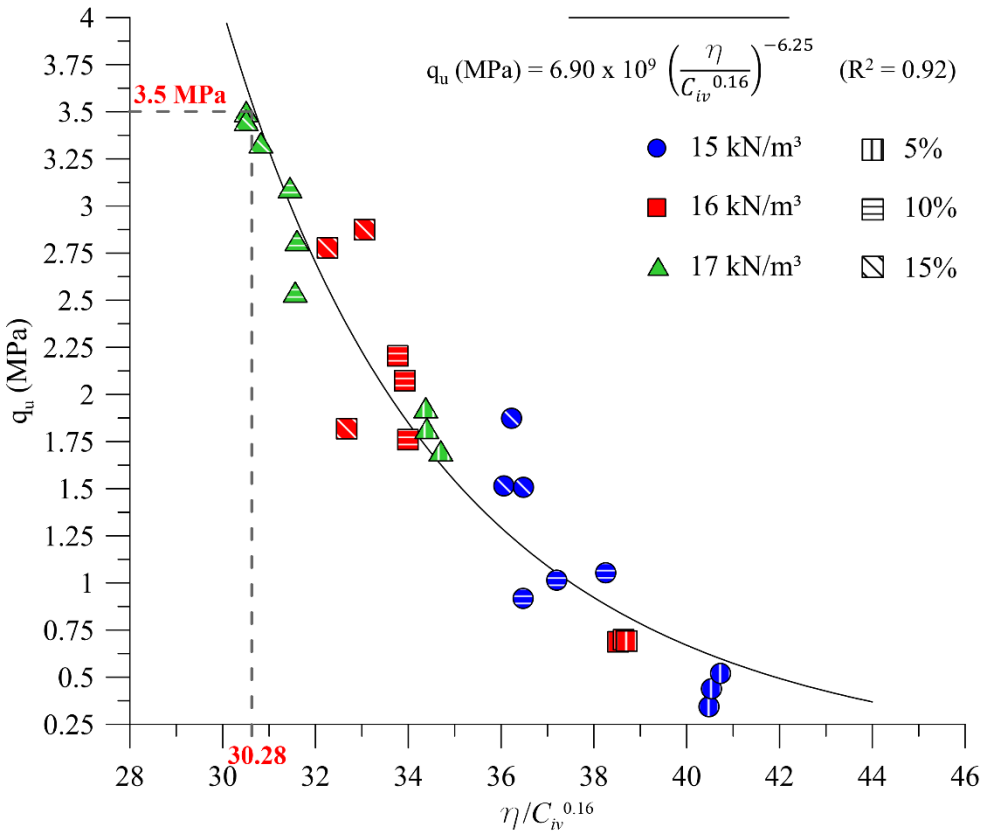

Figure 56: Ordinary sand-ordinary Portland cement unconfined compressive strength in function of the porosity/volumetric cement content index ($\eta/C_{iv}^{0.16}$).

Figure 57 presents the statistical analysis of UCS test results for the ordinary sand-ordinary Portland cement blends. In the case of the ordinary sand matrix and its unconfined compression strength, the frictional strength overcame the strength provided by cementitious compounds precipitation; it reassures the η/C_{iv} index and the exponent of k = 0.16 set to reduce the C_{iv} portion. The dry unit weight-cement content interaction is not statistically significant for this soil matrix.

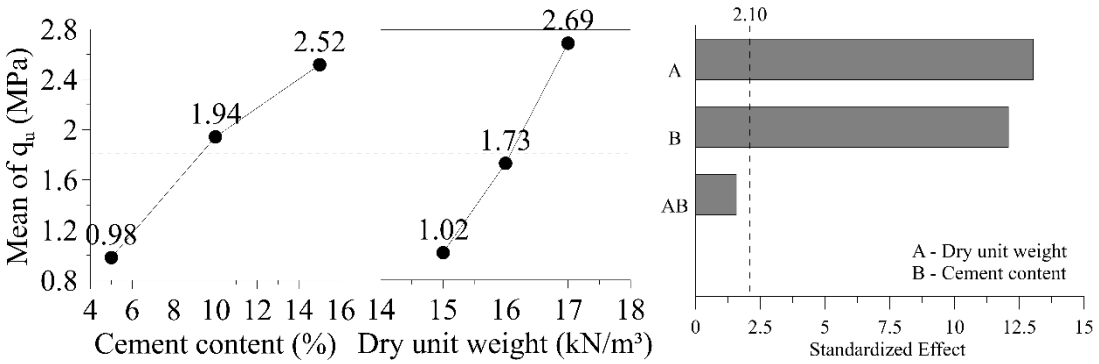

(a) (b)

Figure 57: Unconfined compressive strength statistical analysis.

II. Specimens' secant Young Modulus ($E_{sec\ peak}$)

Figure 58 depicts the large strain stiffness of ordinary sand-ordinary Portland cement blends in function of specimens' porosity, whereas Figure 59 apprises the cement content effect on the same response variable and soil matrix. The trends massively discussed in the previous paragraphs reoccur here for both independent variables-controlled factors, namely, the porosity decrease and cement content increase contributed to specimens stiffness growth.

Specimens' porosity seemingly to be a secondary effect on specimens' stiffness, which it is inferred by Figure 58 and its light impact on $E_{sec\ peak}$ response variable. On the other hand, the cement content increases huge influenced specimens' stiffness, this controlled variable increase rose three times specimens stiffness in some cases.

Such assertions are supported by the statistical analysis which is shown in Figure 61b. Figure 60 depicts the large strain stiffness in function of the η/C_{iv} index where the k exponent preserved. In addition to the η/C_{iv} index joins porosity and cement content into a single parameter, it also helps in suppressing the scatter observed like in Figure 58 where only the porosity variable is apprised.

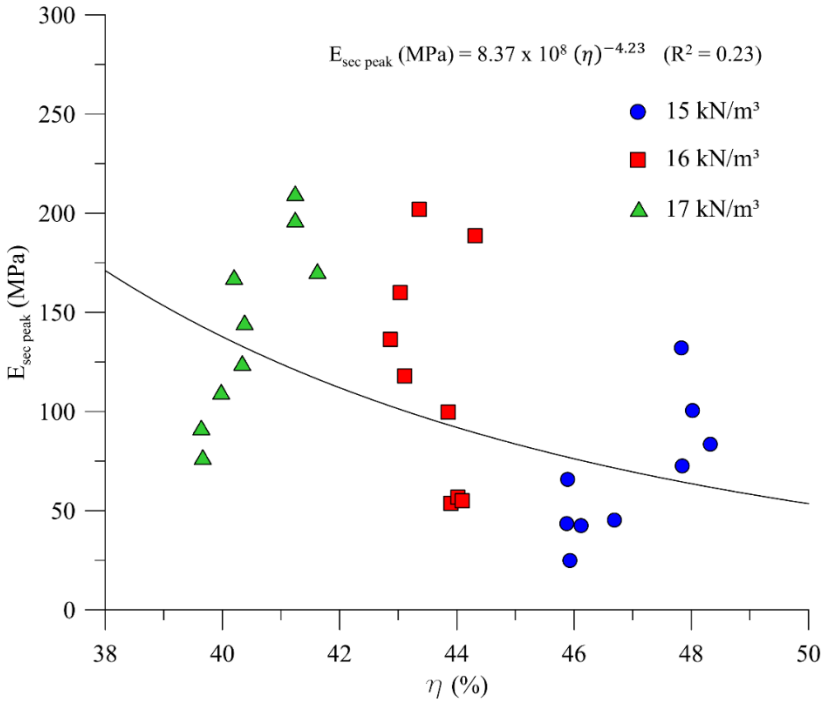

Figure 58: Ordinary sand-ordinary Portland cement Young modulus in function of blends' porosity.

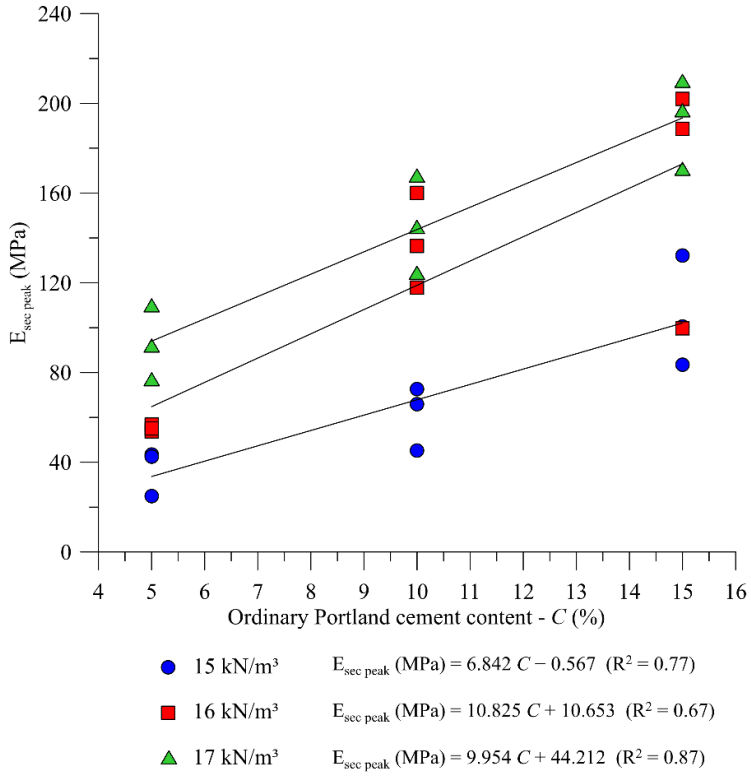

Figure 59: Ordinary sand-ordinary Portland cement Young modulus in function of blends' cement content.

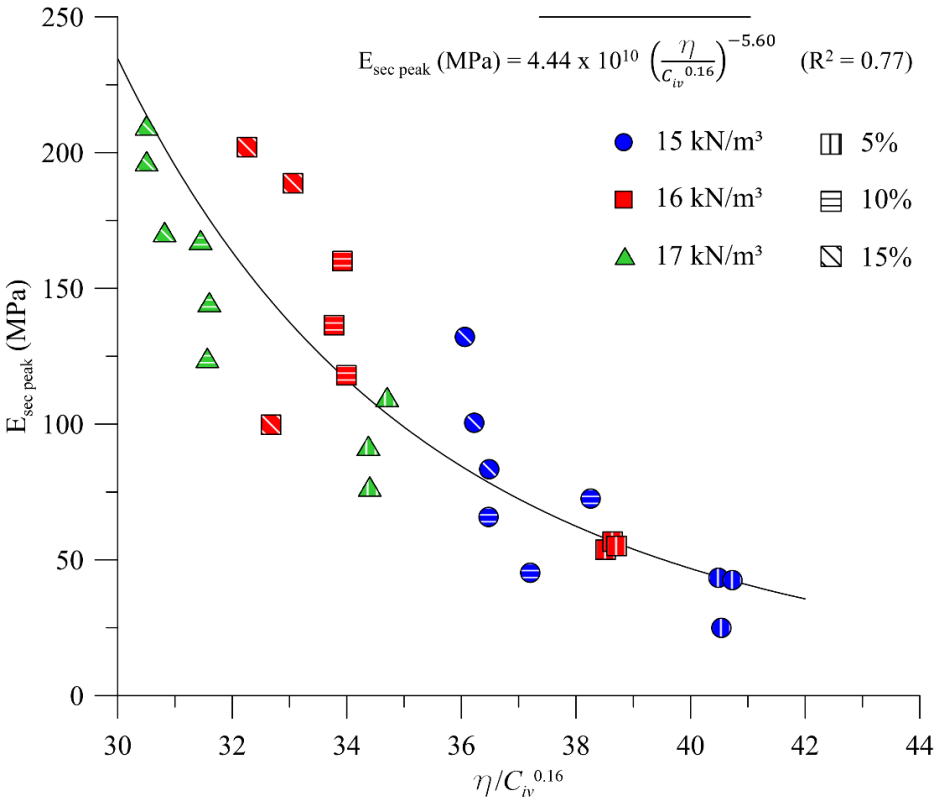

Figure 60: Ordinary sand-ordinary Portland cement unconfined compressive strength in function of the porosity/volumetric cement content index ($\eta/C_{iv}^{0.16}$).

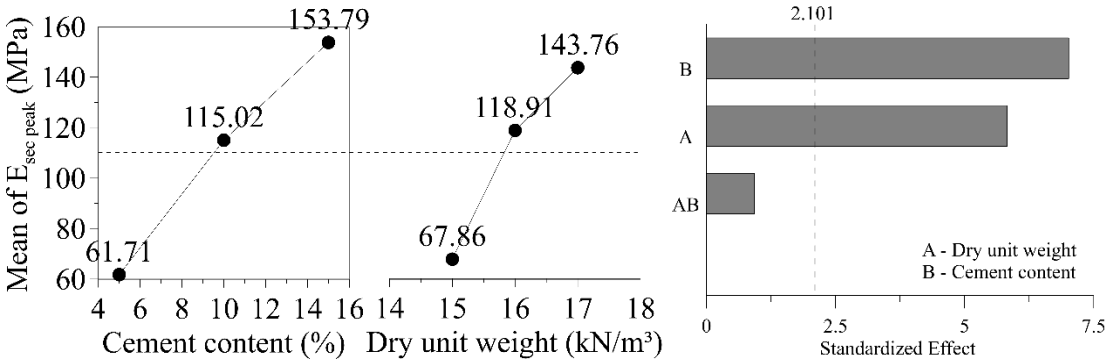

(a) (b)

Figure 61: Young modulus statistical analysis.

4.1.3 Phase I test results summary

The $\eta/C_{iv}^{0.16}$ index demonstrated to be a useful dosage tool for a huge number of engineering properties.

A single impacting pattern was seen for both the dry unit weight and cement content controlled factors, namely, by means decreasing specimens' porosity and increasing the cement content, specimens' obtained both strength and stiffness mechanical properties improvement; the dry unit weight (porosity) impact on specimens' engineering properties is described by a power function, whereas the cement content linearly impacted the same properties for all of the soil matrices and response variables. Properties improvement is due to compaction degree and cement content increase which promotes, in this sequence, particles interaction and samples hardening.

The dry unit weight (porosity) demonstrated to have relative major importance compared to volumetric cement content, which is expressed by the 0.16 exponent applied to the C_{iv} variable. The Young modulus, *i.e.*, the large strain stiffness, is not impacted by the dry unit weight-cement content interaction. On the other hand, this interaction is statistically significant for small strain stiffness (G_0).

Accordingly, once the $\eta/C_{iv}^{0.16}$ index works for the whole response variables apprised here, thus, it will be further applied as a dosage methodology in the Phase II – Advanced tests.

4.2 PHASE II TEST RESULTS

4.2.1 The iron ore tailing-ordinary Portland cement blends test results

This section discuss the iron ore tailing-ordinary Portland cement blends true triaxial test results. Figure 62 to Figure 67 present the deviatoric stress *Vs.* deviatoric strain and deviatoric strain *Vs.* volumetric strain of iron ore tailing-OPC blends tested on *b* values of $b = 0$, 0.5 and 1 respectively; the respective loading θ angle is inserted into each figure. Figure 62a to Figure 67a include the untreated matrix specimens (i.e., pure iron ore tailing specimens), whereas Figure 62b to Figure 67b emphasize on treated matrix specimens (i.e., iron ore tailing-OPC blends). This differentiation is necessary to avoid data misinterpretation, untreated matrix specimens outcome greater strains magnitudes than the treated matrix specimens; this fact impacts on X-axes scales and it may lead to data miscomprehension.

Figure 62 depicts the stress *Vs.* strain behavior of $b = 0$ tested specimens. The ordinary Portland cement benefits are clearly seen in Figure 62a, where the OPC treated specimens accounted for greater strengths and stiffnesses than untreated specimens; in this case, the maximum shear strength observed was adopted as the peak strength. Test interruptions occurred because of the Federal University of Rio Grande do Sul true triaxial main limitations.

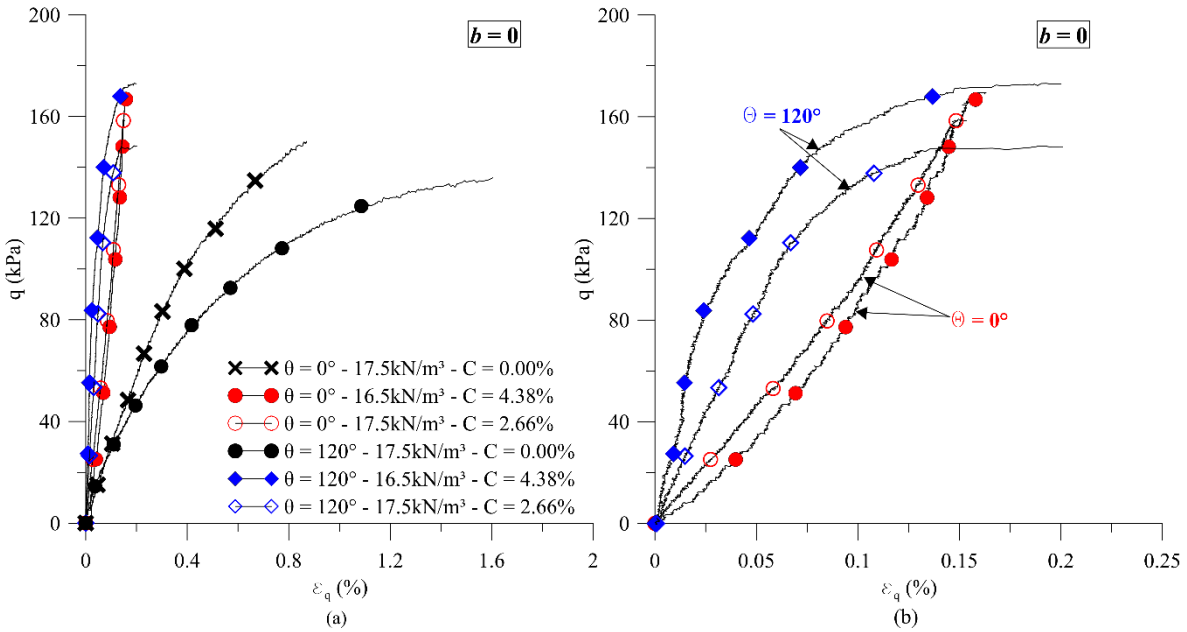

Figure 62: Intermediate stress parameter b = 0 stress *Vs.* strain curves.

The ordinary Portland cement main benefit for the iron ore tailing matrix regards to stiffness improvement, whereas strength gains were limited. OPC treated specimens exhibited an remarkable stiffness gain, in the order of at least 2.5 times higher than untreated specimens. In those cases where the true triaxial tests must be finished because of the true triaxial backpressure limiting condition, the specimens strength slightly increased and shifted from q ≈ 100 kPa for untreated to q ≈180 kPa for treated soil samples; it is important to bear in mind the ultimate strength of 180 kPa expected for these specimens, which were sought by dosing the iron ore tailing-OPC blends with an $\eta/C_{iv}^{0.16}$ of 42.40. Even though the possibility to keep tests ongoing, which were sooner finished because of the true triaxial equipment restrictions, the stress *Vs.* strain curves in Figure 62b go towards a value of 180 kPa. This equity between the dosed and achieved strengths foster the $\eta/C_{iv}^{0.16}$ index workability in spite of the loading condition; remember that the $\eta/C_{iv}^{0.16}$ = 42.40 was chosen based on unconfined compressive test results (axial loading), and the same ultimate strength was achieved for a multiaxial loading condition. In some instance, it was expected that the mean effective stress of 100 kPa could exert some influence on specimens' strength, which was not evidenced. At the same time, this mean effective stress magnitude is small and under the yielding point, thence, the cementitious matrix tends to be dominant in these cases (Consoli et al., 2006; Festugato et al., 2023; da Silva et al., 2024).

Festugato et al. (2013, 2019, 2023) and Silvani et al. (2017, 2022) reported some strength anisotropy attributed to the molding condition, at the same time the authors also report some kind of anisotropy erasing which might be caused by the cementitious matrix provided by the OPC inclusion. This potential anisotropy erasing is also evidenced in Figure 62, where the untreated specimens' stiffness are in function of the loading axes. The untreated $\theta = 0^{o}$ specimen is stiffer than the $\theta = 120^{o}$, probably due to the compaction Z-axis. On the other hand, this stiffness difference among the treated specimens is almost null which might foster the anisotropy erasing theory.

If only the treated specimens are compared, the $\theta = 120°$ specimens turn stiffer than the $\theta = 0°$ specimens after the OPC inclusion, even though a tiny strain difference (strain range of 0 to 0.15%). This suggests that the OPC inclusion might reset the soil fabric, and the soil stiffness would be dependent on the cementitious matrix development (blends' mixture and homogenization, moisture availability, etc.)

Figure 63 depicts the deviatoric strain *Vs.* volumetric strain of the $b = 0$ test specimens loading condition. Untreated specimens experienced a meaningful compressive volumetric strain in the order of 2% (Figure 63a). On the other hand, OPC treated specimens volumetric strain remained beneath of 0.4%; therefore, the OPC treatment assisted on volumetric stabilization as well. In terms of liquefaction susceptibility reduction, which is prone to occur in this kind of soil matrix, the volumetric stabilization comes out as one solution and it was achieved by either 4.38 or 2.66% of cement content. Thence, even OPC small percentages are favorable for liquefaction susceptibility reduction; of course, voids reduction by means soil compaction increase is also an alternative whenever possible. Figure 63b focus on treated specimens only. All the $b = 0$ treated specimens tests exhibited a volumetric compressive behavior, with test curves approaching to the same deviatoric strain/volumetric strain ratio.

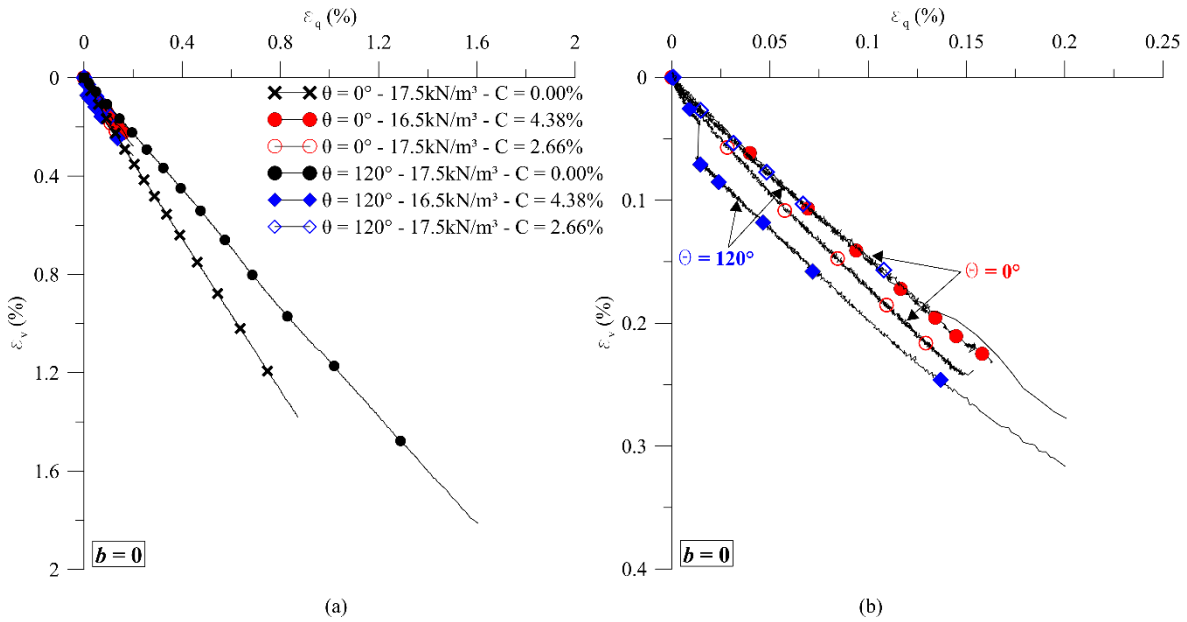

Figure 63: Intermediate stress parameter b = 0 deviatoric strain *Vs.* volumetric strain curves.

The previous test results exhibition pattern is also extended to the b = 0.5 test results. Figure 64 and Figure 65 depict the stress *Vs.* strain and deviatoric strain *Vs.* volumetric strain of the b = 0.5 test specimens loading condition respectively. Samples tested under a plane stress condition (b = 0.5) exhibited even great stiffness when compared to untreated specimens or b = 0 test specimens. This assumption is supported by comparing tests strain ranges like the b = 0 tests experienced a strain range of 0 to 0.20%, whereas the b = 0.5 tests from 0 to 0.075%. Plane stress loading conditions (i.e., θ = 30, 90 and 150° loading stress paths) distinguish because of the σ_2 maintenance throughout the true triaxial tests, namely, σ_1 increases and σ_3 decreases in the same proportion whereas σ_2 remains constant. Therefore, it is reasonable to think that under a plane stress loading condition the ε_2 should be minimal (this is evidenced in Figure 69). This ε_2 limited variation, a consequence of the constant stress in the intermediate axis, may cause specimens' stiffness increase.

Similar b = 0 and b = 0.5 test results were also reported by Lade & Duncan (1973), where great strains-to-failure were noticed to b = 0 tests results; no major differences were detected among b = 0 and b = 0.5 samples strength for these authors.

The b = 0.5 test results also report a kind of cross-section anisotropy for untreated soil specimens. Specimens' stiffness follows this sequence, from the stiffest to the lowest, θ = 30,

90 and 150° (Figure 64a). The θ = 30° stiffest specimen occurs because of the σ_1 loading axis equivalence to the compaction Z-axis. On the other hand, the θ = 90° is characterized to have the σ_1 loading axis on the Y-axis, whereas the σ_3 unloading axis onto the Z-axis; the σ_2 remains constant throughout the test for this loading path, and it occurs on the X-axis. Therefore, the tests results suggest that the initial soil fabric helps to hold at least part of the specimen's stiffness. Fact that does not occur for the θ = 150° loading stress path, and a specimen's stiffness decrease is observed. In this loading condition the compaction Z-axis is not demanded during the test, and only the Y-axis is loaded (σ_1) and X-axis unloaded (σ_3); thence, without the possibility of the initial soil fabric exert some influence on specimen behavior.

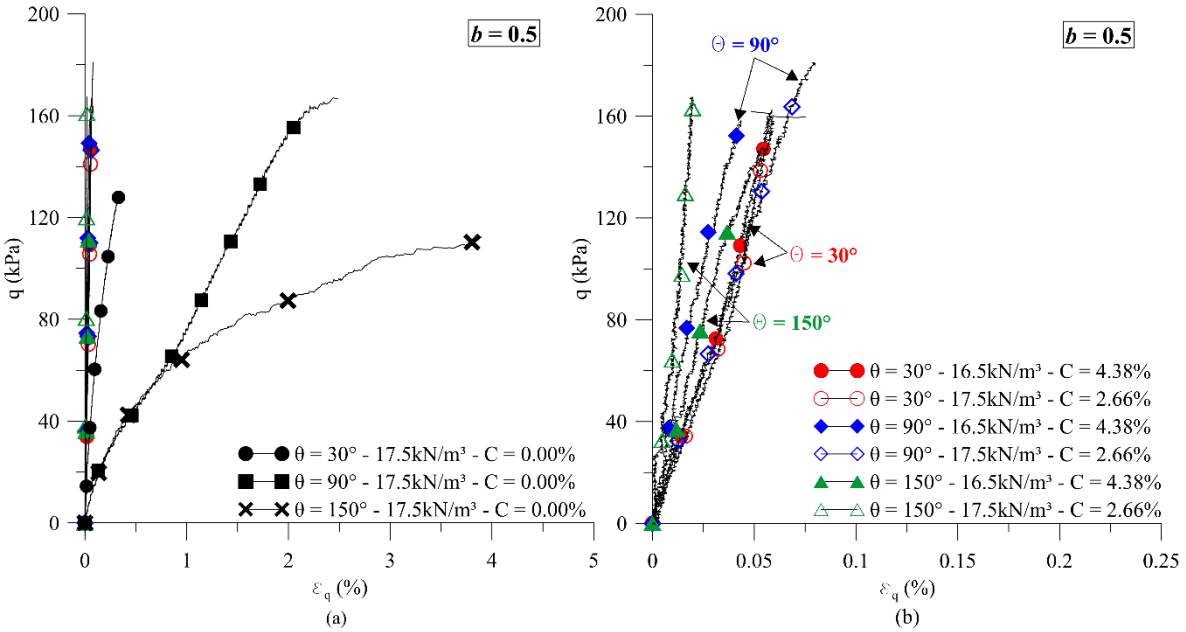

Figure 64: Intermediate stress parameter *b* = 0.5 stress *Vs.* strain curves.

Figure 65 shows the deviatoric strain *Vs.* volumetric strain of *b* = 0.5 iron ore tailing-OPC treated specimens. The *b* = 0.5 treated specimens experienced a half of *b* = 0 volumetric strains. No one of the reviewed authors focused on comparing the *b* = 0.5 test results with other loading conditions. Mostly of them compared the *b* = 0 and *b* = 1 test results, where a volumetric strain and dilation rate increase were noticed when shifted from *b* = 0 to *b* = 1. According to Lade & Duncan (1975), a parameter *b* continuous increase led to ε_1 lower extents, which is also noticed here when *b* shifts from zero to 0.5 and 1 (Figure 68 to Figure

70 support it). Therefore, for a plane stress loading condition it is expected less volumetric instability as seen in Figure 65b for instance.

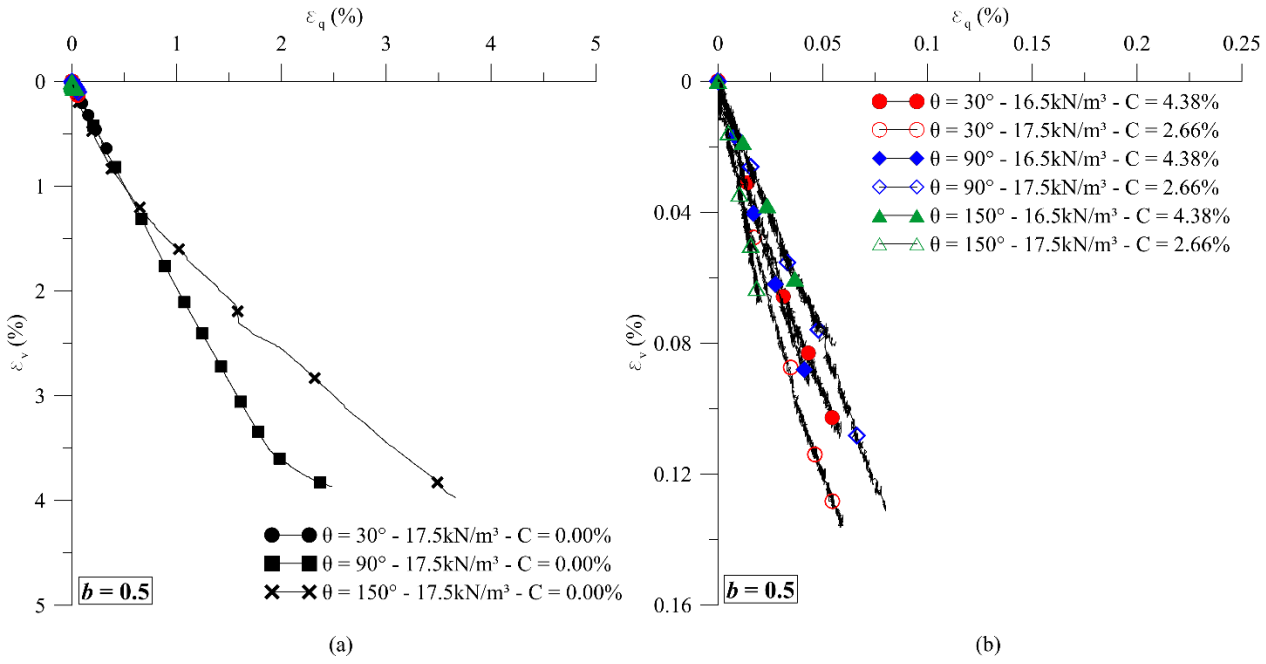

Figure 65: Intermediate stress parameter *b* = 0.5 deviatoric strain *Vs.* volumetric strain curves.

Figure 66 presents the deviatoric stress *Vs*. deviatoric strain of *b* = 1 test results. In line with Corte (2020) and Andreghetto (2022), the true triaxial extension test results also exhibited the lowest samples strength. This is due to the loading stress path severity, where the intermediate principal stress (σ_2) turns equal to the major principal stress (σ_1). The *b* = 1 untreated soil specimens also evidenced a cross-section soil anisotropy provided by Z-axis direction of compaction. The θ = 60° loading stress path occurs by loading both Y and Z-axes, whereas the X-axis is progressively unloaded; the fact of loading the Z-axis in the θ = 60° loading stress path outcome greater specimen's stiffness than the θ = 180° loading stress path (see Figure 66a). This latter loading stress path occurs by loading the X and Y-axes, whereas the Z-axis is progressively unloaded fact that might explain the θ = 180° stiffness substantial decrease.

Figure 67 presents the *b* = 1 specimens' volumetric strain. A dilation rate increased is observed when comparing *b* = 1 and *b* = 0 test results; it goes in agreement with Lade &

Duncan (1975) and Reddy and Saxena (1993) previous assertions. The previous authors also state a volumetric strain increase for b = 1 test results, which is also evidenced here.

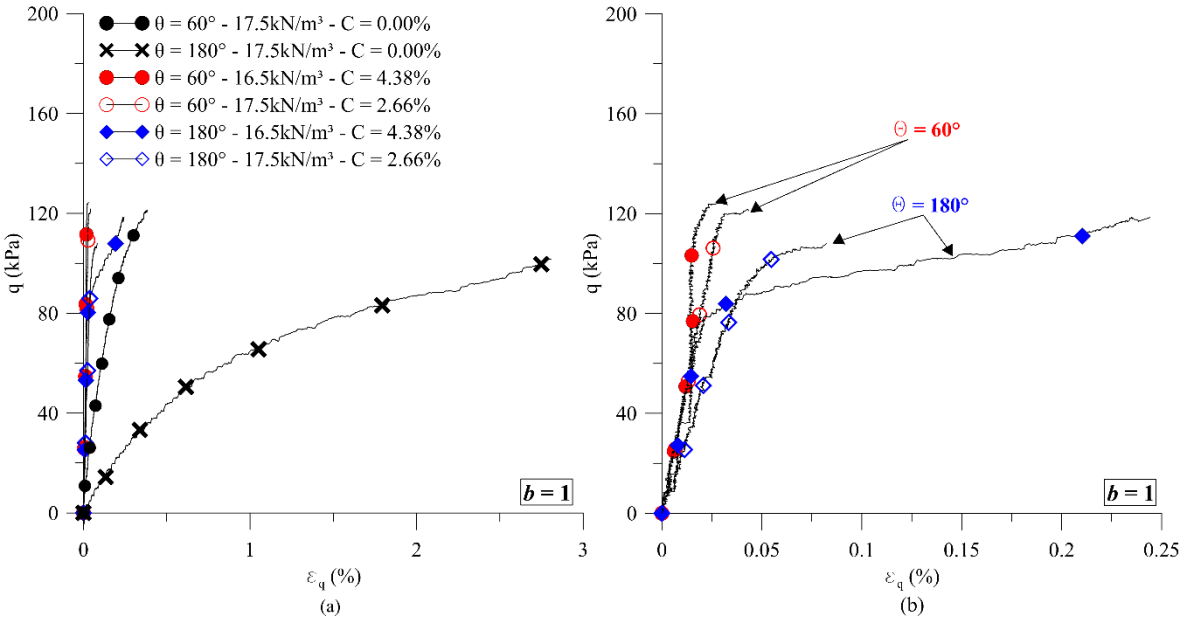

Figure 66: Intermediate stress parameter b = 1 stress *Vs.* strain curves.

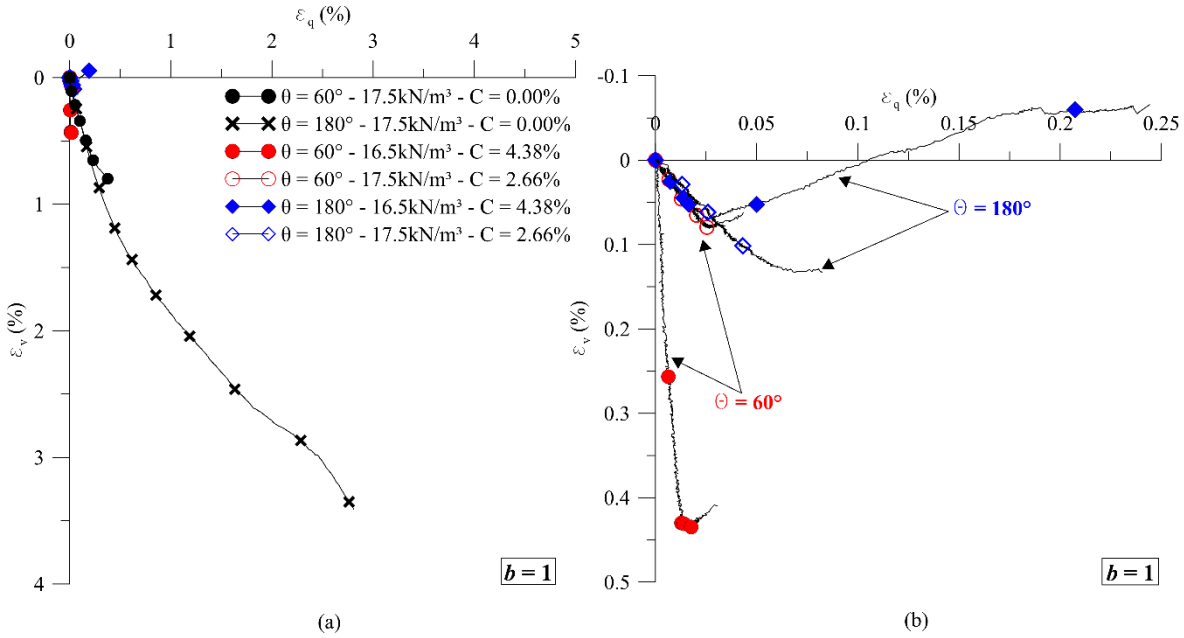

Figure 67: Intermediate stress parameter b = 1 deviatoric strain Vs. volumetric strain curves.

Figure 68 to Figure 70 present the iron ore tailing-OPC blends axial stress *Vs.* axial strain by means each X, Y and Z loading axis; this way of exhibition further helps to detect blends anisotropy if it occurs.

Figure 68 depicts true triaxial tests results of $b = 0$, where figure letter (a) comprehends the $\theta = 0°$ loading condition, and figure letter (b) the $\theta = 120°$ loading condition. Figure 68 also discretizes the $\gamma_d = 16.5$ kN/m³ - C = 4.38% (filled symbols) and $\gamma_d = 17.5$ kN/m³ - C = 2.66% (empty symbols) specimen blends. Firstly, it is emphasizing the blends' stress *Vs.* strain similarity, where both $\gamma_d = 16.5$ kN/m³ - C = 4.38% and $\gamma_d = 17.5$ kN/m³ - C = 2.66% follow almost the same stress *Vs.* strain relation; it is independent of the X, Y and Z axis. This restates the $\eta/C_{iv}^{0.16}$ workability, where dosing by either the cement content or blends' porosity the blends behavior is equivalent. This approach assists in opting for the best dosage option, namely, the field engineer can choose by increasing soil compaction or by adding an equivalent cement content; which will be less expensive or laborious.

Figure 68a and Figure 68b assist to compare the principal strain ranges and directions. For instance, the Z-axis assumes the role of the major principal stress for the $\theta = 0$ loading condition. Therefore, it is expected a great strain range throughout this loading direction. On the other hand, the X and Y-axis assume the role of the intermediate and minor principal stresses due to their progressive equal unloading. Thence, in absence of specimens' anisotropy, it is expected that ε_2 and ε_3 principal strains succeed in the same range and directions; this is evidenced in both Figure 68a and Figure 68b. Therefore, Figure 68a and Figure 68b suggest at least a specimens' cross-section isotropy, because of the X and Y-axis principal strains equivalence.

Another aspect that supports the specimens' isotropy regards to the $\theta = 0º$ and $\theta = 120º$ major principal stresses equivalence; which is here illustrated by the Z-axis for $\theta = 0º$ and by the Y-axis for $\theta = 120º$ (see Figure 68a and Figure 68b). Specimens loaded on the Z-axis like the $\theta = 0º$ tests, would expect great strength and stiffness because of the molding compaction axis that is same; fact that is not evidenced here. This impossibility to distinguish the $\theta = 0º$ and $\theta = 120º$ deviatoric stresses may lead to conjecture specimens' isotropy; the molding compaction did not strengthen the $\theta = 0º$ specimens. Further discussions about a probable specimens' isotropy are addressed in the following paragraphs.

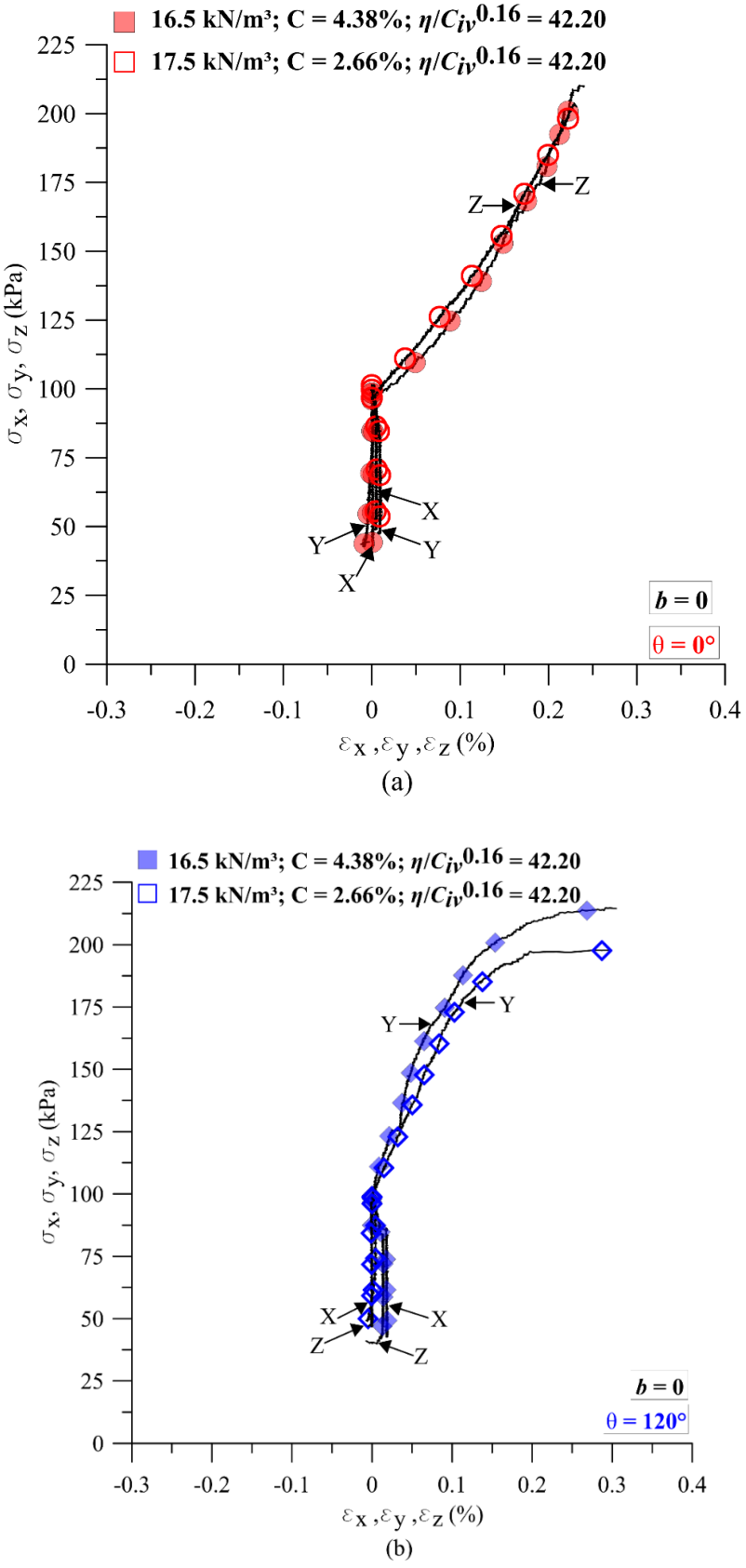

Figure 68: X, Y and Z stress *Vs.* strains curves to *b* = 0: a) θ = 0°; and b) θ = 120°.

Figure 69 shows the *b* = 0.5 test results, these tests have two loading axes whereas the third remains constant at the same stress magnitude. Iron ore tailing-OPC blends stress *Vs.* strain relation are identical in spite of adopted dosage. Both γ_d = 16.5 kN/m³ - C = 4.38% and γ_d = 17.5 kN/m³ - C = 2.66% dosages outcome very similar test results.

The *b* = 0.5 test results were not influenced by some induced compaction anisotropy. This is able to be stated because of the strain and σ_1 magnitudes attained for θ = 30º, 90º and 150º loading conditions, which are fairly identical in spite of the loading axes. The σ_1 loading axes were Z (for θ = 30º) and Y (for θ = 90º and 150º), where a prominent strength and stiffness gain is not evidenced for specimens loaded on the θ = 30º loading stress path. Specimens' behavior convergence suggests blends isotropy, or that the compaction anisotropy could be erased owing to the cement inclusion.

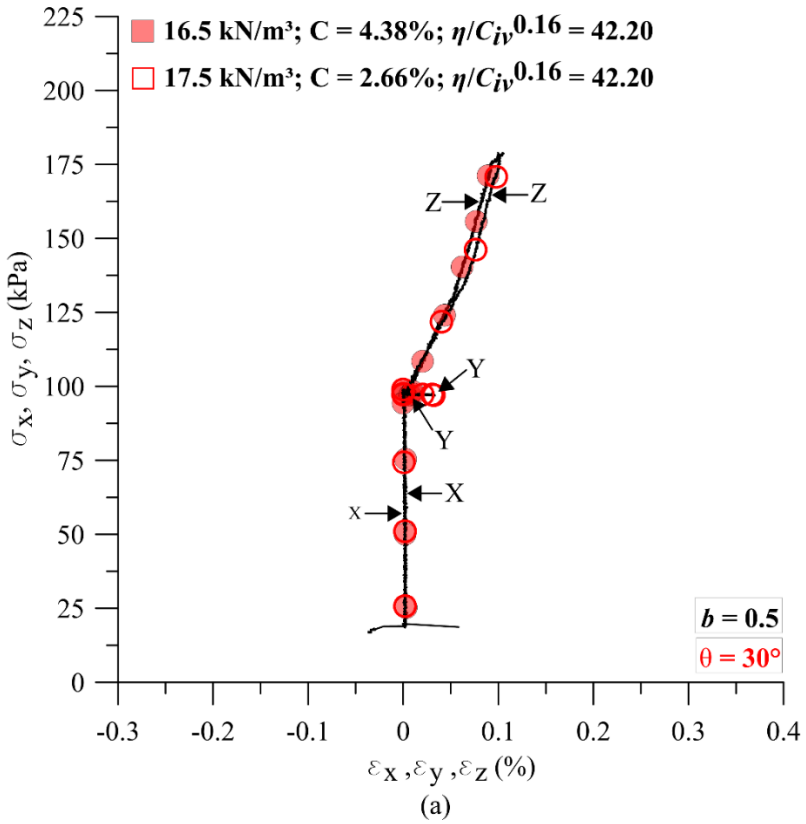

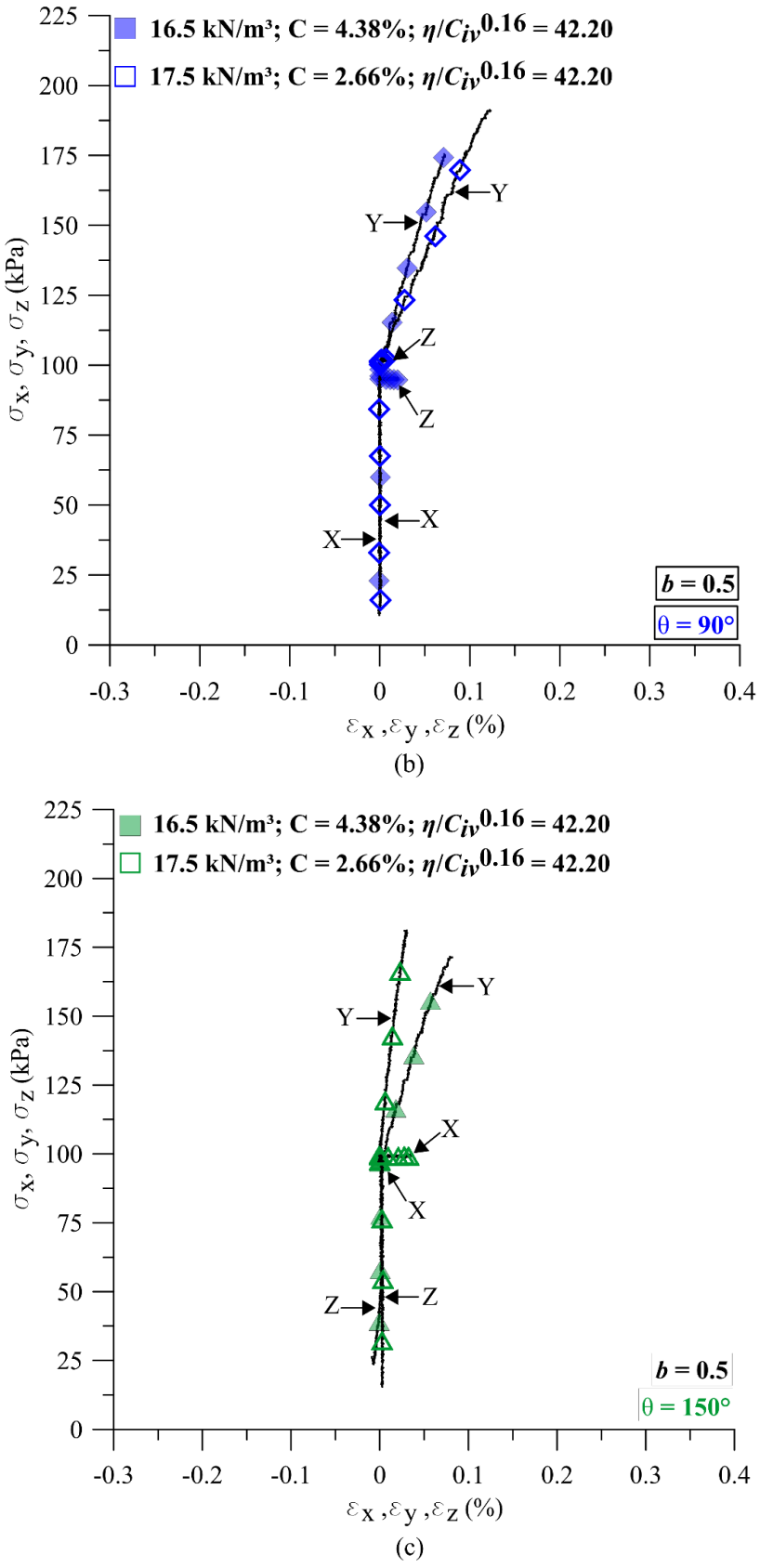

Figure 69: X, Y and Z stress *Vs.* strains curves to *b* = 0.5: a) θ = 30°; b) θ = 90°, and c) θ = 150°.

Figure 70 depicts the *b* = 1 test results, where specimens' isotropy is also noticed at least for the γ_d = 17.5 kN/m³ - C = 2.66% specimen. Lade & Duncan (1973) carried out several true triaxial tests on untreated sandy soil specimens, the authors found that the soil deposition method did not influence the sandy soil behavior, and the soil specimen approached an isotropic body. Silvani et al. (2022) studied Osorio sand-fly ash-lime blends by means true triaxial tests. The authors suggest that the cementing effect might be erasing the inherent anisotropy induced by the specimens' preparation method. Similarly, Andreghetto (2022) noticed Osorio sand-OPC specimens' anisotropy induced by the specimens' preparation method. However, specimens' anisotropy decreased according to the cement content increase; The Andreghetto (2022) cement content range was from 0 to 2.14%, like the content applied here.

On the contrary, Festugato et al. (2019) investigated lightly cemented Hostun RF (S28)-OPC blends by means true triaxial tests. The authors observed that a cement content of 1.8% was not able to erase the inherent compaction anisotropy. Based on the thesis test results and supported by the previous authors, soil anisotropy induced by the specimens' preparation method vary according to particles interaction and cement content in the case of chemically treated soils. Figure 70b restates specimens' isotropy in the present thesis, where both X and Y loading axes vary almost identically along the true triaxial test.

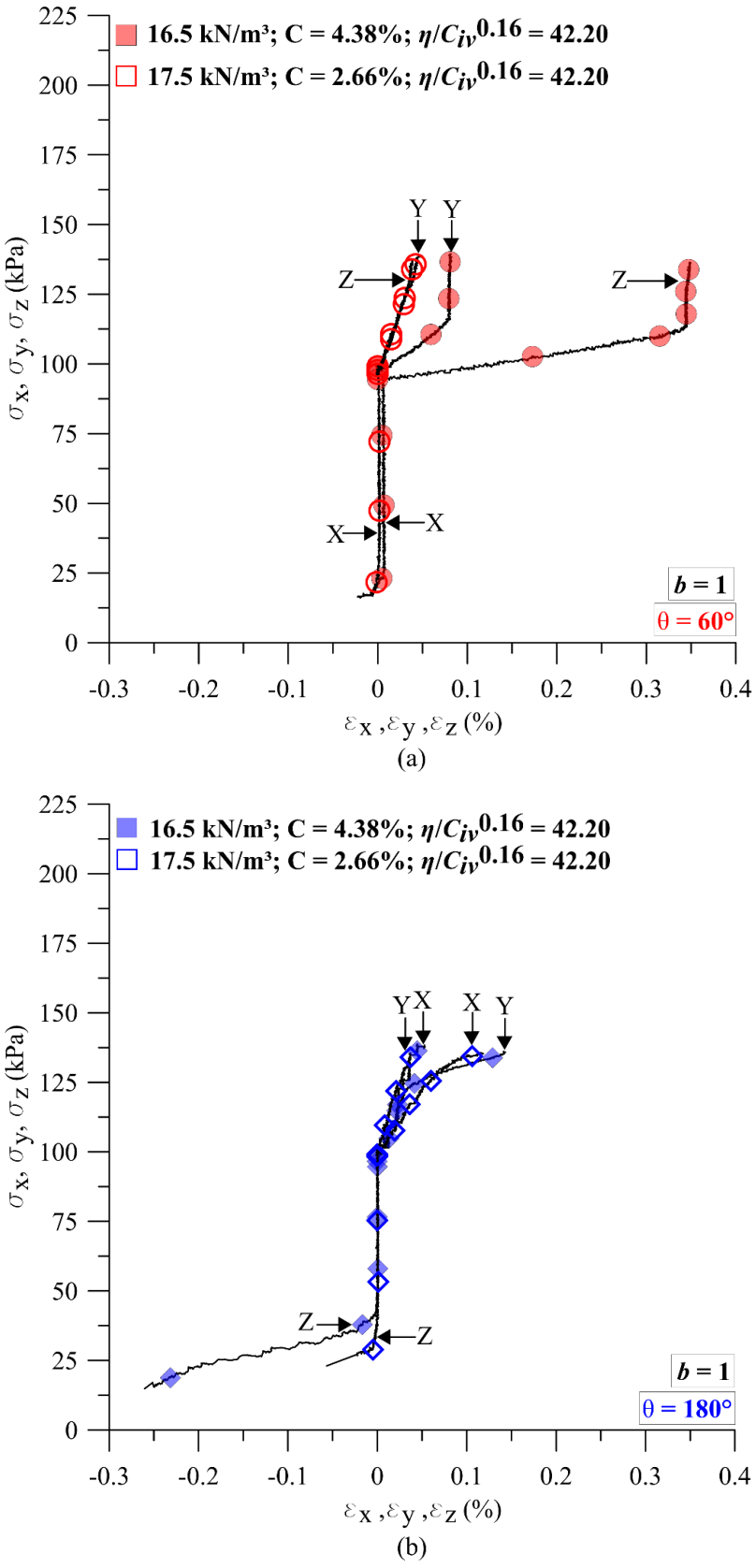

Figure 70: X, Y and Z stress *Vs.* strains curves to *b* = 1: a) θ = 60°; and b) θ = 180°.

Table 9 summarizes the iron ore tailing-OPC blends test results; variables like the test loading condition, specimens' void ratio after the consolidation phase, specimens $\eta/C_{iv}^{0.16}$ index, the maximum deviatoric stress, among others are included in this table. Specimens more detailed aspects can be seen in Appendix B where specimens' pictures are included. As can be seen, the $\eta/C_{iv}^{0.16}$ index remained slightly higher than the 42.40 target for OPC treated specimens. This tiny difference did not impact the test results, which is evidenced comparing the deviatoric stresses of $\theta = 0°$ ($q_{max.}$ = 169.6 kPa) and $\theta = 120°$ ($q_{max.}$ = 173.1 kPa) with the unconfined compressive strength (q_u) target of 180 kPa; when true triaxial compressive stress paths ($\theta = 0°$ and 120°) are compared to the unconfined compressive strength, the strengths converge to a single point that is the target of 180 kPa.

Strengths lower than the target of 180 kPa are due to the loading condition, for example the b = 1 tests results that are the worse multiaxial loading case. Specimens' isotropy and the $\eta/C_{iv}^{0.16}$ workability are also evidenced by the $q_{max.}$ similarity between test results with the same intermediate stress parameter b.

Table 9: Iron ore tailing-OPC blends test results.

Parameters	Dosages																				
	γ_d = 17.5 kN/m^3 C = 0.00 %	γ_d = 16.5 kN/m^3 C = 4.38 %	γ_d = 17.5 kN/m^3 C = 2.66 %	γ_d = 17.5 kN/m^3 C = 0.00 %	γ_d = 16.5 kN/m^3 C = 4.38 %	γ_d = 17.5 kN/m^3 C = 2.66 %	γ_d = 17.5 kN/m^3 C = 0.00 %	γ_d = 16.5 kN/m^3 C = 4.38 %	γ_d = 17.5 kN/m^3 C = 2.66 %	γ_d = 17.5 kN/m^3 C = 0.00 %	γ_d = 16.5 kN/m^3 C = 4.38 %	γ_d = 17.5 kN/m^3 C = 2.66 %	γ_d = 17.5 kN/m^3 C = 0.00 %	γ_d = 16.5 kN/m^3 C = 4.38 %	γ_d = 17.5 kN/m^3 C = 2.66 %	γ_d = 17.5 kN/m^3 C = 0.00 %	γ_d = 16.5 kN/m^3 C = 4.38 %	γ_d = 17.5 kN/m^3 C = 2.66 %	γ_d = 17.5 kN/m^3 C = 0.00 %	γ_d = 16.5 kN/m^3 C = 4.38 %	γ_d = 17.5 kN/m^3 C = 2.66 %
	θ (°)																				
	0°			30°			60°			90°			120°			150°			180°		
b	0			0.5			1			0.5			0			0.5			1		
σ_1	Z			Z			Z and Y			Y			Y			Y			Y and X		
q/p'	1.5	1.7	1.6	1.3	1.7	1.7	1.2	1.3	1.3	1.7	1.6	1.8	1.4	1.7	1.5	1.1	1.5	1.7	1.0	1.2	1.1
q_x (kPa)	0	0	0	47	59	58	88	88	86	118	112	120	95	123	115	39	52	59	0	0	0
q_z (kpa)	140	159	149	94	117	116	60	59	59	0	0	0	-65	-82	-66	-79	-105	-118	-95	-112	-102
$e_{cons.}$[5]	0.746	0.928	0.830	0.780	0.948	0.827	0.687	0.940	0.821	0.685	0.946	0.842	0.716	0.961	0.822	0.610	0.955	0.830	0.648	0.923	0.830
$\eta/C_{iv}^{0.16}$	-	42.8	43.4	-	43.7	43.2	-	43.6	43.1	-	43.8	43.7	-	43.6	43.2	-	43.6	43.3	-	42.7	43.5
$q_{max.}$ (kPa)	150.2	169.6	159.1	128.7	166.9	163.7	121.4	124.3	121.8	167.1	158.4	170.0	135.9	173.1	162.5	112.7	147.6	167.5	101.8	118.6	108.0

[5]Parameter estimated for uncemented specimens. These specimens were molded into the equipment, and their dimensions and weight were not directly measured.

Figure 71 depicts the maximum deviatoric stress attained for each true triaxial test by the loading θ angle. The test results meet with the patterns found by Corte (2020) and Andreghetto (2022), however, diverge from the Lade & Duncan (1973) and Mogi (1981) test results. The test results difference occurs owing to the Lade & Duncan (1973) and Mogi (1981) mean effective stress (p') fluctuation throughout the true triaxial tests, whereas in the Federal University of Rio Grande do Sul true triaxial test results it was maintained constant. On the other hand, this mean effective stress maintenance was not possible in the Colorado School of Mines true triaxial tests and it will be further discussed in section 4.2.2.

Corte (2020) and Andreghetto (2022) found that constant mean effective stress test results or true triaxial test results normalized by the mean effective stress are influenced by the intermediate stress parameter *b* as follows:

1) The $b = 0$ tested specimens were the most competent specimens in terms of soil strength. In this test pattern, the intermediate principal stress (σ_2) turns equal to the minor principal stress (σ_3).
2) The $b = 0.5$ tested specimens attained a fair soil strength. In this test pattern, the intermediate principal stress (σ_2) remains constant throughout the true triaxial test.
3) The $b = 1$ tested specimens were the least competent in terms of soil strength. In this test pattern, the intermediate principal stress (σ_2) turns equal to the major principal stress (σ_3).

The previous pattern is clearly observed for the present thesis uncemented test results (Figure 71 blue-squared symbols). Nonetheless, it does not extend to the cemented test results, where the $b = 0$ and $b = 0.5$ test results soil strength are almost identical. Therefore, it is possible to infer that the soil strength anisotropy was at least partially erased, which occurs when soil samples were subjected to compression and plane-stress loading conditions.

Figure 71 also portrays the OPC stabilization benefits, where great soil strengths were attained after the soil stabilization treatment. Furthermore, it is also highlightable the OPC stabilization low efficiency for tensile stress paths like $\theta = 60°$ and 180°; both cemented and uncemented soil samples attained almost the same soil strength when subjected to $\theta = 60°$ and 180° loading stress paths.

The OPC stabilization low efficiency for tensile stress paths go in line with the reinforced materials theory like fiber and concrete reinforced materials. Where fiber and metal rods are inserted into the main matrix in order to assist materials strength against tensile loadings; reinforcements like the previous mentioned were not considered in the present study, which justifies the OPC treatment lower efficiency for θ = 60° and 180° loading stress paths.

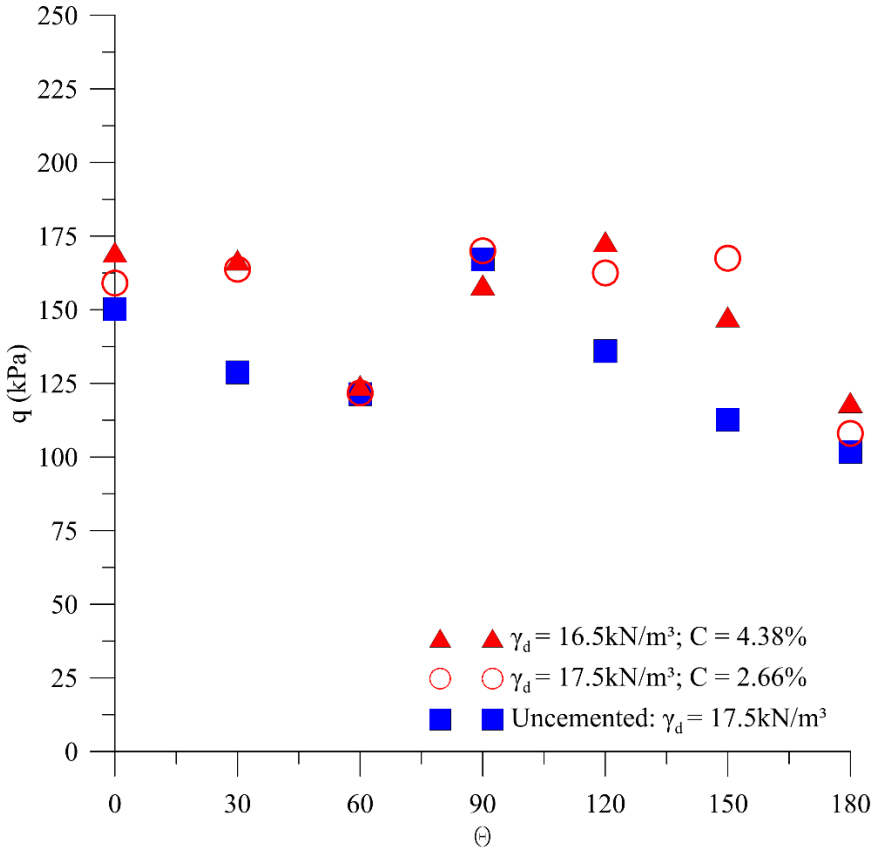

Figure 71: Deviatoric stress – q (kPa) in function of the θ loading angle.

Figure 72 depicts the true triaxial test results on the deviatoric plane, the π plane, by means the orthogonal deviatoric stress components q_x and q_z. These both variables are determined by (Eq. 12) and (Eq. 13).

$$q_x = \frac{\sigma_y - \sigma_x}{\sqrt{2}} \quad \text{(Eq. 12)}$$

$$q_z = \frac{\sigma_z - \sigma_y - \sigma_x}{\sqrt{2}} \quad \text{(Eq. 13)}$$

Figure 72 presents the true triaxial test results on the normalized deviatoric stress plane. The previous conclusions are reassured here, namely, the $\eta/C_{iv}^{0.16}$ index feasibility which is seen by the treated blends test results similarity by the red-rounded-empty and red-triangular-filled symbols superposition. Figure 72 also evidences the OPC treatment impact on the samples ultimate strength, where the apparent failure surface marginally expanded with the OPC insertion. As previously discussed and taking into account the Federal University of Rio Grande do Sul true triaxial boundary conditions, the OPC insertion influenced the soil matrix-strength somewhat and less than expected. On the other hand, soil matrix stiffness was greatly influenced by the OPC treatment which is evidenced throughout Figure 62 to Figure 67.

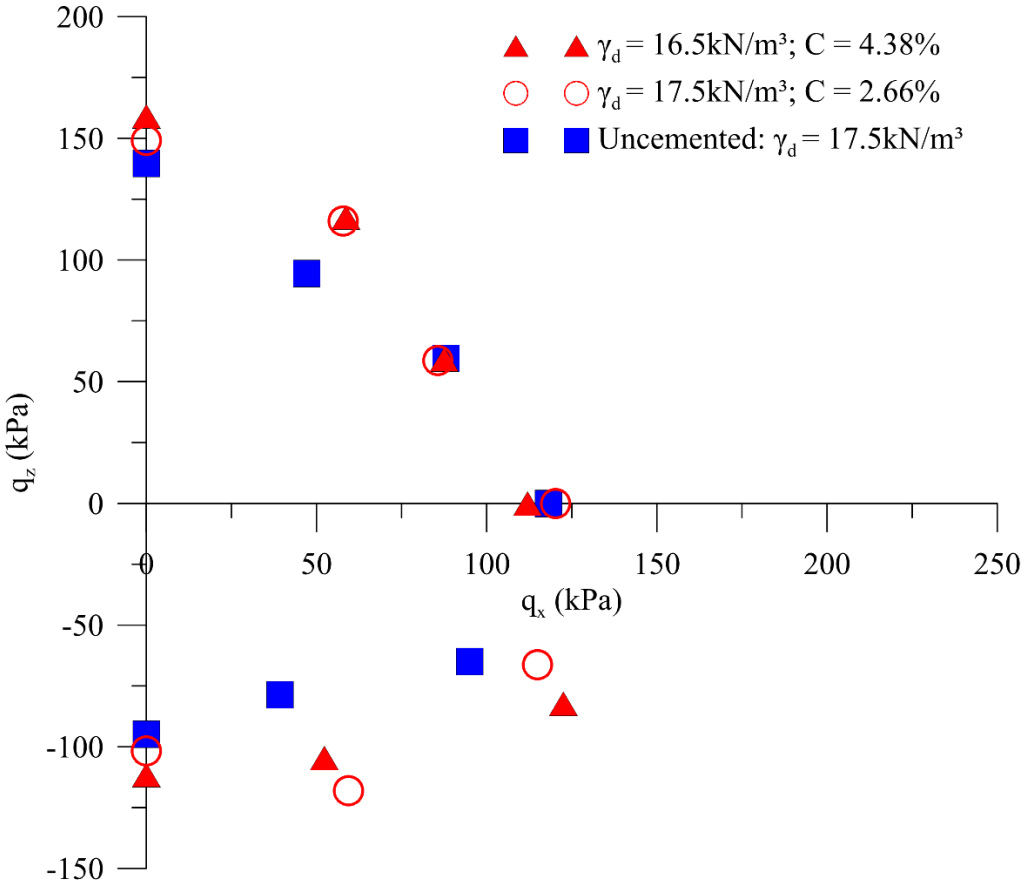

Figure 72: Experimental test results planification on the π plane by means q_z and q_x variables.

Despite of the fact that the Mohr-Coulomb failure criteria does not account for the intermediate principal stress effect, this was chosen to assess the Phase II tests results. Some assumptions were made to turn the test results modelling feasible like: (i) the presumed cohesion intercept due to the OPC insertion was neglected; (ii) the best practice of to be

executing tests on at least three distinct deviatoric stress planes was not considered, and the Mohr-Coulomb failure parameters were determined based on a single deviatoric stress plane of 100 kPa. These restraints were overcame by adjusting the Mohr-Coulomb failure envelope to the θ = 0° experimental test result.

Figure 73 presents the Mohr-Coulomb failure envelopes adjusted for both cemented and uncemented tested specimens' experimental data. These both envelopes were adjusted by adopting internal friction angles of ϕ = 42.3° for uncemented soil matrix, and ϕ = 47° for cemented soil matrix. By adopting these parameters, a fair adjustment is obtained for both untreated and treated soil specimens. Despite the marginal OPC benefit observed for the deviatoric stress tested specimens, its inclusion greatly impacted on the M-C strength parameters expanding the failure envelope.

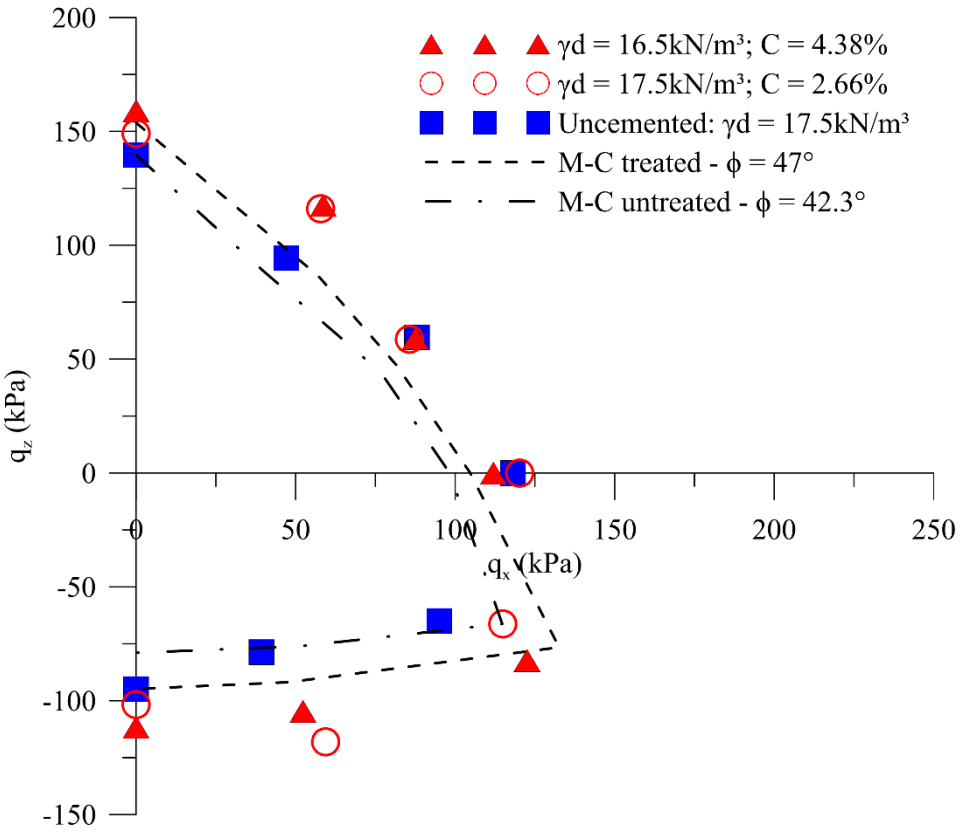

Figure 73: The Mohr-Coulomb failure criterion fitted to the experimental test results.

4.2.2 The ordinary sand-ordinary Portland cement blends test results

Section 4.2.2 and forward present the ordinary sand-ordinary Portland cement blends Phase II test results, which comprises the conventional triaxial and true triaxial test results. Figure 74 and Figure 75 depict the Consolidated Isotropically Undrained (CIU) and Consolidated Isotropically Drained (CID) triaxial test results for ordinary sand and ordinary sand-OPC blends respectively. The present thesis focus on true triaxial tests and the multiaxial loading condition allowed by this kind of test. The conventional triaxial tests carried out in the present study aimed to assist the true triaxial teste results comprehension like in the moment of experimental tests modelling and further aspects of this kind of test will not be addressed.

Despite the conventional triaxial test results portrayed in Figure 74, the natural soil triaxial tests results, show as expected the soil strength in function of the mean effective stress with a not pronounced A parameter (Skempton 1954) in the case of CIU triaxial tests. A traditional internal friction angle of 32º for cohesiveness granular materials was adjusted to the experimental test results.

Still for Figure 75 the conventional triaxial test results for ordinary sand-OPC blends exhibit a soil matrix behavior change owing to the OPC insertion. Among the differences it is possible to verify a huge strength increment and also the dilative behavior portrayed by the CIU triaxial test results. Both these aspects are well documented in the literature and reassure the OPC inclusion benefits like the liquefaction susceptibility prevention.

An internal friction angle of 50º and a cohesion intercept of 150 kPa were adjusted to the experimental test results. Both parameters seem to be high and are not commonly used in the soil mechanics theory. Nonetheless, it is necessary to consider the amount of OCP inserted into the soil matrix, that is, 14.65%, considerably high for OPC soil treatments. Because of the great amount of OPC inserted, it would not be unexpected to analyze this kind of samples in terms of the rock mechanics framework. Alternatively, it would be to consider a non-linear failure envelope and conduct further studies in low mean effective stresses as well.

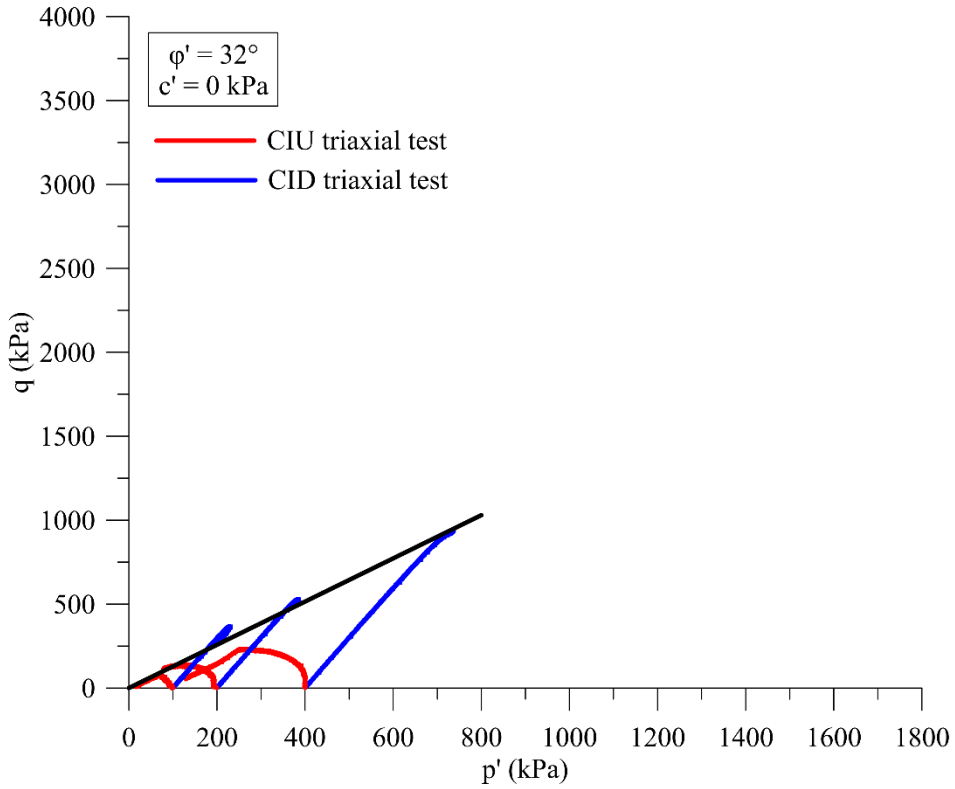

Figure 74: Ordinary sand triaxial test results.

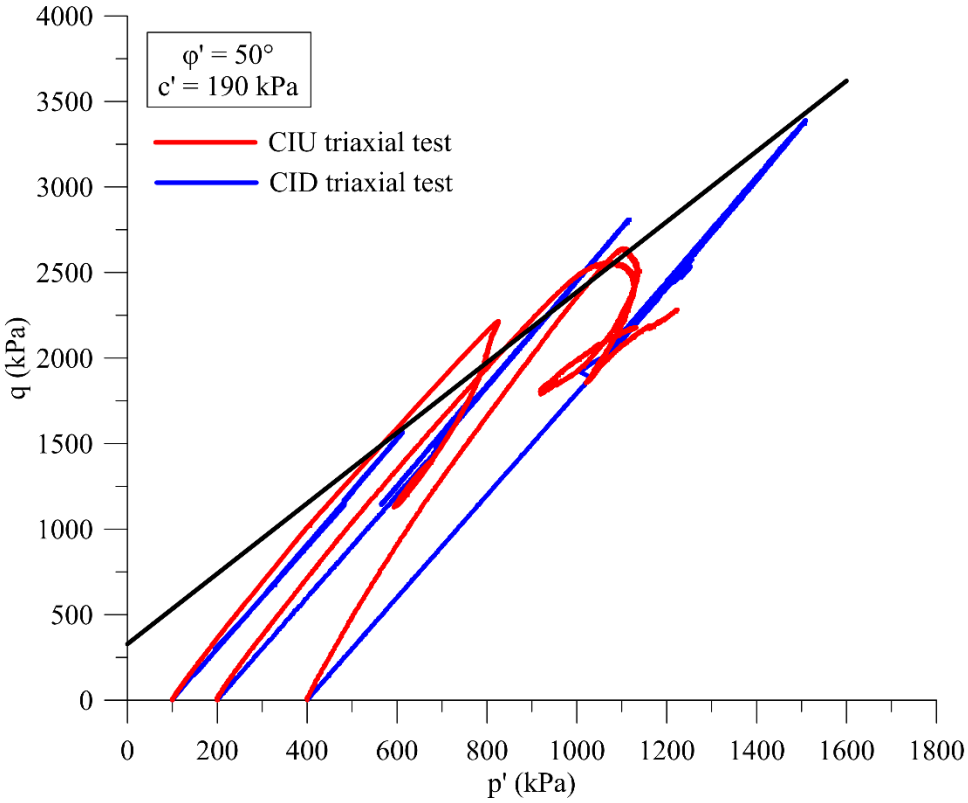

Figure 75: Ordinary sand-OPC blends triaxial test results.

Figure 76 to Figure 81 present the deviatoric stress *Vs.* deviatoric strain and deviatoric strain *Vs.* volumetric strain of true triaxial ordinary sand-OPC blends test results. As previously mentioned in section 1.6, it is important to remember that the Colorado School of Mines true triaxial did not hold a backpressure (porepressure) system. In order to overcome such limitation, the total suction (h) was measured by means the filter paper technique described on ASTM D5298-03 for each treated soil specimen after the shearing procedure. The maximum total suction measured for all tested samples was in the order of 5 kPa, which was considered fair negligible compared to the stress range applied for the Colorado School of Mines true triaxial tests, that is, 2000 kPa and 4000 kPa.

Figure 76 to Figure 81 present the true triaxial test results by means the intermediate stress parameters *b* of 0, 0.5 and 1; test loading conditions like the test parameter *b* and loading θ angle are inserted into each figure. These test results are differentiated by means the initial mean effective stress (p'_0) of each test, thence, the test results are differentiated between tests starting with p'_0 = 2 MPa (filled symbols) and 4 MPa (empty symbols). Despite the loading θ angle, the true triaxial tests were conducted as further as possible, namely, util the minor principal stress reaches its lowest value as possible. After that, the major principal stress was continuously increased whenever possible; this strategy was adopted to have the maximum use of the equipment.

Figure 76 depicts the stress *Vs.* strain behavior of *b* = 0 tested specimens. Figure 76 highlights two main aspects, firstly, the initial mean effective stress impact on the stress *Vs.* strain behavior where samples subjected to a p'_0 = 4 MPa have a great strength and stiffness as well. Secondly, the soil anisotropy maintenance even though the insertion of 14.65% of OPC. This latter conclusion can be inferred by comparing the θ = 0° and θ = 120° test results. The θ = 0° test results are stiffer than the θ = 120° test results, which might be attributed to the molding compaction Z-axis that is the same of the major principal stress in the case of θ = 0°.

Soil anisotropy erasing by OPC inclusion is not a consensus as previous discussed in the iron ore tailings-OPC blends section. Silvani et al. (2022) stated that the induced molding compaction anisotropy could be erased in the case of Osorio sand-fly ash-lime blends. Also, Andreghetto (2022) suggested that the induced molding compaction anisotropy would be

erased according to amount of cement growth for Osorio sand-OPC blends. Conversely, Festugato et al. (2019, 2023) found that 1.8% of OPC inclusion was not sufficient to erase the induced molding compaction anisotropy for Hostun RF (S28)-OPC blends.

In the present thesis we could observe that low extents of cement contents (2.66% and 4.38%) were able to reduce the induced molding compaction anisotropy for iron ore tailings-OPC blends, which might be attributed to the great fines content on this soil matrix. On the other hand, a large cement content of 14.65% was not able to erase the induced molding compaction anisotropy for ordinary sand-OPC blends. The lack of fines in this latter soil matrix might influence the erasing phenomenon. Also, it is necessary to consider the great initial mean effective stresses of each test (2 and 4 MPa) that might promote the cement phase broken hindering it to erase the induced anisotropy.

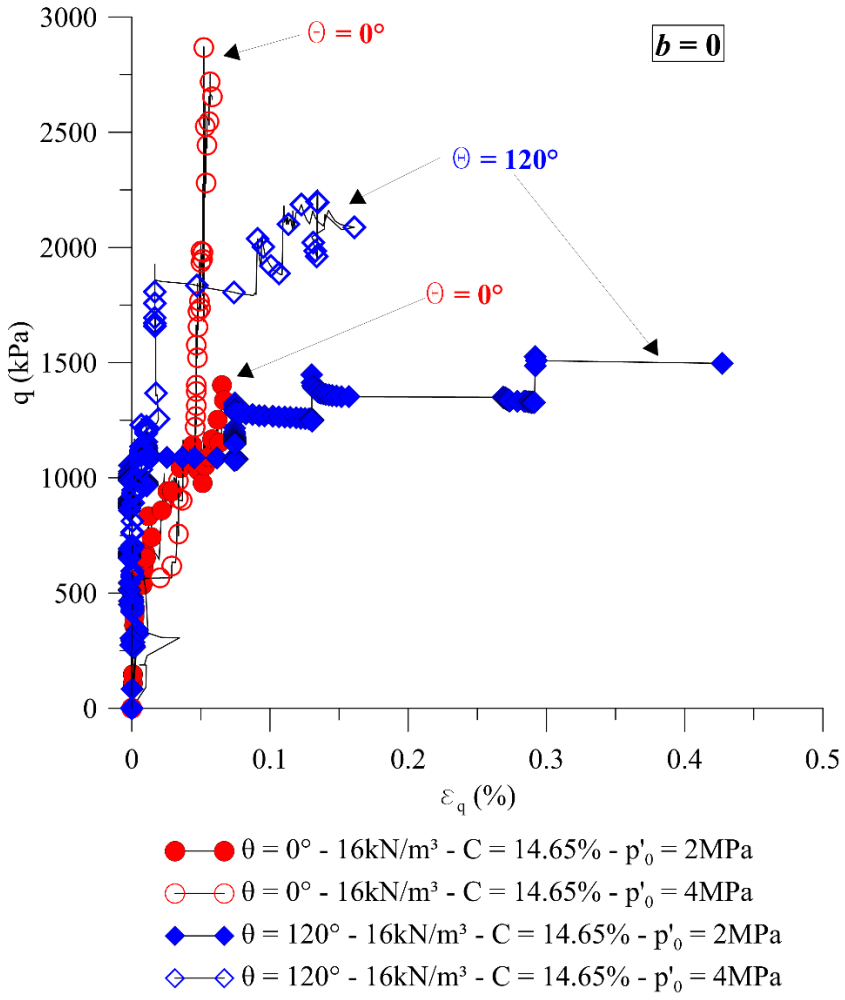

Figure 76: Intermediate stress parameter *b* = 0 stress *Vs.* strain curves.

Figure 77 presents the deviatoric strain *Vs.* volumetric strain of $b = 0$ tested specimens. As described in section 3.2.2, the initial mean effective stresses of 2 and 4 MPa were chosen as controlled variables in order to have mean effective stresses under and over the inferred ordinary sand-OPC blends yielding point of 3.5 MPa. This adoption sought to understand samples behavior in case of the cementing phase broken due to the confining pressure increase. The under and over yielding point mean effective stress impact can be observed in Figure 77. Intermediate stress parameter $b = 0$ test results under the inferred yielding point, namely, the 2 MPa test results, outcame dilative treated soil response. Whereas over the inferred yielding point, namely, the 4 MPa test results, resulted in compressive treated soil response. These findings may indicate a cementing phase broken due to the *p'* increase.

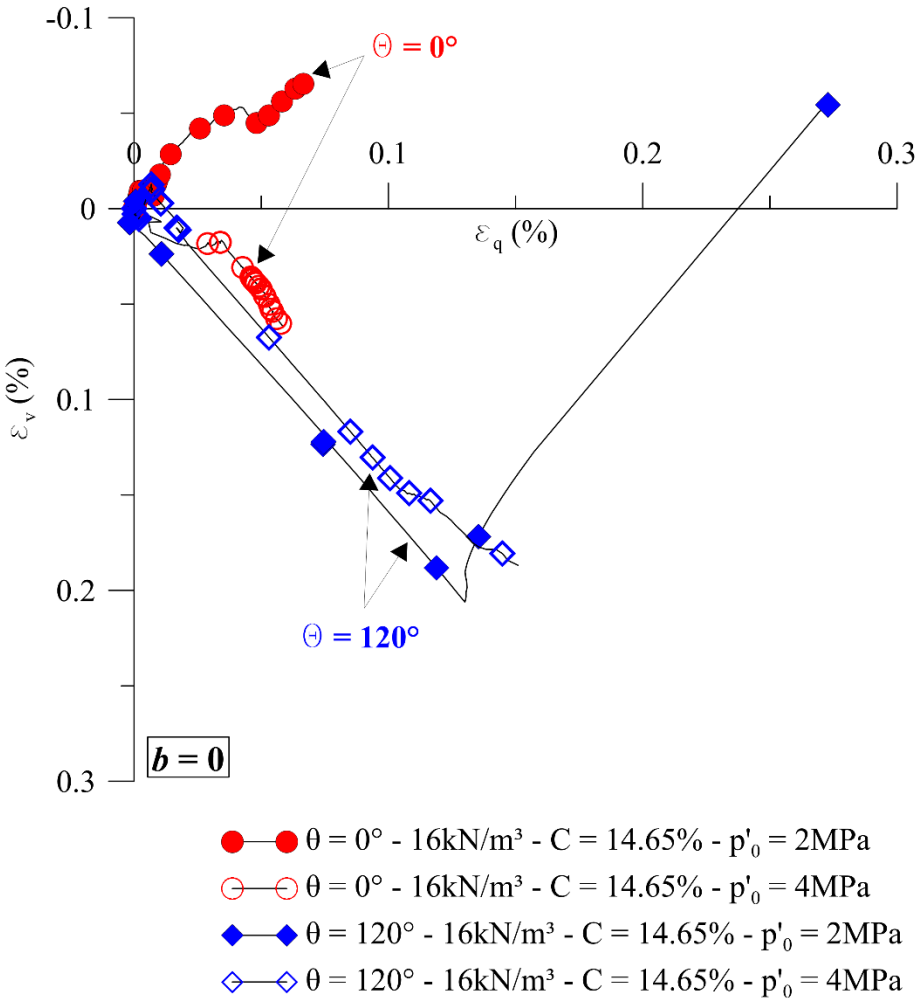

Figure 77: Intermediate stress parameter $b = 0$ deviatoric strain *Vs.* volumetric strain curves.

The stress *Vs.* strain behavior of b = 0.5 tested specimens are depicted in Figure 78. The b = 0.5 tested specimens seem to be somewhat stiffer than the b = 0 tested specimens. The same outcomes were addressed in the iron ore tailings-OPC blends test results. This pattern might be attributed to the loading boundary condition, that is, a plane stress condition. Figure 78 portrays the effect of the mean effective stress on the samples test results, where great deviatoric stresses were attained for p'_0 = 4 MPa tested specimens. Also, the p'_0 = 4 MPa tested specimens seem to be stiffer than the p'_0 = 2 MPa. Even though some cementation phase broke due to mean effective stresses over the yielding point, this higher mean effective stress is also responsible for boosting soil grains interaction. Therefore, specimens' stiffness is a matter of balancing between the cementation phase deterioration and the increase of the mean effective stress (the grains interaction growth).

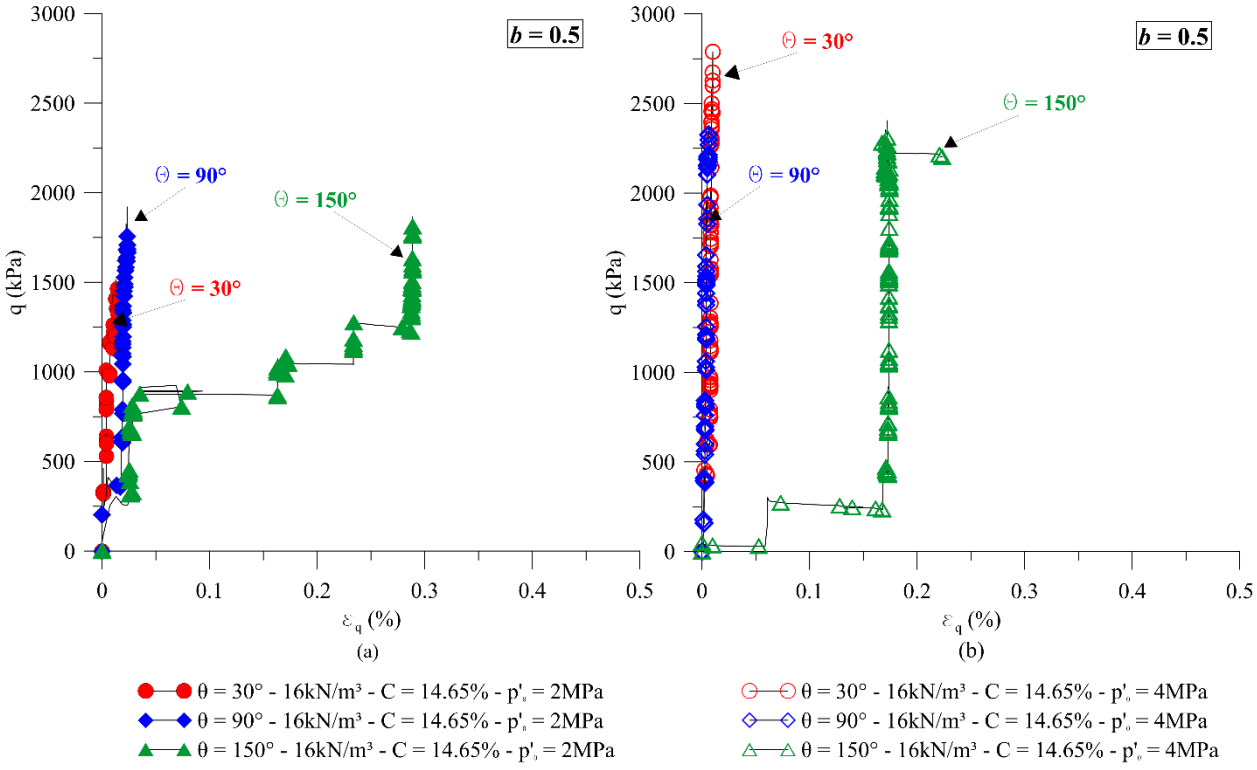

Figure 78: Intermediate stress parameter b = 0.5 stress *Vs.* strain curves.

Another aspect of Figure 78 regards the specimens' stiffness degree for b = 0.5 samples. The b = 0.5 sample stiffness follows, from the stiffen to the weaken, this sequence: θ = 30°, θ = 90°, and θ = 150°. This stiffness variation might be attributed to the compaction molding Z-axis and the loading stress path. The θ = 30° has the σ_1 on the Z-axis, which may justify its

great stiffness. On the other hand, the θ = 150° has the σ_3 on the Z-axis, which may justify its less stiffness on the stress *Vs.* strain response.

The deviatoric strain *Vs.* volumetric strain behavior of *b* = 0.5 tested specimens are depicted in Figure 79. Figure 79 reassures a feasible cement phase broken due to the mean effective stress increase from 2 MPa to 4 MPa, which can be inferred by the dilative and compressive behaviors observed in both p'_0 = 2 MPa and p'_0 = 4 MPa respectively; a more pronounced compressive behavior in the p'_0 = 4 MPa samples may suggest this cementation phase broken. This conclusion can also be addressed by the Appendix B that depicts the specimens' photos after the shearing phase. The p'_0 = 4 MPa photos show severely broken samples at the end of the shearing phase, whereas the p'_0 = 2 MPa show almost intact samples at the end of the shearing phase.

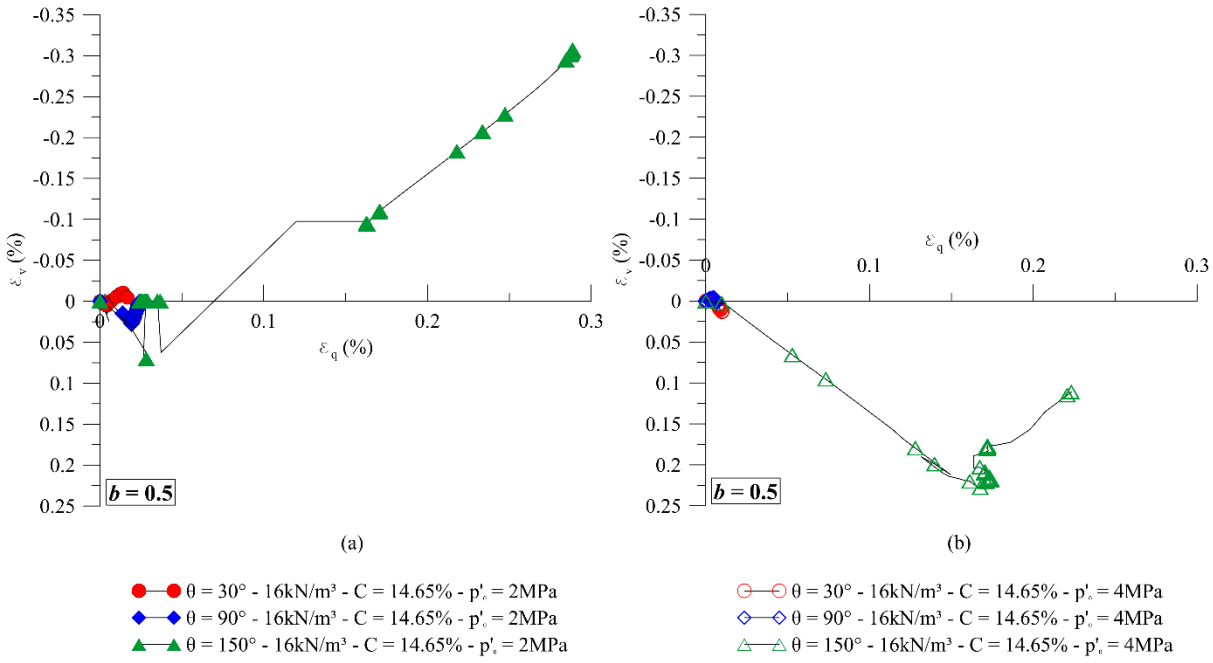

Figure 79: Intermediate stress parameter *b* = 0.5 deviatoric strain *Vs.* volumetric strain curves.

Finally, Figure 80 presents the deviatoric stress *Vs.* deviatoric strain of b = 1 tested samples. The inherent anisotropy induced by the specimens' preparation method seems to persist like in the other loading stress paths. The θ = 60° loading stress path tests got higher strengths

and stiffness than the θ = 180° loading stress path tests. The θ = 60° loading stress path tests are characterized to have the σ_1 in both Y and Z-axes, this latter the same of the molding compaction axis which may justify the θ = 60° tests higher strength and stiffness.

Figure 81 depicts, the deviatoric strain *Vs.* volumetric strain curves of *b* = 1 test results. As expected, both θ = 60° and 180° stress paths are dilative owing to the loading condition. Nonetheless, the θ = 60° stress path outcame less volumetric instability than the θ = 180° stress path, reassuring the previous statement about the inherent anisotropy persistence.

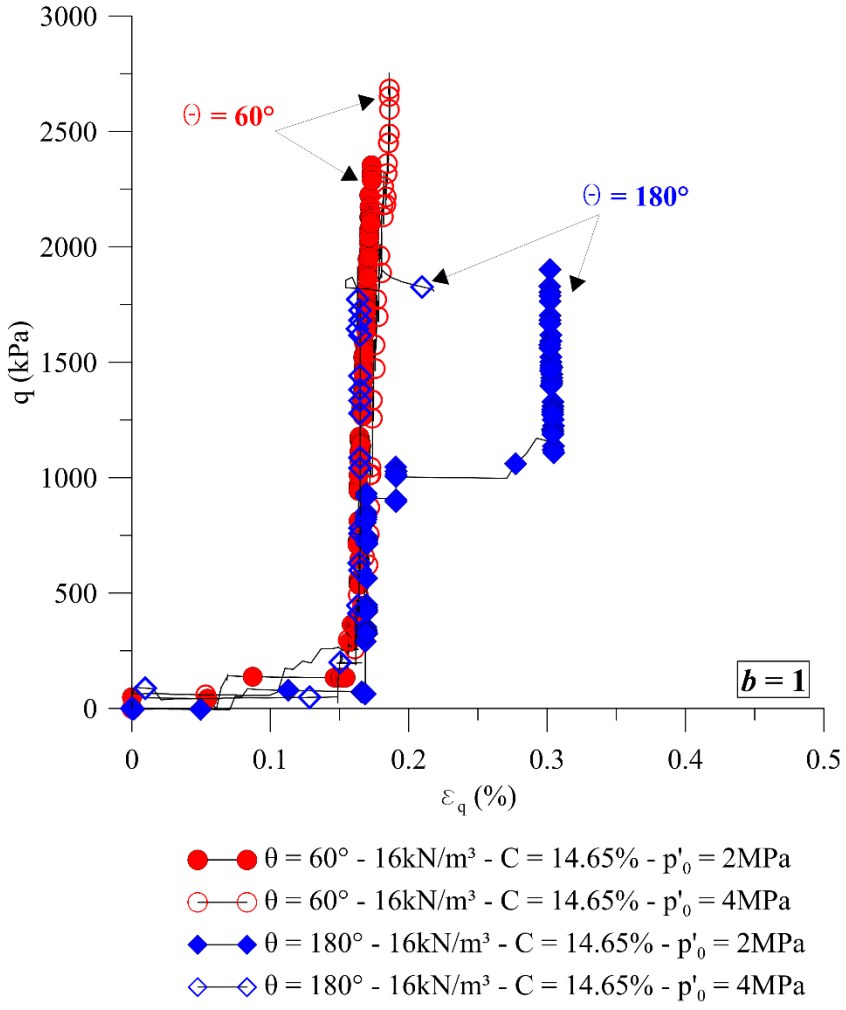

Figure 80: Intermediate stress parameter *b* = 1 stress *Vs.* strain curves.

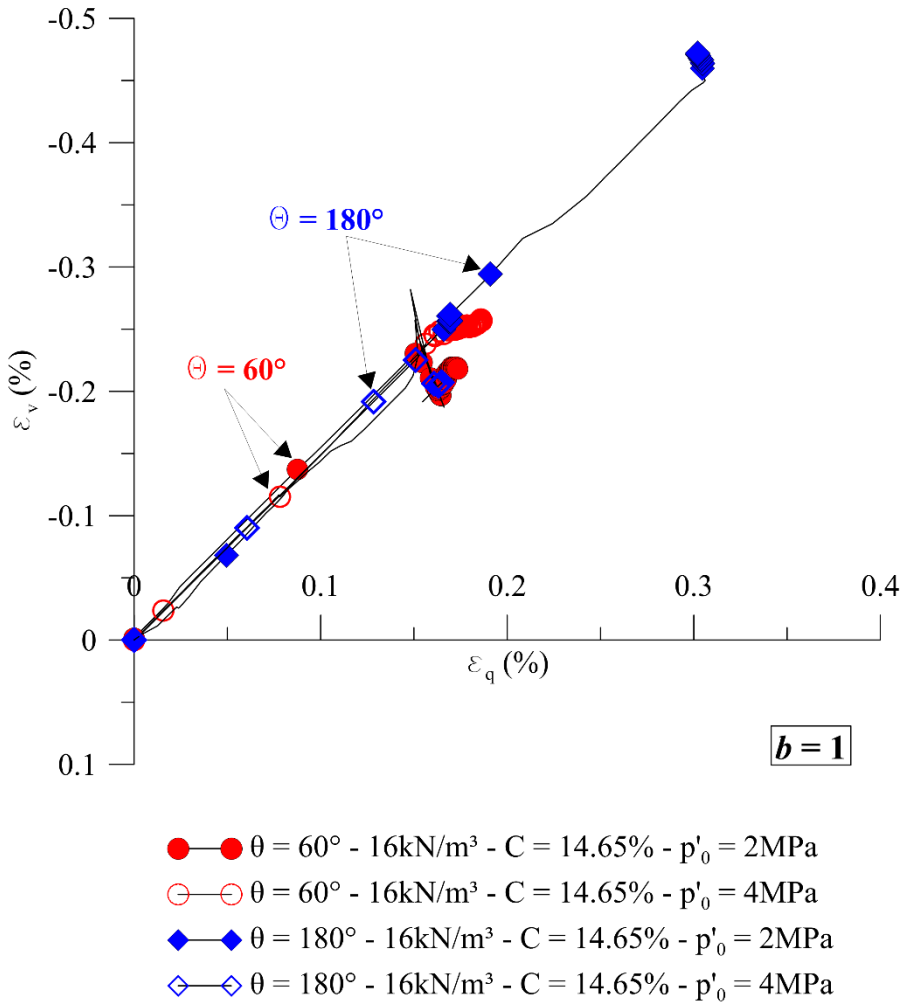

Figure 81: Intermediate stress parameter *b* = 1 deviatoric strain *Vs.* volumetric strain curves.

Figure 82 to Figure 84 present the ordinary sand-OPC blends axial stress *Vs.* axial strain by means each X, Y and Z loading axis.

Figure 82 depicts true triaxial tests results of *b* = 0, where figure letter (a) comprehends the θ = 0° loading condition, and figure letter (b) the θ = 120° loading condition. Figure 82 also discretizes the p'$_0$ = 2 MPa (filled symbols) and p'$_0$ = 4 MPa (empty symbols) test results.

Figure 82a and Figure 82b assist in comparing the principal strain ranges and directions for the *b* = 0 test results. For instance, if we consider the θ = 0° loading condition, where the Z-axis assumes the role of the major principal stress and the X and Y-axis assume the role of

the intermediate and minor principal stresses. Therefore, in the absence of specimens' anisotropy, it is expected that ε_2 and ε_3 principal strains succeed in the same range and directions. This occurs for p'_0 = 2 MPa samples, where both X and Y-axes follow the same strain path (see Figure 82a - the p'_0 = 2 MPa test results). The same conclusions cannot be extended for p'_0 = 4 MPa test results, where the X and Y-axes differ from one another in terms of strain paths (see Figure 82a - the p'_0 = 4 MPa test results).

If we broad our previous analysis for Figure 82b, namely, the θ = 120° loading condition, the same conclusions can be inferred. The θ = 120° loading condition has the major principal stress on the Y-axis, whereas the intermediate and minor principal stresses on the X and Z-axes. These latter axes follow the same strain paths for the p'_0 = 2 MPa test results and differ from one another in the case of the p'_0 = 4 MPa test results.

These former conclusions lead to consider that the p'_0 = 4 MPa may promote the cementation phase disruption, and outcoming in matrix isotropy loss due to the cement insertion. Another aspect that may confirm such assertion regards to the p'_0 = 2 MPa and p'_0 = 4 MPa strain ranges. The p'_0 = 4 MPa strain ranges are considerably higher than the p'_0 = 2 MPa tests.

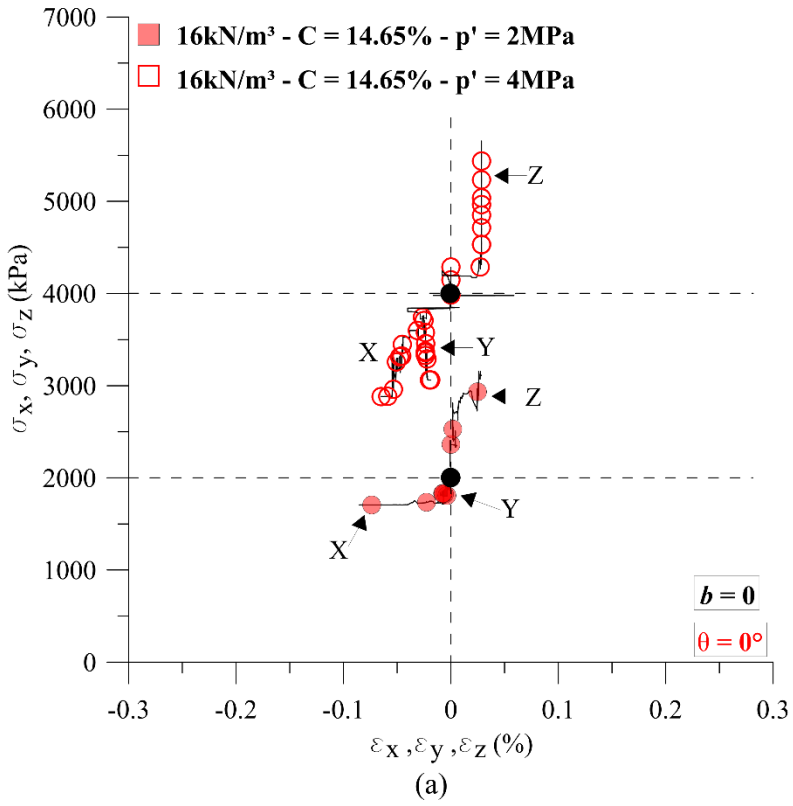

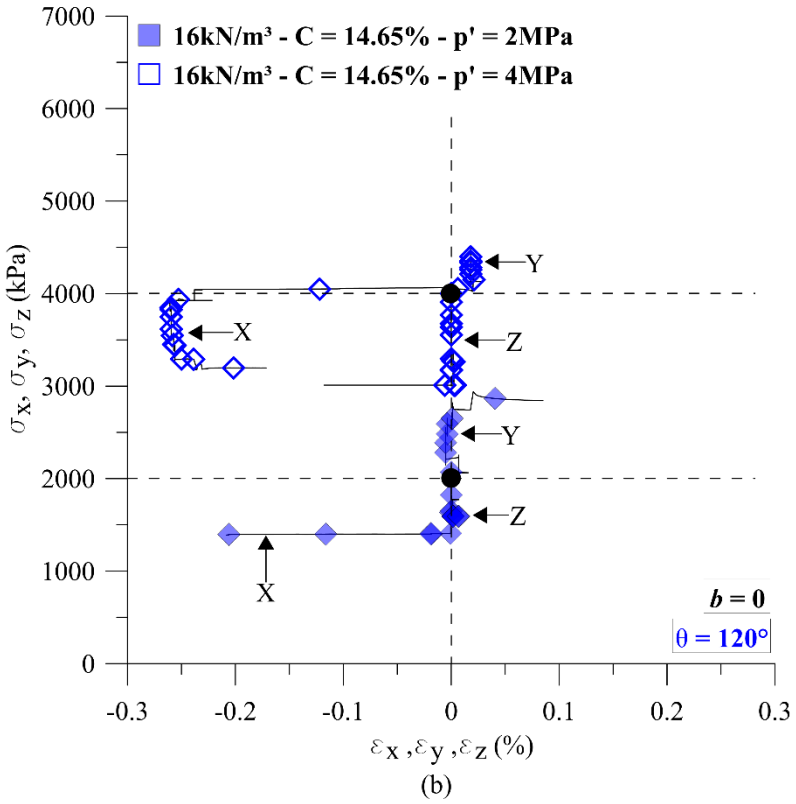

Figure 82: X, Y and Z stress *Vs.* strains curves to b = 0: a) θ = 0°; and b) θ = 120°.

The same pattern previous adopted to present the b = 0 test results is here extended for the b = 0.5 test results in Figure 83. Figure 83 letter (a) comprehends the θ = 30° loading condition, figure letter (b) the θ = 90° loading condition, and figure letter (c) the θ = 150° loading condition. The b = 0.5 test results have two loading axes whereas the third remains constant at the same stress magnitude in order to promote a plane stress loading condition. Parallel conclusions inferred for the b = 0 tests results can also be extended for the b = 0.5 test results.

The induced Z-axis molding compaction anisotropy, which it would be supposed to be erased by the cement inclusion, might switched on again with the cementing phase broken/yielding. In general, the p'_0 = 2 MPa tests outcame strict strain ranges than the p'_0 = 4 MPa true triaxial tests.

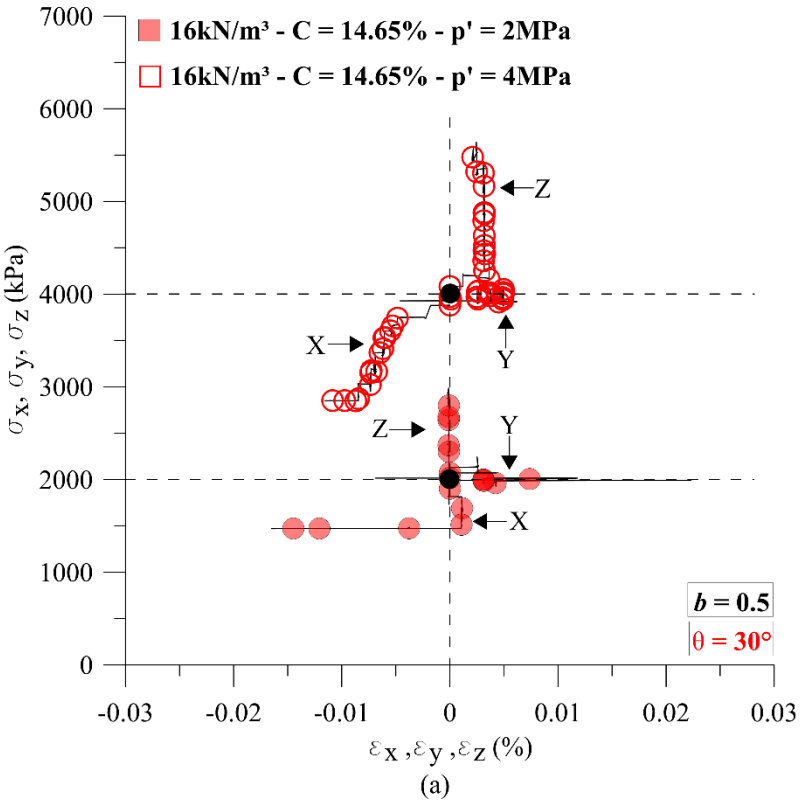
16kN/m³ - C = 14.65% - p' = 2MPa
16kN/m³ - C = 14.65% - p' = 4MPa
7000
6000
5000
4000
3000
2000
1000
0
σx, σy, σz (kPa)
-0.03
-0.02
-0.01
0
0.01
0.02
0.03
εx ,εy ,εz (%)
X
Y
Z
b = 0.5
θ = 30°

(a)

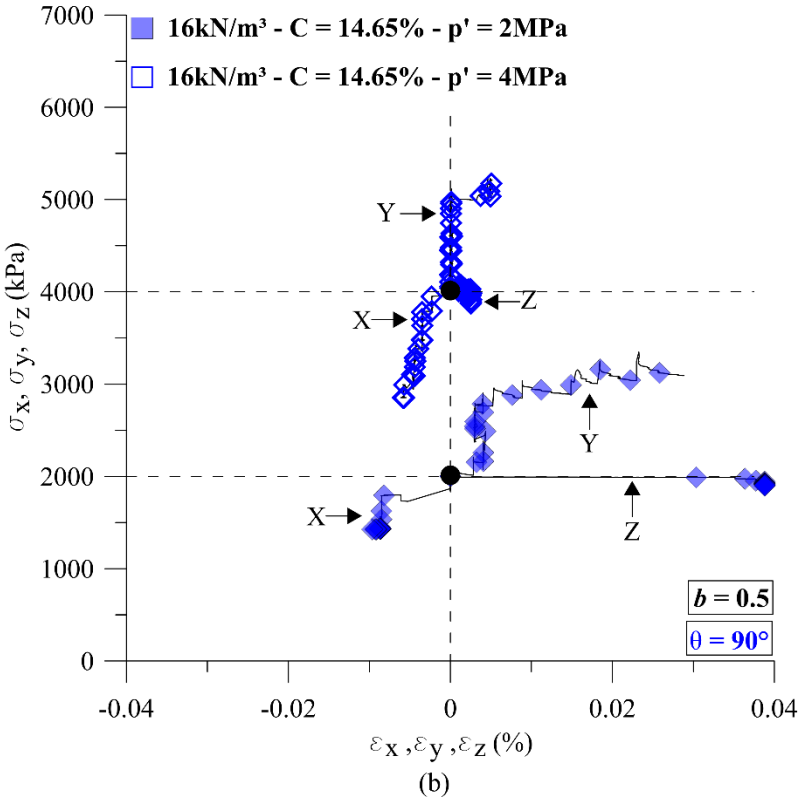
16kN/m³ - C = 14.65% - p' = 2MPa
16kN/m³ - C = 14.65% - p' = 4MPa
7000
6000
5000
4000
3000
2000
1000
0
σx, σy, σz (kPa)
-0.04
-0.02
0
0.02
0.04
εx ,εy ,εz (%)
X
Y
Z
b = 0.5
θ = 90°

(b)

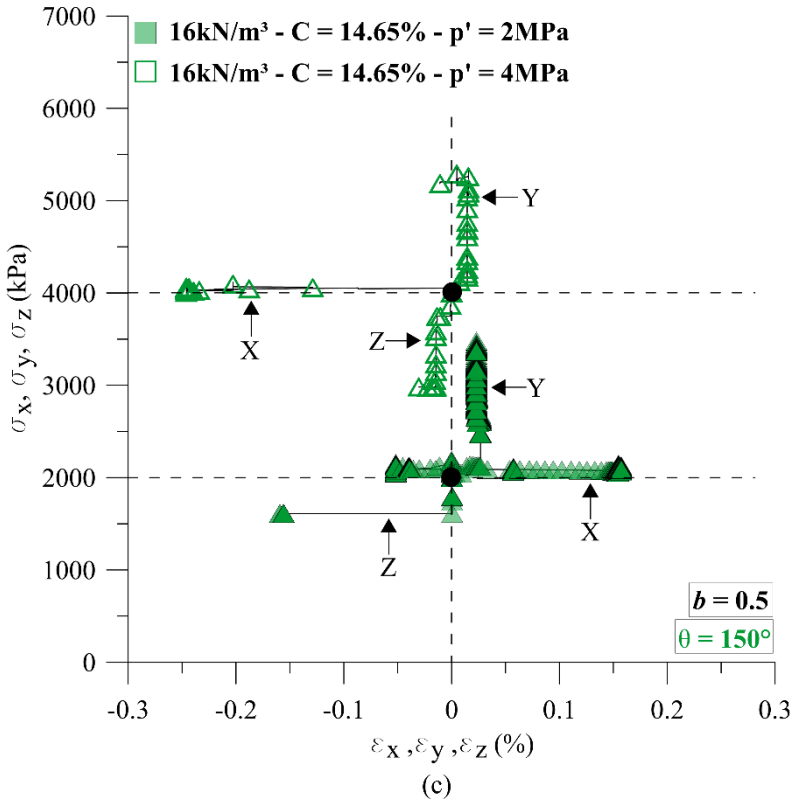

Figure 83: X, Y and Z stress *Vs.* strains curves to b = 0.5: a) θ = 30°; b) θ = 90°; and c) θ = 150°.

Figure 84 depicts true triaxial test results of b = 1, where figure letter (a) comprehends the θ = 60° loading condition, and figure letter (b) the θ = 180° loading condition. Both Figure 84a and Figure 84b restate what was previously addressed, namely, the soil matrix isotropy promoted by the OPC inclusion until the yielding threshold point. Once the soil matrix starts yielding it seems that the soil anisotropy is recoverable. Such statements are addressed based on Figure 84a and Figure 84b test results. In the case of Figure 84a, both Y and Z-axes (the σ_1 axes) are identical for θ = 60° and p'_0 = 2 MPa but differ for θ = 60° and p'_0 = 4 MPa. Somewhat similar occur for Figure 84b and θ = 180°, where the X and Y-axes are identical for p'_0 = 2 MPa and differ for p'_0 = 4 MPa. These findings indicate that the cementation phase may erase the induced anisotropy only under the yielding threshold point.

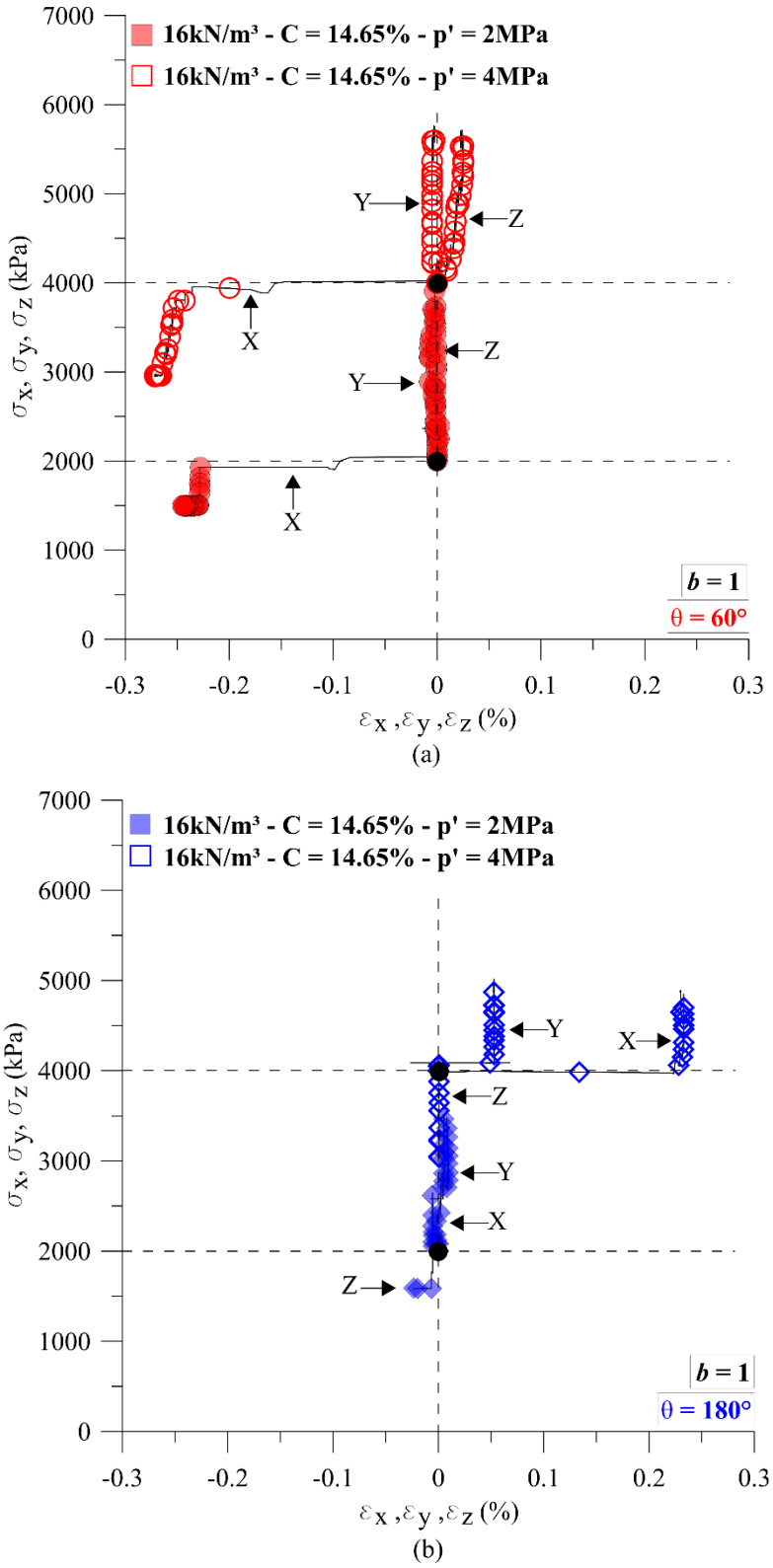

Figure 84: X, Y and Z stress *Vs.* strains curves to *b* = 1: a) θ = 60°; and b) θ = 180°.

Table 10 summarizes the ordinary sand-OPC blends true triaxial test results; variables like the test loading condition, specimens' void ratio after the consolidation phase, specimens $\eta/C_{iv}^{0.16}$ index, the maximum deviatoric stress, among others are included in this table. Specimens more detailed aspects can be seen in Appendix B where specimens' pictures are included. Even though the $q_{max.}$ variable is included in Table 10, it is important to pay attention to the fact that for the Colorado School of Mines true triaxial tests the mean effective stress was not hold constant at the end of the shearing phase. Therefore, for a samples' fair comparison it is necessary to take a look on variables normalized by the mean effective stress (p').

Table 10: Ordinary sand-OPC blends test results.

Parameters	Test characteristics													
	p' = 2MPa γ_d = 16 kN/m³ C = 14.65 %	p' = 4MPa γ_d = 16 kN/m³ C = 14.65 %	p' = 2MPa γ_d = 16 kN/m³ C = 14.65 %	p' = 4MPa γ_d = 16 kN/m³ C = 14.65 %	p' = 2MPa γ_d = 16 kN/m³ C = 14.65 %	p' = 4MPa γ_d = 16 kN/m³ C = 14.65 %	p' = 2MPa γ_d = 16 kN/m³ C = 14.65 %	p' = 4MPa γ_d = 16 kN/m³ C = 14.65 %	p' = 2MPa γ_d = 16 kN/m³ C = 14.65 %	p' = 4MPa γ_d = 16 kN/m³ C = 14.65 %	p' = 2MPa γ_d = 16 kN/m³ C = 14.65 %	p' = 4MPa γ_d = 16 kN/m³ C = 14.65 %	p' = 2MPa γ_d = 16 kN/m³ C = 14.65 %	p' = 4MPa γ_d = 16 kN/m³ C = 14.65 %
	θ (°)													
	0°		30°		60°		90°		120°		150°		180°	
b	0		0.5		1		0.5		0		0.5		1	
σ_1	Z		Z		Z and Y		Y		Y		Y		Y and X	
q/p'	0.6	0.7	0.7	0.7	0.8	0.6	0.9	0.6	0.8	0.6	0.8	0.6	0.7	0.4
p' (kPa)	2222.2	3866.6	2157.9	4169.5	3090.3	4785.2	2225.3	4026.3	1998.6	3705.2	2405.6	4134.9	2853.6	4315.6
q_x (kPa)	0	0	382	824	1449	1678	1358	1680	1481	1621	955	853	0	0
q_z (kpa)	1146	2190	1017	1802	1117	1179	0	0	-680	-863	-973	-1418	-1553	-1974
q_x / p'	0.0	0.0	0.2	0.2	0.5	0.4	0.6	0.4	0.7	0.4	0.4	0.2	0.0	0
q_z / p'	0.5	0.6	0.5	0.4	0.4	0.2	0.0	0.0	-0.3	-0.2	-0.4	-0.3	-0.5	-0.5
$e_{cons.}$	0.720	0.653	0.653	0.674	0.645	0.653	0.660	0.658	0.653	0.653	0.662	0.650	0.661	0.658
$\eta/C_{iv}^{0.16}$	32.09	30.20	30.20	30.80	29.96	30.20	30.39	30.34	30.20	30.20	30.45	30.10	30.43	30.34
$q_{max.}$ (kPa)	1403.1	2872.2	1515.2	2789.5	2381.2	2754.3	1920.4	2375.8	1525.8	2250.9	1866.4	2405.1	1902.1	1912.0

Figure 85 portrays the true triaxial test results in function of the θ loading angle, whereas Figure 86 displays the test results on the deviatoric plane by means of the orthogonal deviatoric stress components q_x and q_z. Figure 85a highlights the initial mean effective stress influence on the maximum deviatoric stress, where p'_0 = 4 MPa tests attained greater strengths than the p'_0 = 2 MPa tests. This pattern is exceptionally not observed for the θ = 180° true triaxial tests. However, Figure 85a may lead to misunderstanding because of the mean effective stress (p') variation at the end of each test, therefore Figure 85b shows the deviatoric stress (q) normalized by its corresponding mean effective stress (q/p'). Figure 85b illustrates the p' influence on each test result, despite the p'_0 = 4 MPa attained greater strengths, they also achieved great mean effective stresses, thence, shifting the red-rounded symbols (4 MPa tests) to under the blue-triangular symbols (2 MPa tests). The same conclusions can also be extended for Figure 86.

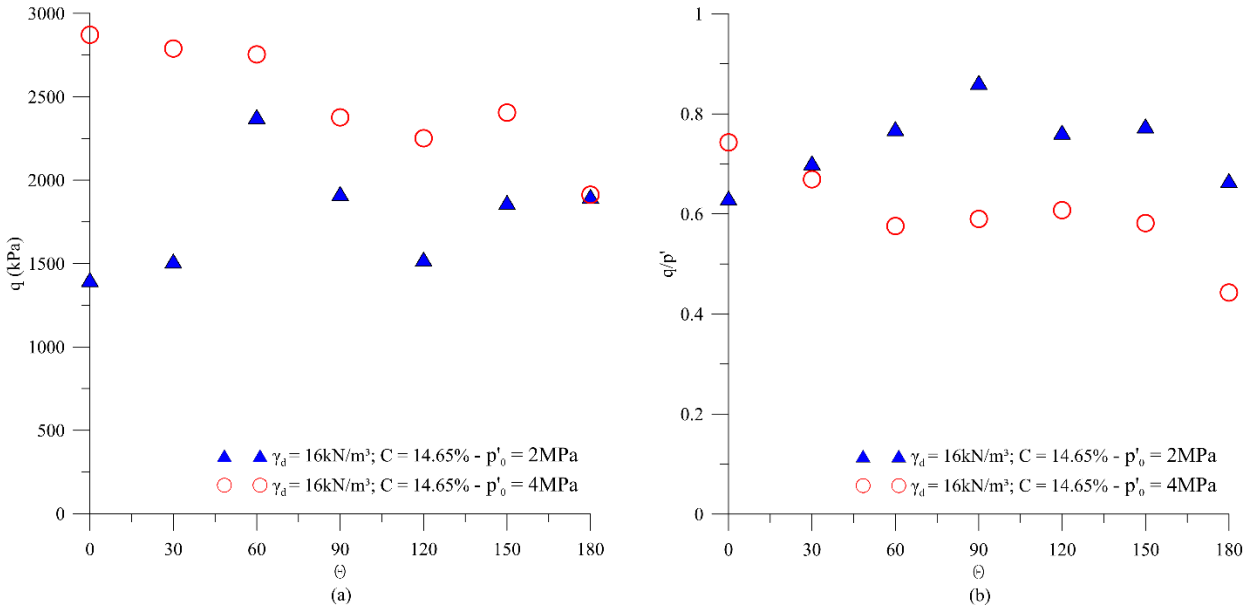

Figure 85: Experimental test results bearing capacity: a) Deviatoric stress (q) in function of the θ loading angle; and b) normalized deviatoric stress (q/p') in function of the θ loading angle.

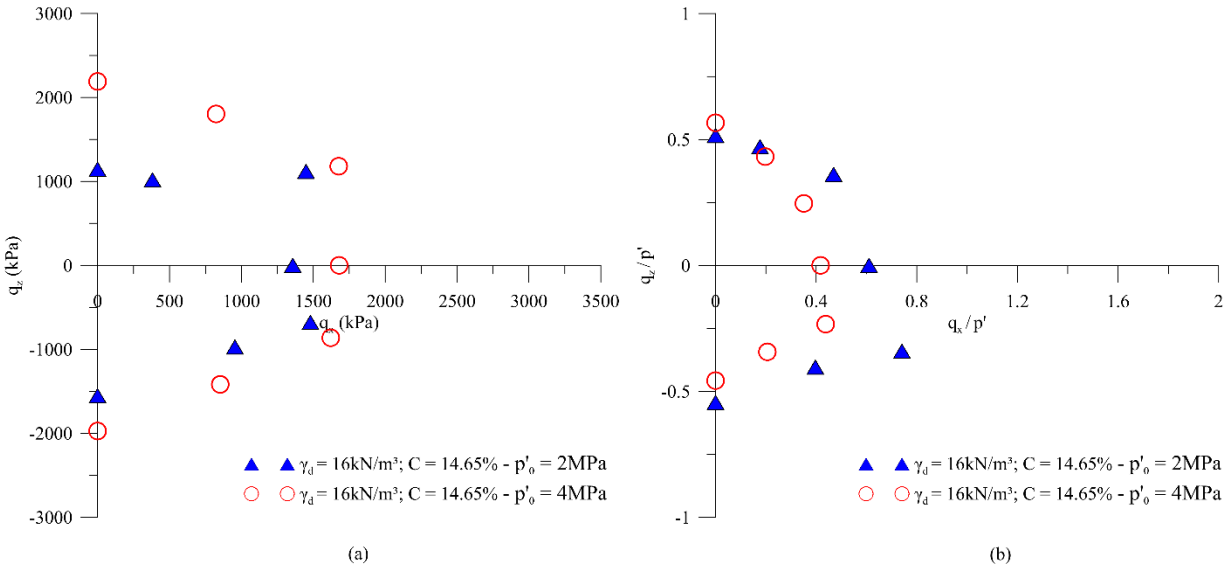

Figure 86: Experimental test results planification on the π plane: a) q_z and q_x variables; and b) normalized q_z/p' and q_x/p' variables.

Figure 87 shows the Mohr-Coulomb failure criteria adjustment for the experimental test results. One of the same assumptions adopted for the iron ore tailing-OPC blends was also extended to these test results like: (i) the presumed cohesion intercept due to the OPC insertion was neglected. The failure envelopes depicted in Figure 87 regard the strength parameters found in the conventional triaxial tests (Figure 74 and Figure 75), where an internal friction angle of $\phi = 32°$ was found for natural soil samples and $\phi = 50°$ for cement-treated soil samples. The present thesis does not have Colorado School of Mines true triaxial tests carried out on natural ordinary sand, therefore the $\phi = 32°$ failure envelope draw in Figure 87 regards to a failure envelope reference. Theoretically speaking, by the Figure 87, both $p'_0 = 2$ MPa and $p'_0 = 4$ MPa tested samples remained far away from the cement treated failure envelope.

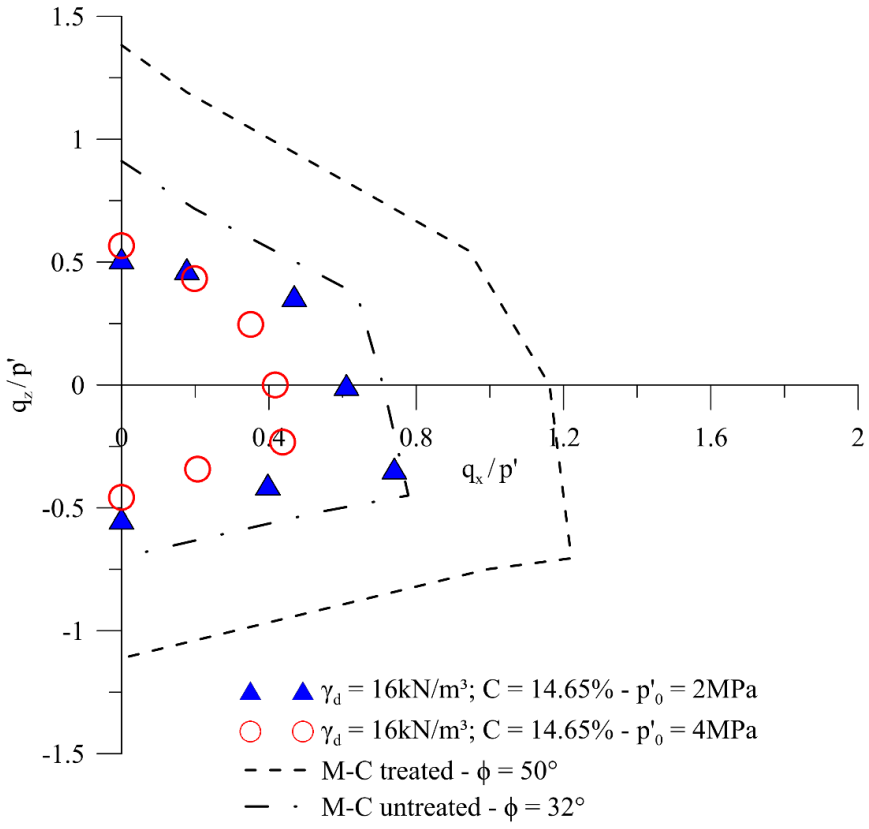

Figure 87: The Mohr-Coulomb failure criterion fitted to the experimental test results.

4.2.3 Phase II test results summary

The $\eta/C_{iv}^{0.16}$ index proves to be useful and a reliable dosage tool for cement-treated soils even for a multiaxial loading condition. Despite of the cement content and porosity combinations, a single η/C_{iv} index value turns to attain the same engineering properties. This opens huge opportunities for the field engineer, who may opt to increase the cement content or the degree of compaction whichever is less expensive.

The effect of ordinary Portland cement inclusion in the iron ore tailing matrix was marginal in terms of strength gain, but substantial in terms of stiffness gain. Festugato et al. (2024) carried out true triaxial tests on cement treated Osório sand specimens, where the Osório sand-OPC samples were cured under atmospheric pressure and afterward isotropically consolidated to 200, 400 and 700 kPa. After the consolidation phase, the tested samples were unloaded and sheared under a mean effective stress of 100 kPa. Somewhat the isotropic consolidation broke the cementing bonds, and the cement inclusion benefit in terms soil strength gain was not relevant when compared with untreated soil samples. This did not extend for the soil stiffness gain, which was maintained even after the cementing bonds breakage. Samples' stiffness maintenance even after the cement bonds breakage may occur because of the voids reduction compensation (soil grains interaction increase). A similar effect might be occurred in the present these for the iron ore tailing-cement treated samples, even though the tests were carried out under the yielding stress point.

The induced Z-axis molding compaction anisotropy was erased for iron ore tailing-OPC blends, which might be attributed to the matrix fines content and cement inclusion (cement contents of 2.66 and 4.38%). On the contrary, for ordinary sand-OPC blends the induced Z-axis molding compaction anisotropy was only erased for samples in which the initial mean effective stress (p'_0) remained under the inferred yielding point. Andreghetto (2022) suggested that the soil anisotropy erasing might be a function of the cement amount added to the soil matrix, which seems to be reasonable. However, the present thesis proved that this statement is only valid for specimens tested under the presumed yielding threshold point.

5 CONCLUSIONS

5.1 SUMMARY OF MAIN CONCLUSIONS

The present thesis main conclusions are as follows:

1) The η/C_{iv} index proves to be useful and a reliable dosage tool for cement-treated soils even for a multiaxial loading condition. Despite of the cement content and porosity combinations, a single η/C_{iv} index value turns to attain the same engineering properties. This opens huge opportunities for the field engineer, who may opt to increase the cement content or the degree of compaction whichever is less expensive.

2) By means of decreasing specimens' porosity and increasing the cement content, specimens obtained both strength and stiffness mechanical properties improvement.

3) The dry unit weight (porosity) impact on specimens' engineering properties is described by a power function, whereas the cement content linearly impacted the same properties.

4) Specimens' stiffness seems not to be impacted by the dry unit weight-cement content interaction. The cement content dictated the specimens' final stiffness.

5) The effect of ordinary Portland cement inclusion in the samples' strength gain depends on the mean effective stress subjected to the soil matrix. Mean effective stresses higher than the yielding threshold point may lessen the cement benefits on the ultimate failure strength. Nonetheless, a mean effective stress higher than the yielding threshold point did not influence specimens' stiffness, where gains were observed even for this kind of condition.

6) The induced Z-axis molding compaction anisotropy is erased with cement inclusion. Nonetheless, this phenomenon is only evidenced for samples tested under the yielding

threshold point. Specimens tested over the yielding threshold point had their induced anisotropy “recovered”.

5.2 FURTHER RESEARCH

The experimental test results exhibited in the present thesis shed light on new geotechnical insight that must be further investigated. Further researches may comprise the following topics:

1) To promote further true triaxial tests with other several cementing agents and soils matrices.
2) To promote true triaxial tests under and over the yielding points among other materials. This topic seeks to ensure the possibility of the matrix anisotropy return if the yielding point is achieved.
3) Carry out tests in more robust equipment like the hollow cylinder equipment in order to check the induced matrix anisotropy and the cement inclusion feasibility in erasing it or not.
4) Evaluate the fines content impact on the induced Z-axis molding compaction anisotropy erasing.

REFERENCES

Abelev, A. V.; Lade, P. V. (2003). **Effects of Cross Anisotropy on Three-Dimensional Behavior of Sand. I: Stress-Strain Behavior and Shear Bending**. *Journal of engineering mechanics*. 129 (2): 160-166. https://doi.org/10.1061/(ASCE)0733-9399(2003)129:2(160)

Agência Nacional de Mineração – ANM (2020). **Sumário Mineral Brasileiro 2018**. p. 28.

Agência Nacional de Mineração – ANM (2021). **Sistema integrado de gestão de barragens de mineração – SIGBM versão pública**. Ministério de Minas e Energias, Governo Federal.

Airey, D. W., Wood, D, M. (1988). **The Cambridge true triaxial apparatus**. ASTM STP 977. West Conshohocken, PA: ASTM.

Aïtcin, P-C. (2000). **Cements of yesterday and today- Concrete of tomorrow**. *Cement and Concrete Research*, 30 (200), pp. 1349-1359. https://doi.org/10.1016/S0008-8846(00)00365-3

Al-Ajmi, A. M.; Zimmerman, R. W. (2005). Relation between the Mogi and the Coulomb failure criteria. International Journal of Rock Mechanics & Mining Sciences, 42(2005), pp. 431-439. https://doi.org/10.1016/j.ijrmms.2004.11.004

Amsden, M.P. (1974). **Ecstall concentrator**. *CIM Bull*., 67 (745), pp. 105-115.

Andersen, K. H. (2009). **Bearing capacity under cyclic loading — offshore, along the coast, and on land**. *In*: The 21st Bjerrum Lecture presented in Oslo, 23 November 2007, *Canadian Geotechnical Journal*, v.46, no. 5, pp. 513–535. https://doi.org/10.1139/t09-003

Andreghetto, D. H. (2022). **Comportamento de areias cimentadas artificialmente sob tensão multiaxial**. 2022. Tese (Doutorado em Engenharia) – Programa de Pós-Graduação em Engenharia Civil, Universidade Federal do Rio Grande do Sul, UFRGS, Porto Alegre.

Andreghetto, D. H.; Festugato, L.; Miguel, G. D.; da Silva, A. (2022). **Automated True Triaxial Apparatus Development for Soil Mechanics Investigation**. *Soils & Rocks*. Accepted for publication.

American Society for Testing and Materials (2003). D5298: Standard Test Method for Measurement of Soil Potential (Suction) Using Filter Paper. United States, p. 6.

_____. (2008). D2845: Standard Test Methods for Laboratory Determination of Pulse Velocities and Ultrasonic Elastic Constants of Rock. United States, p. 7.

_____. (2009). D5102: Standard Test Methods for Unconfined Compressive Strength of Compacted Soil-Lime Mixtures. United States, p. 7.

_____. (2011). D7181: Standard Test Methods for Consolidated Drained Triaxial Compression Test for Soils. United States, p. 11.

_____. (2014). D854: Standard Test Methods for Specific Gravity of Soil Solids by Water Pycnometer. United States, p. 8.

_____. (2015). D559/D559M: Standard Test Method for Wetting and Drying Compacted Soil-Cement Mistures. United States, p. 4.

_____. (2016). D4254: Standard Test Methods for Minimum Index Density and Unit Weight of Soils and Calculation of Relative Density. United States, p. 9.

_____. (2017). D2487: Standard Practice for Classification of Soils for Engineering Purposes (Unified Soil Classification System). United States, p. 10.

_____. (2017). D4318: Standard Test Methods for Liquid Limit, Plastic Limit, and Plasticity Index of Soils. United States, p. 20.

_____. (2017). D6913M: Standard Test Methods for Particle-Size Distribution (Gradation) of Soils Using Sieve Analysis. United States, p. 34.

_____. (2017). C496/C496M: Standard Test Methods for Splitting Tensile Strength of Cylindrical Concrete Specimens. United States, p. 5.

_____. (2019). D4972: Standard Test Methods for pH of Soils. United States, p. 6.

_____. (2021). D698: Standard Test Methods for Laboratory Compaction Characteristics of Soil Using Standard Effort (12,400 ft-lbf/ft³ (600 kN-m/m³)). United States, p. 13.

_____. (2021). D1557: Standard Test Methods for Laboratory Compaction Characteristics of Soil Using Modified Effort (56,000 ft-lbf/ft3 (2,700 kN-m/m3)). United States, p. 13. https://doi.org/10.1520/D0698-12R21

_____. (2021). C150/C150M-21: Standard Specification for Portland Cement. United States, p. 9. https://doi.org/10.1520/C0150_C0150M-21

_____. (2021). C39/C39M-21: Standard Test Method for Compressive Strength of Cylindrical Concrete Specimens. United States, p. 8. https://doi.org/10.1520/C0039_C0039M-21

_____. (2021). C511-21: Standard Specification for Mixing Rooms, Moist Cabinets, Moist Rooms, and Water Storage Tanks Used in the Testing of Hydraulic Cements and Concretes. United States, p. 3. https://doi.org/10.1520/C0511-21

Amini, F.; Qi, G. Z. (2000). **Liquefaction testing of stratified silty sands**. *J. Geotech Geoenviron. Eng.*, 126(3), pp. 208–217. https://doi.org/10.1061/(ASCE)1090-0241(2000)126:3(208)

Arthur, J. R. F.; Menzies, B. K. (1968). **Discussion of 'A new soil testing apparatus' by H. -Y. Ko and R. F. Scott**, *Geotechniqué*, London, England, v. 18, n. 2, pp. 271-272.

Associação Brasileira de Normas Técnicas (2018). **NBR 7181: Solo – Análise Granulométrica Método de Ensaio**. Rio de Janeiro, p. 16.

_____. (2016). **NBR 7182: Solo – Ensaio de compactação**. Rio de Janeiro, p. 13.

Austroads Ltd. (2019). **Guide to Pavement Technology Part 4D: Stabilised Materials**. Ed. Geoff Jameson and Graham Hennessy, Sydney, Autralia.

Azizli, K. A. M.; Chee Yau, T.; Birrel, J. (1995). **Design of the Lohan tailings dam, Mamut Copper Mining Sdn. Bhd., Malaysia**. *Minerals Engineering*, v. 8, n. 6, pp. 705-712.

Baghdadi, Z. A.; Fatani, M. N.; Sabban, N. A. (1995). **Soil Modification by Cement Klin Dust**. *Journal of Materials in Civil Engineering*, Vol. 7, No. 4, pp. 218-222. https://doi.org/10.1061/(ASCE)0899-1561(1995)7:4(218)

Baldovino, J.; dos Santos Izzo, R. L.; Rose, J. L. (2021). **Effects of freeze–thaw cycles and porosity/cement index on durability, strength, and capillary rise of a stabilized silty soil under optimal compaction conditions**. *Geotech. Geol. Eng*., 39 (1), pp. 481–498. https://doi.org/10.1007/s10706-020-01507-y.

Baran, P.A.; Sweezy, P.M. (1968). **Monopoly capital: An essay on the American economic and social order** (Harmondsworth: Penguin Books).

Barbery, G. (1991). **Mineral Liberation, Measurement, Simulation and Practical Use in Mineral Processing**. Les Editions GB, Quebec, Canada.

Baum, W.; Lotter, N. O.; Whittaker, P. J. (2004). **Process mineralogy—a new generation for ore characterization and plant optimization**. 2003 SME Annual Meeting and Exhibit, Denver, CO, USA, Preprint 04-012: 15.

Bayat. E.; Bayat, M. (2012). **Effect of grading characteristics on the undrained shear strength of sand: review with new evidences**. *Arab. J. Geosci*., 6, pp. 4409–4418. https://doi.org/10.1007/s12517-012-0670-y

Been, K.; Jefferies, M. G. (1985). **A state parameter for sands**. *Géotechnique*, 35(2), pp. 99-112. https://doi.org/10.1680/geot.1985.35.2.99

Behnood, A. (2018). **Soil and clay stabilization with calcium- and non-calcium-based additives: A state-of-the-art review of challenges, approaches and techniques**. *Transp. Geotech*. 17 (Dec), pp.14–32. https://doi.org/10.1016/j.trgeo.2018.08.002.

Bell, J. M. (1968). **Discussion of 'A new soil testing apparatus' by H. -Y. Ko and R. F. Scott**, *Geotechniqué*, London, England, v. 18, n. 2, pp. 267-271.

Benghalia, Y.; Bouafia, A.; Canou, J.; Dupla, J. C. (2015). **Liquefaction susceptibility study of sandy soils: effect of low plastic fines**. *Arabian Journal of Geosciences, Springer*, 2015, 8 (2), pp.605-618. https://doi.org/10.1007/s12517-013-1255-0

Benzaazoua, M.; Perez, P.; Belem, T.; Fall, M. (2004). **A laboratory study of the behaviour of surface paste disposal**. *In*: Proc. 8th International Symposium on Miningwith Backfill. Nonferrous Metals Society of China, Beijing, China, pp. 180-192.

Berger, K. C. (2018). **Tailings Dam Inspection And Monitoring**. Accessed in: feb. 2022. < https://africanminingbrief.com/2018/10/04/tailings-dam-inspection-and-monitoring/ >

Bieniawski, Z.T. (1871). **Deformational behaviour of fractured rock under multiaxial compression**. *In*: Structure, Solid Mechanics and Engineering Design. Te'eni, M. (ed.). Proc. Southampton 1969 Civil Engineering Materials Conference. London: Wiley-Interscience, (1971), pp. 589-598.

Bittar Marín, E.J. (2017). **Estudo de Campo e Laboratório do Comportamento Mecânico de Um Solo Sulfatado Estabilizado com Cal**. Dissertação (Mestrado em Engenharia Civil) – Programa de Pós-Graduação em Engenharia Civil, UFRGS, Porto Alegre, Brasil.

Bortolotto, M. S. (2017). **Bender Elements, Ultrasonic Pulse Velocity, and Local Gauges for the Analysis of Stiffness Degradation of an Artificially Cemented Soil**. Dissertação (Mestrado em Engenharia) – Programa de Pós-Graduação em Engenharia Civil, UFRGS, Porto Alegre.

Bruschi, G. J.; dos Santos, C. P.; de Araújo, M. T.; Ferrazzo, S. T.; Marques, S. F. V.; Consoli, N. C. (2021). **Green stabilization of bauxite tailings: A mechanical study on 1 alkali-activated materials**. *Journal of Materials in Civil Engineering*, (accepted for publication).

Bussière, B. (2007). **Colloquium 2004: hydrogeotechnical properties of hard rock tailings from metal mines and emerging geoenvironmental disposal approaches**. *Can. Geotech. J.*, 44 (9), pp. 1019-1052. https://doi.org/10.1139/T07-040

Carvalho, B. C. L. (2012). **Aproveitamento de minérios de ferro de baixo teor: tendências, tecnologias utilizadas e influências no sequenciamento de lavra**. Dissertação de mestrado, Departamento de engenharia de minas, UFOP, Ouro Preto, 2012.

Castro, G. (1969). **Liquefaction of Sand**. Ph.D. Thesis, Division of Engineering and Applied Physics, Harvard University, Cambridge, 1969.

Castro, G.; Poulos, S. J. (1977). **Factors Affecting Liquefaction and Cyclic Mobility**. *Journal of the Geotechnical Engineering Division*, v. 103, n. 6, pp. 501-516. https://doi.org/10.1061/AJGEB6.0000433

Castro, G.; Poulos, S. J.; France, J. W.; Enos, J. L. (1982). **Liquefaction induced by cyclic loading**. *Project 80696 - Report to National Science Foundation*, Washington D. C., March 1982, 353 p.

Chalkley, M. E.; Conard, B. R.; Lakshmanan, V. I.; Wheeland, K. G. (1989). **Tailings and effluent management**. *In*: Proc. International Symposium on Tailings and Effluent Management, Halifax, NS, Canada, 20-24 Aug. 1989.

Chandler, J. L. (1987). **The stacking and solar drying process for disposal of bauxite tailing in Jamaica**. *In*: Wagh, A.S., Desai, P. (Eds.), Bauxite Tailings 'Red Mud'. The Jamaica Bauxite Institute, pp. 101–105.

Chang, N. Y; Yeh, S.T.; Kaufman, L. P. (1982). **Liquefaction potential of clean and silty sands**. *In*: Proceedings of the Third International Earthquake Microzonation Conference, Seattle, USA, 2:1017–1032.

Chen, Q.; Zhang, C.; Yang, C.; Ma, C.; Pan, Z.; Daemen, J. J. K. (2019). **Strength and deformation of tailings with fine-grained interlayers**. *Engineering Geology*, v. 256, pp. 110-120. https://doi.org/10.1016/j.enggeo.2019.04.007

Clough, G. W.; Sitar, N.; Bachus, R. C. (1981). **Cemented Sands Under Static Loading**. *Journal of the Geotechnical Engineering Division*, v. 107, n. 6, p. 799–817, 1981. https://doi.org/10.1061/AJGEB6.0001152

Colombera, P. M.; Want, F. M. (1982). **Bauxite residue disposal and rheology**. *Chem. Eng. Aust*., 7, pp. 36–40.

Consoli, N. C. (1997). **Comparison of the measured and predicted performance of tailings sedimentation**. *Proc. Instn. Civ. Engrs. Geotech. Engng.*, v. 125, n. 3, pp. 179-187. https://doi.org/10.1680/igeng.1997.29468

Consoli, N. C.; Sills, G. C. (2000). **Soil formation from tailings: comparison of predictions and field measurements**. *Géotechnique*, v. 50, n. 1, pp. 25-33. https://doi.org/10.1680/geot.2000.50.1.25

Consoli, N. C.; Montardo, J. P.; Prietto, P. D. M.; Pasa, G. S. (2002). **Engineering Behavior of Sand Reinforced with Plastic Waste**. *Journal of Geotechnical and Geoenviromental Engineering*, Vol. 128, No. 6, pp. 462-472. https://doi.org/10.1061/(ASCE)1090-0241(2002)128:6(462)

Consoli, N. C.; Vendruscolo, M. A.; Prietto, P. D. M. (2003). **Behavior of Plate Load Test on Soil Layers Improved with Cement and Fiber**. *Journal of Geotechnical and Geoenviromental Engineering*, Vol. 129, No. 1, pp. 96-101. https://doi.org/10.1061/(ASCE)1090-0241(2003)129:1(96)

Consoli, N. C.; Casagrande, Dal Toé M.; Coop, M. R. (2005). **Effect of Fiber Reinforcement on the Isotropic Compression Behavior of a Sand**. *Journal of Geotechnical and Geoenviromental Engineering*, Vol. 131, No. 11, pp. 1434-1436. https://doi.org/10.1061/(ASCE)1090-0241(2005)131:11(1434)

Consoli, N. C.; Rotta, G. V.; Prietto, P. D. M. (2006). **Yielding Compressibility-Strength Relationship for an Artificially Cemented Soil Cured under Stress**. *Geotechnique*, Vol. 56, No. 1, pp. 69-72.

Consoli, N. C.; Casagrande, Dal Toé M.; Coop, M. R. (2007a). **Performance of a Fibre-Reinforced Sand at Large Shear Strains**. *Géotechnique*, Vol. 57, No. 9, pp. 751-756. https://doi.org/10.1680/geot.2007.57.9.751

Consoli, N. C.; Heineck, K. S.; Casagrande, Dal Toé M.; Coop, M. R. (2007b). **Shear Strength Behavior of Fiber-Reinforced Sand Considering Triaxial Tests under Distinct Stress Paths**. *Journal of Geotechnical and Geoenviromental Engineering*, Vol. 133, No. 11, pp. 1466-1469. https://doi.org/10.1061/(ASCE)1090-0241(2007)133:11(1466)

Consoli, N. C.; Foppa, D.; Festugato, L.; Heineck, K. S. (2007c). **Key Parameters for Strength Control of Artificially Cemented Soils**. *J. Geotech. Geoenviron. Eng*., Vol. 133, No. 2, pp. 197-205. https://doi.org/10.1061/(ASCE)1090-0241(2007)133:2(197)

Consoli, N. C., da Silva Lopes Jr., L.; Foppa, D.; Heineck, K. S. (2009a). **Key parameters dictating strength of lime/cement-treated soils**. *Proc. Inst. Civ. Eng. Geotech. Eng*., 162 (2), pp. 111–118. https://doi.org/10.1680/geng.2009.162.2.111.

Consoli, N. C.; da Silva Lopes Jr., L.; Heineck. K. S. (2009b). **Key parameters for the strength control of lime stabilized soils**. *J. Mater. Civ. Eng.*, 21 (5), pp. 210–216. https://doi.org/10.1061/(ASCE)0899-1561(2009)21:5(210).

Consoli, N. C.; Viana da Fonseca, A.; Cruz, R. C.; Heineck, K. S. 2009c. **Fundamental parameters for the stiffness and strength control of artificially cemented sand**. *J. Geotech. Geoenviron. Eng.*, 135 (9), pp. 1347–1353. https://doi.org/10.1061/(ASCE)GT.1943-5606.0000008.

Consoli, N. C.; Casagrande, Dal Toé M.; Thomé, A.; Dalla Rosa, F.; Fahey, M. (2009d**). Effect of Relative Density on Plate Loading Tests on Fibre-Reinforced Sand**. *Géotechnique*, Vol. 59. No. 5, pp. 471-476. https://doi.org/10.1680/geot.2007.00063

Consoli, N. C.; Vendruscolo, M. A.; Fonini, A.; Dalla Rosa, F. (2009e). **Fiber Reinforcement Effects on Sand Considering a Wide Cementation Range**. *Geotextiles*

and Geomembranes, Vol. 27, pp. 196-203. https://doi.org/10.1016/j.geotexmem.2008.11.005

Consoli, N. C.; Bassani, M. A.; Festugato, L. (2010a). **Effect of Fiber-Reinforcement on the Strength of Cemented Soils**. *Geotextiles and Geomembranes*, Vol. 28, pp. 344-351. https://doi.org/10.1016/j.geotexmem.2010.01.005

Consoli, N. C.; Cruz, R. C.; Floss, M. F.; Festugato, L. (2010b). **Parameters Contorlling Tensile and Compressive Strength of Artificially Cemented Sand**. *J. of Geotechnical and Geoenvironmental Engineering*, Vol. 136, issue 5, pp. 759-763. https://doi.org/10.1061/_ASCE_GT.1943-5606.0000278

Consoli, N. C.; Cruz, R. C.; Floss, M. F. (2011a). **Variables controlling strength of artificially cemented sand: Influence of curing time**. *J. Mater. Civ. Eng.*, 23 (5), pp. 692–696. https://doi.org/10.1061/(ASCE)MT.1943-5533.0000205.

Consoli, N. C.; Zortéa, F.; de Souza, M.; Festugato, L. (2011b). **Studies on the Dosage of Fiber-Reinforced Cemented Soils**. *Journal of Materials in Civil Engineering*, Vol. 23, pp. 1624-1632. https://doi.org/10.1061/(ASCE)MT.1943-5533.0000343

Consoli, N. C., da Fonseca, A. V.; Silva, S. R.; Cruz, R. C.; Fonini, A. (2012a). **Parameters controlling stiffness and strength of artificially cemented soils**. *Géotechnique*, 62 (2), pp. 177–183. https://doi.org/10.1680/geot.8.P.084.

Consoli, N. C.; Moraez, R. R.; Festugato, L. (2012b). **Parameters Controlling Tensile and Compressive Strength of Fiber –Reinforced Cemented Soil**. *Journal of Materials in Civil Engineering*, p. 14. https://doi.org/10.1061/(ASCE)MT.1943-5533.0000555

Consoli, N. C.; Ruver, C. A.; Girardello, V.; Festugato, L.; Thomé, A. (2012c). **Effect of Polypropylene Fibers on the Upflit Behavior of Model Footings Embedded in Sand**. *Geosynthetics International*, Vol. 19, No. 1, pp. 79-84. https://doi.org/10.1680/gein.2012.19.1.79

Consoli, N. C.; Consoli, B. S.; Festugato, L. (2013). **A practical methodology for the determination of failure envelopes of fiber-reinforced cemented sands**. *Geotext. Geomembr*. 41: 50–54. https://doi.org/10.1016/j.geotexmem.2013.07.010.

Consoli, N. C. (2014). **A Method Proposed for the Assessment of Failure Envelopes Cemented Sandy Soils**. J. Engineering Geology, Vol. 169, pp. 61-68. https://doi.org/10.1016/j.enggeo.2013.11.016

Consoli, N. C.; da Rocha, C. G.; Maghous, S. (2016a). **Strategies for developing more sustainable dosages for soil–coal fly ash–lime blends**. *J. Mater. Civ. Eng.*, 28 (11), pp. 04016130. https://doi.org/10.1061/(ASCE)MT.1943-5533.0001648.

Consoli, N. C.; Samaniego, R. A. Q.; Marques, S. F. V.; Venson, G. I.; Pasche, E.; Velásquez, L. E. G. (2016b). **Single model establishing strength of dispersive clay**

treated with distinct binders. *Can. Geotech. J*., 53 (12), pp. 2072–2079. https://doi.org/10.1139/cgj-2015-0606.

Consoli, N. C.; Vaz Ferreira, P. M.; Tang, C.-S.; Veloso Marques, S. F.; Festugato, L.; Corte, M. B. (2016c). **A unique relationship determining strength of silty/clayey soils Portland cement mixes**. *Soils Found*, 56 (6), pp. 1082–1088. https://doi.org/10.1016/j.sandf.2016.11.011.

Consoli, N. C.; Nierwinski, H. P.; da Silva, A. P; Sosnoski, J. (2017). **Durability and strength of fiber-reinforced compacted gold tailings-cement blends**. *Geotextile and Geomembranes*, v. 45, n. 2, p. 98-102. https://doi.org/10.1016/j.geotexmem.2017.01.001

Consoli, N. C.; da Silva, A. P; Nierwinski, H. P.; Sosnoski, J. (2018a). **Durability, strength, and stiffness of compacted gold tailings-cement mixes**. *Can. Geotech. J.*, v. 55, n. 4, p. 486-494. https://doi.org/10.1139/cgj-2016-0391

Consoli, N. C., and L. F. Tomasi. (2018b). **The impact of dry unit weight and cement content on the durability of sand–cement blends**. *Proc. Inst. Civ. Eng. Ground Improv*., 171 (2): 96–102. https://doi.org/10.1680/jgrim.17.00034.

Consoli, N. C.; Bittar Marín, E. J.; Quiñónez Samaniego, R. A.; Heineck, K. S.; Dalla Rosa Johann, A. (2018c). **Use of Sustainable Binders in Soil Stabilization**. *Journal of Materials in Civil Engineering*, Vol. 31. No. 2, p. 8. https://doi.org/10.1061/(ASCE)MT.1943-5533.0002571

Consoli, N. C.; da Silva, A.; Barcelos, A. M.; Festugato, L.; Favretto, F. (2019a). **Porosity/cement index controlling flexural tensile strength of artificially cemented soils in Brazil**. *Geotech. Geol. Eng.*, 38 (1), pp. 713–722. https://doi.org/10.1007/s10706-019-01059-w.

Consoli, N. C.; Rossi, J. G.; Festugato, L.; Ruver, C. A.; Scheuermann Filho, H. C.; Foppa, D.; Carretta, M. S.; Leon, H. B. (2019b). **Circular-plate load tests on bounded cemented layers above weak cohesive-frictional soil**. *J. Geotech. Geoenviron. Eng*., 145 (10), pp. 06019011. https://doi.org/10.1061/(ASCE)GT.1943-5606.0002144.

Consoli, N. C.; Bittar Marín, E. J.; Quiñónez Samaniego, R. A.; Scheuermann Filho, H. C.; Miranda, T.; Cristelo, N. (2019c). **The effect of mellowing and coal fly ash addition on the behavior of sulfate-rich dispersive clay after lime stabilization**. *J. of Materials in Civil Engineering*, p. 25. https://doi.org/10.1061/(ASCE)MT.1943-5533.0002699

Consoli, N. C.; Carretta, M. S.; Leon, H. B.; Scheuermann Filho, H. C.; Tomasi, L. F. (2019d). **Strength and Stiffness of Ground Waste Glass-Carbide Lime Blends**. *Journal of Materials in Civil Engineering*, p. 8. https://doi.org/10.1061/(ASCE)MT.19435533.0002862

Consoli, N. C.; Festugato, L; Scheuermann Filho, H. C.; Miguel, G. D.; Tebechrani Neto, A.; Andreghetto, D. (2020a). **Durability Assessment of Soil-Pozzolan-Lime Blends**

through Ultrasonic-Pulse Velocity Test. *JOURNAL OF MATERIALS IN CIVIL ENGINEERING*, v. 32, p. 04020223. https://doi.org/10.1061/(ASCE)MT.1943-5533.0003298

Consoli, N. C.; Moreira, E. B.; Festugato, L.; Miguel, G. D. (2020b). **Spread footings bearing on circular and square cement-stabilized sand layers above weakly bonded residual soil**. *SOILS & ROCKS*, v. 43, n. 3, p. 339-349. https://doi.org/10.28927/SR.433339

Consoli, N. C.; Festugato, L.; Miguel, G. D.; Scheuermann Filho, H. C. (2021a). **Swelling Prediction of Green Stabilized Fiber-Reinforced Sulfate-Rich Dispersive Soils**. *Geosynthetics International*, 28(4), p. 394-401, 2020. https://doi.org/10.1680/jgein.20.00050

Consoli, N. C.; Festugato, L.; Miguel, G. D.; Moreira, E. B.; Scheuermann Filho, H. C. (2021b). **Fatigue Life of Green Stabilized Fiber-Reinforced Sulfate-Rich Dispersive Soil**. *JOURNAL OF MATERIALS IN CIVIL ENGINEERING*, v. 33, p. 04021249, 2021. https://doi.org/10.1061/(ASCE)MT.1943-5533.0003842

Consoli, N. C.; Vogt, J. C.; Silva, J. P. S.; Chaves, H. M.; Scheuermann Filho, H. C.; Moreira, E. B.; Lotero, A. (2022). **Behaviour of Compacted Filtered Iron Ore Tailings–Portland Cement Blends: New Brazilian Trend for Tailings Disposal by Stacking**. Applied Science, v. 12, n. 2, p. 836. https://doi.org/10.3390/app12020836

Cooling, D.J.; Glenister, D.J. (1992). **Practical aspects of dry disposal**. *Light Metals*, 1, pp. 25–31.

Corte, M. B. (2020). **Response of cemented sand under multiaxial loading**. Tese (Doutorado em Engenharia) – Programa de Pós-Graduação em Engenharia Civil, Universidade Federal do Rio Grande do Sul, UFRGS, Porto Alegre.

Crystal, C.; Hore, C.; Ezama, I. (2018). **Filter-Pressed Dry Stacking: Design Considerations Based on Practical Experience**. In: Proceedings Tailings and Mine Waste 2018 | Keystone, Colorado, USA | September 30 – October 2, 2018, pp. 209-219.

Danas, K.; Castañeda, P. P. (2012). **Influence of the Lode parameter and the stress triaxiality on the failure of elasto-plastic porous materials**. *International Journal of Solids and Structures*, 49(2012), pp. 1325-1342. https://doi.org/10.1016/j.ijsolstr.2012.02.006

Daronco, J. V. L.; Festugato, L.; Miguel, G. D.; Scheuermann Filho, H. C. (2022). **Discussion of 'Mechanical Strength Improvement of Cement-Stabilized Soil Using Natural Rubber Latex for Pavement Base Applications' by Apinun Buritatun, Thaworn Takaikaew, Suksun Horpibulsuk, Artit Udomchai, Menglim Hoy, Nopparat Vichitcholchai, and Arul Arulrajah**. JOURNAL OF MATERIALS IN CIVIL ENGINEERING, 34(1), p. 1-8. https://doi.org/10.1061/(ASCE)MT.1943-5533.0004057

Daronco, J. V. L. (2022). **Estudo do comportamento geomecânico de rejeito melhorado com cimento**. 2022. Dissertation (Masters in Engineering) – Programa de Pós-Graduação em Engenharia Civil, UFRGS, Porto Alegre. (In Protuguese).

da Silva, A.; Festugato, L.; Daronco, J. V. L.; Miguel, G. D. (2022). **Discussion of 'Soft Clay Stabilization Using Three Industry Byproducts' by Bo Xu and Yaolin Yi**. *JOURNAL OF MATERIALS IN CIVIL ENGINEERING*, v. 34, p. 07022004-1-07022004-1. https://doi.org/10.1061/(ASCE)MT.1943-5533.0004163

da Silva, A.; Festugato, L.; Daronco, J. V. L.; Miguel, G. D. (2024). **Influence of curing under stress on the geomechanical response of cemented iron ore mining tailings subjected to distinct effective stress paths**. *International Journal of Geomechanics*. (accepted for publication).

Davidson, H. - The Guardian (2019). **Rio Tinto's plan to clean up Ranger uranium mine in doubt after hedge fund objects**. Accessed in: feb. 2022. < https://www.theguardian.com/environment/2019/dec/17/rio-tintos-plan-to-clean-up-ranger-uranium-mine-in-doubt-after-hedge-fund-objects >

Davé, N. K.; Vivyurka, A. J. (1994). **Water cover on Acid Generating Uranium Tailings - laboratory and field studies**. *In*: Third International Conference on the Abatement of Acid Mine Drainage, pittsburg, PA, April 24-29, 1994.

Davies, M. P.; Rice, S. (2001). **An Alternative to Conventional Tailings Management – 'Dry Stack' Filtered Tailings**. *AMEC Earth & Environmental*, Vancouver, Canada.

Davies, M. Lupo, J.; Martin, T.; Mcroberts, Ed.; Musse, M.; Ritchie, D. (2011). **Dewatered tailings practice - Trends and observations**. *In*: Tailings and Mine Waste'10 - Proceedings of the 14th International Conference on Tailings and Mine Waste, pp. 133-142. https://doi.org/10.1201/b10569-19.

De Paula, T. M.; Consoli, N. C.; Festugato, L.; Favretto, F.; Daronco, J. V. L. (2019). **Behaviour of fibre-reinforced cemented sand under flexural tensile stress**. *In*: Vol. 92 of Proc., E3S Web of Conf., 12005. Les Ulis Cedex, France: EDP Sciences. https://doi.org/10.1051/e3sconf/20199212005.

Dermatas, D. (1995). **Ettringite-induced swelling in soils: State-of-the-art**. Part of Mechanics of swelling, edited by Theodoros k. Karalis, American Society of Mechanical Engineers, vol. 48, no. 10, pp. 659-673.

Diambra, A.; Ibraim, E.; Consoli, N. C.; Festugato, L. (2017). **Theoretical Derivation of Artificially Cemented Granular Soil Strength**. *Journal of Geotechnical and Geoenviromental Engineering*, V. 143(5), pp. 1-9. https://doi.org/10.1061/(ASCE)GT.1943-5606.0001646

Dixon-Hardy, D. W.; Engels, J. M. (2007). **Methods for the disposal and storage of mine tailings**. *Land Contamination & Reclamation*, v. 15, n. 3, pp. 301-318. https://doi.org/10.2462/09670513.832

Dutra, M. R. **Geomechanical behaviour of iron ore tailings from low to high confining stress**. 2021. M.Sc. Dissertation – Department of Civil Engineering, UFRGS, Porto Alegre.

EPA (1995). **Best Practice Environmental Management in Mining – Tailings Containment**. Australian Environmental Protection Agency: ISBN 0642194238 of the series 0642194181

Espósito, T. J. (2000). **Metodologia probabilística e observacional aplicada a barragens de rejeito construídas por aterro hidráulico**. Tese de doutorado, Departamento de Engenharia Civil e Ambiental, UNB, Brasília, 2000.

European Commission (EC) (2004) **Draft Reference Document on Best variable techniques for Management of Tailings and Waste-Rock in Mining Activities**. European Commission, Edificio EXPO, Seville, Spain.

Evans, C.L.; Wightman, E. M.; Manlapig, E. V.; Coulter, B. L. (2011). **Application of process mineralogy as a tool in sustainable processing**. Miner. Eng. 24 (12), 12421248. https://doi.org/10.1016/j.mineng.2011.03.017

Fabre, J. S. (2019). **Ensaios Triaxiais de Extensão em Rejeito de Minério de Ferro**. Dissertação (Mestrado em Engenharia) – o Programa de Pós-graduação em Engenharia Civil, COPPE, Rio de Janeiro, Brasil.

Festugato, L.; Fourie, A.; Consoli, N. C. (2013). **Cyclic shear response of fibre-reinforced cemented paste backfill**. *Géotechnique Letters*, v. 3, No. 1, 5–12. https://doi.org/10.1680/geolett.12.00042

Festugato, L.; Consoli, N. C.; Fourie, A. (2015). **Cyclic shear behaviour of fibre-reinforced mine tailings**. *Geosynthetics International*, v.22, no. 2, pp. 196-206. https://doi.org/10.1680/gein.15.00005
Google (2021). Google Maps: Minas Gerais State. United States of America.

Festugato, L.; Menger, E.; Benezra, F.; Kipper, E. A.; Consoli, N. C. (2017). **Fibre-reinforced cemented soils compressive and tensile strength assessment as a function of filament length**. *Geotext. Geomembr*., 45 (1), pp. 77–82. https://doi.org/10.1016/j.geotexmem.2016.09.001.

Festugato, L.; Corte, M. B.; Ibraim, E.; Diambra, A. (2019). **Artificially cemented sand under multiaxial loading**. *In*: Proc., 7th Int. Symp. On Deformation Characteristics of Geomaterials, IS-Glasgow 2019: Open Access Proceedings in Environment, Energy and Earth Sciences, edited by E. Ibraim and A. Tarantino. Paris: EDP Sciences. https://doi.org/10.1051/e3sconf/20199211011

Festugato, L.; Gálvez, J. H. F.; Miguel, G. D.; Consoli, N. C. (2022). **Cyclic Response of Fibre Reinforced Dense Sand**. *Transportation Geotechnics*, Volume 37, November 2022, 100811. https://doi.org/10.1016/j.trgeo.2022.100811

Festugato, L.; Ibraim, E.; Corte, M. B.; Diambra, A. (2023). **Multiaxial Behavior of Compacted Artificially Lightly Cemented Sands**. *Journal of Geotechnical and Geoenvironmental Engineering*, Volume 149, Issue 12. https://doi.org/10.1061/JGGEFK.GTENG-11389

Figueredo, M. M. **Estudo de metodologias alternativas de disposição de rejeitos para a mineração Casa de Pedra – Congonhas/MG**. Dissertação de mestrado, programa de pós-graduação em geotecnia, UFOP, Ouro Preto, 2007

Foppa, D. (2005). **Análise de Variáveis-Chave no Controle da Resistência Mecânica de Solos Artificialmente Cimentados**. Dissertação (Mestrado em Engenharia), Programa de Pós-Graduação em Engenharia Civil, UFRGS, Porto Alegre.

Fredlund, G. D. (2016). **State Variables in Saturated-Unsaturated Soil Mechanics**. *Soils and Rocks*, v. 39, n. 1, pp. 3-17.

Gao, Z.; Diambra, A. (2021). **A multiaxial constitutive model for fibre-reinforced sand**. Géotechnique 71, No. 6, pp. 548–560 https://doi.org/10.1680/jgeot.19.P.250

Godoy, V. B. (2018). **Desempenho de Misturas de Distintos Materiais com Cinza Volante e Cal Submetidos a Condições Climáticas Severas**. Dissertação (Mestrado em Engenharia), Programa de Pós-Graduação em Engenharia Civil, UFRGS, Porto Alegre.

Google (2021). Google Maps: Minas Gerais state region. United States of America.

Gray, P.M.J., 1984. **Metallurgy of the complex sulphide ores**. Mining Mag. Oct, 315321.

Green, G. E. (1971). **Strength and deformation of sand measured in an independent stress control cell**. Stress-Strain Behaviour of Soils: Proceedings of the Roscoe Memorial Symposium, G. T. Foulis & Co. Ltd., Henley-on-Thames, pp. 285-323.

Guerra, F. (1973). **Characteristics of Tailings from a Soils Engineer's Viewpoint**. *In*: 1st Int. Tailing Symposium, Aplin, C., and Argall, G. (eds.), Miller Freeman, San Francisco, pp. 102-137.

Guerra, F. (1979). **Controlling the Phreatic Surface**. *In*: 2nd Int. Tailing Symp., Argall, G. (ed.), Miller Freeman, San Francisco, pp. 292-326.

Guerney, P. J.; Laplante, A. R.; O'Leary, S. (2003). **Gravity recoverable gold and the Mineral Liberation Analyser**. *In*: 35th Annual Meeting of the Canadian Mineral Processors Conf. CIM, Ottawa, ON, Canada, pp. 401416.

Habib, P. (1953). **Influence de la variation de la contrainte principale moyenne sur la résistance au cisaillement des sols**. *In*: Proc. Third International Conference on Soil Mechanics and Foundation Engineering, v. 1, p. 100-105.

Hambly, E. C. (1969). **A new true triaxial apparatus**. *Géotechnique*, 19, No. 2, 307-309.

Handin, J.; Heard, H.C.; Magouirk, J.N.(1967). **Effects of the intermediate principal stress on the failure of limestone, dolomite, and glass at different temperatures and strain rates**. *J. Geophys. Res*., 72, (1967), pp. 611-640.

Harrisson, A. M. (2019). **Chapter 4: Constitution and Specification of Portland Cement**. In: Lea's Chemistry of Cement and Concrete, Eds. Peter C. Hewlett and Martin Liska, 5th Ed., Butterworth-Heinemann, Elsevier, 868 p.

Hausmann, M. R. (1990). **Engineering Principles of Ground Modification**. McGraw-Hili Book Co., Inc., New York, N.Y.

Heinzen, R. T.; Arulanandan, K. (1977). **Factors Influencing Dispersive Clays and Methods of Identification**. Dispersive Clays, Related Piping, and Erosion in Geotechnical Projects, ASTM STP 623, J. L. Sherard and R. S. Decker, Eds., American Society for Testing and Materials, pp. 202-217.

Henzinger, C.; Schömig, P. (2020). **Prognose der Festigkeitse wicklung zementbehandelter Böden mit dem porosity/binder-index**. [In German.] *Geotechnik*, 43 (1), pp. 14–25. https://doi.org/10.1002/gete.201900017.

Herzog, A.; Mitchell, J. K. (1963). **Reactions Accompanying Stabilization of Clay with Cement**. Paper sponsored by Committee on Soil-Portland Cement Stabilization, pp. 146-171.

Hoal, K. O; Stammer, J. G.; Appleby, S. K.; Botha, J.; Ross, J. K.; Botha, P. W. (2009). Research in quantitative mineralogy: examples from diverse applications. *Miner. Eng*. 22 (4), 402408. https://doi.org/10.1016/j.mineng.2008.11.003

Holmgren, G. G. S.; Flanagan, C. P. (1977). **Factors Affecting Spontaneous Dispersion of Soil Materials as Evidenced by the Crumb Test**. Dispersive Clays, Related Piping, and Erosion in Geotechnical Projects, ASTM STP 623, J. L. Sherard and R. S. Decker, Eds., American Society for Testing and Materials, pp. 218-239.

Hu, L.; Wu, H.; Zhang, L.; Zhang, P.; Wen, Q. (2017). **Geotechnical properties of mine tailings**. *Journal of Materials in Civil Engineering*, v. 29, n.2, 04016220. https://doi.org/10.1061/(ASCE)MT.1943-5533.0001736

Ingles, O. G,; Metcalf, J. B. (1972). **Soil Stabilization: Principles and Practice**. Sydney: Butterworths, 1972, 374 p.

Instituto Brasileiro de Mineração – IBRAM (2020). **Economia Mineral – fevereiro de 2020**. p. 19.

Ishihara, K.; Troncoso, J.; Kawase, Y.; Takahashi, Y. (1980). **Cyclic strength characteristics of tailings materials**. *Soils Found*., 20(4), pp. 127–142. https://doi.org/10.3208/sandf1972.20.4_127

James, M.; Aubertin, M.; Wijewickreme, D.; Wilson, G. W. (2011). **A laboratory investigation of the dynamic properties of tailings**. *Canadian Geotechnical Journal*, v. 48, n. 11, pp. 1587-1600. https://doi.org/10.1139/t11-060

Jefferies, M. G.; Been, K. (2015). **Soil liquefaction: A critical state approach**. CRC Press: Boca Raton, FL, USA, 2015.

Kanazawa, N. M. (2015). **Durabilidade, rigidez e análise do ciclo de vida de um solo dispersivo estabilizado com cal**. Dissertação (Metrado em Engenharia) – Programa de Pós-Graduação em Engenharia Civil, UFRGS, Porto Alegre, Brasil.

Kingman, S. W.; Jackson, K.; Cumbane, A.; Bradshaw, S. M. (2004). **Recent developments in microwave-assisted comminution**. *Int. J. Miner. Process*. 74 (1-4), 7183. https://doi.org/10.1016/j.minpro.2003.09.006

Kjellman, W. (1936). **Om undersökning av jordarters deformationsegenskaper**. Teknisk Tidskrift, Väg- och Vattenbyggnadskonst, Stockholm, Häfte 8, 85-91.

Klohn, E., (1979). **Taconite Tailings Disposal Practices**. Current Geotechnical Practice in Mine Waste Disposal, ASCE, pp. 202-241.

Ko, H. Y.; Scott, R. F. (1967). **A new soil testing apparatus**. *Géotechnique*,17 (1): 40–57. https://doi.org/10.1680/geot.1967.17.1.40.

Ko, H. Y.; Scott, R. F. (1968). **Deformation of sand at failure**. Journal of the Soil Mechanics and Foundations Division, ASCE, v. 94, no. SM4, Proc. Paper 6028, July, 1968, pp. 883-898.

Kossoff, D.; Dubbin, W.; Alfredsson, M.; Edwards, S.; Macklin, M.; Hudson-Edwards, K. (2014). **Mine tailings dams: Characteristics, failure, environmental impacts, and remediation**. *Appl. Geochem.*, v. 51, pp. 229–245. https://doi.org/10.1016/j.apgeochem.2014.09.010

Ladd, R. S. (1978). **Preparing test specimens using under-compaction**. *Geotech. Test. J*., 1 (1), pp. 16–23. https://doi.org/10.1520/GTJ10364J.

Lade, P. V., Duncan, J. M. (1973). **Cubical triaxial tests on cohesionless soils**. *J. Soil Mech. Found. Div.*, 99 (10): 793–812. https://doi.org/10.1061/JSFEAQ.0001934.

Lade, P. V.; Duncan, J. M. (1975). **Elastoplastic Stress-Strain Theory for Cohesionless Soil**. *Journal of the Geotechnical Engineering Division*, v. 101, n. 10, p. 1037-1053. https://doi.org/10.1061/AJGEB6.0000204

Lade, P. V. 2016. Triaxial testing of soils. Hoboken, NJ: Wiley.

Lambe, T. W.; Whitman, R. V. (1979). **Soil Mechanics, SI Version**. With assistance of H. G. Poulos, John Wiley & Sons Inc., New York, p. 553.

Lambe, T. W.; Michaels, A. S.; Moh, Z. C. (1960). **Improvement of Soil-Cement with Alkali Metal Compounds**. *HRB Bull*. 241, pp. 67-108 (1960).

Li, W.; Coop, M.; Senetakis, K.; Schnaid, F. (2018a). **The mechanics of a silt-sized gold tailing**. *Eng. Geol*., 241, 97–108. https://doi.org/10.1016/j.enggeo.2018.05.014

Li, W.; Coop, M. R. (2018b). **Mechanical behaviour of Panzhihua iron tailings**. *Canadian Geotechnical Journal*, v. 56, n. 3, pp. 420-435. https://doi.org/10.1139/cgj-2018-0032

Lindolfo, S. (2010). **Barragem de rejeitos**. Centro de tecnologia mineral CETEM/MCT, Rio de Janeiro, 2010.

Lopes, M. C. O. (2000). **Disposição hidráulica de rejeitos arenosos e influência dos parâmetros de resistência**. Dissertação de mestrado, Departamento de Engenharia Civil e Ambiental, UNB, Brasília, 2000.

Lotter, N.O. (2011). **Modern process mineralogy: an integrated multidisciplined approach to flowsheeting**. Miner. Eng., 24(12), 12291237. https://doi.org/10.1016/j.mineng.2011.03.004

Luz, A. B.; Lins, F. A. (2010). **Introdução ao tratamento de minérios**. Centro de tecnologia mineral CETEM/MCT, Rio de Janeiro, 2010.

Marto, A.; Tan, C. S.; Makhtar, A. M.; Jusoh, S. N. (2016). **Cyclic behaviour of Johor sand**. *International Journal of GEOMATE*, v.10, n. 21, pp. 1891-1898. https://doi.org/10.21660/2016.21.5394

Mateos, M. (1961). **Physical and Mineralogical Factors in Stabilization of Iowa Soils with Lime and Fly Ash**. Tese (Doctor of Phylosophy) – Iowa State University of Science and Technology, Ames, 1961.

McElroy, C. H. (1987). **Using Hydrated Lime to Control Erosion of Dispersive Clays**. Lime for Environmental Uses, ASTM STP 931, K. A. Gutschick, Ed., American Society for Testing and Materials, Philadelphia, pp. 100-114.

Miguel, G. D. (2020). **Performance and Mechanical Behavior of a Sulfate-Rich Dispersive Soil Treated with Carbide Lime-Artificial Pozzolan Blends and Reinforced with Fiber Glass**. 2020. Thesis (Masters in Engineering) – Programa de Pós-Graduação em Engenharia Civil, UFRGS, Porto Alegre. (*In Protuguese*). https://doi.org/10.13140/RG.2.2.27481.67687/1

Miguel, G. D.; Festugato, L.; Marques, S. F. V.; Venson, G. I. (2021a). **Discussion of 'Engineering Properties of Biocementation Coarse- and Fine-Grained Sand Catalyzed by Bacterial Cells and Bacterial Enzyme' by Tung Hoang, James Alleman, Bora Cetin, and Sun-Gyu Choi**. *JOURNAL OF MATERIALS IN CIVIL ENGINEERING*, v. 33, p. 07021006. https://doi.org/10.1061/(ASCE)MT.1943-5533.0003757

Miguel, G. D.; Scheuermann Filho, H. C.; Festugato, L.; Corte, M. B. (2021b). **Discussion of 'Cement, Lime, and Fly Ashes in Stabilizing Expansive Soils: Performance Evaluation and Comparison' by Masrur Mahedi, Bora Cetin, and David J. White**. *JOURNAL OF MATERIALS IN CIVIL ENGINEERING*, v. 33, p. 07021012. https://doi.org/10.1061/(ASCE)MT.1943-5533.0003867

Miguel, G. D.; Festugato, L.; Moreira, E. B.; Corte, M. B. (2021c). **Discussion of 'Geopolymers Based on Recycled Glass Powder for Soil Stabilization' Jair de Jesús Arrieta Baldovino; Ronaldo dos Santos Izzo; Juliana Lundgren Rose; Mônica Angélica Avanci.** *GEOTECHNICAL AND GEOLOGICAL ENGINEERING*, 3(4). https://doi.org/10.1061/(ASCE)MT.1943-5533.0003676

Miguel, G. D.; Festugato, L.; Scheuermann Filho, H. C; Daronco, J. V. L. (2022a). **Discussion of 'Fiber-Reinforced Cement-Stabilized Macadam with Various Polyvinyl Alcohol Fiber Contents and Lengths' by Chunhua Zhao, Naixing Liang, Xiaolong Zhu, Lingqing Yuan, and Bo Zhou**. *JOURNAL OF MATERIALS IN CIVIL ENGINEERING*, 34(3). https://doi.org/10.1061/(ASCE)MT.1943-5533.0004291

Miguel, G. D.; Ssaldanha, R. B.; da Silva, A.; Festugato, L.; Chaves, H. M.; Mendes, C. C. (2022b). **Life Cycle Assessment Comparison of Distinct Soil Stabilizations Methods: An Environmental and Cost Approach to the Soil Improvement**. *Proceedings of the ICE - Ground Improvement*, p. 1-41, (Ahead of Print). https://doi.org/10.1680/jgrim.21.00006a

Mine Environment Neutral Drainage – MEND (2017). **Dry stacking facilities around world**. Sponsored by The Mining Association of Canada (MAC). 164 p. Accessed in: feb. 2022. < http://mend-nedem.org/wp-content/uploads/2.50.1Tailings_Management_TechnologiesL.pdf >

Ministério de Minas e Energias – MME (2021). **Boletim do Setor Mineral 2020**. p. 28.

Mitchell, J. K. (1981). **Soil improvement: State-of-the-art report**. *In*: Proc., 10th Int. Conf. on Soil Mechanics and Foundation Engineering, pp. 509–565. Stockholm, Sweden: International Society of Soil Mechanics and Foundation Engineering.

Mitchell, J. K.; Dermatas, D. (1992). **Clay Soil Heave Caused by Lime-Sulfate Reactions**. Inovations and Uses for Lime, ASTM STP 1135, D. D. Walker, Jr., T. B. Hardy, D. C. Hoffman, and D. D.Stanley, Eds., American Society for Testing and Materials, Philadelphia, pp. 41-64.

Mogi, K. (1967). **Effect of the intermediate principal stress on rock failure**. *J. Geophys. Res.*, 72, (1967), pp. 5117-5131.

Mogi, K. (1981). **Flow and fracture of rocks under general triaxial compression**. Applied Mathematics and Mechanics, v. 2, n. 6., pp. 635-651.

Mola-Abasi, H.; Khajeh, A.; Naderi Semsani, S. (2017). **Variables controlling tensile strength of stabilized sand with cement and zeolite**. *J. Adhes. Sci. Technol*., 32 (9), pp. 947–962. https://doi.org/10.1080/01694243.2017.1388052.

Montgomery, D. C. (2001). **Design and Analysis of Experiments**. John Wiley & Sons, INC., 5th ed., United States of America, p. 684.

Murrell, S.A.F. (1965). **The effect of triaxial stress systems on the strength of rocks at atmospheric temperatures**. *Geophys. J*., 10, (1965), pp. 231-282.

Nalbantoglu, Z. (2006). **Chapter 23: Lime Stabilization of Expansive Clay**. *Part of*: Expansive Soils: Recent Advances in Characterization and Treatment, Eds. Amer Ali Al-Rawas & Mattheus F. A. Goosen, p. 341.

Nguyen, Q. D.; Boger, D.V. (1987). **The rheology of concentrated bauxite residue suspensions — a complete story**. In: Wagh, A.S., Desai, P. (Eds.), Bauxite Tailings 'Red Mud'. The Jamaica Bauxite Institute, pp. 53–65.

Nguyen, Q. D.; Boger, D. V. (1998). **Application of rheology to solving tailings disposal problems**. *International Journal of Mineral Processing*, v. 54, n. 3-4, pp. 217–233. https://doi.org/10.1016/S0301-7516(98)00011-8

Niwa, Y.; Koyanagi, W.; Kobayashi, S. (1967). **Failure criterion of lightweight concrete to triaxial compression**. *Proc. Japan soc. Civil. Eng.*, 143, (1967), pp. 28-35.

Organização das Nações Unidas – ONU (2019). **População mundial deve chegar a 9,7 bilhões de pessoas em 2050, diz relatório da ONU**. Accessed in: Mar. 2022. Available at: < https://brasil.un.org/pt-br/83427-populacao-mundial-deve-chegar-97-bilhoes-de-pessoas-em-2050-diz-relatorio-da-onu >.

Pasche, E. (2016). **Estudo da Resistência e da Rigidez de uma Mistura de Material Fresado Asfáltico e Pó-de-Pedra com Adição de Cimento**. Dissertação (Mestrado em Engenharia), Programa de Pós-Graduação em Engenharia Civil, UFRGS, Porto Alegre.

Pearce, J. A. (1970). **The behaviour of soft clay in a new true triaxial apparatus**. PhD thesis,

University of Cambridge.

Pearce, J. A. (1971). **A new true triaxial apparatus**. Stress-Strain Behaviour of Soils: Proceedings of the Roscoe Memorial Symposium, G. T. Foulis & Co. Ltd., Henley-on-Thames, pp. 330-339.

Pereira, E. L. **Estudo do potencial de liquefação de rejeitos de minério de ferro sob carregamento estático**. Dissertação de mestrado, programa de pós-graduação do departamento de engenharia civil, UFOP, Ouro Preto, 2005.

Perlea, V. G.; Koester, J. P.; Prakash, S. (1999). **How liquefiable are cohesive soils?**. *In*: Proceedings of the Second International Conference on Earthquake Geotechnical Engineering, Lisboa, Portugal, pp 611–618.

Portland Cement Association (PCA) (1995). **Soil-Cement Construction Handbook EB003.10S**. p.44.

Pohland, H. H.; Tielens, A. J. (1987). **Design and operation of non-decanting red mud ponds in Ludwigshafen**. *In*: Wagh, A.S., Desai, P. (Eds.), Bauxite Tailings 'Red Mud'. The Jamaica Bauxite Institute, pp. 87–90.

Quaresma, L. F. (2009). **Relatório Técnico 18: Perfil da Mineração de ferro**. Ministério de Minas e Energia – MME, agosto 2009.

Quiñonez Samaniego, R. A. (2015). **Estabilização de um solo dispersivo com adição de cal**. Dissertação (Mestrado em Engenharia) – Programa de Pós-Graduação em Engenharia Civil, UFRGS, Porto Alegre, Brasil.

Radziszewski, P. (2013). **Energy recovery potential in comminution processes**. *Miner. Eng*. 46-47, pp. 83-88. http://dx.doi.org/10.1016/j.mineng.2012.12.002

Reddy, K. R.; Saxena, S. K.; Budiman, J. S. (1992). **Development of a true triaxial testing apparatus**. *Geotech. Test. J*., 15 (2): 89–105. https://doi.org/10.1520/GTJ10231J.

Reddy, K. R.; Saxena, S. K. (1993). **Effects of cementation on stress-strain and strength characteristics of sands**. *Soils and Foundations*, v. 33, n. 4, p. 121–134, 1993. https://doi.org/10.3208/sandf1972.33.4_121

Rezende, V. A. Estudo do comportamento de barragem de rejeito arenoso alteada por montante. Dissertação de mestrado, programa de pós-graduação em geotecnia, UFOP, Ouro Preto, 2013.

Ribeiro, J. L. D.; Caten, C. S. ten (2014). **Série Monográfica Qualidade: Projeto de Experimentos**. Andréia Leal, Fabíolla Granata, Gustavo Schroeder e Marcelo Pereira, Eds., UFRGS, Porto Alegre, p. 169.

Ribeiro, L. F. M.; Assis, A. P. (1999). **Experimental simulation of the hydraulic deposition process in tailings dams**. *In*: XI Panamerican Conference on Soil Mechanics and Geotechnical Engineering, Foz do Iguaçu, Brasil, pp. 1113-1120.

Rio Tinto (2022). **Tailings Storage Facilities**. Acessed in: Feb. 2022. <https://www.riotinto.com/sustainability/environment/tailings >.

Rios, S.; Viana da Fonseca, A.; Baudet, B. A. (2012). **Effect of the porosity/cement ratio on the compression of cemented soil**. *J. Geotech. Geoenviron*. Eng. 138 (11): 1422–1426. https://doi.org/10.1061/(ASCE)GT.1943-5606.0000698.

Rios, S.; Viana da Fonseca, A.; Consoli, N. C.; Floss, M. F.; Cristelo, N. (2013). **Influence of grain size and mineralogy on the porosity/cement ratio**. *Géotech. Lett*., 3 (3), pp. 130–136. https://doi.org/10.1680/geolett.13.00003.

Ritcey, G.M. (1989). **Tailings Management: Problems and Solutions in the Mining Industry**. (Vol. 6). Elsevier, Amsterdam, New York. ISBN: 0444873740

Robertson, P. K.; Melo, L.; Williams, D. J.; Wilson, G. W. (2019). **Report of the expert panel on the technical causes of the failure of Feijão Dam I**. 2019.

Robinsky, E. I. (1987). **Current status of sloped thickened tailing disposal system**. In: Wagh, A.S., Desai, P. (Eds.), Bauxite Tailings 'Red Mud'. The Jamaica Bauxite Institute, pp. 91–100.

Robinsky, E.I. (1999). **Thickened Tailings Disposal in the Mining Industry**. E.I. Robinsky Associates Ltd (Publisher), Toronto, ON,Canada.

Rodriguez, N. M.; Lade, P. V. (2013). **True Triaxial Tests on Cross-Anisotropic Deposits of Fine Nevada Sand**. *International Journal of Geomechanics*. Vol 13(6), 779-793. https://doi.org/10.1061/(ASCE)GM.1943-5622.0000282.

Rong-Rong, Z.; Dong-Dong, M. (2020). **Effects of Curing Time on the Mechanical Property and Microstructure Characteristics of Metakaolin-Based Geopolymer Cement-Stabilized Silty Clay**. *Advances in Materials Science and Engineering*, v. 2020, p. 9. https://doi.org/10.1155/2020/9605941

Sadek, T. (2006). **The Multiaxial Behavior and Elastic Stiffness of Hostun Sand**. Dissertation (Doctor of Philosophy) – Department of Civil Engineering, University of Bristol.

Sakurai, S; Serata, S. (1967). **Mechanical properties of rock salt under three dimensional loading conditions**. *Proc. Japan Congr. Tect. Mater.*, 10th, (1967), pp. 139-142.

Santamarina, J. C.; Torres-Cruz, L. A.; Bachus, R. C. (2019). **Why coal ash and tailings dam disasters occur**. *Science*, v. 364, n. 6440, pp.526–528. https://doi.org/10.1126/science.aax1927

Santamarina, J. C.; Klein, J. C.; Fam, M. A. (2001). **Soils and waves: particulate materials behavior, characterization and process monitoring**. [s.l.] John Wiley & Sons Ltd, 2001, p. 488.

Santos, W, K. (2009). **Rotas de processo para concentração de minérios itabiríticos e hematíticos da mina de fábrica**. Belo Horizonte: Escola de Engenharia da UFMG, 2009. p. 9-10.

Sarsby, R. W. (2013). **Environmental Geotechnics**. Second edition, ICE Publishing, London, 2013.

Sas, W.; Gluchowski, A. (2013). **Effects of stabilization with cement on mechanical properties of cohesive soil – sandy-silty clay**. *In*: Annals of Warsaw University of Life

Saxena, S. K; Lastrico, R. M. (1978). **Static properties of lightly cemented sand**. *Journal of the Soil Mechanics and Foundations Division*, ASCE, v. 104, n. 12, p. 1449–1464, 1978. https://doi.org/10.1061/AJGEB6.0000728

Sciences – SGGW, Land Reclamation, 45(2), pp. 193-205. https://doi.org/10.2478/sggw-2013-0016

Scheuermann Filho, H. C. (2019). **Estabilização de um solo dispersivo com pó de vidro e cal de carbureto**. Dissertação (Mestrado em Engenharia) – Programa de Pós-Graduação em Engenharia Civil, UFRGS, Porto Alegre, Brasil.

Scheuermann Filho, H. C.; Miguel, G. D.; Festugato, L.; Corte, M. B. (2021a). **Discussion of 'Suppressing Ettringite-Induced Swelling of Gypseous Soil by Using Magnesia-Activated Ground Granulated Blast-Furnace Slag' by Wentao Li, Yaolin Yi, and Anand J. Puppala**. *Journal of Geotechnical and Geoenvironmental Engineering*, v. 147, p. 07021010-1. https://doi.org/10.1061/(ASCE)GT.1943-5606.0002557

Scheuermann Filho, H. C.; Miguel, G. D.; Daronco, J. V. L.; Menezes, R. J. W.; Festugato, L. (2021b). **Discussion of 'Expansive and Compressibility Behavior of Lime Stabilized Fiber-Reinforced Marine Clay' by Vihan Shenal Jayawardane, Vivi Anggraini, Endene Emmanuel, Lee Li Yong, and Mehdi Mirzababaei**. *JOURNAL OF MATERIALS IN CIVIL ENGINEERING*, v. 33, p. 07021014. https://doi.org/10.1061/(ASCE)MT.1943-5533.0003977

Scheuermann Filho, H. C. (2022). **Adjusted Porosity/Cement Index: mechanical behavior and microstructure over a wide range of dosages**. Thesis (Doctor of Engineering) – Graduate Program of Civil Engineering, UFRGS, Porto Alegre, Brazil.

Scheuermann Filho, H. C.; Miguel, G. D.; Consoli, N. C. (2022). **Porosity/Cement Index over a Wide Range of Porosities and Cement Contents**. *J. Mater. Civ. Eng*., 2022, 34(3): 06021011. https://doi.org/10.1061/(ASCE)MT.1943-5533.0004115

Schnaid, F.; Nierwinski, H. P.; Odebrecht, E. (2020). **Classification and state parameter assessment of granular soils using the seismic cone**. J. Geotech. and Geoenvironmental Engng., 146(8). https://doi.org/10.1061/(ASCE)GT.1943-5606.0002306

Shukin, W.; Olsen, M. (1980). **Quebec Cartier-Mount Wright Tailings Disposal**. *In*: Symp. on Design and Construction of Tailings Dams, Colorado School of Mines, pp. I II18.

Silva, A.; Miguel, G. D.; Daronco, J. V. L.; Coelho, P.; Festugato, L. (2024). **Influence of curing under stress on the geomechanical response of cemented iron ore mining tailings subjected to distinct effective stress paths**. *International Journal of Geomechanics*. (accepted for publication).

Silvani, C. (2013). **Influência da Temperatura de Cura no Comportamento Mecânico da Mistura Areia-Cinza Volante-Cal**. Dissertação (Metre em Engenharia), Programa de Pós-Graduação em Engenharia Civil, UFRS, Porto Alegre.

Silvani, C. (2017). **Solos Artificialmente Cimentados em Célula Cúbica: Isotropia a Pequenas Deformações e na Ruptura**. Tese (Doutorado em Engenharia), Programa de Pós-Graduação em Engenharia Civil, UFRS, Porto Alegre.

Silvani, C.; Ibraim, E.; Scheuermann Filho, H. C.; Festugato, L.; Diambra, A.; Consoli, N. C. (2022). **Sand-Fly Ash-Lime Blends: Mechanical Behavior under Multiaxial Stress Condition**. Journal of Materials in Civil Engineering, 34(5), 04022059. https://doi.org/10.1061/(ASCE)MT.1943-5533.0004199.

Skempton, A.W. (1954). **The pore-pressure coefficients A and B**. *Geotechnique*, 4(4), pp. 143-147. https://doi.org/10.1680/geot.1954.4.4.143

SLR Consulting (2016). **Schedule 2: Assessment of Alternatives for Mine Waste Management, Magino Gold Project**. Prodigy Gold, Inc. Markham, ON, Canadá.

Smythe, D.M.; Lombard, A.; Coetzee, L. L. (2013). **Rare earth element deportment studies utilizing QEMSCAN technology**. *Miner. Eng*. 52, 5261. https://doi.org/10.1016/j.mineng.2013.03.010

Sture, S.; Desai, C. S. (1979). **Fluid Cushion Truly Triaxial or Multiaxial Testing Device**. *Geotechnical Testing Journal*, 2, No. 1, 20-33.

Tarazona, C. F. (2015). **Estudo da Alteração em Laboratório de Rejeitos de Mineração de Ferro para Análise em Longo Prazo**. Tese (Doutorado em Engenharia) – Programa de Pós-graduação em Engenharia Civil, Universidade Federal do Rio de Janeiro, COPPE, Rio de Janeiro, Brasil.

Terzaghi, K.; Peck, R. B.; Mesri, G. (1996). **Soil Mechanics in Engineering Practice**. 3rd Edition, John Wiley and Sons, Inc., New York.

Thompson, M. R. (1966). **Lime Reactivity of Illinois Soil**. *Journal of Soil Mechanics Foundation Division*, ASCE, 92(5), pp. 67-72.

Tuncer, E. R.; Basma, A. A. (1991). **Strength and Stress-Strain Characyeristics of Lime Treated Cohesive Soil**. Transportation Research Record, 1295, pp. 70-79.

U.S. Army Corps of Engineers (1984). **Soil Stabilization for Pavements Mobilization Construction**. Department of the Army Corps of Engineers, Office of the Chief of Engineers, Washington, D.C., p. 32.

Vale S.A. (2019). **Relatório de Impacto Ambiental (RIMA) - Projeto Pilha de Disposição de Rejeitos Filtrados – PDR Tamanduá**. p. 131. Acessado em: fev. 2022. < http://www.vale.com/brasil/PT/aboutvale/servicos-para-comunidade/minas-gerais/Documents/projetos/STE-CVD257-RIA-INT-PDF001-FF-PR(1).pdf >

Van Niekerk, H. J.; Viljoen, M. J. (2005). **Causes and consequences of the Merriespruit and other tailings-dam failures**. *Land Degradation & Development*, v. 16, n. 2, pp. 201–212. https://doi.org/10.1002/ldr.681

Van Olphen, H. (1963). **An Introduction to Clay Colloid Chemistry**. *Interscience Publishers*, Div. of John Wiley & Sons, New York, p. 301.

Vick, S. G. (1984). **A systematic approach to tailings impoundment siting**. Mining Sci. Technol. 1 (4), pp. 285-297. https://doi.org/10.1016/S0167-9031(84)90329-3

Vick, S. G. (1990). **Planning, Design and Analysis of Tailings Dams**. 2nd ed. BiTech, Vancouver. ISBN: 0921095120

Wijewickreme, D.; Sanin, M. V.; Greenaway, G. R. (2005). **Cyclic shear response of fine-grained mine tailings**. Can. Geotech. J., 42(5), 1408–1421. https://doi.org/10.1139/t05-058

Williams, H. S. (2004). **Development of a true triaxial apparatus for soil testing**. Master's Thesis (Master of Science in Civil Engineering), Agricultural and Mechanical College, Louisiana State University, 2004, 1811.

Wills, B. A.; Atkinson, K. (1993). **Some observations on the fracture and liberation of mineral assemblies**. *Miner. Eng*. 6 (7), 697706. https://doi.org/10.1016/0892-6875(93)90001-4

Wills, B.A.; Finch, J. A. (2015). **Mineral processing technology: An introduction to the practical aspects of ore treatment and mineral recovery**. Elsevier Ltda., p. 498. https://doi.org/10.1016/C2010-0-65478-2

Wood, D. M. (1974). Some aspects of the mechanical behaviour of Kaolin under truly triaxial conditions of stress and strain. PhD thesis, University of Cambridge.

Wood, D. (1991). **Soil Behaviour and Critical State Soil Mechanics**. Cambridge: Cambridge University Press. doi:10.1017/CBO9781139878272.001

World Information Service on Energy (WISE). (2021). **Chronology of major tailings dam failures**. Last updated 13 Jun. 2021. Available at: < https://www.wise-uranium.org/mdaf.html >. Accessed in: July 2021.

Wu, S.; Yang, C.; Zhang, C.; Zhang, X.; Wang, G. (2017). **The effect of silt content on the mechanical properties of tailings**. *Chinese Journal of Rock Mechanics and Engineering*, v. 36, n. 8, pp. 2007-2017. https://doi.org/10.13722/j.cnki.jrme.2016.1456

Yin, G.; Wei, Z.; Wang, J. G.; Wan, L.; Shen, L. (2008). **Interaction characteristics of geosynthetics with fine tailings in pullout test**. *Geosynthetics International*, v. 15, no. 6, pp. 428–436. https://doi.org/10.1680/gein.2008.15.6.428

Yin, G.; Li, G.; Wei, Z.; Wan, L.; Shui, G.; Jing, X. (2011). **Stability analysis of a copper tailings dam via laboratory model tests: A Chinese case study**. *Minerals Engineering*, v. 24, n. 2, pp. 122-130. https://doi.org/10.1016/j.mineng.2010.10.014

Zhang, C.; Chen, Q.; Pan, Z.; Ma, C. (2020). **Mechanical behavior and particle breakage of tailings under high confining pressure**. *Engineering Geology*, v. 265, 105419. https://doi.org/10.1016/j.enggeo.2019.105419

Xiao, H,; Lee, F-H. (2008). **Curing Time Effect on Behavior of Cement Treated Marine Clay**. *World Academy of Science, Engineering, and Technology*, v. 43, pp. 71-78.

Appendix A: Phase I test results

- Iron ore tailing-ordinary Portland cement blends

Experimental run	Ordinary Portland cement content (%)	Dry unit weight (kN/m³)	q_u (MPa)	q_t (MPa)	G_0 (MPa)	$E_{sec\ peak}$ (MPa)
1	3	17.5	0.25	0.02	229.07	18.78
2	3	19	0.54	0.04	459.33	45.97
3	3	20.5	0.93	0.07	910.52	74.16
4	3	22	1.47	0.13	1279.63	82.09
5	5	17.5	0.38	0.03	565.25	31.58
6	5	19	0.84	0.06	854.35	67.93
7	5	20.5	1.67	0.12	1415.56	105.07
8	5	22	2.52	0.22	1862.66	120.44
9	7	17.5	0.50	0.05	732.67	33.27
10	7	19	1.25	0.08	1127.52	66.52
11	7	20.5	1.80	0.17	1512.71	119.18
12	7	22	3.14	0.19	2276.52	182.86
13	3	17.5	0.13	0.02	245.72	8.11
14	3	19	0.58	0.03	529.11	30.28
15	3	20.5	1.05	0.03	836.57	73.98
16	3	22	1.59	0.07	1250.26	93.31
17	5	17.5	0.46	0.03	569.07	39.94
18	5	19	1.06	0.07	891.51	79.68
19	5	20.5	1.49	0.08	1344.17	62.61
20	5	22	2.24	0.14	1639.95	142.07
21	7	17.5	0.60	0.05	671.36	70.09
22	7	19	1.19	0.06	1087.05	69.61
23	7	20.5	2.01	0.10	1609.83	111.27
24	7	22	2.85	0.27	2158.39	126.04
25	3	17.5	0.24	0.02	250.23	14.71
26	3	19	0.64	0.06	492.47	41.42
27	3	20.5	1.02	0.11	815.75	59.80
28	3	22	1.69	0.10	1309.44	102.70
29	5	17.5	0.38	0.03	500.32	20.64
30	5	19	0.92	0.09	845.80	59.28
31	5	20.5	1.67	0.14	1290.02	97.72
32	5	22	2.51	0.27	1823.52	122.59
33	7	17.5	0.55	0.04	715.56	55.86
34	7	19	1.10	0.16	1117.51	62.28
35	7	20.5	1.99	0.19	1617.02	142.06
36	7	22	2.99	0.24	2176.76	159.39

- Ordinary sand-ordinary Portland cement blends

Experimental run	Ordinary Portland cement content (%)	Dry unit weight (kN/m³)	q_u (MPa)	$E_{sec\ peak}$ (MPa)
1	15	15	1.51	132.14
2	15	17	3.50	210.00
3	5	16	0.69	53.74
4	10	17	2.54	124.43
5	10	16	2.07	159.99
6	10	16	1.76	117.93
7	10	17	2.82	144.96
8	5	15	0.34	43.45
9	10	17	3.10	167.78
10	5	15	0.44	24.90
11	15	16	2.87	188.65
12	15	17	3.33	170.81
13	10	15	1.02	45.26
14	10	15	1.05	72.61
15	10	16	2.21	136.36
16	5	16	0.70	56.77
17	15	15	1.87	100.55
18	5	17	1.70	110.00
19	15	17	3.45	196.82
20	15	16	2.78	201.94
21	5	17	1.82	77.00
22	15	16	1.82	99.74
23	15	15	1.51	83.44
24	10	15	0.92	65.84
25	5	16	0.69	55.05
26	5	17	1.93	92.00
27	5	15	0.52	42.51

Appendix B: Phase II specimens' pictures

- Iron ore tailing-ordinary Portland cement blends

1) Cemented_16.5 kN/m³_C = 4.38%_θ = 0

2) Cemented_16.5 kN/m³_C = 4.38%_θ = 30

3) Cemented_16.5 kN/m³_C = 4.38%_θ = 60

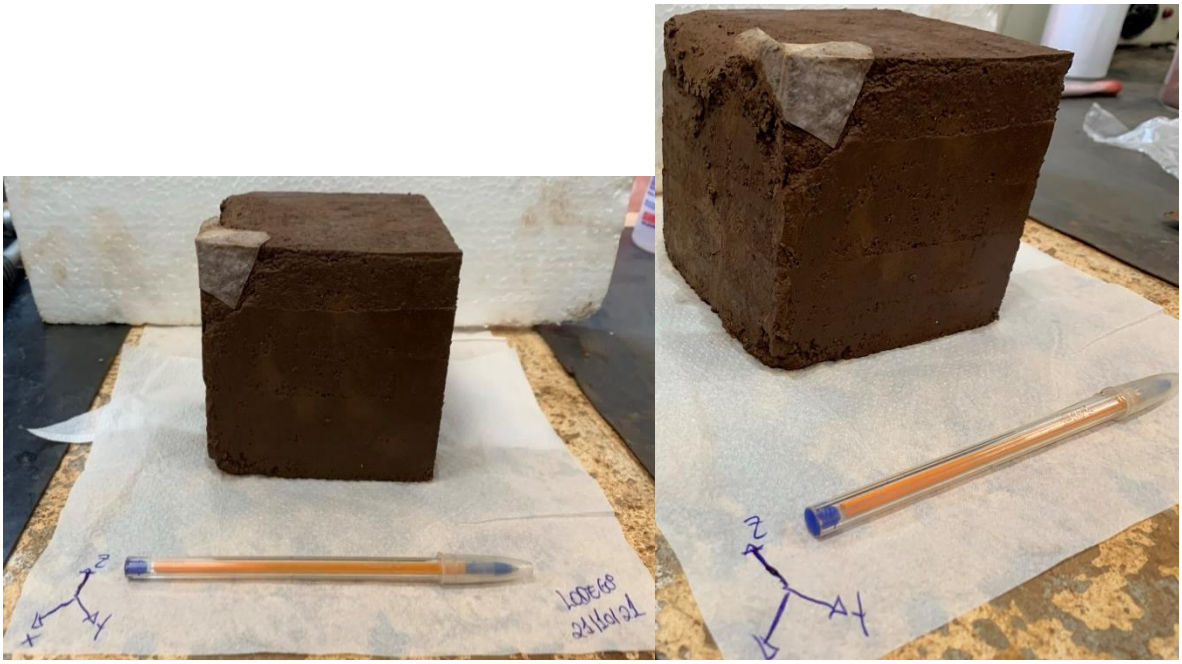

4) Cemented_16.5 kN/m³_C = 4.38%_θ = 90

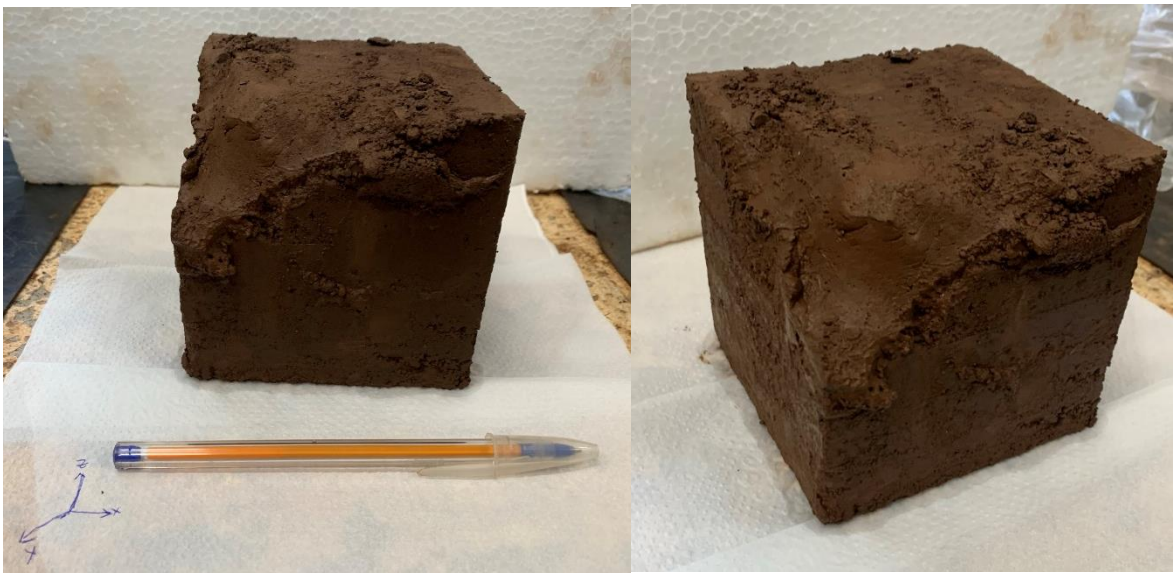

5) Cemented_16.5 kN/m³_C = 4.38%_θ = 120

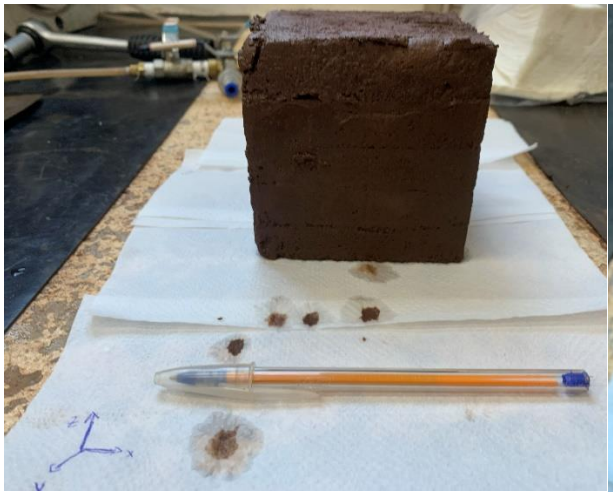

6) Cemented_16.5 kN/m³_C = 4.38%_θ = 150

7) Cemented_16.5 kN/m³_C = 4.38%_θ = 180

8) Cemented_17.5 kN/m³_C = 2.66%_θ = 0

9) Cemented_17.5 kN/m³_C = 2.66%_θ = 30

10) Cemented_17.5 kN/m³_C = 2.66%_θ = 60

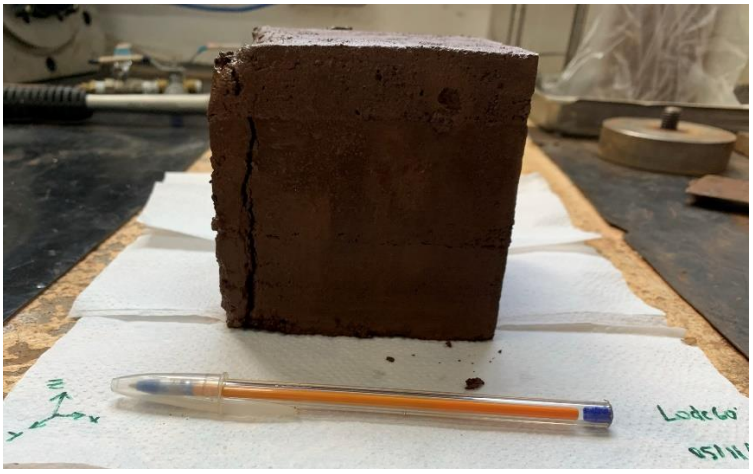

11) Cemented_17.5 kN/m³_C = 2.66%_θ = 90

12) Cemented_17.5 kN/m³_C = 2.66%_θ = 120

13) Cemented_17.5 kN/m³_C = 2.66%_θ = 150

14) Cemented_17.5 kN/m³_C = 2.66%_θ = 180

- Ordinary sand-ordinary Portland cement blends

1) Cemented_16 kN/m³_C = 14.65%_θ = 0_ p’ = 2MPa

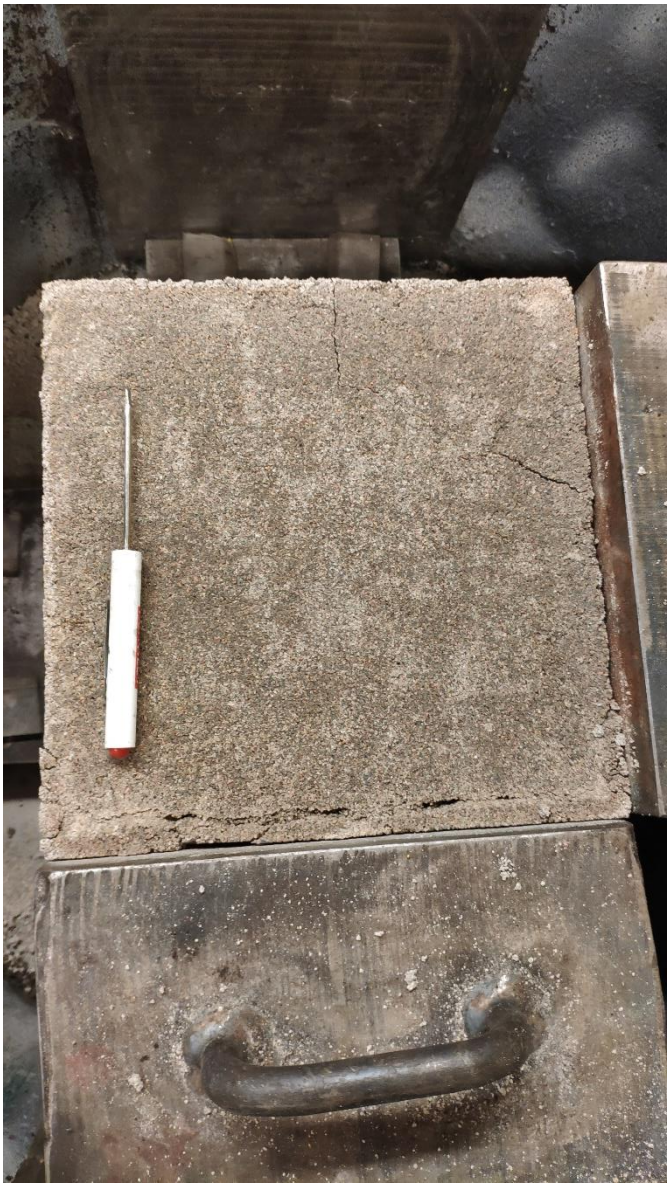

2) Cemented_16 kN/m³_C = 14.65%_θ = 30_ p’ = 2MPa

3) Cemented_16 kN/m³_C = 14.65%_θ = 60_ p’ = 2MPa

4) Cemented_16 kN/m³_C = 14.65%_θ = 90_ p’ = 2MPa

5) Cemented_16 kN/m³_C = 14.65%_θ = 120_ p’ = 2MPa

6) Cemented_16 kN/m³_C = 14.65%_θ = 150_ p’ = 2MPa

7) Cemented_16 kN/m³_C = 14.65%_θ = 180_ p’ = 2MPa

8) Cemented_16 kN/m³_C = 14.65%_θ = 0_ p’ = 4MPa

9) Cemented_16 kN/m³_C = 14.65%_θ = 30_ p’ = 4MPa

10) Cemented_16 kN/m³_C = 14.65%_θ = 60_ p’ = 4MPa

11) Cemented_16 kN/m³_C = 14.65%_θ = 90_ p’ = 4MPa

12) Cemented_16 kN/m³_C = 14.65%_θ = 120_ p’ = 4MPa


Y
X

13) Cemented_16 kN/m³_C = 14.65%_θ = 150_ p’ = 4MPa

14) Cemented_16 kN/m³_C = 14.65%_θ = 180_ p’ = 4MPa